Enterprise-Level Migration to Micro Frontends in a Multi-Vendor Environment

István Pölöskei[1], Udo Bub[2]

[1]adesso Hungary Software Kft.
Infopark sétány 1, 1117 Budapest, Hungary
E-mail: istvan.poeloeskei@adesso.eu
[2]Eötvös Lóránt University (ELTE) Budapest, Faculty of Informatics
Pázmány Péter sétány 1/C, 1117 Budapest, Hungary
E-mail: udobub@inf.elte.hu

Abstract: With new web applications rapid growth in size, the monolithic frontend approach has been increasingly challenged over the last years. The micro frontends concept has been proposed to match the architectural needs facing increasing complexity, e.g. for newly emerging cloud-native solutions. It provides function-level granularity and lets the developer adjust each process's performance. In the majority of relevant cases for which the micro frontends paradigm is considered, the system should be migrated, or an existing monolith should be converted to new technologies, whereas, the scientific community mainly focuses on greenfield designs. In this paper, we validate the paradigm, with a case study, in the context of migration for enterprise information systems, in a multi-vendor environment. Based on our analysis, we propose a method for the migration of frontend monoliths, along with guidelines and recommendations for future work.

Keywords: micro frontends; multi-vendor; migration

1 Introduction

Web interaction layers are crucial for rendering a feature-rich browser application. The service is deployed online through a pointer like a public web endpoint, serving a frontend as a target web application user interface. This layer's code is growing bigger because some of the new logic implementation. The latest applications are behavior-driven; the frontend application may also contain some business logic. Concentrating on the frontend is reasonable because the administered components may affect the global usability of the product.

Some frameworks and principles have been revealed to enhance its general effectiveness in recent years, like service composition and web services [1]. The introduced concepts have delivered software elements for accomplishing the business needs based on technology, being controlled by different developers and

teams or organizations. Few of the designed architecture components have become legacy later because they are built on a deprecated technology or framework.

In enterprise applications, typically, the components have been developed evolutionally. It implies that the applied frameworks have been replaced continuously. Modern software architectural concepts should sustain the coexisting of different approaches. Without a modern frontend framework, realizing such an outstanding frontend application involves additional complexities [2].

The monolithic strategy has been challenged in the last years. In an enterprise software system, the code-base can regularly be so huge that it is not maintainable. The first advances were the modularization and component-based solutions, leading to the service-oriented architecture paradigm [3], where e.g. [4] gives an overview. Recently it has evolved further to a micro-service or micro frontends architecture (Figure 1) for getting the dynamism of cloud computing [5].

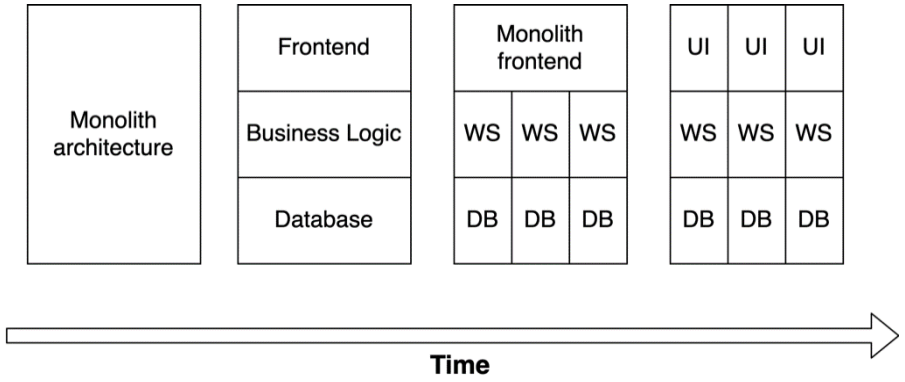

Figure 1

Evolution of architectures from the frontend point of view. Monolith – 3 layered – Micro-services/SOA – Micro frontends. While systems are growing, it involves the growing diversity of technology. WS (Web Service), DB (Database), UI (User Interface).

The current research examines an efficient monolith frontend migration strategy to the cloud by using a compound approach to find a cost-effective way to migrate the UI tier.

2 Frontend Approaches

2.1 Micro-Services and Frontends

Micro-services are getting more and more popular. Some corporations have preferred this architecture against the conventional monolithic one. Initially, this strategy was more or less restricted to backend services. It was intuitive, splitting the entire backend logic into miniature independent services. Each service is accessible through the API, realizing the REST principle. Although, a comparable breakdown had not proceeded with the frontend tier.

The growth of the frontend was also commenced but barely on the code level. After server-side rendering, contemporary JavaScript-based frameworks were becoming popular. Nowadays, some organizations attempt to realize their Single Page Application (SPA) based software in their landscape, presenting a single HTML page with dynamically loaded page content [2].

In brief, the monolithic frontends survived, along with service-oriented architecture and micro-service backend design, where they were still generally used [6]. In that case, the backend was innovative, but the frontend tier remained conventional. The frontend code had not evolved; it used just the traditional modular strategy, a bright compilation of tiny applications. The deployment of a complex bundle was challenging as well.

The micro-service architecture advantages are formulated, but why does the industry not use it on frontend projects [5]? It might have some positive consequences, producing the features of the same domain by a single team. However, there are still some dependencies between the frontend and backend. It makes it more complicated to discover a bug in the productive system if there is no transparent responsibility for the business domain's set of features [6].

An uncomplicated solution to the dilemmas discussed above is the micro frontend design, which complements the micro-services architecture in the presentation layer. Each company has its resolution to this obstacle, using the equivalent principle as micro-services. They were directed to the same outcome while producing micro-apps using isolated endpoints; they experienced some positive attributes [5]. The isolated applications can be merged into a portal-like single page application as well. From the user perspective, it remains only one application, but architecturally, they are self-governing entries.

By the micro frontends pattern, the frontend element synthesis is done in the client's browser. Frontend services are implemented by the frontend (JavaScript) code; through the web applications, the backend services can be requested. The host application assembles the components as services, qualified only for the routing, component selection, and communication [7].

2.2 Frontend Monolith

As the brand-new web applications are getting bigger and bigger, it serves unusual, unique difficulties to the architects. For example, the monolith frontends may suffer performance issues because it is not a trivial task to fine-tune each unit's performance.

The deployment of such a big client bundle is also challenging since DevOps pipelines are not well supported by the monolith architecture [8]. Moreover, the reusability of each unit is also not irrelevant. As a result, the complexity remains high compared to the well-structured applications.

The introduction of new technologies is not trivial in this landscape. Some parts must be reworked before a different element has been injected. The platform dependencies are potential bottlenecks in massive projects.

2.3 Main Features of Micro Frontends

The functional division has its benefits. The main one is scalability. This concept fits well into the latest cloud-native solutions [9]. A function can be scaled freely. The architecture remains on the frontend side as adjustable as on the backend side. A process with a more extraordinary load (request number) can take more extra resources by allocating more instances. It could be achieved in a "self-driving" manner through modern auto-scaling solutions [10].

The advantages of this pattern are identical to working with a cloud-native architecture. Each project can be managed by separate repositories (multi-repo approach) [11]. The separation, on the code level, establishes the final software structure. An arrangement by autonomous repositories makes it attainable to have a well-defined system in the organization [11]. A product could be developed in a flat structure; the teams can be systematized according to their business domains. Only a thin architect layer is obliged to define the direction of the entire application. It also decreases the business dependencies between teams. It has some privileges in grouping the functionalities by areas [6].

The deployment is also a necessary aspect. The micro frontends concept fits not only into cloud-native landscapes but also into DevOps philosophy [12]. It promotes the more durable build and release cycles natively. The small chunks have another positive characteristic as well, more satisfying testability. Atomic automatized tests can be executed if the complexity is low.

The application can handle different technologies (Figure 2), but the synthesis remains manageable. Each team is free to use its own preferences to formulate its unique user interface. From a product point of view, the implementation of each micro-app is hidden. The provided application does not depend on the built-in technologies. The micro apps are framework agnostic, but following some usual guidelines and naming conventions is advised for the complete picture.

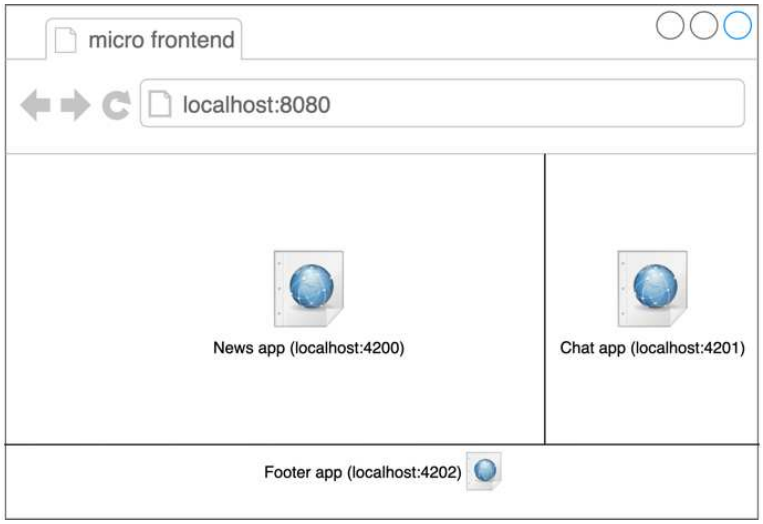

Figure 2
Frontend as a set of applications from different endpoints

2.4 Micro Frontends in a Cloud-Native Environment

Cloud-native solutions, like Kubernetes, provide their open-source container orchestration services [13]. Scaling and deploying the application is sufficient with multiple instances, allocating further resources for business-critical processes. This method actively supports the micro frontends theory because the well-defined granularity lets the orchestrator adjust each process's performance.

2.5 Drawbacks

This approach with multi-repositories involves a complexity baseline. The communication between each micro application has overhead; the polyrepo is recommended only for huge enterprise solutions, providing the choice of organic evolution [11]. Because of built-in complexity, some expertise is required for the micro frontends.

Debugging such an intricate and fragmented landscape is a complicated task. It may take time to locate a bug among dependencies, and they might easily get outsourced. Issues seldom occur during the authentication (single sign-on) mechanism because the creation of the tokens' transportations can be problematic. Since current browsers could apparently handle several built-in applications on the same screen, it might suggest different logins claiming three authentication mechanisms. For fixing this issue, introducing the backend for the frontend (BFF) layer is recommended (Figure 3). BFF can regulate the backend API calls [14].

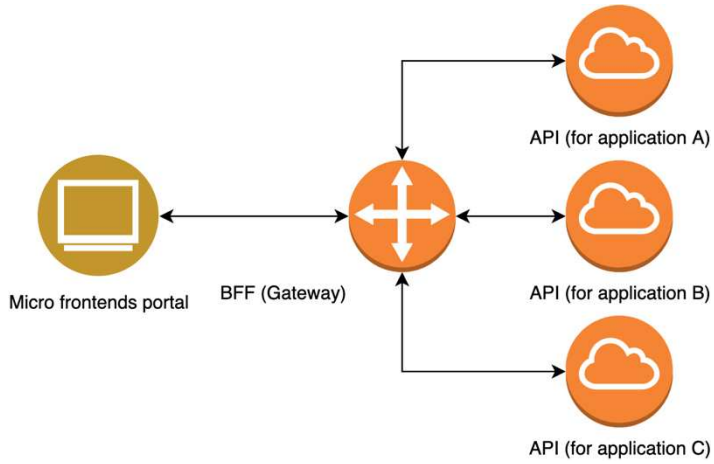

Figure 3
Backend for frontend pattern

Standard guidelines are required. In a portal-like structure, the apps should follow the same design principles. Redundancy in the source code may occur because the framework elements and base controllers could be bundled together in each micro application.

2.6 Domain-driven Approach

Assume an application that has some sovereign functionalities. Despite having enough developers, it could be challenging to handle it. Providing the necessary business knowledge for each developer is a hurdle, but it is possible to organize the human resource according to business domains or architectural layers during the preparation.

The micro frontends concept is a modern approach where teams own the feature sets of business areas. They are independent or loosely coupled, oriented by business domains and specialists. The teamwork is full-stack, affecting each layer, from the database until the user interface.

The implementation is effective. The team can use the DevOps features at their full capacity [12]. The micro applications are detached; they may have their versions. The versions are independent of the other releases. The micro-app can be introduced individually.

The procedure is matching well the agile methodology. Achieving in increments is also a potent compound with micro frontends architecture. The combination of new features or redesigning the traditional ones is feasible in tiny increments. This mixture continuously contributes business value through the project [15].

3 Integration Techniques

3.1 Multiple Endpoints

The original approach of multiplied endpoints is not an imperative section of the micro frontends idea, but historically it is the main root and initial trigger. It means a set of applications, which live under different endpoints (for example, each route is provided by reverse proxy). This approach does not use the advantage of Single Page Application. After switching the route, complete side reloading is required.

3.2 Iframes in a Single Page Application

The first, native HTML5 based approach uses Iframes [16]. They can split a compact web application into smaller elements; the components get isolation and security by the Iframe. These parts are assembled into a frame-like formation. Currently, it is one of the most generally used solutions. It realizes the simple combination of technologies, by providing a certain degree of sovereignty among Iframes.

Through its native API, communication between components is feasible. While providing separation, the event flow is also possible. The Event bus (like message queue) is the state-of-the-art recommendation for extending the communication between Iframes [16].

The usage of Iframes is not such a universal solution [7]. It can provide a remote endpoint as a built-in frame, but it is not such a flexible structure. Providing a responsive modern application requires some additional structures and complexities. The usage of other solutions based on the modern JavaScript frameworks is recommended because some unexpected issues may occur during the routing and navigation between Iframes [7].

3.3 Web Components

Since 1995, JavaScript became the number one language of the web. Currently, the websites frequently use one of the three main JavaScript frameworks: Angular, React, and Vue [17]. Since enterprises frequently choose an Angular framework, its features as a web component supportive framework will be described.

The Web Components concept is a standard by W3C; some modern browsers have already implemented it, providing a run-time integration possibility for the components [7]. The web component concept is the remote extension of the original components approach. According to the DRY (“Don’t Repeat Yourself”) principle, any web application can easily import the frontend components. This way, the entire frontend application can also be imported from diverse

remote locations; like serving a remote resource, the pieces are encapsulated apart from the host code.

The User Interface components provider is a service, which is not just a conventional REST endpoint; it also publishes the required User Interface components. The web component can encapsulate various technologies and frameworks, as well. Through the provided UI component, the business logic is also available by calling the backend services.

Since the web components use the browser API, some compatibility issues may occur [18]. It is not guaranteed to be compatible with all possible browsers. If too many components are imported from remote sources, some network performance issues may occur. Since the implementation may involve some complexities, popular UI frameworks are recommended, like Angular Elements [18].

By custom elements, each micro frontend service can be converted into components [6]. A published element is a reusable component with its CSS and JavaScript logic. It could be installed directly on the shell web application. Each team can develop its traits and declare them as a pure service. They can also be extended by lifecycle hooks, as call-backs. It is possible to assign properties to them. The events are triggered if DOM's manipulation occurs. DOM (Document Object Model) means the abstract tree-like model of the HTML page, where the injected components are inserted or rendered. This technique includes some intercommunications with DOM; each element fits into the original DOM by using namespaces.

If the micro applications are Angular applications, they can be pushed as angular libraries (like NodeJS modules) into a shared repository. The published modules can be loaded in a lazy loading manner to reduce network traffic [19].

4 General Frontend Migration Use-Case

4.1 Problems with the Frontend Migration

Enterprises try to realize efficiency gains by using cutting-edge technologies once they are mature enough to compensate for the attached efforts. A new frontend framework serves some advantages. It increases the user experience, making the developer's work more efficient and effective [17].

Upgrading the existing landscape is challenging; it slows down the introduction of new business features. Some new functionalities can be restricted by technology constraints on the frontend side as well. Getting rid of legacy factors is never simple because they include complexity based on last years' developments. Since the implementation is growing over the years based on new technologies, the complexity mirrors this trend because its volume is more significant.

The migration use case was increasingly crucial for service-oriented concepts [4] and has gained further momentum nowadays [14].

In most cases, when the micro frontends pattern is under consideration, the system should be migrated, or the existing monolith should be converted to new technologies. This pattern allows continuous modernization by operating the legacy components until they have been replaced.

The migration of monolith systems is not a trivial task. Some necessary backend services might belong to the frontend applications, not only strongly UI applications. One migration methodology fits well to the backend dependencies; another one might be better for the UI use-cases. Businesses need to be cost-conscious. The migration to the cloud is managed cost-effectively. The migration to the new technology involves potentially cost-savings.

Our research question targets the effective frontend migration strategy. Based on our literature research, the various frontend applications can be handled as a micro frontend portal. To identify the appropriate method for migration, we investigate the different approaches in the area of migration to synthesize a compound one for our use case. The applied strategy needs to improve the company's overall productivity.

4.2 Proposed Solution

At the beginning of the product lifecycle, a single frontend monolith method is a popular strategy. It's suitable until the volume becomes too huge. After a critical size, the structure becomes a limitation; the development becomes unscalable. The introduction of modern cloud-based solutions could not cooperate with a frontend monolith. It involves some difficulties to the development. Domain separation presents independence for the developers.

The preparation for the migration and transformation between the monolith and micro frontends should begin with identifying bounded contexts and domains. The domain-driven design is an undecayed approach for discovering monolith landscapes. It involves some code investigations as well. After the modeling of the AS-IS landscape, the granularity of the migration can be defined. The costs are critical because the granularity of the redesign is considerably influencing it.

The commonly used migration strategies are mainly applied in cloud migration projects: lift-and-shift, re-platforming, refactoring [20]. Lift-and-shift is the most straightforward and cheapest strategy. State-of-the-art public cloud services can practically automate it. The combination with other techniques is also possible since the remaining two methods could be more effectively managed if the application is hosted by the cloud initially. The primary rehosting by lift-and-shift approach is a good milestone before the notable restructuration while using the public cloud services as soon as possible. The re-platforming involves a few

modifications on the application level as well. The cloud services frequently require at least a few changes on the application's side, setting the necessary interfaces. The re-architecting necessitates an in-depth business review to fulfill the function and non-functional requirements. Since the reimplementation takes some time, the operation and implementation costs are higher.

The migration is advised when the previous application turns too complex or architectural modernization is essential. The agile mindset is vital in cloud migration projects, bypassing the big bang implementation style. The Minimum Viable Product (MVP) milestone is a valid option for collecting the customers' feedback. The migration projects strive to minimalize the expenses, pushing the lift and shift approach [21]. This could also be performed by re-platforming the original applications. The refactoring is costlier, but provides the option to use the serverless technology that makes it possible to hide the dependency of the servers by the services of the public cloud providers, providing a more affordable and productive usage of cloud computing. The contemporary design methods fit well in the event-driven logic.

5 Frontend Migration Case-Study

We will validate the applicability of the approach for migration in a case study. It is structured as proposed in [22] with the following sections: Situation Faced, Action Taken, Results Achieved, and Lessons Learned.

5.1 Situation Faced

According to the global decommission program, a particular location of a multi-national company gets rid of the legacy software elements. This process has been made together with infrastructural modernization and cloudification. The demand is to migrate the legacy on-premise service-oriented architecture to the united micro-services-based architecture. The examined work-stream focuses on migrating the presentation layers to find an adequate way to migrate frontend monoliths. The existing monolith frontend applications should be reconstructed for a more stable usability. The outcome of the study is discussed in the following sections.

During the migration, the critical measurement is the costs. A superior but costly solution can be achieved by reapplying each feature as a new project based on recent technologies. In real-world projects, the budget is restricted. Bound resources should realize the relative best technology level. It comprises some cost-effective methodologies.

Based on the existing design documents, and architectural snapshot has been created for having an input for the migration (Figure 4). The architecture is high level, focuses only on the separation of layers and endpoints.

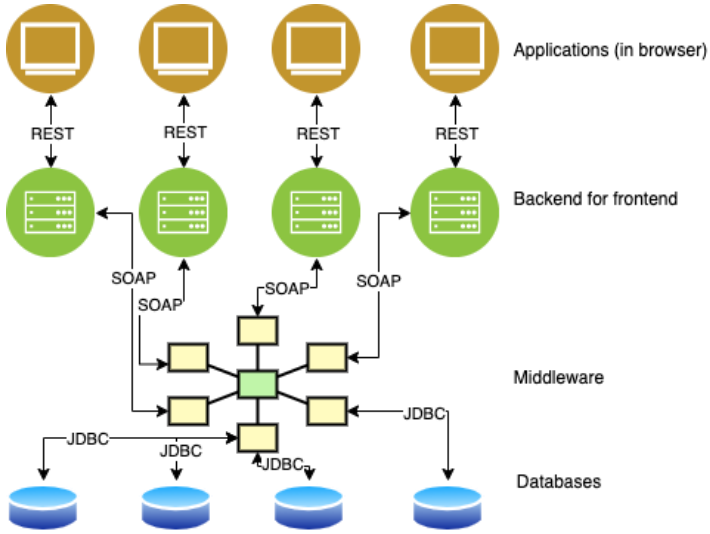

Figure 4

High-level enterprise AS-IS architecture. Each monolith frontend application has its backend for the frontend provider. Through middleware, the backend for the frontend layer can communicate with databases. On the database layer, some logic has been implemented.

The system is service-oriented and on-premise. The service-broker middleware element provides the services. The backend functionalities are accessible through the backend for the frontend layer for consolidating the API. The migration of the backend part is not part of the scope, but the new frontend must connect to the legacy and new backend services. The original goal is the migration of the full set of business processes. Current research focuses only on the frontend; this paper will not describe the migration of the backend side.

5.2 Action Taken: Target-Architecture Design

The proposed target architecture will serve as a target solution for global technical requirements. The main requirement is cloud-nativeness for implementing a modern architecture in the location. The frontend layer needs to support and extend cloud-based approaches. The new architecture should be compatible with the guidelines and cost-effective as well.

During the preparation, the potential approaches of the scientific literature have been investigated. The architectural guidelines already determined the set of concepts. The combination of a portal-like frontend as a collection of micro

applications has been chosen. The related proof of concepts has clarified the implementation details.

Functionally, the applications are getting united. Owning only one application has a tremendous user experience and business value. The frontend codes are behavior-driven; they contain some JavaScript parts as well. However, it increases the complexity and the size of the bundle in the browser. Lazy-loading is necessary for satisfactory client-side performance. The required modules should be loaded if they are necessitated. Reusability is also a fundamental aspect; some frontend functionalities might be served directly to the various platforms.

Previously discussed integration methodologies have already been reviewed: route level separation by reverse-proxy, Iframe, Web Components, Angular specific web-components implementation. For this business need and baseline architecture, the introduction of Angular-based web components serves potentially a robust solution. A Proof of Concept has proved this statement. It is possible to handle the existing applications as independent components by web components, but they are merged into a portal frame. Transformation of each element to web components is not challenging. Its micro frontend service can host this component. Each frontend service must provide the UI with the exact design requirements. The introduction of an ordinarily used framework or style is reasonable.

The Angular framework is often used in enterprise-grade complex frontend solutions. Some organizations have built their application portfolio like islands, having separate web endpoints for each service or just navigating between them, but managing a massive monolith might be less productive.

With micro frontends, merging the whole distributed application portfolio is conceivable by implementing a single portal for all purposes (Figure 5). Therefore, the research has been looking for the best option of merging some individual applications into one modern single-page application.

First of all, the project manager should clarify the scope. The AS-IS architecture probably contains some legacy or deprecated elements. Over the years, some processes or components might be deprecated from a business perspective. The management can cut unnecessary costs by planning the migration precisely. The detailed plan contains the migration schedule of each dependency as well.

Concerning scheduling, providing results as early as possible is essential. The migration must start with the core modules or the low complex ones. The minimal viable product involves some support from the management side. This approach is strongly supported by micro frontends architecture. By them, old on-premise applications and modern cloud-based ones can be served together in the same portal shell. At the early stage, the portal can publish the old on-premise applications; after each sprint, they can be replaced easily without effort.

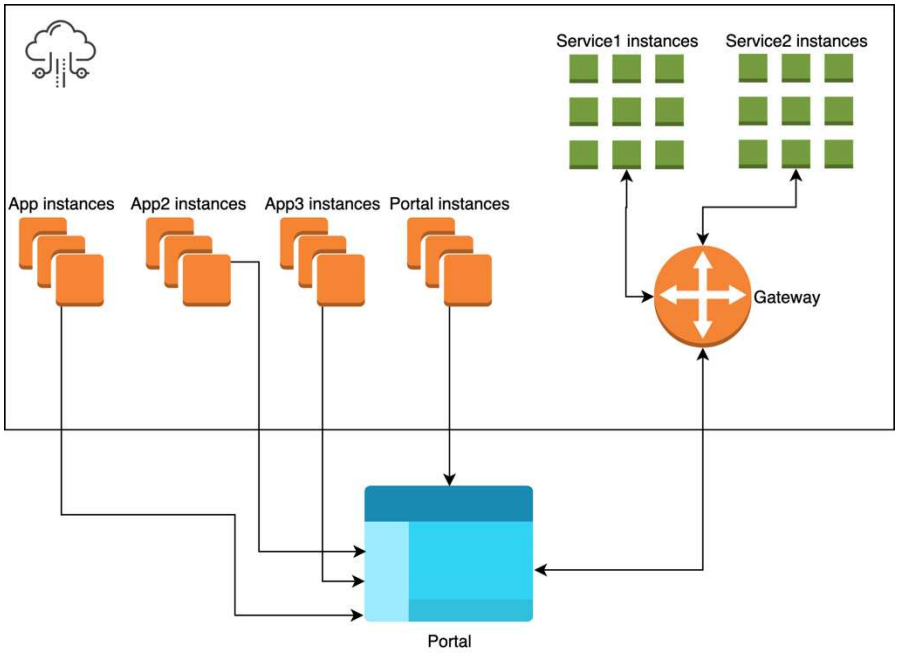

Figure 5

The proposed high-level target architecture in a cloud-native environment [13]. Each application provides its user interface. Each app is integrated into the portal frame. The applications can use the backend API through a consolidated gateway (Backend for frontend pattern).

The Micro-services approach supports the usage of different technologies for each component. The simplest method is the implementation of web components. They created independent web components that can be easily injected into a Single Page Application Container [16].

For building such a system, some other dependencies are needed. The modern JavaScript ecosystem natively supports the implementation of micro frontends by web components. Each component is a different app; they listen to different ports. The Single Page Application Container (host or shell application) will merge and serve them as a single website. From the user perspective, the fragments seem to be a homogeneous web-application.

Modern JavaScript frameworks can create components. They need to be encapsulated into web components, to publish them through the network. In Angular, the AppModule root module should export the whole (micro) application as a web component. In React and Vue, the implementation is a bit more complicated than in Angular, but each frequently used framework has its solution. Angular has another added benefit: Angular CLI supports the whole build – the deployment process natively. For other modern frameworks, some build and deployment tools are required, like webpack.

There are many possible ways to build micro frontends based portal applications. The most obvious choice is the usage of Web Components or Iframe with an event transmitting system. These native elements can fulfill this goal, but some bottlenecks may occur, like the poor communication between elements and code redundancy. For avoiding the weaknesses, some frameworks were introduced [17].

The Angular elements library was created for sharing components between applications; it provides simple integration for the micro frontends. Angular is a well-known product in the industry. It is a battle-tested solution from Google for enterprises because unknown open-source libraries and frameworks might contain some security vulnerabilities. A possible alternative of Angular Elements is the injection of Angular modules for reaching additional code-level features. In that case, both applications should use the Angular framework [19].

The cloud-native techniques are used to reach the cloud goals, based on a containerized infrastructure, not being dependent on a cloud provider. The cloud-native deployment can be effectively supported by DevOps tools, serving the demand of high deployment frequency [12]. The migration tries to minimize the development costs, applying the lift-and-shift approach as many times as possible [21]. For the introduction of a container-based platform, the refinement of the modules is needed. The modules contain the backend for frontend (BBF) parts as well. In a frontend project, the BBF layer is mainly responsible for serving the frontend code and applying the authentication mechanism, transforming the middleware services into REST API. In our case, the processes' refinement is just optional because the containers can be launched without any problems.

The pages and applications should have the same design. The integration from the user perspective should be smooth. The inconsistencies might damage the customer's satisfaction. In our case, the design of each application should be the same based on a shared library. The library provides common design elements and components.

5.3 Results Achieved

The current enterprise's primary goals are cloud migration, merging frontend applications supporting a portal-like structure; each built-in application will be rendered in the same style. The migration is driven by cost optimization; it involves a low amount of resources for attaining the goals.

The migration of frontend applications uses different migration strategies to combine lift-and-shift, re-platforming, and refactoring. Since the core backend services contain an inefficient and difficult code basis, the lift-and-shift strategy was the only option. Without the necessary expertise of the legacy services, their migration will be done at a later stage. The frontend application migration offers more extensive flexibility. Without much risk, the User Interface can be re-

architected according to a different approach. It also gives the possibility to present functionally noticeable results directly to the end-user.

Angular-based web components support the theory of micro frontends. The application can be bundled into a single JavaScript file, and each backend serves it for the frontend instance. The portal frame on the client-side can manage the provided applications like a native angular component, merging them, hide, or make them visible according to the client's credentials.

This architecture can use the cloud native's full potential on the frontend side as well. The migration to cloud-based micro frontends architecture lessens the calculated operational costs in the above-discussed case.

The accomplished proof of concept is built on Angular Elements web components. The elements are united into a portal structure. The main benefit of the polyrepo approach is separation. The idea extends the micro-services, providing a platform for accessing the old and new functionalities together.

Strengths:

- The newest Angular versions support the Ivy compiler; the generated components are reusable by other frameworks
- Only the relevant apps are loaded in the portal frame
- Independent repositories can manage the project. Repositories have their version number
- Short deployment cycles
- The flexibility of the structure
- There are no compatibility problems with the frame's Angular-based logic
- The effort for the integration of the existing applications is reduced
- Project security is improved, the repository access can be limited to the application, which is helpful in a multi-vendor environment
- Applications can have their dependency versions
- Legacy and modern can live together

Weaknesses:

- Some dependencies are redundant; each web component may include its own
- Memory and the network load are higher because of redundant dependencies
- Analysis of the issues is challenging because of dependencies
- Merging the application's frontend code into one bundle makes debugging challenging

Modifications made:

- The applications are being embedded into an Angular shell application
- Usage of shared libraries. They are registered in the global scope

5.4 Lessons Learned

The above-discussed proposal is a good fit for the migration use case. Current applications are behavior-driven, a huge code-base for complex business logic is demanding for the client and network.

The containerization-based lift-and-shift approach provides a valid option for promptly migrating the core standard services, like having a suitable wrapper around the application. It gives a further granularization, after the central cloud re-platform step since the lift-and-shift initially doesn't reach the cloud-natives principal gains. Like breaking down the software into services and bigger units, several elementary modifications can serve the scalability. For the most cloud-optimized result, strong refactoring is needed.

The approach supports the incremental delivery natively, being a good combination with the agile paradigm. Having a flexible software structure is a real advantage. Old on-premise frontend applications can be integrated into a micro frontends frame as non-native components instead of navigating to a new tab in the browser. The legacy components can be replaced later by a native sub-application if the feature has been migrated to the cloud. Resource constraints sometimes limit migration projects. The project manager needs to find the simplest solution for realizing the target. Part results and milestones are essential for getting the support of project sponsors.

Conclusions and Future Work

During our research, the polyrepo micro frontend solutions were investigated. The principal goal was to determine the optimal solution for our migration use case. For being cloud-native and having some separate applications on the frontend side, the implementation needs to follow the micro frontends pattern, with a polyrepo approach. This approach provides a run-time native integration in the browser. The cloud-native multi-instance environment can allocate additional resources to each process, giving a dynamic response to higher request quantities at any point of the designed system. This guarantees higher efficiency and lower costs.

The case study presents an example of the potential use-case of the micro frontends pattern. In an enterprise, each application can be delivered by vendors. In a multi-vendor environment, each legacy app has its restricted know-how. If the target is a common standardized portal, the baseline diversity makes the designing troublesome. The micro frontends concept grants freedom for the implementation teams, but it has its obligations as well. The standardization of the UI design and

having a well-defined integration methodology is a necessity. The teams are limited to their domain by their own repository. It provides built-in security, in a multi-vendor environment.

The web components have been used in the case study. For an enterprise-level Angular project with distinct teams, the micro frontends pattern should be considered. The benefits concerning the separation of applications could be helpful to migration and re-architecting projects.

The concept of micro frontends is a business-oriented strategy. Business domains separate teams and applications. The members of each team are specialists. Since the micro frontends provide flexibility, each business need could be realized through the best fitting technology.

The micro frontends pattern is used in industry, but still, there is room for improvement. Based on the careful evaluation of the state-of-the-art and the above-discussed case study, a new generic strategy could be introduced, for micro-frontends-based migration.

References

[1] A. L. Lemos, F. Daniel, and B. Benatallah, "Web service composition: A survey of techniques and tools," *ACM Computing Surveys*, Vol. 48, No. 3, 2015, doi: 10.1145/2831270

[2] F. Shahzad, "Modern and Responsive Mobile-enabled Web Applications," *Procedia Computer Science*, Vol. 110, pp. 410-415, 2017, doi: 10.1016/j.procs.2017.06.105

[3] P. Offermann and U. Bub, "A method for information systems development according to SOA," *15th Americas Conference on Information Systems 2009, AMCIS 2009*, Vol. 2, pp. 908-918, 2009

[4] P. Offermann, M. Hoffmann, and U. Bub, "Benefits of SOA: Evaluation of an implemented scenario against alternative architectures," *Proceedings - IEEE International Enterprise Distributed Object Computing Workshop, EDOC*, pp. 352-359, 2009, doi: 10.1109/EDOCW.2009.5331973

[5] J. Bogner, J. Fritzsch, S. Wagner, and A. Zimmermann, "Microservices in Industry: Insights into Technologies, Characteristics, and Software Quality," *Proceedings - 2019 IEEE International Conference on Software Architecture - Companion, ICSA-C 2019*, No. March, pp. 187-195, 2019, doi: 10.1109/ICSA-C.2019.00041

[6] C. Yang, C. Liu, and Z. Su, "Research and Application of Micro Frontends," *IOP Conference Series: Materials Science and Engineering*, Vol. 490, No. 6, 2019, doi: 10.1088/1757-899X/490/6/062082

[7] A. Pavlenko, N. Askarbekuly, S. Megha, and M. Mazzara, "Micro-frontends: Application of microservices to web frontends," *Journal of Internet Services and Information Security*, Vol. 10, No. 2, pp. 49-66, 2020,

doi: 10.22667/JISIS.2020.05.31.049.

[8] M. Waseem, P. Liang, and M. Shahin, "A Systematic Mapping Study on Microservices Architecture in DevOps," *Journal of Systems and Software*, Vol. 170, p. 110798, 2020, doi: 10.1016/j.jss.2020.110798

[9] N. Kratzke and P. C. Quint, "Understanding cloud-native applications after 10 years of cloud computing - A systematic mapping study," *Journal of Systems and Software*, Vol. 126, pp. 1-16, 2017, doi: 10.1016/j.jss.2017.01.001

[10] S. Kho Lin *et al.*, "Auto-Scaling a Defence Application across the Cloud Using Docker and Kubernetes," *Proceedings - 11th IEEE/ACM International Conference on Utility and Cloud Computing Companion, UCC Companion 2018*, pp. 327-334, 2019, doi: 10.1109/UCC-Companion.2018.00076

[11] N. Brousse, "The issue of monorepo and polyrepo in large enterprises," *ACM International Conference Proceeding Series*, 2019, doi: 10.1145/3328433.3328435

[12] E. Dornenburg, "The Path to DevOps," *IEEE Software*, Vol. 35, No. 5, pp. 71-75, 2018, doi: 10.1109/MS.2018.290110337

[13] K. Indrasiri and P. Siriwardena, *Microservices for the Enterprise: Designing, Developing, and Deploying*. 2018

[14] A. Henry and Y. Ridene, *Assessing Your Microservice Migration*. 2020

[15] D. Sjödin, V. Parida, M. Kohtamäki, and J. Wincent, "An agile co-creation process for digital servitization: A micro-service innovation approach," *Journal of Business Research*, Vol. 112, No. January, pp. 478-491, 2020, doi: 10.1016/j.jbusres.2020.01.009

[16] M. Mena, A. Corral, L. Iribarne, and J. Criado, "A Progressive Web Application Based on Microservices Combining Geospatial Data and the Internet of Things," *IEEE Access*, Vol. 7, pp. 104577-104590, 2019, doi: 10.1109/access.2019.2932196

[17] S. Peltonen, L. Mezzalira, and D. Taibi, "Motivations, Benefits, and Issues for Adopting Micro-Frontends: A Multivocal Literature Review," *arXiv*, 2020

[18] P. J. Molina, "Quid: Prototyping web components on the web," *Proceedings of the ACM SIGCHI Symposium on Engineering Interactive Computing Systems, EICS 2019*, 2019, doi: 10.1145/3319499.3330294

[19] M. Hajian, *Progressive Web Apps with Angular*. 2019

[20] N. Ahmad, Q. N. Naveed, and N. Hoda, "Strategy and procedures for Migration to the Cloud Computing," *2018 IEEE 5th International Conference on Engineering Technologies and Applied Sciences, ICETAS*

2018, pp. 1-5, 2019, doi: 10.1109/ICETAS.2018.8629101

[21] D. S. Linthicum, "Cloud-Native Applications and Cloud Migration: The Good, the Bad, and the Points between," *IEEE Cloud Computing*, Vol. 4, No. 5, pp. 12-14, 2017, doi: 10.1109/MCC.2017.4250932

[22] J. vom Brocke and J. Mendling, "Frameworks for Business Process Management: A Taxonomy for Business Process Management Cases," pp. 1-17, 2018, doi: 10.1007/978-3-319-58307-5_1

Design Modifications and Thermal Analysis of Visco-Dampers for Extending Silicone Oil Durability

Márk Venczel[1], Michael Steidl[2], Árpád Veress[1,3]

[1]Budapest University of Technology and Economics, Faculty of Transportation Engineering and Vehicle Engineering, Department of Aeronautics and Naval Architecture, Műegyetem rkp. 3, H-1111 Budapest, Hungary
e-mail: mvenczel@vrht.bme.hu
[2]Hasse und Wrede, Georg-Knorr-Straße 4, 12681 Berlin, Germany
e-mail: Michael.Steidl@hassewrede.de
[3]Knorr-Bremse R&D Center Budapest, Engineering Calculations, Major u. 69, H-1119 Budapest, Hungary
e-mail: Arpad.Veress@knorr-bremse.com

Abstract: The application of torsional vibration dampers is reasonable in every internal combustion engine with high performance output, where the unbalanced gas and inertial forces cause harmful torsional oscillations on the crankshaft. These oscillations can lead to the fatigue and damage of engine components. A visco-damper is a type of torsional vibration damper. Temperature represents one of the highest effects, on the lifetime of its operational fluid, in this case, silicone oil. Design solutions are proposed and realized for increasing cooling capabilities and the durability of the silicone oil. The heat transfer processes inside and outside of the damper are determined by coupled fluid dynamics and heat transfer simulations. The plausibility of the results is confirmed by using a modified version of the Iwamoto equation. A temperature-based lifetime prediction method has been used for determining the lifespan of the synthetic damping medium. The proposed geometrical modifications, decrease the level of the temperature distributions and thereby, improve the durability of the silicone oil.

Keywords: torsional vibration damper; silicone oil; design modifications; thermal and life-time management; CFD

1 Introduction

Nowadays, the Transportation and Vehicle industry are some of the most dynamically evolving sectors; significant amounts of research is going on, not only in the area of e-mobility – including autonomous driving [1] – and traffic safety [2] but in the field of structural mechanics, as well, to provide longer

lifetimes and higher levels of reliability and availability for vehicle systems and components in present and future.

Amongst the many different structural parts, torsional vibration dampers are found in the piston engines with the aim of damping torsional vibration of the crankshaft. Torsional vibration dampers are widespread from maritime applications through sports cars to heavy-duty vehicles due to their simple construction, high degree of reliability and relatively long lifetime. Considering the development trends in the field of internal combustion engines (ICE), they would eventually become smaller with a requirement for higher power output leading to an increase in the load on torsional vibration dampers in the future. Due to this evolution, there is a certain need for accurate methodologies and analyses to simulate the damper's function, as well as the lifespan influencing factors to be able to design the most suitable damper for any type of engine application. This is especially important for viscous torsional vibration dampers or shortly visco-dampers, which use silicone oil as operational fluid. The temperature is one of the most dominant factors for influencing its durability. Conducting thermal analysis on the silicone film situated inside the visco-damper poses a challenge as there are no practical and real time reliable techniques available so far. However, numerical methods – catering to the complex geometry and multidisciplinary physics – provide a plausible range of thermal distribution and can be replicated for various designs and their modifications.

This article provides an insight into the research and development process of visco-dampers, utilizing the relationship between the temperature of the silicone oil during operation and its effect on service life. Two different visco-damper geometries are considered in the presented analysis, both being in their early design phase.

1.1 Torsional Vibration Dampers

According to Figure 1, as the fuel burns in the piston cylinders of an ICE (1), thermal energy is released and converted into mechanical load (torque) by connecting rods (2) on the crankshaft (3). The continuous repetition of momentary angular acceleration (determined by the ignition and injection sequence) causes irregular and periodic oscillations on the shaft and significant mechanical stresses in the drivetrain. These oscillations are responsible for noise, higher stresses and ultimately, engine failure. Fatigue occurs when the frequency of the oscillation corresponds to the natural frequency of the crankshaft and driven components. [3] [4]

To prevent this failure and reduce the amplitude of vibration, a torsional vibration damper (4) can be mounted onto the free-end of the crankshaft or integrated into the flywheel (5). Several types of torsional vibration damper are available such as frictional, spring, rubber and viscous [3].

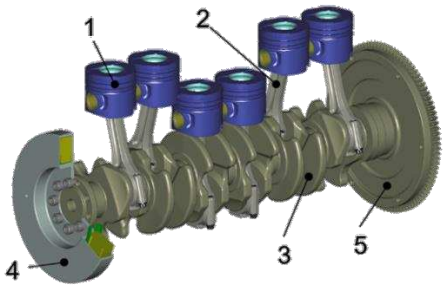

Figure 1
Torsional vibration damper mounted on the free-end of crankshaft [3]

Visco-dampers are some of the simplest devices, in damping technology. They consist of a closed annular space, called a housing, with a freely moving inertia ring within it as seen in Figure 2 (left). The inertia ring is guided by polymer slide bearings and surrounded by a thin film of damping medium. Regarding the operation of the device, the damping effect can be explained as follow. In the case of undisturbed rotation of the crankshaft without superposed oscillations, the inertia ring rotates together with the housing without any slip. With the onset of torsional oscillations, a relative motion between the housing and the ring occurs, which causes tangential shear stress in the damping medium. The damping effect is the sum of the shear stresses developing on the friction surfaces between the housing and the ring. Silicone oil is a non-Newtonian fluid and it has a different response to external forces compared to other conventional (Newtonian) fluids. Because of this characteristic, the relative velocity between the housing and the inertia ring influences the viscosity and thus the damping characteristics of the oil. During operation, the damping fluid is exposed to high thermal load originating from the friction and shear of the oil layer and from the engine and surrounding air as heat sources. The viscosity of the silicone oil varies with the change in temperature, thus cooling fin plates may be mounted onto the housing or onto the cover in one or two rows (see Figure 2 (right)) to keep the operational temperature within the designed range. [3] [5]

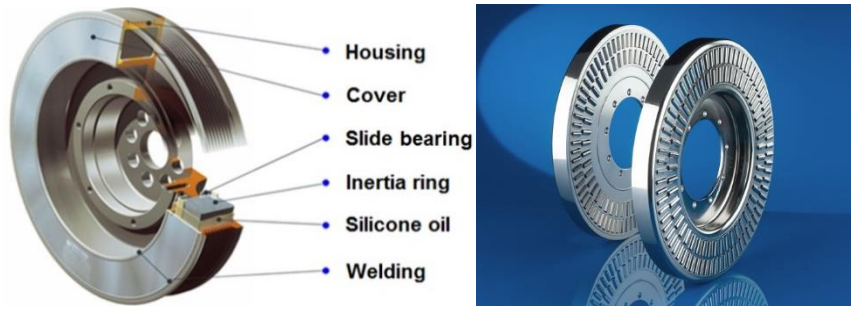

Figure 2
Structure of a visco-damper (left) [3] and cooling fins in two rows on the damper (right) [6]

There has been much research in conjunction with torsional vibration dampers in recent times. Homik [7] investigated the torsional and longitudinal vibrations of crankshafts of vessels and discussed the possibilities for vibration damping thoroughly. The characteristics of shaft amplitudes for rubber and viscous type of torsional vibration damper were analyzed and compared through resonance measurements.

Do-Kwan et al. [8] in their study provided an insight into the multidisciplinary design process of vibration dampers, in which a visco-damper for high performance crankshaft system of a transporting machine was developed by using reverse engineering, structural stability analysis and manufacturing techniques. Several prototypes were made with inertia rings of different sizes and masses and profound performance tests were conducted.

Damping properties play an important role in the determination of dynamic response of a crankshaft and a visco-damper however, these damping parameters are very scarce and cannot be deduced deterministically from other structural properties. Thus, experiments must be conducted on complete devices of similar characteristics. One such parameter is the damping coefficient. In the work of Navale et al. [9] a test rig was developed to find out the damping coefficient of a viscous damper. The verification of the experimental results was performed by comparing them with analytical results. The damping coefficient (obtained from the test setup) can be used to check the quality and the usage of a damper with ease.

A different type of torsional vibration damper – known as magnetorheological damper – has been recently investigated. This damper is filled with magnetorheological fluid (MRF), which is controlled by a magnetic field generated by an electromagnet. As the intensity of the electromagnet increases, the viscosity of fluid changes (increases) as well. Ehab et al. [10] developed a hybrid torsional vibration damper incorporating conventional centrifugal pendulum absorber and magnetorheological damper and demonstrated the superior performance of the proposed design. More details can be found about MRF technology for visco-dampers in Anant et al.'s work [11].

1.2 Silicone Oils for Torsional Vibration Damping

Silicone oils belong to the silicon-based lubricants and include every type of polymerized liquid siloxane, in which the molecules contain organic side chains. [12] Polydimethylsiloxane (PDMS) is a special type of silicone oil, which is one of the most suitable materials for visco-dampers due to its favorable tensile strength, density and low friction properties. It mitigates efficiently the unwanted oscillations in a wide frequency range. Its chemical formula is $(H_3C)_3[Si(CH_3)_2O]_uSi(CH_3)_3$ where u is the number of repeating monomer units. The higher this number, the higher is the viscosity of the oil sample. [13]

Today, the viscous behavior of the silicone oils has been well studied and is relatively well understood. Czirják and Kőkuti [14] [15] made efforts to describe the non-linear viscoelasticity and thixotropy of silicone oils in mathematical way and they created different rheological models for research and development purpose.

Several scientific researches deal with thermal and material stability, improvements and the response of PDMS molecular structure to high temperature. As it turned out from the study of Camino et al. [16] [17], thermal volatilization and weight loss of PDMS oil occurs during a molecular mechanism at lower temperature with formation of cyclic oligomers through Si-O backbone scission. This kind of decomposition of the investigated material is directly proportional to the rate of heat increase that takes place and is determined by the diffusion and evaporation of produced oligomers following first order Arrhenius behavior and having activation energy of ~ 27 kcal mol^{-1}. At higher temperatures, a radical mechanism occurs through homolytic Si-CH_3 bond scission followed by hydrogen abstraction and leads to the formation of methane. The flexibility of PDMS chain is reduced by the cross-linking of macro-radical groups and further splitting of cyclic oligomers is restricted. The oxidative cross-linking and the reorganization of split bonds improve the thermal stability of the material and produces ceramic silicon-oxycarbide.

Different methods were developed to improve the thermal stability and resistance of PDMS. Dongzhi et al. [18] for example described a way to enhance the properties by preparation of PDMS composites using polyvinyl silsesquioxanes (PVS) as reinforcing agent by hydrolytic condensation in the presence of organotin catalyst. Experimental results show that the thermal and mechanical properties of the novel composites were improved greatly by adding PVS and their resistance to thermal oxidation in nitrogen, increased as well. However, no differences, in the case of the air environment, were observed.

For damping applications, there are some uncertainties in the preliminary design phase of visco-dampers related to operation such as the rate of change of viscosity of PDMS oil in the damper, heat generated and dissipated, damping performance and the temperature distribution. In Wang et al.'s report [19] an engine-damper matching calculation method is introduced based on the heat equilibrium. The accuracy and the validation of the implemented calculation process were demonstrated by measurement results on a real diesel engine equipped with an operational visco-damper.

The present introductory chapter primarily dealt with an overview about the types, the structures and the general operation of torsional vibration dampers with a special focus on visco-ones. Background on the damping medium (in our case, silicone oil), the general effects of temperature change and the continuous research and development on increasing the operational temperature range were also discussed. However, in case of extreme operational conditions, where power

dissipation and the ambient temperature both are high, a special design methodology is required to limit the oil temperature to tolerable values. Hence, a computational fluid dynamics-based (CFD) methodology has been introduced during the design phase of torsional visco-dampers to control the thermal degradation process and thus the service life of silicone oil.

1.3 Iwamoto Equation for Temperature Estimation

A half empirical analytical expression, developed by Shoichi Iwamoto, is applied for preliminary thermal analysis of viscous torsional vibration dampers to estimate the outer surface temperature of the damper housing under operation.

A modified version of the original Iwamoto Eq. (1.1) [5] is considered in the present case. The calculated value by the equation will be used in the plausibility analysis of the CFD results. The circumferentially averaged temperature distribution of the case will be compared with the results of the numerical analyses described in the forthcoming part of the article and conclusions are going to be drawn about the reliability of the analyses.

$$T_{case} = \frac{Q_{damp} - c \cdot A_{ring}}{d \cdot \left(-g \cdot \frac{D_0}{D_{ring}} + h\right) \cdot n_{case}^{k} \cdot (p \cdot A_{ring})^{r}} + T_{ambient} \tag{1.1}$$

The parameters in Eq. (1.1) are next:

Q_{damp} is damping performance which converts into heat [W]; A_{ring} is inertia ring wetted surface [m^2]; n is crankshaft rotational speed [RPM]; D_0 is damper outer diameter [m]; D_{ring} is inertia ring inner diameter [m]; $T_{ambient}$ is ambient temperature [K]; c, d, g, h, k, p, r are Iwamoto parameters [-].

2 Degradation of Silicone Oil

The best method for monitoring the degradation of the silicone oil is determining the viscosity change. The viscosity is one of the most important properties of the damping media; it describes the degree of internal friction among the fluid layers, which in turn result energy loss.

Based on static degradation measurements, the viscosity and the lifespan of PDMS oil depend strongly on the operational temperature. The following technical factors can be considered to influence the operation of a torsional visco-damper: [20]

- Type of silicone oil (initial viscosity)
- Speed of rotation (damping performance)
- Gap-sizes between the housing and the inertia ring (gap-size investigation)

- Positioning of the cooling fins (cooling fin mounting investigation)

This paper investigates the effect of different gap-sizes and the side-positions of the cooling fin geometries on thermal load and on the service life of PDMS oil. It also considers the material aspects integrated into the lifetime of the oil discussed below. A theoretical variable, called Degradation Factor (*DF*), is introduced for lifetime calculations. *DF* provides information about the rate of change of viscosity of a given silicone oil under continuous thermal load at constant operational temperature for one day as shown by Eq. (2.1) [20]

$$DF = \frac{\eta_0 - \eta_1}{\eta_0} \cdot 100 \tag{2.1}$$

where *DF* is the degradation factor [%/day]; η_0 is the initial dynamic viscosity [Pa s] and η_1 is the changed dynamic viscosity after one day [Pa s].

Since *DF* is the function of the temperature [20], the temperature distribution in the damper, especially in the silicone oil, must be determined to calculate the degradation factor of the PDMS oil. The maximum change in viscosity allowed $\Delta\eta_{allowed}$ [%] can be calculated by Eq. 2.2 by using the values of the initial viscosity η_0 [Pa s] and the minimum allowed viscosity $\eta_{\min}$ [Pa s].

$$\Delta\eta_{allowed} = \frac{\eta_0 - \eta_{\min}}{\eta_0} \cdot 100 \tag{2.2}$$

As the degradation (considering in the range from the oil's initial state to the allowable degree of degradation state) is linear function of time, dividing the maximum change in viscosity allowed $\Delta\eta_{allowed}$ [%] by DF [%/day] will provide the service life $t_{service}$ [day] of the fluid as presented in Eq. 2.3.

$$t_{service} = \frac{\Delta\eta_{allowed}}{DF} \tag{2.3}$$

3 Design Methodologies, Numerical Analyses and Silicone Oil Durability

The enhancement of effectiveness in the vehicle industry is a general expectation, there are several innovative researches in this field [21] [22]. In the last decade, the attention of product development is focused more on technical modelling and simulation activity including CFD, which are becoming an essential part and a powerful tool for design, development and researches as it is shown by [23] and [24].

Bicsák et al. [25] used CFD techniques to introduce a minimum requirement demanding method for investigating the effect of an aircraft propeller in low Mach number flow regime. The results of Actuator Disk Method (ADM) with induced velocities and total pressure were compared to a reference solution generated by Rotating Domain Model (RDM). It turned out from the numerical investigation

that ADM with total pressure boundary condition provides acceptably close results to RDM solution. In terms of computational time, ADM with total pressure boundary condition required less time by 95% to provide converged simulation results compared to RDM simulation.

Kátai et al. [26] performed CFD analysis on a novel mobile refrigerated container. The cooling air velocity distribution in empty and fully loaded cases was investigated while the shape of inlet air profile and the necessity of auxiliary ventilator installation were also tested. The outcome of the CFD calculation was supported by hydrodynamic experimental small-scale test. Both the CFD calculation and the experimental model proved the fact, that the original container design is not suitable for proper cooling due to the lack of generated air circulation. By applying multijet technology with auxiliary fans installed on bottom of the partition wall and directed evaporator blow-out, the quality of cooling can be improved.

CFD is an appropriate tool not only for investigating flow characteristics but to understand the combustion phenomena and pollution composition of an ICE as well. Akbarian et al. studied in their work [27] the effect of fuel combination (natural gas and diesel fuel) on the performance and emissions of a dual-fueled engine under constant speed with different loads. According to the results, the dual-fueled mode of the engine causes lower CO2, NOx and particle materials (PM) emission under all load conditions compared to the diesel mode. The authors suggest to use the engine in the dual mode at 30% and 50% of the pilot fuel (diesel) ratio in full and half loads respectively for significant reduction in emission and fuel consumption.

Fabio et al. [28] used CFD method for proposing and testing an alternative wall function model to calculate more reliable heat fluxes on the wall of high-performance spark ignition engines. Four currently produced and direct injection spark ignition turbocharged engines had been selected with different operating conditions for heat transfer model improvement purpose. Experimental engine thermal survey and point-wise temperature measurement data were used to validate their developed wall heat transfer model.

CFD enables also damper developers to better understand the complex fluid flow and the detailed thermal distribution inside a visco-damper during operation. ANSYS CFX commercial code has been used in this work for numerical modelling and analysis. The general conservation law for mass, momentum and energy are discretized into a system of algebraic equations. Time discretization is achieved by ‘First or Second Order Implicit Backward Euler’ scheme, which solves a multidimensional nonlinear algebraic equation in each iteration. The discretized system of algebraic equations is then determined numerically over the predefined control volumes through iteration steps with the ‘Multigrid Accelerated Incomplete Lower Upper Factorization’ technique to render the solution field. [29]

3.1 Geometry – Design Modifications for Lifetime Extension

As discussed in Chapter 2, the service life of silicone oil is heavily dependent on the temperature. The goal of the visco-damper developments is to design appropriate geometry in such a way that the operational temperature remains in favorable range, prolonging the lifetime of the lubricant. The temperature distribution of the oil can be influenced either by properly selected gap-sizes, which determine the amount of fluid and the film thickness between the moving components (housing and inertia ring) and by application of advanced cooling fin plates on the outer surface of the damper (either the housing or the cover side). The goal of the present investigation is to decide, whether the smaller gap-sizes improve or degrade the service life of the silicone oil and which side of the housing is suitable for mounting the cooling fin plate to hold the temperature of the visco-damper at a lower degree.

In terms of gap-sizes, the axial (X) and radial (Y) gap-sizes of the initial model (INIT1) are shown in Figure 3 (left). Besides keeping the design specifications, the operational temperature can be affected by the gap-sizes as the heat is generated in the silicone oil due to the dissipated energy and spread to the environment by heat transfer. The reduction of the distance between the inertia ring and housing (if the expected wet lubrication of surfaces is ensured) allows less amount of fluid stored in the damper and makes the oil film thinner. In case of the modified damper geometry (MOD1) (see Figure 3 (left)) the axial gap size (X) is reduced by 18.6% and the radial gap-size (Y) is decreased by 12.5% thus the amount of stored oil in the damper is reduced by 9.6%. Due to this modification, the oil content inside the damper is expected to store less amount of heat and keep the inner components at a comparatively lower temperature.

As far as cooling fin mounting is concerned, several cooling fin designs were tested previously, and it turned out that not the shape but the length, the height and the mounting position of the fins have a significant effect on the heat transfer process and thus on the cooling efficiency. [5] The initial model (INIT2) for mounting investigation with ‘tunnel type’ cooling fins assembled on the engine-side is shown in Figure 3 (right). In this case the gap-sizes remain unchanged. Considering the proximity of the engine and the heat transfer characteristics of the cooling fins, it would be advisable to relocate the fin plate onto the other side (free-side) of the damper housing.

As the damper rotates together with the engine crankshaft, free-stream of ambient air cools the fins more efficiently and more amount of heat can be discharged from the fins compared to the engine-side of the housing where the air close to the fins is rather stagnated with limited ventilation. Figure 3 (right) also shows the modified cooling fin mounting model (MOD2) for CFD investigation.

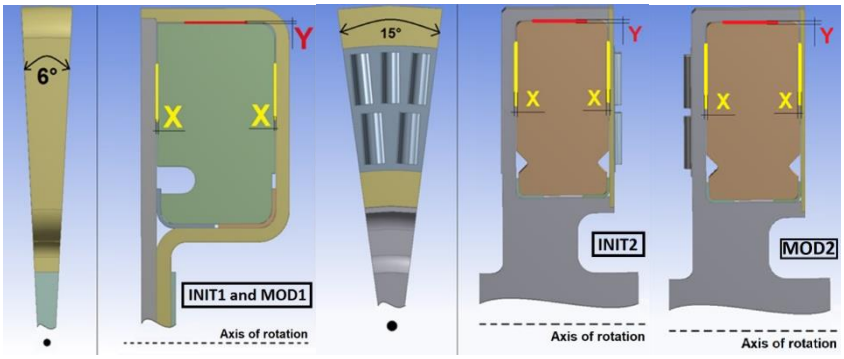

Figure 3
Initial and modified geometries for gap-size (left) and for mounting investigation (right)

To reduce the calculation time but maintain the accuracy of the results, only a sector of the whole damper-shaft-engine geometry is investigated considering the rotational periodicity. In case of gap-size simulations (INIT1 and MOD1) the investigated sector angle is $\beta_1 = 6°$ while in case of cooling fin mounting simulations (INIT2 and MOD2) a sector angle of $\beta_2 = 15°$ is considered. The greater β_2 provides enough width for fulfilling the periodicity conditions for the flow field including fins.

The geometries are prepared by Creo Parametric. The simplified geometries with the crankshaft, engine and flow fields are finalized in Ansys "Design Modeler" submodule. The slide bearings are removed since their effect on the oil has already been considered in the lifetime analysis. The housing and cover are merged (called case or casing in the following subchapters) because they are made of the same material and welded. The boundaries of the ambient are set far away from the investigated damper-shaft-engine system to protect it from the flow-disturbing effects of the structure.

3.2 Numerical Mesh

Generating mesh is the crucial part of numerical calculations. The smaller the mesh size, the more accurate the results would be, resulting in, however, a longer calculation time. Results can also be influenced by properly selecting and creating mesh elements. Hence, mesh size sensitivity and quality analysis has been completed to find the most suitable mesh configurations, keeping in mind the accuracy (maximum acceptable skewness, aspect ratio, etc.), the optimum cell number (for resolving heat transfer processes) and effort needed for mesh generation.

As denser mesh at the wall (or inflation layer) has a prominent role in modelling heat transfer processes accurately, preliminary calculations for Reynolds number, dynamic and kinematic viscosity, shear velocity, wall shear stress, skin friction

coefficient, first cell height and the boundary layer thickness are determined and used as described in [30].

The final mesh, in case of INIT1 and MOD1, is built up from approximately 11 million elements, whereas, in the case of INIT2 and MOD2 (see Figure 4), the cell number is approximately 15 million. In each case the y+ (dimensionless distance from the wall) is less than 1 and the boundary layer is split up to 15 sublayers, resulting in the CFD software using „Near-Wall Model Approach" technique. In this approximation, the discretized form of the transport equations is solved directly till the wall and provide more accurate results unlike using logarithmic-based wall functions.

The surrounding of cooling fin plate is called fin-zone, where a finer mesh must be used to take full advantage of the wall resolving approach. This region of air moves together with the fin plate and forms a transition between the static ambient domain and the rotating fins.

3.3 Boundary Conditions and Program Settings

After importing the final mesh into Ansys CFX submodule, the next step is defining material properties, boundary conditions and solver settings.

Silicone oil and air gap (rotating volumes) in the damper are modelled as solid domains (with density, viscosity, specific heat, thermal conductivity and considering energy conservation law) for two reasons. On the one hand, the effect

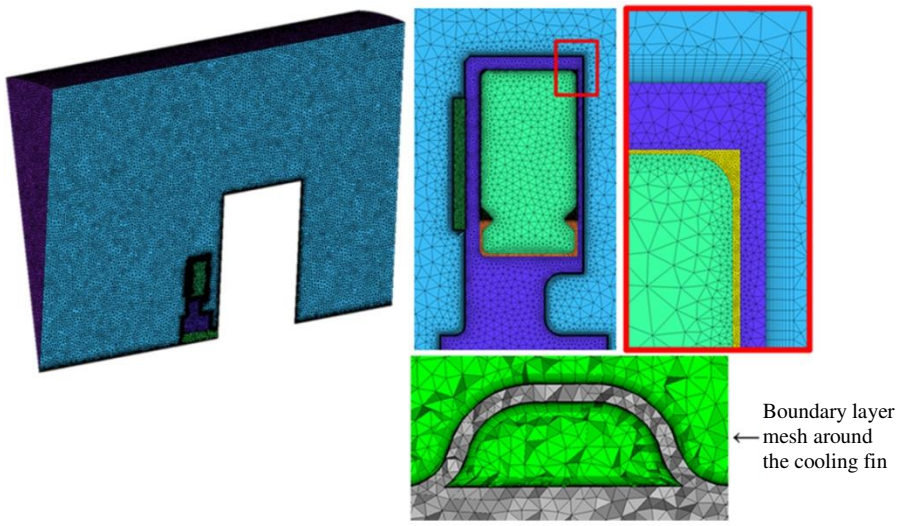

Figure 4
Numerical mesh (MOD2) with inflation layers for mounting investigation

of heat convection is negligible due to the rather stiff silicone oil at an elevated centrifugal force, thus heat can only be conducted as in a solid domain. On the other hand, calculating solid domain requires a shorter calculation time if the scope of the simulation is to determine the temperature distribution inside the damper. Shaft, case and ring (rotating solid domains) are defined with density, specific heat, thermal conductivity and with considering energy conservation law also. Ambient (stationary domain) and fin-zone (rotating domain) are set to flow domain with SST turbulence modelling, automatic wall function and with considering total energy conservation law. The applied material properties are found in Table 1.

Table 1
Materials and parameters used in the simulations

Material	Air	Silicone fluid	Steel components
Density [kg/m^3]	1.185	973	7854
Specific heat capacity [J/kg/K]	1004.4	550	434
Thermal conductivity [W/m/K]	0.0261	0.15	60.5

1500 RPM speed has been applied at silicone oil gap-size investigation and 1900 RPM is considered at cooling fin mounting investigation for the rotating domains.

The heat source (defined on the oil domain segment) is calculated by Eq. (3.1).

$$Q_V = \frac{Q_{damp}}{V^{oil} \cdot \frac{360°}{\beta}} \tag{3.1}$$

where Q_V is oil segment heat source [W/m^3]; Q_{damp} is damping performance [W]; V^{oil} is oil segment volume [m^3]; β is investigated sector angle [deg].

2000 W damping performance is considered at silicone oil gap-size investigation and 1000 W is at cooling fin mounting investigation.

Interface connections are defined between the adjacent surfaces of the relevant domains as follows. Each domain connecting with itself circumferentially has rotational periodicity interface; there is a heat resistance free contact between case and shaft; fin-zone has a rotating wall interface at the connection with ambient air while the shaft and case are in a rotating solid wall interface connection with the ambient air. Finally, perfect heat transfer interface is defined between fin-zone and case, oil and case, air gap and case, air gap and oil, oil and ring, and air gap and ring. These connections are shown in Figure 5 (right) for cooling fin mounting investigation.

The boundary conditions for cooling fin geometry investigation case are presented in Figure 5 (left). The ambient domain contains stationary walls (next to the surfaces of the engine with a constant temperature) and rotating walls (next to the surfaces of the damper, the fin-zone and the shaft). The far field surfaces of the

ambient domain are set to be Opening (Entrainment) with constant static temperature 50° C, relative static pressure 0 bar and „Opening pressure and Direction" option.

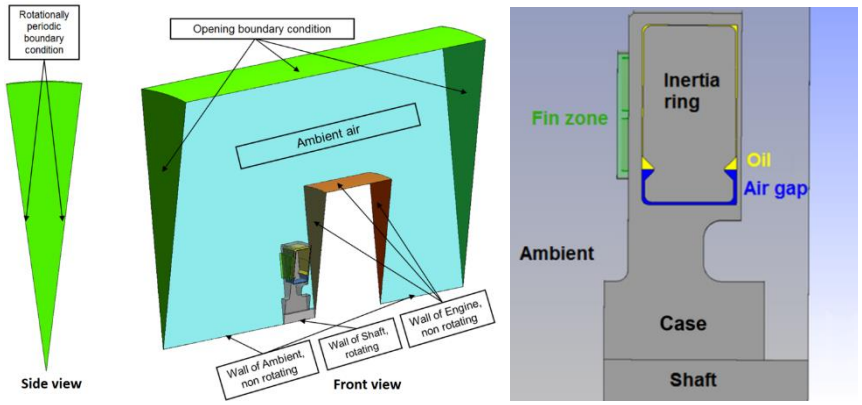

Figure 5
Boundary conditions (left) and interface connections (right) for mounting investigation

The turbulent intensity is set to be medium (5%). Nine monitoring points (in the function of radius) are defined on the casing to monitor the convergence of temperature and the area-averaged temperature during the numerical calculation. The last step is the solver settings in the software setup. 'High resolution' advection scheme is used, while turbulence numeric is defined to be 'First order'. The number of maximum allowed iteration steps is 5000.

Timescale control is specified by a timescale factor of 30 for fluid domains and 10 for solid domains. Convergence criteria are given by the residual target of RMS 10^{-6} and the conservation target of imbalances is 1%.

3.4 Evaluation of Numerical Results

3.4.1 Gap-Size Investigation

Figure 6 shows the convergence curves of temperatures at different monitoring points in case of INIT1 analysis. The graph proves the convergence; the constant temperatures are reached after 2500 iterations for INIT1. The convergence-increase around 1800th iteration can be explained by the fact that the time scale factor in the solver has been changed to improve convergence and reduce the calculation time. The convergence is also reached for the MOD1 simulation after 1000 iterations. MOD1 simulation needed less iteration steps to reach convergence because of the fact, that the calculation has been initialized from the converged results of INIT1 simulation. In each analysis results the residuum reached the residual 10^{-4} and each imbalance goes below 1% conservation target at the end of the calculation.

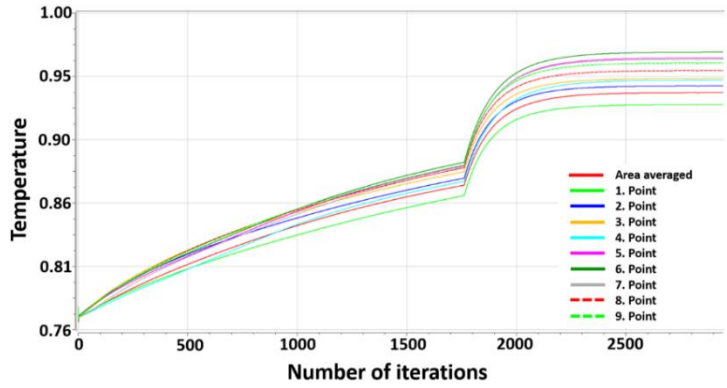

Figure 6

Temperature convergence of INIT1 analysis at gap-size investigation

Figure 7 shows the normalized temperature distribution in the dampers (on the left) and the heat flux on the outer side of the case (on the right) for INIT1 and MOD1. The outside area-averaged temperature of the case shows 1.7% difference from the pre-calculated value by Eq. (1.1) at the same conditions, thus the presented simulation results are plausible, and the simulation is suitable for further engineering purpose. The location of the heat source and a stagnant flow region of air between the engine and the damper can be identified in the left side of the figure. This latter region has poor cooling efficiency; the average temperature here is higher than the ambient temperature by 11.7%. That can be proven also by the intensity of heat transfer on the outer side of the case (see Figure 7 (right)). It turns out that the pattern of cooling intensities shows similarities for both geometries and they are the function of radius.

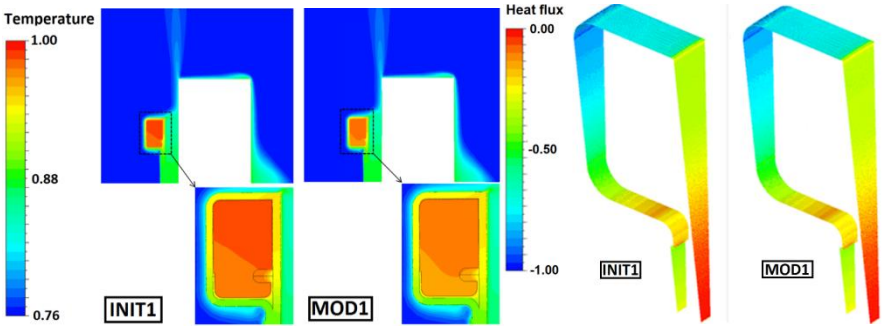

Figure 7

Normalized temperature distribution (left) and heat flux of the case (right) at gap-size investigation

Figure 8 shows the temperature distribution in the oil region for INIT1 (on the left) and for MOD1 (on the right) geometries. There is a difference on the inner side of the oil rings. In case of MOD1 geometry, the temperature is lower, and the peak temperature of the oil is less by 1% compared to the baseline geometry.

The temperature values of both oil domains have been exported and a *DF* value has been calculated for each exported temperature based on [20]. After averaging the gained *DF* values in both oil domains, the lifetime for each investigated case has been determined by Eq. 2.3. The results present that the suggested gap-size modification (corresponds to less amount of oil by 9.6%) causes a lifetime increment by 25.8% compared to the initial geometry (INIT1) on average.

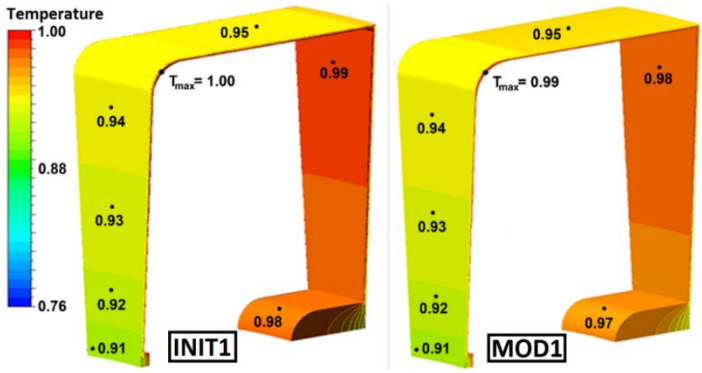

Figure 8
Temperature distribution in the oil rings at gap-size investigation

3.4.2 Cooling Fin Mounting Investigation

INIT2 and MOD2 simulations provided similar convergence curves to Figure 6. The calculation is converged for INIT2 when the constant temperatures are reached after 5000 and for MOD2 after 1400 iterations respectively. In both calculations the residuum reached 10^{-4} and each imbalance goes below 1% target at the end of the iteration steps.

Figure 9 shows the temperature distribution in the dampers (on the left) and the heat fluxes on the outer side of the case (on the right) for INIT2 and MOD2 variants. The outside area-averaged temperature of the case shows 2.6% difference from the pre-calculated value by Eq. (1.1), so the presented simulation results are suitable from plausibility point of view. The heat generation domain and the stagnant flow conditions between the damper and the engine are well visible also in the figure. Here, in this enclosed zone, the flow temperature is higher by 7.1% in average compared to the ambient temperature. The cooling fins show a poor cooling efficiency when they are mounted on the engine side. This can also be seen by the intensity of heat transfer on the outer side of the case (see Figure 9 (right)). The temperature varies along the radius of the case, from higher (near the center) to lower on the periphery, and hence, the cooling intensity can be determined to be a function of the radius of the case also. With the cooling fins mounted on the free side of the case, the overall temperature observed is lower as compared to when the cooling fins are situated on the engine side, so this variant has higher cooling efficiency.

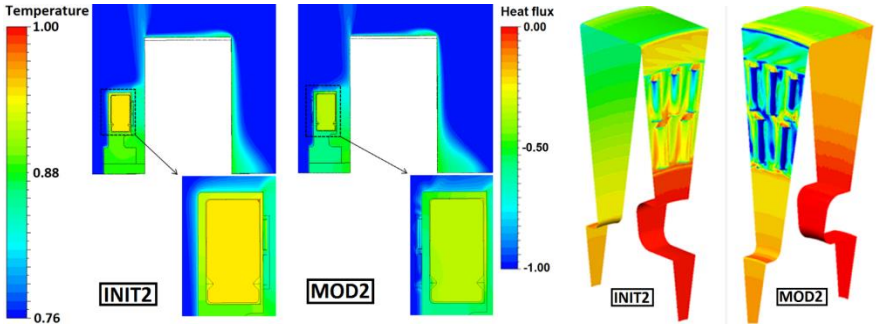

Figure 9

Normalized temperature distribution (left) and heat flux of the case (right) at cooling fin mounting investigation

Figure 10 shows the temperature distribution in the oil segment for INIT2 (on the left) and for MOD2 (on the right) geometries. There is a significant difference both on the outer and inner sides of the oil regions. In case of MOD2, not only the peak temperature of the oil is lower but the temperature distribution throughout the oil region is less compared to INIT2. Similarly, to the gap-size investigation case, the temperature values of both oil domains were exported and lifetime calculations were performed based on [20] with help of Eq. 2.3. It turned out that the suggested cooling fin mounting modification (MOD2) causes a lifetime increment of 133.2% in comparison with the initial geometry (INIT2).

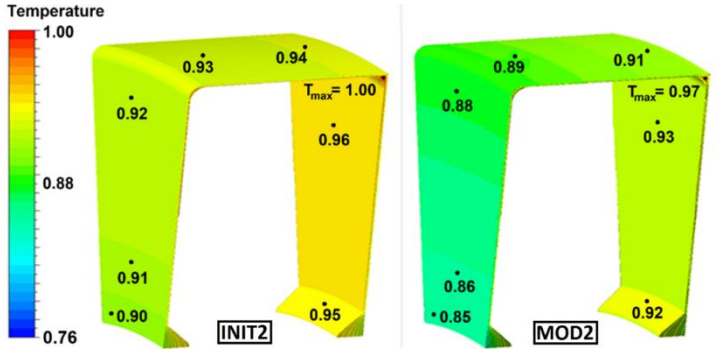

Figure 10

Normalized temperature distributions in the oil rings at cooling fin mounting investigation

Conclusions

Viscous torsional vibration dampers are essential accessories of high performance and/or downsized piston engines and are exposed to complex mechanical, thermal and chemical loads, within their componentry. The lifespan of visco-dampers is influenced, primarily, by the usage of its working medium, which is strongly affected by the operational temperature. Hence, it is always necessary, in the

preliminary design phase, to properly estimate and control the oil temperature for slowing down the thermal degradation process. Analytical and numerical methods have been used in this work to determine the temperature distribution and its plausibility. Design modifications have been suggested and thoroughly analyzed, by coupled fluid dynamic and heat transfer simulations, to check their effect on the temperature and service life of the damping medium.

The influence of gap-sizes and positioning of the mounted cooling fins on the lifespan of the silicone oil, has been brought to light, with the help of CFD simulations. MOD1 geometry with smaller gap-sizes and lesser quantity of silicone oil by 9.6% provides longer lifespan by 25.8% compared to the original INIT1 geometry. The MOD2 geometry places the cooling fins on the free side, away from the engine, providing a lower temperature level and a lifetime is 2.33 times longer as compared to the INIT2 geometry.

The visco-damper technology depends strongly on the degradation properties of the silicone oil. Thus, the improvement of recently applied lifetime estimation method, is indispensable for increasing accuracy. Hence, the next step within the framework of the present study, is to update the available lifetime prediction method, by means of completing further degradation measurements, at lower operational temperatures. Future simulations are planned, including validation under different operational conditions, including advanced cooling fin geometries, to better understand and improve thermal behavior and therefore, the durability.

Acknowledgement

This work was supported by the Pro Progressio Foundation. We would like to express our special thanks to Sándor Kovács and Gábor Rácz from the Engineering Calculations Team at Knorr-Bremse R&D Center Budapest for their technical support in CFD. We would like to show appreciation to Mr. Shayan Asim at Hasse und Wrede GmbH in Berlin for his valuable help in revision and improvements the quality of the paper.

References

[1] Szalay, Zs., Tettamanti, T., Esztergár-Kiss, D., Varga, I. and Bartolini, C.: Development of a Test Track for Driverless Cars: Vehicle Design, Track Configuration, and Liability Considerations, Periodica Polytechnica Transportation Engineering, 46:(1), pp. 29-35, 2017, DOI: https://doi.org/10.3311/PPtr.10753

[2] Sándor, Z.: Effects of Weather Related Safety Messages on the Motorway Traffic Parameters, Periodica Polytechnica Transportation Engineering, 45:(2), pp. 58-66, 2017, DOI: https://doi.org/10.3311/PPtr.9117

[3] Érsek, P.: Numerische Untersuchung der Auffüllung eines Torsiondämpfers mit Silikonöl, Knorr-Bremse R&D Center Budapest, Technische und Wirtshaftwissenschaftliche Universität Budapest, Lehrstuhl für Hydrodynamische Systeme, Diplomarbeit, Budapest, 2008

[4] http://www.lezo.hu/szerkezettan/hajtas/motor/szerkezet/forgattyustengely/forgattyus-tengely.html (Accessed: 23.08.2017)

[5] Hafner, K. E., Maass, H.: Torsionsschwingungen in der Verbrennungskraftmaschine, Die Verbrennungskraftmaschine, Neue Folge, Band 4, Springer-Verlag Wien-New York, pp. 392, 1985

[6] http://www.hassewrede.de/media/pictures/produkte/vd_r6_nfz_510ps.jpg (Accessed: 23.08.2017)

[7] Homik, W.: Torsional vibration silencers used in vessels propulsion systems, Scientific Journals, 40:(112), pp. 9-16, 2014, ISSN 1733-8670

[8] Do-Kwan, H., Chan-Woo, A., Jae-Joon, S., Sang-Suk, L., Young-Duk, J.: Development and Experimental Performance Validation of Torsional Viscosity Damper for Crank Shaft System of Transporting Machine, International Journal of Precision Engineering and Manufacturing, 16:(7), pp. 1591-1597, 2015, DOI: https://doi.org/10.1007/s12541-015-0209-8

[9] Navale, V. R., Dr. Dhamejani, C. L.: Analysis of Damping Coefficient for Viscous Damper, International Journal of Innovations in Engineering Research and Technology, 2:(7), 2015, ISSN: 2394-3696

[10] Ehab, A., Rama, B., Ramin, S.: Development of a new torsional vibration damper incorporating conventional centrifugal pendulum absorber and magnetorheological damper, Journal of Intelligent Material Systems and Structures, 27:(7), pp. 980-992, 2015, DOI: https://doi.org/10.1177/1045389X15590275

[11] Anant, C., Nigam, S. P.: Magnetorheological Fluids in Viscous Friction Torsional Vibration Dampers, International Journal of Mechanical and Production Engineering, 3:(3), 2015, ISSN: 2320-2092

[12] https://en.wikipedia.org/wiki/Silicone_oil (Accessed: 23.08.2017)

[13] https://en.wikipedia.org/wiki/Polydimethylsiloxane (Accessed:23.08.2017)

[14] Kőkuti, Z., van Gruijthuijsen, K., Jenei, M., Tóth Molnár, G., Czirják, A., Kokavecz, J., Ailer, P., Palkovics, L., Völker, A. C., Szabó, G.: High-frequency rheology of a high viscosity silicone oil using diffusing wave spectroscopy, Applied Rheology, 24 (2014) 63984, 2014, DOI: http://doi.org/10.3933/ApplRheol-24-63984

[15] Kőkuti, Z., Völker-Pop, L., Brandstätter, M., Kokavecz, J., Ailer, P., Palkovics, L., Szabó, G., Czirják, A.: Exploring the nonlinear viscoelasticity of a high viscosity silicone oil with LAOS, Applied Rheology, 26 (2016) 14289, 2016, DOI: http://doi.org/10.3933/ApplRheol-26-14289

[16] Camino, G., Lomakin, S. M., Lazzari, M.: Polydimethylsiloxane Thermal Degradation Part 1, Kinetic Aspects, Polymer, 42:(2001), pp. 2395-2402, 2001, DOI: https://doi.org/10.1016/S0032-3861(00)00652-2

[17] Camino, G., Lomakin, S. M., Lazzari, M.: Polydimethylsiloxane Thermal Degradation Part 2, The Degradation Mechanism, Polymer, 43:(2002), pp. 2011-2015, 2002, DOI: https://doi.org/10.1016/S0032-3861(01)00785-6

[18] Dongzhi, C., Xiaoyun, H., Hongwei, Z., Xianze, Y., Yingshan, Z.: Preparation and Properties of Novel Polydimethylsiloxane Composites Using Polyvinylsilsesquioxanes as Reinforcing Agent, Polymer Degradation and Stability, 111, pp. 124-130, 2015, DOI: https://doi.org/10.1016/j.polymdegradstab.2014.10.026

[19] Wang, M., Zhou, R., Xu, X.: The Engine Silicone-oil Damper Matching Calculation Method Based on the Heat Balance, Research Journal of Applied Sciences, Engineering and Technology, 4:(16), pp. 2773-2777, 2012, ISSN: 2040-7467

[20] Érsek, P., Nagy, I., Kiss, Cs., Németh, H.: Silicone Oil Degradation Tests, Knorr-Bremse R&D Center Budapest, Internal Project Report, Budapest, 2014

[21] Bera, J., Pokorádi, L.: Monte-Carlo simulation of helicopter noise, Acta Polytechnica Hungarica, Vol. 12, No. 2, pp. 21-32, 2015

[22] Sziroczák, D., Jankovics, I., Gál, I., Rohács, D.: Conceptual design of small aircraft with hybrid-electric propulsion systems, Energy, Vol. 204, 2020, ISSN 0360-5442, https://doi.org/10.1016/j.energy.2020.117937

[23] Beneda, K.: Numerical Simulation of MEMS-based Blade Load Distribution Control in Centrifugal Compressor Surge Suppression, in ICNPAA 2012 Congress: Mathematical Problems in Engineering, Aerospace and Sciences, Vienna, Austria, 2012

[24] Beneda, K.: CFD Simulation of Blade Load Distribution Control as Active Centrifugal Compressor Surge Suppression, ACTA AVIONICA, Vol. 15, No. 25, pp. 13-20, 2013

[25] Bicsák, Gy., Veress, Á.: New Adaptation of Actuator Disc Method for Aircraft Propeller CFD Analyses, Acta Polytechnica Hungarica, 14:(6), pp. 95-114, 2017, DOI: https://doi.org/10.12700/APH.14.6.2017.6.6

[26] Kátai, L., Várszegi, T., Oldal I., Zsidai. L.: Hydrodynamic Modelling and Analysis of a New-Developed Mobile Refrigerated Container, Acta Polytechnica Hungarica, 13:(5), pp. 83-104, 2016, DOI: https://doi.org/10.12700/aph.13.5.2016.5.5

[27] Akbarian, E., Najafi, B., Jafari, M., Ardabili, S. F., Shamshirband, S., Chau, K. W.: Experimental and Computational Fluid Dynamics-Based Numerical Simulation of Using Natural Gas in a Dual-Fueled Diesel Engine, Engineering Applications of Computational Fluid Mechanics, 12:(1), pp. 517-534, 2018, DOI: https://doi.org/10.1080/19942060.2018.1472670

[28] Fabio, B., Giuseppe, C., Stefano, F.: A Modified Thermal Wall Function for the Estimation of Gas-To-Wall Heat Fluxes in CFD In-Cylinder Simulations of High Performance Spark-Ignition Engines, Applied Thermal Engineering, 115, pp. 1045-1062, 2017, DOI: https://doi.org/10.1016/j.applthermaleng.2017.01.055

[29] ANSYS, ANSYS CFX-Solver Theory Guide, Release 14.5, Southpointe, 275 Technology Drive, Canonsburg, PA 15317, 2012

[30] http://imechanica.org/files/fluent_13.0_lecture06-turbulence.pdf (Accessed: 17.09.2017)

Transforming Hierarchical Data Structures – a PSVDAG–SVDAG Conversion Algorithm

Branislav Madoš, Norbert Ádám

Department of Computers and Informatics, Faculty of Electrical Engineering and Informatics, Technical University of Košice, Letná 9/A, 042 00 Košice, Slovakia
e-mail: branislav.mados@tuke.sk, norbert.adam@tuke.sk

Abstract: This paper examines the issues of domain-specific hierarchical data structures, based on directed acyclic graphs, dedicated to the representation of the geometry of three-dimensional scenes. In this paper, the authors introduce two versions (out-of-core and semi-out-of-core) of an algorithm to transform hierarchical data structures – pointerless sparse voxel directed acyclic graphs, into sparse voxel directed acyclic graphs. Pointerless sparse voxel directed acyclic graphs are not suitable for immediate traversing, due to the absence of pointers to the child nodes; however, they are suitable for archiving and streaming, as they have a more compact binary-level representation. Sparse voxel directed acyclic graphs, on the other hand, allow quick traversing during visualization or other forms of processing, since their nodes include pointers to child nodes. The disadvantage of this, is that the binary-level representation, requires more operating memory or secondary storage space. Both hierarchical data structures – sparse voxel directed acyclic graphs and pointerless sparse voxel directed acyclic graphs – and both versions of the proposed conversion algorithm are described in the first part of the paper. Results of tests, performed on various models – previously surface polygonal models, stored in the Wavefront Technologies geometry definition file format (OBJ) – now voxelized to the respective resolutions, are summarized in the second part of the paper. The binary-level representation lengths of both data structures, along with the time consumption of both versions of the proposed conversion algorithms, are detailed in the last part of the paper.

Keywords: pointerless sparse voxel octrees; PSVO; sparse voxel octrees; SVO; pointerless sparse voxel directed acyclic graphs; PSVDAG; sparse voxel directed acyclic graphs; SVDAG; hierarchical data structures; volume dataset; three-dimensional image; lossless data compression

1 Introduction

Hierarchical data structures (HDS), based on the use of octant trees (octrees) and Directed Acyclic Graphs (DAGs), are popular solutions to represent the geometry of three-dimensional scenes, especially if the scenes are voxelized from three-dimensional polygonal surface models [1]. In voxelized scenes, the uncompressed

geometry is represented as a three-dimensional regular grid, using 1 b per voxel – active (filled) voxels are encoded as "1" bits and passive (empty) voxels are encoded as "0" bits. In such scenes, most voxels are passive (often, these represent 99.99% of all voxels, or even more).

Hierarchical data structures, based on octrees and directed acyclic graphs, can cope with this sparsity and use it in lossless data compression, and that is why they can store scene geometry using unprecedentedly small space. A compression level of 10^{-5} bits per voxel (b/vox) can be achieved in case of a 64 K^3 scene (65536 × 65536 × 65536 voxels), using 315.3 MB of space to store the particular scene geometry [2] [3]. In comparison, to store this geometry in its uncompressed form, as a regular three-dimensional grid of 1b/vox, one needs 256 TB of space. Another common feature of voxelized scenes based on polygonal surface models is the high probability of occurrence of identical subspaces. Hierarchical data structures use this feature to achieve lossless compression, via Common Subtree Merging (CSM). Applying this technique, octrees are transformed into DAGs.

There are octree-based hierarchical data structures allowing space-saving representation of the scene geometry without having any child node pointers encoded in their nodes – these are Pointerless Sparse Voxel Octrees (PSVOs). Pointerless hierarchical data structures are suitable for archiving and streaming purposes, but are less suitable for immediate traversing. Their disadvantage is that they don't allow using the CSM technique. Sparse Voxel Directed Acyclic Graphs (SVDAGs) include pointers for quick traversing and CSM. Pointers, though, require a significant amount of space in SVDAGs. However, the possibility to use CSM can outweigh this disadvantage. That is why, in total, SVDAGs can be more space-efficient, compared to PSVOs.

In our previous research, we developed Pointerless Sparse Voxel Directed Acyclic Graphs (PSVDAGs) [4] – hierarchical data structures incorporating advantages of both PSVOs and SVDAGs [5]. Due to pointerless encoding, this data structure saves space, and, due the concept of variable-length Labels/Callers, it allows the use of CSM. PSVDAGs can exceed the compression ratio of PSVOs and SVDAGs. However, the absence of pointers makes this data structure unsuitable for quick traversing. That is why the PSVDAG data structure incorporates a feature – active child node count (ACHNC) – allowing quick transformation into SVDAGs. In this paper, we propose and describe two versions of the conversion algorithm allowing the transformation of PSVDAGs into SVDAGs: an out-of-core and a semi-out-of-core version.

The contribution of the paper is in the following:

The design of two versions of the PSVDAG – SVDAG conversion algorithm: an out-of-core and a semi-out-of-core version.

Section 2, hereof summarizes the related works in the field of multi-dimensional data linearization, hierarchical data structures used to represent the geometry of

three-dimensional scenes and out-of-core algorithms for the creation of those data structures. Due to the vast number of papers published in the field, only closely related works are mentioned.

Section 3, provides a description of the SVDAG and PSVDAG hierarchical data structures, not only their formal description using the Backus-Naur Form, but also a brief explanation of their fundamental properties.

Section 4, is an introduction to the main contribution of the paper, i.e. the out-of-core and semi-out-of-core versions of the conversion algorithm that transforms PSVDAGs into SVDAGs.

Section 5, describes the results of the tests performed on various three-dimensional scenes, originally stored in the Wavefront Technologies geometry definition file format (OBJ), subsequently voxelized to the respective resolutions and then stored as PSVDAGs. Using the algorithm described in Section 4, the transformation of their representation from PSVDAG into SVDAG was tested.

Section 6, the last section of the paper, draws conclusions from the test results stated in the previous section of the paper.

2 Related Work

Due to the vast number of papers published in this field, this section lists only the closely related works.

Linearization of multi-dimensional data. Space-Filling Curves (SFC), introduced by Peano and Hilbert at the end of the 19th Century [6] [7], are used to linearize multi-dimensional data. Very popular in computer graphics is the Morton order [8]. Hilbert Space Filling-Curves (HSFCs) are used in computer science for better locality preserving [9]. Examples of linearization of a two-dimensional space using Morton order and Hilbert SFCs of levels 1 and 2 are depicted in Figure 1.

Hierarchical data structures for three-dimensional data representation. Octrees – hierarchical data structures – have been used for representation of three-dimensional scenes for decades. Works from the 1980s include Srihari [10], Rubin and Whitted [11], Jackins and Tanimoto [12] and Meagher [13] [14] [15], to name only a few. Different encoding schemes of child node header tags in PSVO leveraging fixed-length and variable-length header tags appeared in [16].

Not only homogenously empty subtrees, but also homogenously filled subtrees were removed: PSVOs – hierarchical data structures allowing the removal of not only homogenously empty subtrees, but also those homogenously filled with any symbol from a defined set of symbols – were proposed in [17]. The symbol set can be encoded using a fixed-length or variable-length binary-level representation.

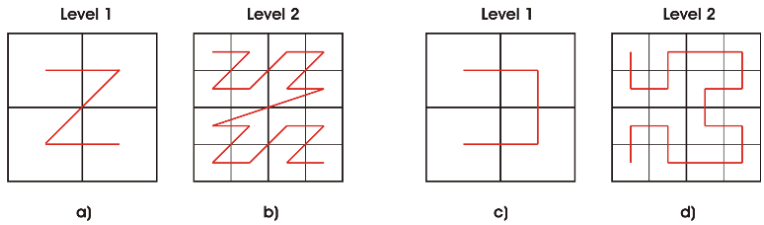

Figure 1
Linearization of the two-dimensional space of various levels,
using a, b) Morton order and c, d) Hilbert curves

Efficient Sparse Voxel Octrees (ESVOs), introduced in 2010, are sparse voxel octrees, in which whole subtrees may be efficiently replaced with 32 b-long contour information (i.e. a 24 b-long contour pointer and an 8 b-long contour mask) [18].

High Resolution Sparse Voxel Directed Acyclic Graphs (SVDAGs), proposed in 2013, are DAGs incorporating pointers to the child nodes into their internal nodes and allowing common subtree merging, when two or more child node pointers point to the same node of the data structure [5]. Child node pointers are 0 b and 32 b-long, respectively. Each part of the data structure is 32 b-aligned. In 2016, Symmetry-aware Sparse Voxel Directed Acyclic Graphs (SSVDAG) were introduced in [2] [3]; these incorporate pointers to the child nodes of 0 b, 16 b, 32 b and 33 b lengths, which is why 2 b header tags of the child node mask with an overall length of 16 b are used. Three bits of child node pointers are used to encode a reflective symmetry transformation (separately, in each main axis of the scene) when common subtree merging is used, for improved lossless compression of the data structure. CSM is applicable not only to identical subtrees, but also to subtrees identical after applying reflective symmetry transformation.

SSVDAG* is a small modification of the SSVDAG data structure, proposed in 2019 in [19], replacing 33 b-long pointers with another 16 b-long pointer without the symmetry transformation representation. This allows a higher compression ratio but smaller overall size of the binary representation of the data structure, due to the smaller overall addressing space of pointers in each level of data structure.

Pointerless Sparse Voxel Directed Acyclic Graphs (PSVDAGs) were proposed in 2020 in [4]. This hierarchical data structure allows common subtree merging using the concept of Labels/Callers, with variable-length and their frequency-based compaction. See subsection 3.2 for further details.

Out-of-core construction of Sparse Voxel Octrees (SVOs) from triangle meshes was introduced in [20] [21]. The algorithm consists of two basic steps. The first is a voxelization process, in which the triangles representing the scene form an intermediate product – a high-resolution three-dimensional voxel grid. In the second step, this intermediate product is transformed into SVOs. The algorithm

allows the size of the binary representation of the input triangle mesh, the output SVO, and the intermediate product – a three-dimensional voxel grid generated at a high resolution and represented by a Morton order – to exceed the available computer memory by far. Compared to the in-core algorithm, it uses only a fraction of the memory and has comparable processing time.

3 Hierarchical Data Structures

This section describes the SVDAG and PSVDAG data structures – the formal description in the Backus-Naur Form (BNF) is accompanied by a brief explanation of the basic features of those data structures.

3.1 Sparse Voxel Directed Acyclic Graphs

The formal description of the SVDAG hierarchical data structure using Backus-Naur Form is as follows:

$$
\begin{aligned}
&\textit{SVDAG ::= (n) <NODE>}\\
&\textit{NODE ::= <INODE> | <LNODE>}\\
&\textit{INODE ::= <CHNM> (p) <BIT> <PTS>}\\
&\textit{LNODE ::= <CHNM> (q) <BIT>}\\
&\textit{CHNM ::= (8) <HT>}\\
&\textit{PTS ::=(1) * (8) <PT>}\\
&\textit{PT ::= (r) <BIT>}\\
&\textit{HT ::= <BIT>}\\
&\textit{BIT ::= “0“ | “1“}
\end{aligned}
\tag{1}
$$

Where the following applies:

<SYM> - mandatory non-terminal symbol SYM,

“sym“ – terminal symbol sym,

(n) <SYM> - symbol SYM, concatenated n times,

(n)(m) <SYM> - symbol SYM, concatenated from n to m times*

| - alternative

Juxtaposition – concatenation.

SVDAGs represent the three-dimensional grid of voxels R that comprises N^3 voxels, where $N \geq 2$; $N = 2^m$. If $N = 2$, the root node of the SVDAG data structure is constructed as the leaf node *LNODE*. If N >2, the root node of the SVDAG data structure is constructed as the internal node *INODE*.

Each internal node (*INODE*) of the data structure comprises a Child Node Mask (*CHNM*) and an array of pointers (*PTS*). The *CHNM* comprises 8 b, where each potential child node is represented by a 1 b header tag (HT). If HT is set to 0, the related subDAG of the grid *R* is homogenously filled by passive voxels and there is no need for pointer representation, because the subDAG is pruned out. If HT is set to 1, it represents the subDAG of the grid *R*, in which at least one of the voxels is active, and therefore the child node is present in the data structure and the related pointer *PT* is included in the *PTS*. The *CHNM* is concatenated with *p* reserved bits, to align the size of this part of the node. The next part of the node is the *PTS,* containing 1 to 8 pointers *PT,* each of them *r* bits long. The order of *HTs* in the *CHNM* and that of the pointers in the *PTS* depends on the selected linearization.

Two or more pointers from different nodes at the same level *n* of the data structure and even from the same node may point to the same address and therefore to the same node (their child node) in level $n + 1$ of the data structure. This allows common subtree merging and further lossless compression without any decompression overhead in comparison to the octree version of the data structure, which does not allow two pointers to point to the same node. In SVDAGs proposed in [5], each part of the node and therefore each node and the overall data structure is 32 b-aligned, when parameters *p* and *q* are set to 24 and *r* is set to 32.

Figure 2 shows an example of a two-dimensional (for the sake of simplicity) grid of pixels and the corresponding directed acyclic graph that can be transformed into a binary-represented SVDAG. Each node has four potential child nodes in the Morton order [8]. Passive pixels are set in white, active pixels in red. Two subgrids of 4×4 pixels are pruned out along with four 2×2 subgrids. Each of the two other subgrids of 2×2 pixels is represented in the grid twice; that is why common subtree merging is performed two times. For linearization, we used the Morton order.

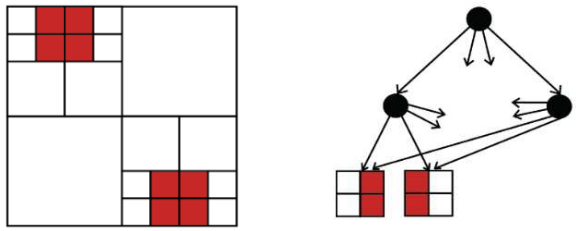

a) b)

Figure 2

Example of a) a two-dimensional grid of pixels with passive voxels (white) and active voxels (red); and b) a directed acyclic graph that can be transformed into a sparse voxel directed acyclic graph using common subtree merging

3.2 Pointerless Sparse Voxel Directed Acyclic Graphs

The formal description of the PSVDAG hierarchical data structure using the Backus-Naur Form is as follows:

$$
\begin{aligned}
&PSVDAG ::= \langle NODE \rangle \\
&NODE ::= \langle INODE \rangle \mid \langle LNODE \rangle \\
&INODE ::= \langle ACHNC \rangle \ \langle CHNM \rangle \\
&ACHNC ::= (3)\ \langle BIT \rangle \\
&CHNM ::= (1)*(8)\ \langle HT \rangle \\
&HT ::= \text{“00“} \mid \text{“01“}\ \langle LAB \rangle\ \langle NODE \rangle \mid \text{“10“}\ \langle CAL \rangle \mid \text{“11“}\ \langle NODE \rangle \\
&LAB ::= \langle SIZ \rangle \langle VAL \rangle \\
&CAL ::= \langle SIZ \rangle \langle VAL \rangle \\
&SIZ ::= (5)*\langle BIT \rangle \\
&VAL ::= (1)*(32)\ \langle BIT \rangle \\
&LNODE ::= (8)\ \langle BIT \rangle \\
&BIT ::= \text{“0“} \mid \text{“1“}
\end{aligned}
\tag{2}
$$

A PSVDAG represents a three-dimensional grid of voxels R comprising N^3 voxels, where $N \geq 2;\ N = 2^m$. The *PSVDAG* data structure comprises the root node (*NODE*) that represents the overall 3D scene. If $N = 2$, the root node of the PSVDAG data structure is constructed as the leaf node *LNODE*. If N > 2, the root node of the PSVDAG data structure is constructed as the internal node *INODE* and is further iteratively decomposed into 8 child nodes, dividing the scene into 8 suboctants. Each node can be either an *INODE* or an *LNODE (*if the node is located in the last level of the hierarchical data structure).

The *INODE* consists of the *Active Child Node Count* (*ACHNC*) and the *Child Node Mask* (*CHNM*). The *ACHNC* is a 3 b unsigned integer value showing the number of active child nodes of the particular node (using a value decremented by 1). It allows potential lossless compression of the *CHNM*. The *ACHNC* facilitates the reconstruction of pointers in the PSVDAG–SVDAG transformation process. The *Child Node Mask* comprises header tags *HT* ordered according to the selected linearization. All *HT*s indicating passive child nodes (set to “00”), placed beyond the last active child node *HT* (the active child node indicator *HT* is encoded as “01”,”10” or ”11”) in the *CHNM* are omitted, as it can be seen in Figure 3, in which 4 *HT*s are omitted.

ACHNC	HT0	HT1	HT2	HT3	HT4	HT5	HT6	HT7
001	11	00	00	01	00	00	00	00

Figure 3

An example of the node structure, where *ACHNC* set to 1 indicates 2 active child nodes (here: HT0 and HT3) and four omitted HTs (HT4 to HT7). For the sake of simplicity, only *HT* indicators are represented, without concatenated Labels and Callers.

The meaning of *HT* indicator values is as follows:

- **00** – a passive child node header tag indicating that there is no active voxel in the corresponding suboctant of the grid R. There is no further information concatenated (the passive subtree is pruned out).
- **01** – an active child node header tag indicating a child node being the root node of a subtree present in the data structure multiple times. The header tag indicator is concatenated with the Label along with the representation of that child node.
- **10** – an active child node header tag indicating a child node being the root node of a subtree present in the data structure multiple times. The HT is concatenated with the Caller. No other information is needed, because the whole subtree is pruned out.
- **11** – an active child node header tag, concatenated with the root node of the subtree, present in the data structure only once.

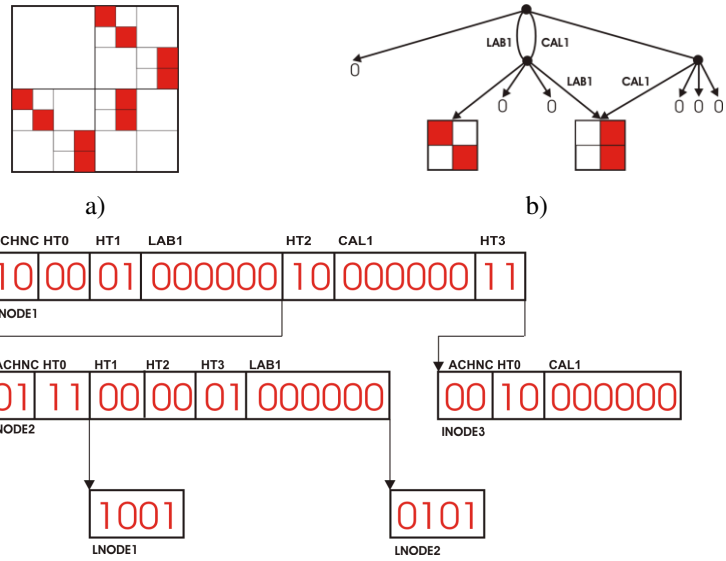

Figure 4

An example of a) a two-dimensional grid of 8×8 pixels, b) a quadtree with labels and callers marked to illustrate the relation to the PSVDAG, c) the structure of PSVDAG nodes and d) the final binary representation of the PSVDAG data structure in its version for 2D where only two bits are used for the active child node count (ACHNC)

PSVDAGs are pointerless data structures allowing merging of common subtrees (CSM). If two or more subtrees are identical in the data structure, only one full decomposition of the subtree is present in the data structure: in its root node, the *HT* is set to "01", concatenated with the Label. For all other instances of this subtree, the *HT* is set to "10" and a Caller (with the same binary representation as the Label) is used, but the subtree is not decomposed (its root node and whole decomposition is pruned out and the Caller represents the link to the template subtree used instead when traversing the data structure). This way, complete representations of subtrees can be referenced in PSVDAGs, multiple times. When depth-first traversing the PSVDAG, to the first occurrence of this common subtree, the Label is assigned and to all other occurrences, the Caller.

The Label has two components – label size (*SIZ*), which is a 5 b unsigned integer and value (*VAL*). *SIZ* represents the length of the value *VAL* in bits, decremented by 1. If *SIZ* is *n*, the length of value is $n + 1$ bits. *VAL* can be from the range of $\langle 0; 2^{n+1}-1 \rangle$. For each level *l* of the data structure nodes, the labels are generated separately, from the smallest value of *SIZ* and *VAL* (SIZ = 0 and VAL = 0). For each following label in a particular level, the value of *VAL* is incremented and when the capacity of this size of *VAL* is filled, size *SIZ* is incremented and *VAL* is set to 0 for the next label. Taking only *SIZ* and *VAL* into account, each Label within level *l* is unique. Considering level *l*, *SIZ* and *VAL*, each label within the whole data structure is unique – see Figure 4.

The Caller structure follows the same principles as that of the Label, when it comprises *SIZ* and *VAL*. A Caller with the same values of *l*, *SIZ* and *VAL* as the particular Label points to the subtree labelled with this particular Label. This allows common subtree merging, using the concept of variable-length Labels/Callers.

To each level *l* of the data structure, frequency-based compaction is applied, when all nodes referenced from level $l - 1$ more than once are ordered by their frequency of referencing in descending order and labels generated for this level of nodes are ordered by their binary-representation length *SIZ* and value of the *VAL* in ascending order. The most frequently referenced node in the level is therefore assigned the label with the shortest binary-level representation and vice versa. This allows to obtain the lowermost possible number of bits forming Labels/Callers for this principle of Label/Caller-encoding.

Leaf nodes (*LNODE*) contain one bit per voxel – active voxels are set to 1, passive voxels are set to 0. In the leaf node, voxels are ordered according to the selected linearization (Morton order [8] in Figure 4).

For detailed information regarding PSVDAG encoding principles and features, refer to [4].

4 The Proposed Conversion Algorithm

One of the basic features of PSVDAGs is that considering binary-level encoding, internal nodes are not encoded as uninterrupted sequences of bits, but quite the opposite: binary-level representations of internal nodes are intermittent, when child node representations are inserted. Internal node representation can be therefore distributed across the whole data structure. Child node pointers are absent, while some of them are replaced by Labels and Callers having a variable-length binary-level representation.

The *CHNM* of the internal nodes can have a variable-length binary representation and *HT* indicators are encoded using 2 b. On the contrary, in SVDAGs, internal nodes are encoded as uninterrupted sequences of their binary-level representation, the *CHNM* has a constant length with 1b *HT*s and child nodes are referenced using constant-length pointers.

The conversion algorithm must therefore perform four important tasks:

- Extract the binary-level representation of the PSVDAGs internal nodes and transform them into compact sequences of binary-level representation, as used in SVDAGs
- Transform the PSVDAG *CHNM* into the SVDAG *CHNM*, i.e. transform 2 b PSVDAG *HT* indicators into 1b SVDAG *HT*s
- Generate child node pointers referencing child nodes in SVDAG internal nodes and those that are missing in PSVDAG HDS
- Replace PSVDAG Labels and Callers by SVDAG pointers to the child nodes in SVDAG in the way allowing CSM

The binary-level representation of the PSVDAG is the linearized form of the HDS, obtained as the product of depth-first traversing of the particular directed acyclic graph. When processed by the transformation algorithm, it is transformed into a SVDAG in one pass, progressively generating particular internal and leaf nodes of the target SVDAG, processing only one SVDAG node at a time, for each level of nodes. During the processing, we use a data structure having a significantly shorter binary representation than the whole input PSVDAG and the output SVDAG and store this structure in the main memory of the computer. During the transformation, a Label Transformation Table (LTT) – to convert Labels/ Callers into child node pointers – is needed; the binary representation of the LTT can be considerably larger. Thus, if this table is stored in the main memory of the computer, the algorithm is considered to be the semi-out-of-core version and if the LTT table is stored in secondary storage, it is considered to be the out-of-core version.

When the conversion of the PSVDAG internal node starts, the nearest free address in the SVDAG is assigned to this node as the final address where this node will be stored as the new SVDAG internal node; it will be finalized after its conversion.

This address is 32 b-long; its value will be used also when child node pointers to this child node will be constructed. Using the ACHNC of the PSVDAG node, which is also stored in the operating memory during node transformation and which was read as the first part of the PSVDAG node when its transformation started, it is possible to determine the length of the binary-level representation of the corresponding SVDAG node, although not all components of this node have been read and transformed yet. Therefore, it is possible to evaluate the next free address in the SVDAG for the next node to be transformed. This allows to determine addresses and binary-level representation lengths for all nodes processed at this time. As soon as one of those nodes gets finally processed, this node may be stored at the final address in the target HDS immediately.

The *ACHNC* of internal PSVDAG node stores the number of active child nodes of the corresponding SVDAG internal node, decremented by 1. In the SVDAG node, each active child node will have its 32 b child node pointer and another 32 b will comprise the 8 b *CHNM* of the node and 24 reserved bits (to align this part of the node to 32 b). The size of the SVDAG node $SVDAG_{nodesize}$ in bits can be calculated from the *ACHNC* of the related PSVDAG node using this formula:

$$SVDAG_{nodesize} = (ACHNC + 2) * 4\ [B] \quad (3)$$

Another component describing the SVDAG node is an 8 b vector, representing its child node mask *CHNM*. While in PSVDAGs, the *CHNM* of the child nodes is represented using 2 b *HT* indicators and some of those *HT*s can be omitted, in SVDAGs, there are always eight 1 b *HT*s in the *CHNM*. When transforming the PSVDAG *CHNM,* the passive child node – i.e. the node encoded in the PSVDAG node as the "00" *HT* indicator – is transformed into *HT* "0" in SVDAG. Active child nodes – nodes encoded in the PSVDAG node with the "01", "10" or "11" *HT* indicator – are transformed into *HT* "1" in SVDAG. *HT*s omitted in the PSVDAG node are inserted into the SVDAG, encoded as *HT* "0". Due to the selected linearization, the HT order in the SVDAG HDR will be the same as the one in the PSVDAG HDR.

Another part of the SVDAG node is the array of pointers *PTS*, where each pointer has a constant – 32 b – length. Their number varies from 1 to 8. When processing PSVDAG nodes, each processed node has an array for 8 potential pointers, each 32 b-long. Each processed node has also a pointer *ptpt* showing where the next pointer can be stored in the *PTS* array of the node.

When constructing a node pointer to the child node that is indicated by HT "11" in the PSVDAG *CHNM*, in the SVDAG, the address of the child node will be – after its completion – the next free address, stored in the variable *nnadr*. This address is also used as the value of the pointer to this child node. Considering that this child node is referenced by the pointer in the HDS only once, there is no need to store the value of this pointer in the operating memory after it has been generated and stored into the node and after the child node's address has been assigned. After this step, the algorithm starts the conversion of the child node.

When constructing the child node pointer for the active child node that is indicated by the *HT* set to "01" in the PSVDAG *CHNM*, the corresponding Label of the child node – containing *SIZ* and *VAL* – is read. Level *l,* representing the level of the particular node, is also known. The next free address in the SVDAG, stored in the *nnadr* variable, is assigned to this child node and this child node will be stored at this address in the SVDAG after its finalization. This address is used as the value of the pointer to this child node and as the value of the corresponding Label in the *LTT*. After the pointer is generated and stored into the node and the address is assigned to the child node, the processing of this child node starts.

During the PSVDAG data structure transformation, there is need to store information about addresses assigned to the particular labels, because those addresses will be used one or more times when processing the Callers. That is why the particular Labels and their addresses are progressively stored in the Label Transformation Table (*LTT*). For each triplet [*level*, *SIZ*, *VAL*] of a particular Label, the address assigned to this Label is written into the *LTT*. If the *LTT* is stored in the operating memory of the computer, the semi-out-of-core version of the algorithm is used; if the *LTT* is stored in the secondary storage of the computer, the out-of-core version of the algorithm is used.

When constructing the child node pointer for the child node indicated by the HT set to "10" in the PSVDAG *CHNM*, the related Caller of the child node – containing *SIZ* and *VAL* – is read. Level *l,* representing the level of the particular node, is also known. The value of the pointer to this child node that will be used when constructing the SVDAG node is then read from the LTT table, where it may be found using the triplet [*level*, *SIZ*, *VAL*] of the Caller when the same triplet of the Label is found and the assigned address is used as the pointer.

For each constructed internal node of the SVDAG, the 32 b target address, stored in *adr* is known. The number of active child nodes, calculated from the *ACHNC*, is stored in the 8 b *achnc* variable. There is a 32 b *chnm* variable, representing the node's *CHNM*. The *pts* array may store at most 8 child node pointers, 32 b each. The number of node pointers actually processed for this node is stored in the 8 b *ptpt*. Each node is therefore represented in memory by the 336 b structure *node*, consisting of *adr*, *achnc*, *chnm*, *pts* and *ptpt*. The array *nodes* comprise one *node* structure for each level of internal nodes of the HDS. After each pointer is added to the *pts* array of the particular *node*, the algorithm checks if it was the last pointer expected for this node. If yes, the node is finalized and stored at the *adr* address in the SVDAG. The related *node* structure is then initialized and prepared for processing another node of the same level.

The proposed conversion algorithm has three steps. ***Step 3*** is called iteratively.

Step 1 *nnadr = 0; level = 0;*

if (*maxl == 1*) ***Step 2; end;***

if *(maxl >1)* ***Step 3; end;***

```
Step 2   readLNODE();
         writeLNODE();
         nnadr += 4;
         return;
Step 3   level++;
         nodes[level].achnc = readACHNC() + 1;
         nodes[level].adr = nnadr;
         nnadr += (nodes[level].achnc + 1) * 4;
         nodes[level].ptpt = 0;
         until (nodes[level].achnc > nodes[level].ptpt) {

         ht = readHT();
            switch (ht) {

                  case 0:  updateCHNM(nodes[level].chnm, 0);
                           break;
                  case 1:  updateCHNM(nodes[level].chnm, 1);
                           [siz, val] = readLabel();
                           putInLTT(level, siz, val, nnadr);
                           updatePTS(nodes[level].pts[ptpt++], nnadr);
                           if (level < lmax-2) Step 3;
                           if (level == lmax-2) Step 2;
                           break;
                  case 2:  updateCHNM(nodes[level].chnm, 1);
                           [siz, val] = readCaller();
                           adr = getFromLTT(level, siz, val);
                           updatePTS(nodes[level].pts[ptpt++], adr);
                           break;
                  case 3:  updateCHNM(nodes[level].chnm, 1);
                           updatePTS(nodes[level].pts[ptpt++], nnadr);
                           if (level < lmax-2) Step 3;
                           if (level == lmax-2) Step 2;
                           break;
            }
         }
         writeINODE(nodes[level]);
         return;
```

The input of the proposed conversion algorithm is represented by the stream of bits of the binary-level representation of the PSVDAG (described in subsection 3.2), and *maxl*, the number of node levels in this data structure (*maxl* > *0*). Node levels are from the range of *<0; maxl - 1>*: the root node is located in level 0, the internal nodes are located in levels *<0; maxl - 2>*, the leaf nodes are located in level *maxl - 1*.

Step 1 of the algorithm sets the next node variable *nnadr* to 0, as well as the PSVDAG node level indicator, the variable *level*. Subsequently, it has to be tested if the root node of the PSVDAG data structure is a leaf node or an internal node. If the input parameter *maxl* is set to 1, the root node of the PSVDAG is a leaf node, ***Step 2*** of the algorithm is performed and then execution of the algorithm ends. If the input parameter *maxl* > 1, the root node of the PSVDAG is an internal node, ***Step 3*** of the algorithm is performed and then the execution of the algorithm ends.

Step 2 processes the leaf node of the PSVDAG, encoded in the PSVDAG as an 8-bit vector, where each bit represents one voxel. ***readLNODE()*** reads 8 bits from the input stream. ***writeLNODE()*** writes an 8-bit vector representing the leaf node of the SVDAG data structure and adds 24 reserved bits to the output stream at the address *nnadr*. The value of *nnadr* (in bytes) is then incremented by 4.

Step 3 processes an internal node of the PSVDAG. The *level* value is incremented and the *ACHNC,* a 3-bit vector, is read from the input stream. Its incremented value shows how many child node pointers will the SVDAG node have. Its final address is set to the *nnadr* value and stored in *adr*. The value of *nnadr* (next new node address) is computed, and pointer *ptpt* is set to 0.

Until the last active child node *HT* is read, the following is repeated:

ht is read using ***readHT()***.

If the *ht* is set to 0 (“00“), *chnm* in the *node* structure of SVDAG nodes, stored in *nodes* array, is updated using ***updateCHNM()***, setting the corresponding HT to 0.

If *ht* is set to 1 (“01“), *chnm* in the *node* structure of SVDAG nodes, stored in the *nodes* array, is updated using ***updateCHNM()***, setting *HT* to 1. The Label is read using ***readLabel()*** and *LTT* table is updated using ***putInLTT()***, using the particular *level*, *siz* and *val* values to set the Label address to *nnadr*. The pointer array *pts* of the particular structure *node* is updated using ***updatePTS()*** – the new pointer is written into this array and *ptpt,* showing the number of pointers stored for this node, is incremented. Then, child node construction starts and – depending on the level in which it is stored – ***Step 3*** (if the child node is an *INODE)* or ***Step 2*** (if it is an *LNODE*) is performed.

If *ht* is set to 2 (“10“), *chnm* in the *node* structure of SVDAG nodes, stored in the *nodes* array, is updated using ***updateCHNM()***, setting the related *HT* to 1. The caller is read using ***readCaller()***, and from the *LTT* table, the address is retrieved for particular *level*, *siz* and *val* values, using ***getFromLTT()***. The pointer

array *pts* of the particular structure *node* is updated using ***updatePTS()*** – the new pointer is written into this array and *ptpt,* showing the number of pointers stored for this node, is incremented.

If *ht* is set to 3 ("11"), *chnm* in the *node* structure of SVDAG nodes, stored in the *nodes* array, is updated using ***updateCHNM()***, setting the related *HT* to 1. The pointer array *pts* of the particular structure *node* is updated using ***updatePTS()*** – the new pointer is written into this array and *ptpt,* showing the number of pointers stored for this node, is incremented. Then, child node construction and – depending on the level in which it is stored – ***Step 3*** (if the child node is an *INODE)* or ***Step 2*** (if it is an *LNODE*) is performed.

After all active child node *HT*s are processed, the particular INODE is written to the output using ***writeINODE()***.

5 Results

Various 3D scenes, originally stored in Wavefront OBJ geometry definition file format (examples of those scenes with their visualizations are in Figure 5), were used for test purposes. The "Angel Lucy" model consisted of 488 880 triangles, the "Skull" model had 80 016 triangles and the "Porsche" model had 22 011 triangles. These were voxelized to different resolutions, ranging from 128^3 to 1024^3 ($1\ K^3$). The voxelized scenes were then encoded as PSVDAG hierarchical data structures.

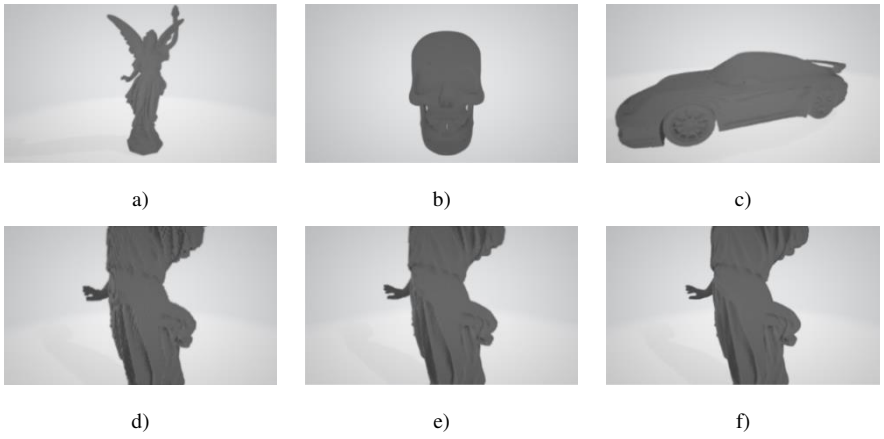

Figure 5
Visualization of voxelized scenes for testing purposes: a) "Angel Lucy" 512^3; b) "Skull" 512^3; c) "Porsche" 512^3; d) detail of the "Angel Lucy" 256^3 model; e) detail of the "Angel Lucy" 512^3 model; f) detail of the "Angel Lucy" $1\ K^3$ model

Details of particular models and their particular voxelizations to the respective resolutions can be found in Table 1.

Table 1
Parameters of particular models, voxelized to the particular resolutions and stored as PSVDAGs, for test purposes

		Active voxels					
		Angel Lucy		Skull		Porsche	
Resolution [vox]	**Voxels [×2^{20}]**	**[×10^3]**	**[%]**	**[×10^3]**	**[%]**	**[×10^3]**	**[%]**
128^3	2	22,48	8,78	74,10	28,95	54,20	21,17
256^3	16	91,52	4,47	298,85	14,59	233,04	11,38
512^3	128	366,58	2,24	1192,04	7,28	969,11	5,91

By converting PSVDAGs into SVDAGs, the space needed to store the scene geometry increased. In case of the particular models and voxelization resolutions, the increase ranged from 3.01-fold (in case of the "Skull" model at 1 K^3 scene voxelization resolution) to 3.70-fold (in case of the "Angel Lucy" model at 128^3 scene voxelization resolution). So, in general, higher voxelization resolutions led to smaller inflation rates. See Table 2 for absolute sizes of the PSVDAGs and SVDAGs (in KB) for the respective models and voxelization resolutions.

Table 2
Size of particular models at various voxelization resolutions, stored as PSVDAG and SVDAG hierarchical data structures

Size [KB]		**Resolution**		
		128^3	**256^3**	**512^3**
Angel Lucy	**PSVDAG**	8.62	35.10	132.37
	SVDAG	31.88	127.01	462.85
Skull	**PSVDAG**	28.11	104.31	366.48
	SVDAG	100.39	356.75	1182.45
Porsche	**PSVDAG**	15.80	61.28	227.13
	SVDAG	56.78	222.41	788.76

During the conversion process, it was necessary to maintain 32 b addresses assigned to the individual Labels in the LTT table. The smallest number of these addresses (182) was needed for the Angel Lucy 128^3 model, requiring 0.71 KB of space. The largest number of these addresses (9179) was needed in the case of the Skull 512^3 model, requiring 35.86 KB of space.

The semi-out-of-core version of the conversion algorithm that stores the Label Transformation Table in the operating memory, transformed PSVDAGs into SVDAGs with a higher data throughput and therefore faster for each model and voxelization resolution, in comparison to the out-of-core algorithm storing the Label Transformation Table in the secondary storage.

Table 3
Time in seconds and data throughput in MB for particular models at various voxelization resolutions – conversion from PSVDAG hierarchical data structure into SVDAG hierarchical data structure, for the semi-out-of-core (SOoC) and out-of-core (OoC) versions of the algorithm

Time [s] **Data throughput [KB/s]**		**Resolution**		
		128^3	**256^3**	**512^3**
Angel Lucy	**SOoC**	0.28[*1] 112[*2]	1.14 111	4.62 100
	OoC	0.30[*1] 106[*2]	1.21 105	4.73 98
Skull	**SOoC**	0.81[*1] 124[*2]	3.24 110	13.59 87
	OoC	0.85[*1] 118[*2]	3.43 104	14.44 82
Porsche	**SOoC**	0.44[*1] 129[*2]	1.97 113	7.33 108
	OoC	0.47[*1] 121[*2]	2.04 109	7.51 105

[*1] Conversion time in seconds
[*2] Data throughput measured on the output in KB/s

The time required for the conversion of the particular models and voxelization resolutions ranged from 0.28 s for the "Angel Lucy" model at 128^3 resolution and the semi-out-of-core version to 14.44 ms for the "Skull" model at 512^3 resolution and the out-of-core version. The time consumption of the out-of-core version was 1.024–1.057-times higher than that of the semi-out-of-core version.

Data throughput was 82 KB/s – 129 KB/s and was strongly affected by the seek operation, performed when storing the completed nodes in the final output file. Output data throughput at the level of 34.5 MB/s was achieved in the case when a fully in-core transformation was performed on the model "Skull" having a 512^3 resolution. Both the PSVDAG and the LTT structures were stored in the computer's operating memory, together with the SVDAG hierarchical data structure, which was consecutively stored into the secondary storage after its finalization.

Conclusions

This paper examined the issues related to three-dimensional scene geometry representation, using domain-specific hierarchical data structures, building on previous work in the field – Pointerless Sparse Voxel Directed Acyclic Graphs. This data structure is well suited for archiving and streaming purposes; however, quick traversing requires reconstruction of pointers. That is why PSVDAG incorporates a feature that facilitates pointers reconstruction. Two versions – an out-of-core and a semi-out-of-core – of the PSVDAG–SVDAG conversion

algorithm were proposed and introduced as the contribution of this paper, along with test results that were performed on different models voxelized to various resolutions.

During the conversion of PSVDAGs into SVDAGs, pointers are generated. Pointers take significant amount of space in SVDAGs, so conversion causes inflation of the space required for storing this HDS, in the operating memory of computer or in the memory of the graphics card. For particular models and voxelization resolutions, the resulting inflation ranged from 3.01-fold (in case of the "Skull" model at a 1 K^3 scene voxelization resolution) to 3.70-fold (in case of the "Angel Lucy" model at a 128^3 scene voxelization resolution). In general, higher voxelization resolutions need more space for Labels/Callers in PSVDAGs, which results in a relatively smaller inflation ratio when converting to the SVDAG data structure. Considering conversion time, the out-of-core version of the algorithm (storing the Label Transformation Table on secondary storage), has a disadvantage, compared to the semi-out-of-core version of the algorithm (storing the Label Transformation Table in the operating memory of the computer). Thus, the out-of-core version of the algorithm was 1.024 to 1.057 times slower than the semi-out-of-core version of the algorithm, for all models and voxelization resolutions. When testing the in-core version of the algorithm, a data throughput 34.5 MB/s was achieved.

Acknowledgement

This research was supported by the Slovak Research and Development Agency, project number APVV-18-0214 and by KEGA 002TUKE-4/2021 Implementation of Modern Methods and Education Forms in the Area of Cybersecurity towards Requirements of Labour Market.

References

[1] C. Crassin, F. Neyret, S. Lefebvre and E. Eisemann, GigaVoxels: Ray-Guided Streaming for Efficient and Detailed Voxel Rendering. ACM SIGGRAPH Symposium on Interactive 3D Graphics and Games (I3D. 10.1145/1507149.1507152

[2] A. J. Villanueva, F. Marton and E. Gobbetti, Symmetry-aware Sparse Voxel DAGs (SSVDAGs) for compression-domain tracing of high-resolution geometric scenes, Journal of Computer Graphics Techniques (JCGT), May 8, 2017, Vol. 6, No. 2, p. 30, 2017, ISSN 2331-7418, http://jcgt. org/ published/0006/02/01/

[3] A. J. Villanueva, F. Marton, and E. Gobbetti, SSVDAGs: Symmetry-aware Sparse Voxel DAGs. In Proceedings of the 20th ACM SIGGRAPH Symposium on Interactive 3D Graphics and Games (I3D '16) February 27-28, 2016, Redmond, WA, USA, pp. 7-14, ACM, New York, NY, USA, ISBN: 978-1-4503-4043-4/16/03, DOI: https://doi.org/ 10.1145/285 6400.2856420

[4] L. Vokorokos, B. Madoš and Z. Bilanová, PSVDAG: Compact Voxelized Representation of 3D Scenes Using Pointerless Sparse Voxel Directed Acyclic Graphs", In: Computing and Informatics: Computers and Artificial Intelligence - Bratislava (Slovakia), Vol. 39, No. 3 (2020), pp. 587-616, [print] - ISSN 1335-9150

[5] V. Kämpe, E. Sintorn, and U. Assarsson., High Resolution Sparse Voxel DAGs. ACM Transactions on Graphics. 32, 4, Article 101 (July 2013), pp. 8, ISSN 0730-0301, DOI: https://doi.org/10.1145/2461912.246 2024

[6] A. Laszloffy, J. Long and A. K. Patra, Simple data management, scheduling and solution strategies for managing the irregularities in parallel adaptive finite element simulations. Parallel Computing, 26, ISSN 1765-1788

[7] H. Sagan, Space-Filling Curves, Springer Verlag, 1994, ISSN 978-1-4612-0871-6, ISBN 978-0-387-94265-0, DOI 10.1007/978-1-4612-0871-6

[8] G. M. Morton, A Computer Oriented Geodetic Data Base and a New Technique in File Sequencing, Research Report. International Business Machines Corporation (IBM), Ottawa, Canada, 20, p. 20, March 1st, 1966, Available: https://dominoweb.draco.res.ibm.com/reports/Morton1966.pdf

[9] D. Hilbert, Via the continuous mapping of a line onto a patch of area. Mathematical annals (orig. Über die stetige Abbildung einer Linie auf ein Flächenstück. Mathematische Annalen) 38 (1891), pp. 459-460

[10] S. N. Srihari, Representation of Three Dimensional Digital Images. Technical Report No. 162, Department of Computer Science, State University of New York at Bufallo, Amherst, New York, pp. 26, 1980

[11] S. M. Rubin, T. Whitted, A 3-Dimensional Representation for Fast Rendering of Complex Scenes. Proceedings of the 7th Annual Conference on Computer Graphics and Interactive Techniques (SIGGRAPH '80), ACM, 1980, pp. 110-116, doi: 10.1145/800250.807479

[12] C. L. Jackins and S. L. Tanimoto, Octrees and Their Use in Representing Three-Dimensional Objects. Computer Graphics and Image Processing, 1980, Vol. 14, No. 3, pp. 249-270, doi: 10.1016/0146-664X(80)90055-6

[13] D. J. R Meagher, Octree Encoding: A New Technique for the Representation, Manipulation, and Display of Arbitrary 3-D Objects by Computer. Technical Report No. IPL-TR-80-111, Rensselaer Polytechnic Institute, Troy, NY, 1980

[14] D. J. R. Meagher, Geometric Modeling Using Octree Encoding. Computer Graphics and Image Processing, 1982, Vol. 19, No. 2, pp. 129-147, doi: 10.1016/0146-664X(82)90104-6

[15] D. J. R. Meagher, The Octree Encoding Method for Efficient Solid Modeling. Technical Report IPL-TR-032, Image Processing Laboratory, Rensselaer Polytechnic Institute, Troy, New York, 1982

[16] B. Madoš, E. Chovancová and M. Hasin, Evaluation of Pointerless Sparse Voxel Octrees Encoding Schemes Using Huffman Encoding for Dense Volume Datasets Storage, In: ICETA 2020: 18th IEEE International conference on emerging elearning technologies and applications: Information and communication technologies in learning: proceedings - Denver (USA): Institute of Electrical and Electronics Engineers pp. 424-430, ISBN 978-0-7381-2366-0

[17] B. Madoš, N. Ádám and M. Štancel, Representation of Dense Volume Datasets Using Pointerless Sparse Voxel Octrees With Variable and Fixed-Length Encoding, IEEE 19th World Symposium on Applied Machine Intelligence and Informatics, SAMI 2021, Herľany, Slovakia, January, 21-23, 2021, p. 6

[18] S Laine and T. Karras, Efficient Sparse Voxel Octrees. In Proceedings of ACM SIGGRAPH 2010 Symposium on Interactive 3D Graphics and Games. I3D '10, Washington D.C, pp. 55-63, ACM Press, New York, NY, USA, ISBN: 978-1-60558-939-8, DOI: 10.1145/1730804.1730814

[19] P. Čerešník, B. Madoš, A. Baláž and Z. Bilanová, SSVDAG*: Efficient Volume Data Representation Using Enhanced Symmetry-Aware Sparse Voxel Directed Acyclic Graph, In: IEEE 15th International Scientific Conference on Informatics: proceedings - New York (USA): Institute of Electrical and Electronics Engineers, pp. 70-75 [print] - ISBN 978-1-7281-3178-8

[20] J. Baert, A. Lagae and Ph. Dutré, Out-of-core Construction of Sparse Voxel Octrees. In Proceedings of the 5th High-Performance Graphics Conference. HPG ’13, July 19-21, Anaheim, California, pp. 27-32, ACM, New York, NY, USA, ISBN: 978-1-4503-2135-8/13/07

[21] J. Baert, A. Lagae and Ph. Dutré, Out-of-Core Construction of Sparse Voxel Octrees, Computer Graphics Forum Vol. 33, No. 6, pp. 220-227, ISSN 0167-7055, https://doi.org/10.1111/cgf.12345

Cyber Security Awareness and Behavior of Youth in Smartphone Usage: A Comparative Study between University Students in Hungary and Vietnam

Phuong Thao Mai[1], **Andrea Tick**[2]

[1] Doctoral School on Safety and Security Sciences, Óbuda University
Népszínház u. 8, 1081 Budapest, Hungary, thao.mai@stud.uni-obuda.hu

[2] Keleti Károly Faculty of Business and Management, Óbuda University,
Népszínház u. 8, 1081 Budapest, Hungary, tick.andrea@uni-obuda.hu

Abstract: Within the digital culture, the increasing internet consumption and the constant development of technology, especially smartphones have made cyber awareness turn to be increasingly urgent. This study focuses on comparing the level of cyber security awareness, knowledge and behavior among university students in general and between Hungary and Vietnam in particular. Research data was collected, using a set of questionnaires and the 313 responses from University Students, in different school years and fields of study, in Hungary and Vietnam. Quantitative analysis was conducted using SPSS. Results show that all respondents possess a lack of knowledge of cyber security, leading to a low level of cyber threat awareness, beyond the differences in respondent countries. However, there are minor differences in the behavior, between respondents in Hungary and Vietnam, which were measured through four dimensions of cyber security: malware items, password usage issues, social engineering and online scam issues. This research helps to raise awareness of differences in cyber security mindfulness, due to cultural characteristics, that can be considered, when developing global mega-systems, such as, social platforms.

Keywords: Cyber security; internet security; online threats; smartphone usage; student awareness; student behavior; Hungary, Vietnam

1 Introduction

The rapid and dramatic development of information technology, over the recent decade, cannot be denied. Especially in the current context of the Industry 4.0, the massive global rates of internet consumption by individuals and organizations in all of governmental, industrial and also academic sectors, together with the diverse development of smartphone and digital applications have significantly transformed the society as well as daily life [1, 2]. Regarding education sector, the

information and knowledge society in the "digital society" has generated enormous challenges to universities and academic institutions regarding the digitalization in education system such as the comprehensive integration of digital, online, e-learning educational forms, the exploration of industrial and business academic programs, and the possibility of their complex integration into higher education at all levels. Across the globe, the spread of novel coronavirus COVID-19 since early 2020 has led to profound challenges in social interaction, organization as well as the education sector. When the policies on lockdown and social distancing are taken place in most of the countries in the world, one of the most urgent responses to the pandemic applied to maintain educational activities in any higher education institutions is switching all face-to-face forms of education to e-learning/digital learning forms. With the emergent current situation due to the pandemic, the digital competences, skills and practices are indispensable. Along with immediate getting used with the new form of study, students' security awareness in the digital learning environment has been raised as one of the most concerned issues that need to be addressed recently.

Based on distinctions in economic, cultural and social aspects, Vietnam is currently a developing country which has been strongly stimulated to become a high-income economy by 2045 [3]; meanwhile, Hungary is a high-income economy, which was transformed from a developing to developed country. The paper aims to compile a comparative study on the cyber security behavior of students in Hungary and Vietnam. It raises the questions whether in the virtual society created by social networks, the internet where global mega-systems can be used by anyone all over the world, the differences of nations, cultures and educations should be considered at all in relation with cyber security on smart phone. The question arises whether there are peculiarities regarding cyber security on smart phone in the various cultures and countries among students in higher education that must be kept in mind. This paper initially focuses on two different cultures, Hungary and Vietnam and makes an effort to show the differences, linked to the cyber security on smart phone, between these two cultures, among the higher educated students. As a first step, two countries were chosen from a developing and transition economy, on purpose, aiming to reveal the differences. The research findings would help to compare these countries to countries of similar economic and cultural backgrounds. Furthermore, it is expected that the research results of this study would provide the input to future research, in which, the research scale of countries could be expanded. With this goal, more countries with different economic and cultural backgrounds will be compared.

2 Literature Review

2.1 Digital Society in 2020 - the Comparative Context between Hungary and Vietnam

Digital, mobile, and social media have played a vital role in people's everyday life all over the world. Digitalization together with information technology has revolutionized both products and services [4]. It is emphasized that human lives have entered a whole new global age in which countless unfolded opportunities would touch every aspect of life. According to the international official report on digital world in 2020 [5], over 4.5 billion people have been using the internet which account for 59% of total population in the world, meanwhile social media users have passed the 3.8 billion mark. As stated in statistics from January 2020 [6], the total number of people around the world using the internet have increased by 7% with 298 million compared to the corresponding period last year that make the total internet users reach to 4.54 billion. In particular country scale regarding this study, compared to the total population of Hungary in 2020 (9.67 million), there have been 7.64 million internet users until January 2020 which account for 79% [7]. In Vietnam, there have been 68.17 million internet users in 2020 which make up 70% of total population of the country; Compared to January 2019, the number increased by 6.2 million (10.0%) [8]. Thanks to the huge number, Vietnam is ranked as the top 9th worldwide for the internet growth. It is claimed that mobile phone has accounted for over half of total time that people spent on when being online using the internet of people [6]. Specifically, nearly 246 million mobile connections in Vietnam in January 2020 (equivalent to 150% of the total population) in which up to 93% of the total internet users aged from 16 to 64 using smartphone. It is noticed that the daily time accessed the internet via smartphone by internet users aged from 16 to 64 in Vietnam is 3 hours 8 minutes which is considered as a half of the worldwide average time per day spent using the internet by the same age range of respondents. Regarding the mobile connections in Hungary in 2020, there have been more than 11.6 million mobile connections until January that increased by 2.2% compared to the corresponding period last year (equivalent to 120% of the total population) [7] [8]. According to Figure 1, there is a big difference in the rate of smartphone owners, the average download speed for fixed internet connections (MBps/100), and in mobile connections between Hungary and Vietnam.

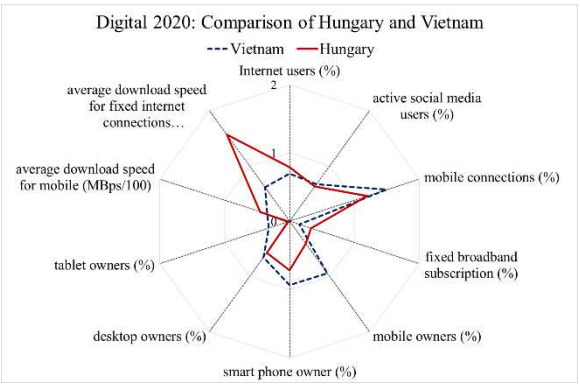

Figure 1
Digital 2020: Comparison of Hungary and Vietnam [5-10]

2.2 The Impact of Internet and Cyber Risk on Society and Individuals

An evolution of the internet, followed by a booming of digital media has brought about drastic changes in learning, information access and knowledge construction. Particularly, cyberspace has facilitated the way people communicate and socialize. Because of the increasing connection with high technology, people use internet for more social connecting in both personal and professional environments such as daily conversation, business work, online services (banking, education and virtual healthcare, etc.). In this line, even operation manner of businesses has been changed thanks to the emergence of the internet and high technologies. It is certain that internet became the fastest-growing communications medium in the last decades [11]. This means that the internet consumption buttressed by information technology improvements has been increasing dramatically. However, being continuously connected, also causes more cyber security risks, which could be cyber threats against a critical infrastructure and economy. To individual internet users, cyber security risks can result in threats to confidential identity, identity as well as privacy [12]. Furthermore, the existence of cyber risks also emerges which are explicitly cybersex, pornography, personal information exposure, cyber addiction, online fraud, addiction towards gaming and gambling, which have negative effects on adults and children [13]. The authors of the study [14] emphasized the effect of the cyberspace toward the daily life: "In our technology and information-infused world, cyberspace is an integral part of the modern-day society. In both personal and professional contexts, cyberspace is a highly effective tool in, and enabler of, most people's daily digitally transposed activities." In the meantime, another study [2] has emphasized that the majority of internet users still lack sufficient awareness of various internet threats/ cyber hazards.

Online study has become an integral part of higher education thanks to the availability of internet resources and constantly has been critical for the future of higher education [15, 16]. At the same time, it is emphasized that internet access together with information technology provide a great extent of flexibility and autonomy for the students [17]. Thus, attitude and perception of the students to cyber security would play a vital role in their self-protection from online threats to their daily online activities. It is noticed that people are recently more dependent on the internet technologies for their daily tasks which have facilitated the extending scale of the involvement in cyber-related activities; whilst the fundamental knowledge needed for preventing from cyber threats correspondingly is lagging [18]. Furthermore, it is also argued that even the basic level cyber security awareness is not sufficient enough for mitigating cyber risks and threats [2, 18]. A study [19] found out that cyber security in mobile phone using has been largely studied in technical aspect while the role of the human aspect who interact with technology is overlooked. As such, further studies cause concern regarding more insights and practices would be critical, to not only individuals, but also the educational sector and other related organizations.

Regarding research topics on cyber security and individual cyber engagement, individual attitudes and behaviors concerning cyber threats have attracted the attention of both academic scholars and practitioners [20, 21]. There have been also a number of studies about cyber security awareness of individual and organization, and the effect of cyber-attacks to internet users. To be more specific, studies on information security awareness in both governmental organizations and private sectors on the level of individual resilience with cyber security awareness as a cause of job stress [22, 23]. Similarly, studies [24, 25] provided more insights about understanding of how employee awareness and attitudes contribute to a company or organization's cyber security, as well as focusing on cyber regulations and the establishment of security policies. Regarding studies on cyber security awareness in education sector, authors of the research [26] have measured the influence of a cyber-security awareness campaign for school youth. After conducting their study based on carrying on the campaign, they found a great impact on cyber security awareness of the targeted school youth when compared with their existing knowledge related to cyber security hazards. However, authors in the study [2] strongly emphasizes that lack of cyber awareness is still a serious global problem while there is still little attention to research on the relationships between individual cyber security awareness, knowledge and behavior which is based on comparative analysis between countries; especially, in smartphone using. In fact, the comparative approach for studies in this area plays a crucial role for the creation of intervention programs [27]. Furthermore, the new milestone in the development of smartphone thanks to the endless innovation in its technology and convenience could not be denied. Simultaneously, the number of internet users who access the internet via smartphone has been constantly increased with up to 91% until January 2020 [6]. This implies that more potential cyber threats could attack not only individuals, but also organizations, education institutions as well as

governments at any time and this could be the most concerned topic than ever. Therefore, further research on cyber security in smartphone use, particularly as a comparative evaluation of the level of awareness across different countries, is crucial, not only for individuals, but, also, the educational sector and other related organizations and governments.

3 Research Methodology and Research Questions

This study was conducted, seeking to answer the following research questions:

1) What is the different state of cyber security awareness of higher education students between Hungarian and Vietnamese students?
2) What are the main factors impacting on the difference level of cyber security awareness of students between Hungary and Vietnam?
3) How similarly do university students behave between the two countries regarding using smartphone through cyber security dimensions?
4) What segments of students regarding cyber security awareness can be found and which are the most influential factors in creating the segments?

Quantitative research method is applied in this study which uses both primary and secondary data for the analysis. Specifically, the statistics analysis is chosen for this study to collect primary data through online questionnaire surveys. The respondents are selected using samples of target population and the purpose. The research population for this research comprised university students in the two countries: Hungary and Vietnam. Because of the large population sizes, researcher was unable to test every person in the total population due to some contrasts in time and budget, especially under the current circumstances of Covid-19. Therefore, this research relied on sampling and applied non-probability, convenience sample. The research data was collected using a set of online questionnaires answered by 313 university students in different school years and different field of study in Hungary and Vietnam in which 191 respondents are students in Hungary (61%) and 122 respondents are from Vietnam (39%).

The targeted respondents received the survey via social media and e-mail, and they were asked to spend from 5 to 7 minutes on this questionnaire. The questionnaire included three parts, (a) personal demographic information, (b) a set of 15 questions on the awareness of cyber security on smartphone – both parts comprise both types of Yes/No and multiple choices questions – (c) respondents were requested to indicate their rate of agreement with statements on cyber security dimensions. The instrument in part three was structured in the Likert fashion, on a 5–point scale, ranging from:

1 - Totally disagree

2 - Partly disagree

3 - Neutral

4 - Partly agree

5 - Strongly agree

A pilot testing for confirming the validation of the questionnaire was done by a number of random students at university level in different countries such as Australia, Hungary, the USA, the United Kingdom and Vietnam excluded from the targeted audience group who actually participated in the study's result contribution.

For the purpose of the study Pearson's Chi-squares test of independence, independent samples t-tests and the decision tree method were applied to reveal the similarities and differences in the cyber security behavior of students in Hungary and Vietnam when using smartphones.

4 Results and Analysis

4.1 Demographic Profile

The study respondents were university students of Óbuda University in Hungary and the University of Danang in Vietnam. In the total 313 respondents of the survey, up to 99.7% of respondents are using smartphone. Table 1 displays the respondents' demographic information. Regarding gender, it is shown that in general, female students make up the highest percentage which is 53.7%, followed by male student with 45.4% and others with 0.9%. In both Hungary and Vietnam, the majority of respondents are in the age between 19-22 years old which account for 63.6% of total number of respondents. The second highest percentage in age range of the respondents in both countries is 24.9% which represents for students in the age of 22-25 years old. This number has illustrated that the survey has approached well to the targeted respondents who are the most suitable research objectives for this study. Regarding the fields of study, up to 70.9% of total respondent percentage are studying in the field of Economics or Business Management. In addition, Engineering, Mathematics or Natural Sciences is the field of study that is second most studied by total respondents (13.7%), followed by other fields (11.8%), Medicine (3.2%) and Laws fields (0.3%). Due to the fact that the majority of the respondents study economics, not engineering or informatics, the behavioral attitude is expected to give valuable results. Further studies will be conducted to extend the sample to make it representative.

The duration of time using smartphone taken into account in this study could be an important factor affecting the experience of cyber security issues. Accordingly, there are up to 101 students using smartphone in 7-10 years in Hungary which account for the highest rate in all four periods of time with 32.3%. Meanwhile, the majority of respondents in Vietnam have been using smartphone in 3-6 years and 7-10 years, which account for 37.7% and 35.2% respectively. It is to be noted that up to 24% of total respondents in Hungary and 21% of total respondents in Vietnam who are in the range age of under young adults have experienced smartphone for over 10 years.

Table 1
Respondent's demographic information (in %)

Country	**Hungary**	**Vietnam**	**Total**
Gender: Male	50.0%	38.1%	45.4%
Female	49.0%	61.9%	53.7%
Others	1.0%	0.0%	0.9%
Age: Under 19	2.1%	5.9%	3.5%
19 - 22	63.4%	63.9%	63.6%
23 - 25	25.8%	23.5%	24.9%
Over 25	8.8%	6.7%	8.0%
Smartphone Usage: Yes	100.0%	99.2%	99.7%
No	0.0%	0.8%	0.3%
Fields of Study: Economics or Business Administration	82.0%	52.9%	70.9%
Engineering, Mathematics or Natural Sciences	10.3%	19.3%	13.7%
Medicine	0.5%	7.6%	3.2%
Law	0.0%	0.8%	0.3%
Other fields	7.2%	19.3%	11.8%
Duration of using smartphone: Under 3 years	2.1%	6.1%	3.5%
3-6 years	21.1%	37.7%	27.5%
7-10 years	52.8%	35.2%	46.0%
Over 10 years	24.0%	21.0%	23.0%

Based on the responses of the question about online activities, all the respondents claimed that they spent most of the online time via their smartphone. The respondents were asked to choose at least three activities that they spend time the most daily. As shown in Figure 2, accessing social networking sites is the activity that most of respondents in both Hungary and Vietnam choose, which means they are heavy social networking users.

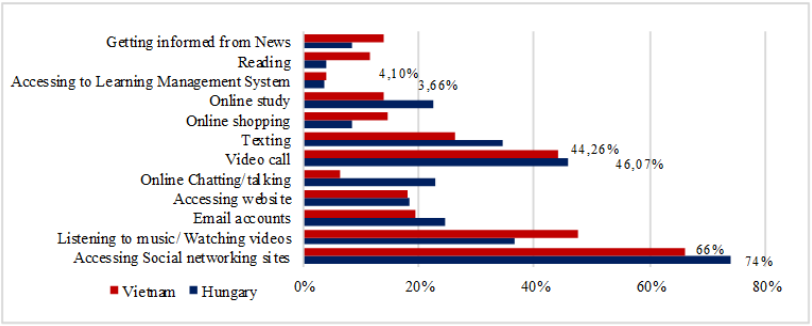

Figure 2

Online activities participated by the respondents in Hungary and Vietnam (in %) (Source: edited by authors)

Specifically, over 70% of total respondents in Hungary use smartphone to access social networking sites such as Facebook, Instagram, etc., and up to 66% of total respondents from Vietnam chose the same activities. In Vietnam, there have been up to 67% of total population using social media [8]. According to a research on Vietnamese students using social-internet-network [28], 100% of respondents ascertained that they got more than one social network accounts and the majority of students spend time on social networking from 1-3 hours per day. Furthermore, Figure 1, also shows that University Students in both Hungary and Vietnam, use their smartphones for mostly, entertainment activities (listening to music/watching videos) and communication (texting, chatting, video calls); instead of, for study purposes (emailing, reading book, online study, accessing websites).

Together with Figure 3, it is stated, that up to 70.2% of total respondents in Hungary and 61.5% of total respondents in Vietnam, are not willing to use a smartphone for accessing online study systems/applications or even getting online materials for their study. Preferences of students in Hungary and Vietnam are similar regarding the access of online learning management system via smartphone, as justified by the CHI^2 test supposing relationship between the preference and the country of origin (CHI^2=2.529, p=0.112).

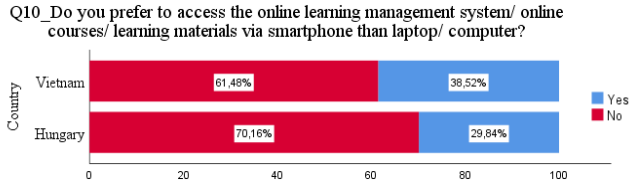

Figure 3

The intention of students to use smartphone for only study activities (Source: edited by authors)

The difference between online activities pursued by students in Hungary and Vietnam proved to be significant, despite the close percentages and some individual similarities, regarding certain activities (CHI^2=39.222, p=0.000).

4.2 Findings on Awareness of Cyber Security on Smartphone

The general awareness of cyber security of all respondents was analyzed with the question "Have you ever heard/ known about the term of cyber security?". Figure 3 shows the results of this question for comparing the knowledge of respondents in Hungary and Vietnam combined with the responses on the question of "desire to learn more on cyber security". Accordingly, it could be clearly seen, that the number of respondents in Hungary who know about cyber security is higher than in Vietnam, accounting for 84.8% of total respondents in Hungary; while the percentage of university students knowing about this term is 73.8%. When asked about their willingness to learn more about cyber security, 89.3% of respondents in Vietnam answered "Yes" while only 69% of respondents in Hungary gave the same answer. It is to be noticed that up to the nearly 40% of the "No" answers for this question to all respondents in Hungary is a relatively high ratio, which ought to be taken into account when 100% of them use smartphone daily and can face unexpected cyber threats from their phone at any time. Testing and comparing the difference of student behavior in Hungary and Vietnam on the above two questions a significant difference was detected between student behavior (CHI^2=26.963, p=0.000), which is due to the difference in the wish to learn more on cyber security being either aware of the term or not. The difference can be captured in Figure 4 illustrating how knowledge of cyber security leads to the desire to learn more on cyber security in Hungary, Vietnam and in total. The difference is well manifest in the "No" groups. In total, a larger proportion of students who answered "No" for the knowledge of the term Cyber security wishes to learn more about it, while the path is the opposite in Vietnam but similar in Hungary. It has to be highlighted that students who learnt about the term cyber security wish to learn more on it in both countries. The balance swings based on student awareness of the importance of cyber security. There is a higher awareness, in the case of Hungary, since student behavior shows that those who already knew about cyber security and might have realized the importance of being prepared for unpredictable cyber threats, are willing to study more about cyber security.

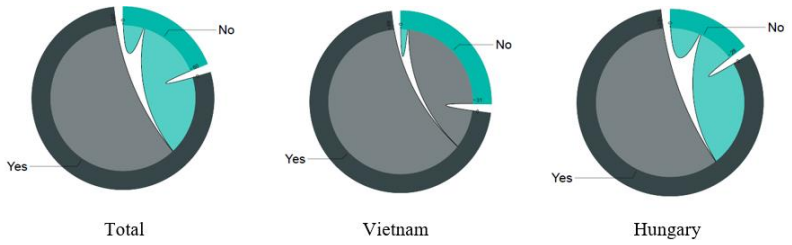

Figure 4
Knowledge of cyber security leads to desire to learn more on cyber security (Source: edited by authors)

The source of difference is shown in Table 2, stating that balance is turned to Hungary for the knowledge while it is turned to Vietnam for desire to learn.

Table 2
The significant difference in student behavior on the knowledge of the term Cyber security (Source: edited by authors)

Comparisons of Column Proportions		Country	
		Hungary (A)	Vietnam (B)
Cyber security knowledge	Q14_Have you ever heard or known about the term of "Cyber security"?	B (0.000)	
	Q16_Do you desire to learn more on security?		A (0.000)
Results are based on two-sided tests. For each significant pair, the key of the category with the smaller column proportion appears in the category with the larger column proportion. Significance level for upper case letters (A, B, C): .05			
a. Tests are adjusted for all pairwise comparisons within a row of each innermost sub-table using the Bonferroni correction.			

Furthermore, the awareness of respondents to cyber security while using smartphone and the difference between respondents in the two counties are also presented by analyzing the answers to specific questions. Accordingly, even though respondents are with their phone every day and spend time on them with many purposes (Figure 1), about half of all the respondents, in both countries, are not sure about their smartphone being virus infected, when their phone is not responding correctly, while 32% and 21% of respondents in Hungary and Vietnam, respectively, have no idea about this issue. For the aim of comparing the behavior of students in Hungary and Vietnam a significant difference was detected in case of the belief of the need of protection on smartphone (CHI^2=11.713, p=0.003) as shown in Table 3. The percentage of respondents in Vietnam is higher for "Yes" (76.2%) which implies that they are more skeptical about security protection while students in Hungary trust more their smartphones and care less about security protection with up to more than 40% of respondents are unsure and deny the necessity of security applications in their smartphone.

Table 3
Awareness of respondents on the need of smartphone security

Q18_Do you think that your smartphone needs security protection? (e.g.: antivirus application) * Country Crosstabulation				
	Country	**Hungary**	**Vietnam**	**Total**
Do you think that your smartphone needs security protection? (e.g.: antivirus application)	Yes	113_a	93_b	206
	No	58_a	17_b	75
	Not sure	20_a	12_a	32
Total		191	122	313
Each subscript letter denotes a subset of Country categories whose column proportions do not differ significantly from each other at the .05 level.				

Regarding the questions on the "possibility of a virus affected device in case of no response of smartphone" and "auto saving login information in smartphone", in both countries students behave similarly and approximately half of the students do not believe saving auto login information in smartphone as a good action from a security perspective (CHI^2=4.298, p=0.117 and CHI^2=5.797, p=0.055, respectively). With a significance level smaller than 5.5% there is a difference in auto login behavior of respondents between the two countries. A larger proportion of students in Vietnam compared to Hungary is not sure about the relation of security breach and auto login data savings meanwhile 54.5% and 48.4% in Hungary and Vietnam respectively are sure about the security concerns. What affirms the need of cyber security education is the relatively high percentage of students (28.3% and 23% in Hungary and Vietnam respectively) trusting saving auto login information. On contrary to the similar behaviors in case of the two questions above, students' approach to the need of smartphone security protection (e.g. antivirus app) in these two countries differ significantly (CHI^2=11.713, p=0.003). This significant difference makes the behavior different in the combination of the three concerns (CHI^2=8.232, p=0.041) as shown in Table 4.

Table 4

Students approach to security protection on smart phone (Column N %)

Country	Hungary	Vietnam	Total
Q17_Have you noticed that when your smartphone is not responding, it is most probably considered as a virus infected device?	27.7%	29.7%	28.6%
Q18_Do you think that your smartphone needs security protection? (e.g., antivirus application)	82.5%	92.1%	86.6%
Q19_Do you think that saving auto login information in your smartphone is good from a security perspective?	39.4%	27.7%	34.5%
The table contains a multiple response set with "Yes" answers as percentage of group totals exclusively.			

Together with the improvement of smartphone, mobile banking has developed by the diffusion of mobile communication technology to become an innovative and essential service to people around the world. Mobile banking is defined as "the financial services delivered via mobile networks and performed on a mobile phone" which is the recent trend in banking transition [29]. The era of mobile banking has arrived; applications can be downloaded for the simplest mobile banking facilities onto mobile phones. Pop-up windows often induce one to save credit card information for future online services without calling attention to its dangers. Students in Hungary and Vietnam behave similarly in the use of mobile banking and submission of credit card information (country comparison: CHI^2=2.831, p=0.304) i.e. the more students use mobile banking the more they save their credit card information (Hungary: CHI^2=34.392, p=0.000; Vietnam CHI^2=9.923, p=0.000 and Cramer's V equals 0.421 and 0.289 respectively).

4.3 Cyber Security Dimension Items

Table 5 describes the summative descriptive analysis of the variables in the four dimensions applied for evaluating the cyber security behavior of respondents. The present analysis shows the Mean, Median, Mode and the Interquartile Range (IQR) in descending order. The dimension on password and online scam issues were the most relevant while in the other two dimensions, there were some constant items. It could be seen that all the respondents in general show their highest awareness in the case of not considering any amount of money for services offered by an online site. Due to the number of constant responses, university students in both countries have shown the least aware behavior in the dimension of social engineering issues.

This study applied the Cronbach's alpha to assess the reliability of the instrument. The statistical validation was performed for each item as well as for the overall model as shown in Table 5. The Cronbach's alpha values were in the range from 0.782 to 0.791 (Table 5) in which each item had a Cronbach's alpha coefficient over 0.78. The overall Cronbach's alpha value, of all four dimensions in Hungary, was 0.79 while the value, when texting all respondents in Vietnam, only was 0.804. Reliability is considered acceptable when this score exceeds 0.70 (Hair et al, 1998). The overall reliability is 0.794 with all the items included.

Table 5
Descriptive analytics and reliability of Cyber security dimension items

Item	*Mean*	*Median*	*Mode*	*IQR*	*Cronbach's Alpha if Item Deleted*
Dimension 1. Cyber security behavior on malware items					
29. I prefer to update information on my study via computer	3.78	4	5	2	Deleted
27. I trust any information sent from my university online learning management system	3.59	4	4	1	0.786
24. I can sense something is wrong if my smartphone runs extremely slow.	3.55	4	3	2	0.788
26. I will apply security patches to my phone as soon as possible.	3.38	3	3	1	0.791
28. I prefer to update information on my study via my smartphone	3.03	3	3	2	0.789
23. An interesting subject line makes me open an email attachment.	2.42	2	1	2	0.790
25. I'm willing to download materials from unsecure sites.	2.30	2	1	2	0.790
22. I'm willing to open email or message attachments from strangers.	2.18	2	1	2	0.786

Dimension 2. Cyber security behavior on password usage issues					
30. My password consists of lowercase, uppercase, numbers, special characters.	3.87	4	5	2	0.789
30. My password doesn't follow keyboard pattern.	3.35	3	5	3	0.790
36. I do use the "Remember my password" option in my phone.	3.15	3	4	2	0.785
32. I use a similar password for different applications.	3.12	3	4	2	0.782
34. My passwords are based on my personal information.	2.71	3	1	3	0.786
35. I never change passwords.	2.55	3	3	2	0.784
37. I keep my password somewhere in my phone.	2.41	2	1	3	0.789
31. I can share passwords with other people.	1.86	1	1	2	0.790
Dimension 3. Cyber security behavior on social engineering issues					
44. I wouldn't reveal any confidential information under any circumstances.	3.73	4	5	2	0.787
42. I check the authorization or identity of someone before talking on any issues.	3.55	4	3	1	0.788
43. I wouldn't communicate with a stranger although his/her looks warrant sympathy.	3.35	3	3	1	0.787
41. I'm not willing to respond to calls, SMS, or email messages to friendly/ non-threatening strangers.	3.28	3	3	2	0.785
40. I think I'm not a target of social engineering attacks due to student status.	2.78	3	3	1	0.785
39. I'm not interested in reading social engineering issues.	2.76	3	3	2	0.785
Dimension 4. Cyber security behavior on online scam issues					
47. I never trust strangers identity information given on the Internet.	3.45	3	3	2	0.791
49. I'm aware of and able to identify the latest online scams.	3.38	3	3	1	0.785
48. I never consider any amount of money for services offered by an online site.	3.19	3	3	3	0.786
50. I wouldn't hesitate to meet internet friends in person.	2.75	3	3	2	0.788
45. I established trusted online relationship with strangers.	2.36	2	1	1	0.786
46. I respond to SMS announcing contests involving huge sums of money.	1.96	1	1	2	0.794

The visual representation of the mean responses (Figure 5) shows a slight or weak difference between the responses of the students in the countries separately (the numbers represent the index of the statements in the Table 6). The correlation of mean responses for the items between Hungary and Vietnam, is r=0.985, which also suggests similar behavior, so further tools – independent samples t-test and the CHAID decision tree method for segmentation of categorical data – helped to find similarities and differences between the countries.

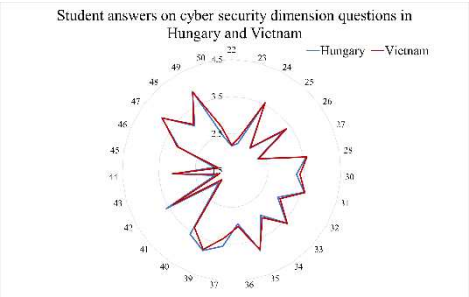

Figure 5

Student responses on cyber security dimension questions (source: edited by authors)

4.1.1 Significance of Cyber Security Dimension Items

The comprehensive reliability of the items in the dimensions of cyber security on smartphone for the two countries in question and the reliability of the individual items allow a comparative analysis between the students in these countries. In order to find the significant items in the dimension's independent samples t-tests were conducted on the items to compare the behavior in Hungary and in Vietnam (Table 6).

Table 6

Significant differences between Hungary and Vietnam

Independent Samples t-test	Levene's Test for Equality of Variances		t-test for Equality of Means		
	F	Sig.	t	df	Sig. (2-tailed)
23. An interesting subject line makes me open an email attachment.	1.030	0.311	-3.022	311	0.003
26. I will apply security patches to my phone as soon as possible.	0.091	0.763	-1.965	311	0.050
30. My password doesn't follow keyboard pattern.	3.608	0.058	3.515	311	0.001
31. I can share passwords with other people.	3.379	0.067	2.271	311	0.024

34. My passwords are based on my personal information.	0.491	0.484	-4.715	311	0.000
42. I check the authorization or identity of someone before talking on any issues.	0.481	0.488	-2.060	311	0.040

Out of the 27 items the behavior of students showed significant difference in case of 6 questions. Two items came from behavior on malware items, three from password usage and one from social engineering. Regarding the individual online scam issue items students behave similarly in these countries. In each case the variances proved to be equal in the population and in each case the p value for the independent t-test was below 5%, thus the test was significant. Most of the statements were on private and very personal aspect of cyber security like curiosity, personal password practices and trust in unknown individuals, which statements rather belong to cyber safety and there was only one statement specifically belonging to cyber security. The significant difference was confirmed with CHI^2 analysis due to the ordinal scale nature of responses in which process item 23, 30 and 34 also showed significant difference in the behavior.

5 Discussion on Behavior toward Cyber Security on Smartphone

The next step in the comparative analysis was to confirm these significant dimension items and to reveal further ones along which the behavior of the students is different in these two countries. For the specific analysis the CHAID (CHI-squared Automatic Interaction Detector) decision tree method was applied, which is a multivariable recursive classification process that can be used for categorical variable and can also be a segmentation process [30, 31, 32]. The categorical variable in this case is the country while the independent variables are the dimension items. The decision tree is applied because it provides a visual representation of the significant dimension items and represents the relationships between the dependent and the independent variables in a tree structure and makes the interpretation easier. The advantage of the CHAID method is that there are no restrictions on the measuring scale of the variables and their distribution, categorical variables can be used, as well as numerical variables for dependent and independent variables. Splitting is based on CHI^2 tests, and the algorithm first unifies the categories that are the least different concerning the categorical variable then splits according to the strength of the dependent variable. It stops when it finds an optimal tree depth and no relevant changes would happen in the segments. The Exhaustive CHAID method differs from CHAID by not having a stopping criterion. The decision tree method is used in the research to reveal the significant differences between Hungary and Vietnam. The splitting variables will be used to characterize the different behavior of students and identify the areas.

The SPSS program was used for growing the tree. All the statements were used as independent variables and the target variable was set to Hungary (Vietnam was set as target variable for a second running and resulted in the same decision tree), with the following criteria: the splitting node significance level was set to α=0.05, the minimum number of cases in the parent node was set to 30 while that of the child note to 10 due to the fact that the number of students from Vietnam was 124 and the goal was to gain a decision tree with sufficient depth. The maximum tree depth was set to 5 in order to gain as many significant splitting variables as possible. Even though, the decision tree grew 3 levels (Figure 6).

The decision tree levels show the significant items and also gives a priority order of significant items in the cyber security behaviors of students on smart phones. The 0 level presents the percentage and the numeric distribution of the students. The algorithm step by step selects the most significant items and creates segments in which the distribution of students from the two countries can be found. It can be concluded that students are split into three groups by item 34, then 2 items (24 and 30) with the same impact became the splitting items.

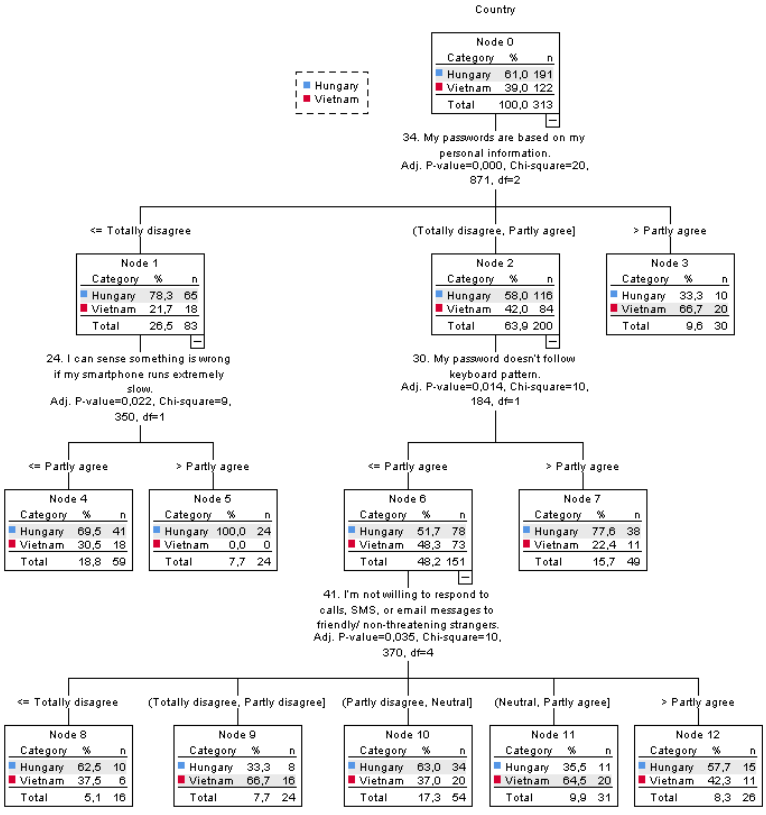

Figure 6
Splitting statements concerning behavior of students in Hungary and Vietnam

The level 1 splitting (34) put only 10 students from Hungary in the group more characteristic to the Vietnamese group. The *leftmost group* at level 1 is dominated by the students in **Hungary** which group is characterized by *high awareness of non-personal data for passwords* and *skeptical behavior with slow running of smart phones.* The *rightmost leaf* is *the least aware of password usage*, which group is assigned to **Vietnamese students**. The *second group*, which *pays attention to password usage on smart phones, avoids using keyboard patterns* (a second splitting item at level 2) but still *uses personal information* is also assigned to students in **Hungary**, in which case the less careful are further split into 5 groups by the item 41 linked to *social engineering*. At level 3 two groups are assigned to students in Vietnam and three groups to students in Hungary, and their behavior does not follow a consistent pattern. The behavior of students in this particular branch calls for the highest degree of education and awareness raising. It has to be noted that with the application of CHAID instead of exhaustive CHAID algorithm, the *rightmost group* at level 1 is further split by item 35 (I never change password) which further confirms *this group's lower level of awareness of password usage.* (The tree is not presented in the paper due to its length). At the same time in case of the most unsure group being either from Hungary or from Vietnam at level 3 (item 30 <= Partly agree) a new variable has become influential (item 31 – I can share passwords with other people.) and segments two groups one assigned to Vietnam (<= Neutral) and one to Hungary (>=Neutral).

Most of the students belong to the uncertain branch. The Exclusive CHAID algorithm reduces the decision uncertainty from 39% to 17.89% by level 4 ([6+8+20+11+11]/313=0.1789) which is a 21% reduction in uncertainty (i.e. error) compared to level 0. Table 7 gives the representation of the decision tree.

Table 7

The representation of the decision tree

Node	Hungary		Vietnam		Predicted Category		
	N	Percent	N	Percent		Sig.[a]	Split Values
0	191	61.0%	122	39.0%	Hungary		
1	65	78.3%	18	21.7%	Hungary	0.000	<= Totally disagree
2	116	58.0%	84	42.0%	Hungary	0.000	(Totally disagree, partly agree]
3	10	33.3%	20	66.7%	**Vietnam**	0.000	> Partly agree
4	41	69.5%	18	30.5%	Hungary	0.022	<= Partly agree
5	24	100.0%	0	0.0%	Hungary	0.022	> Partly agree
6	78	51.7%	73	48.3%	Hungary	0.014	<= Partly agree
7	38	77.6%	11	22.4%	Hungary	0.014	> Partly agree
8	10	62.5%	6	37.5%	Hungary	0.035	<= Totally disagree
9	8	33.3%	16	66.7%	**Vietnam**	0.035	(Totally disagree, partly disagree]

10	34	63.0%	20	37.0%	Hungary	0.035	(Partly disagree, Neutral]
11	11	35.5%	20	64.5%	**Vietnam**	0.035	(Neutral, partly agree]
12	15	57.7%	11	42.3%	Hungary	0.035	> Partly agree
a. Bonferroni adjusted							

Table 8 gives information about the leaves in the decision tree. The "node" information is the number of students in the segmented group and the proportion to the total number of students. The "Gain" shows the number of students segmented to the target group by the algorithm and the proportion to the total number of students in Hungary. The "response" is the proportion of students segmented by the target within the group and the "Index" is the ratio of the response % and the root target %. The higher the index the impact of the rule leading to that group is larger.

The model used to find extra significant variables that cause a different behavior of students in Vietnam and Hungary related to cyber security on smart phone is 69.6% accurate so there is a 30.4% probability of misclassification.

Table 8

Final segmentation by the decision tree

Node	Node		Gain		Response	Index
	N	Percent	N	Percent		
5	24	7.7%	24	12.6%	100.0%	163.9%
7	49	15.7%	38	19.9%	77.6%	127.1%
4	59	18.8%	41	21.5%	69.5%	113.9%
10	54	17.3%	34	17.8%	63.0%	103.2%
8	16	5.1%	10	5.2%	62.5%	102.4%
12	26	8.3%	15	7.9%	57.7%	94.5%
11	31	9.9%	11	5.8%	35.5%	58.1%
3	30	9.6%	10	5.2%	33.3%	54.6%
9	24	7.7%	8	4.2%	33.3%	54.6%

The decision tree method used allowed the researchers to identify two-two (item 24 and 41, and item 31 and 35) extra significant variables by the CHAID and the exhaustive CHAID methods while the significance of three variables that make the behavior of the students different were confirmed. Most of these variables belong to *password usage* while one belongs to *smart phone security* and *protection* and one to *social engineering*.

To answer the hypotheses questions, concerning the comparison of cyber security behavior of students in Hungary and Vietnam on smart phones, three methods were used and certain similarities and differences were found. Student behave *similarly concerning the use of LMS on smartphone* as well as *using mobile*

banking services and *saving credit card information* or *auto saving login information*. Analyzing the four dimensions of cyber security, student behavior proved to be relatively similar in the dimension of online scam, the *differences* cropped up regarding *password usage* – students in Vietnam tend to be less aware of cyber secure password usage than students in Hungary, on *smartphone security* issues and their *knowledge of cyber security and intention to learn more* on it (Figure 7).

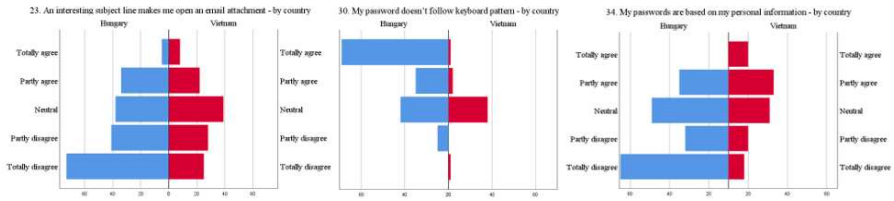

Figure 7

Differences in overall student behavior in three questions (item 23, 30, 34)

At the same time, the more uncertain students, tend to behave similarly both in Hungary and Vietnam and their behavior on certain social engineering issues proved to be significantly different. The exhaustive CHAID decision tree enables student segmentation identifying **highly aware students (Hungary), the least aware students (Vietnam)** and the **uncertain group** (partly Hungary and partly Vietnam) mainly *segmented by password issues and social engineering*.

The results confirm the need of education and training, at an early age, and also confirms that there are cultural differences in cyber security practices, in these two countries.

Conclusions

This study has targeted University Students' self-evaluating issues, in relation to cyber security dimensions, through survey for the purpose to investigate the level of awareness and behavior in cyber security via using smartphone. By choosing Hungary and Vietnam as the two countries for comparative analysis, the similarity and differences in the level of existing knowledge of cyber security, the level of awareness and behavior in cyber security, using smartphones were discovered and discussed. The findings of this study have shown results in all aspects, chosen for evaluating the current level of awareness and behavior in cyber security of respondents in both countries. It should be noted, that without any barriers of the different countries, the majority of all respondents, who are currently University Students, in different fields of study, are lacking not only a fundamental knowledge of cyber security, but also, good practices in their daily experiences while using their smartphones, beyond the differences in respondent's country. Importantly, the respondents have also shown their neglect of self-protection from threats of cyber security, by ignoring minor potential risks, while using their smartphone while connected to the Internet. Based on the research results, as

discussed herein, the study emphasizes the importance of a cyber-security formal education, that could directly support young users with a fundamental knowledge of this global issue, for self-prevention, from cyber threats. Through a comparative analysis between Hungary and Vietnam, it is shown that the findings of this research, contribute to the International Academic scheme, especially in the field of cyber-security for smartphones, using a different lens. Finally, the information in this study, can also provide basic data, for further relevant research, particularly in any comparative research for this emerging global issue.

References

[1] Jalali, M. S., Siegel, M., and Madnick, S.: "Decision-making and Biases in Cybersecurity Capability Development: Evidence from a Simulation Game Experiment". *Journal of Strategic Information System*, 28(1) 2019, pp. 66-82

[2] Zwilling, M., Klien, G., Lesjak, D., Wiechetek, Ł., Cetin, F., and Basim, H. N.: "Cyber Security Awareness, Knowledge and Behavior: A Comparative Study", *Journal of Computer Information Systems*, 2020, pp. 1-16

[3] World Bank Group.: "Vibrant Vietnam, Forging the Foundation of a High-Income Economy", The World Bank, Washington, 2020, World Bank Document

[4] Pieskä, S., Luimula, M., and Suominen, T.: "Fast Experimentations with Virtual Technologies Pave the Way for Experience Economy". *Acta Polytechnica Hungarica*, 16 (6), 2020, pp. 9-26

[5] Digital in 2020//We are social, 2020 [Online] URL: https://wearesocial.com/digital-2020

[6] Digital 2020: Global Digital Overview // Datareportal, 2020 [Online] URL: https://datareportal.com/reports/digital-2020-global-digital-overview

[7] Digital 2020: Hungary//Datareportal, 2020 [Online] URL: https://datareportal.com/reports/digital-2020-hungary

[8] Digital 2020: Vietnam//Datareportal, 2020 [Online] URL: https://datareportal.com/reports/digital-2020-vietnam

[9] The World Bank Open Data,: 2021 [Online] URL: World Bank Open Data | Data

[10] O'Dea, S.: "Forecast of smartphone user numbers in Hungary from 2015 to 2025", Statista, 2020 [Online] URL: https://www.statista.com/statistics/566122/predicted-number-of-smartphone-users-in-hungary/

[11] Karabasevic, D., Stanujkic, D., Maksimović, M., Popovic, G., and Momcilovic, O.: "An Approach to Evaluating the Quality of Websites Based on the Weighted Sum Preferred Levels of Performances Method". *Acta Polytechnica Hungarica*, 16 (5), 2019, pp. 195-215

[12] Senthilkumar, K., Sathishkumar, E.: "*A Survey on Cyber Security awareness among college students in Tamil Nadu*". IOP Conference Series: Materials Science and Engineering, 2017, 263, pp. 1-10

[13] Khalid, F., Daud, M. Y., Rahman, M. J. A., and Nasir, M. K. M.: "An Investigation of University Students' Awareness on Cyber Security". *International Journal of Engineering & Technology*, 7(4), 2017, pp. 11-14

[14] Reid, R., and Niekerk, J.: "*A Cyber Security Culture Fostering Campaign through the Lens of Active Audience Theory*". In Proceedings of the nineth International Symposium on Human Aspects of Information Security & Assurance, 2015, pp. 34-44

[15] Allen, I. E., and Seaman, J.: "*Learning on demand: Online education in the United States*". Sloan Consortium, Newburyport, 2010

[16] Luyt, I.: "Bridging spaces: Cross-cultural perspectives on promoting positive online learning experiences". *Journal of Educational Technology Systems*, 42, 2013, pp. 3-20

[17] Ivanova, M.: "ELearning Informatics: From Automation of Educational Activities to Intelligent Solutions Building". *Informatics in Education*, 19(2), 2020, pp. 257-282

[18] Abawajy J.: "User Preference of Cyber Security Awareness Delivery Methods". *Behavior Information Technology*, 33(3), 2014, pp. 237-48

[19] Chin, A. G., Etudo, U., and Harris, M. A.: "On Mobile Device Security Practices and Training Efficacy: An Empirical Study". *Informatics in Education*, 15(2), 2016, pp. 235-25

[20] Lehto, M.: "*Cyber security competencies: cyber security education and research in Finnish universities*". ECCWS2015-Proceedings of the 14th European Conference on CyberWarfare & Security: ECCWS 2015, University of Hertfordshire, Academic Conferences and Publishing International Limited, 2015, pp. 179-88

[21] Shropshire, J., Warkentin, M., Johnston, A., and Schmidt, M.: "*Personality and IT security: an application of the five-factor model*". AMCIS 2006 Proceedings, Acapulco, Mexico, 2006

[22] Parsons, K., McCormac, A., Pattinson, M., Butavicius, M., and Jerram, C.: "A study of information security awareness in Australian government organizations". *Information Management & Computer Security*, 22 (4), 2014, pp. 334-345

[23] McCormac, A., Calic, D., Parsons, K., Butavicius, M., Pattinson, and M., Lillie, M.: "The effect of resilience and job stress on information security awareness". *Information Computer Security*, 26(3), 2018, pp. 277-289

[24] Hadlington, L.: "Employees Attitudes Towards Cyber Security and Risky Online Behaviours: An Empirical Assessment In The United Kingdom". *International Journal of Cyber Criminology*, 12(1), 2018, pp. 269-81

[25] Pendley, J. A.: "Finance and accounting professionals and cybersecurity awareness". *Journal of Corporate Accounting Finance*, 29(1), 2018, pp. 53-58

[26] Reid, R., and Van Niekerk, J.: "Decoding audience interpretations of awareness campaign messages". *Information Computer Security*, 24(2), 2016, pp. 177-93

[27] McCormac, A., Zwaans, T., Parsons, K., Calic, D., Butavicius, M., and Pattinson, M.: "Individual differences and information security awareness". *Comput Human Behav*, 69, 2017, pp. 151-56

[28] Xu, T. D. T., Polyakova, N., and Shipilova, S. S.: "*Social Internet-networks in the life of Vietnamese students*". HS Web of Conferences, 28 (01101), 2016

[29] Alampay, E. A., and Moshi, G. C.: "Impact of mobile financial services in low-and lower-middle-income countries: A systematic review". *Information Technologies & International Development*, 14, 2018, pp. 164-181

[30] Dudás, P.: "Segmentation using a decision tree", *Economica New* 9(2), 2018, pp. 49-54

[31] Kass, G.: "An exploratory technique for investigating large quantities of categorical data", *Applied Statistics*, 29(2), 1980, pp. 119-127

[32] Hámori, G.: "Characteristics of CHAID-based decision trees (A CHAID alapú döntési fák jellemzői)", *Hungarian Statistical Review* (*Statisztikai Szemle)* 79(8), 2001, pp. 703-710

Internet of Digital Reality: Infrastructural Background – Part II

György Wersényi[1], Ádám Csapó[2], Tamás Budai[1], Péter Baranyi[2]

[1] Dept. of Telecommunications, Széchenyi István University
Egyetem tér 1, Győr, Hungary
wersenyi@sze.hu, budai.tamas@sze.hu

[2] Dept. of Computer Science, Széchenyi István University
Egyetem tér 1, Győr, Hungary
csapo.adam@sze.hu, baranyi.peter@sze.hu

Abstract: Internet of Digital Reality (IoD) is a concept that extends the Internet of Things (IoT) with the management, transmission and harmonization of digital realities. IoD covers aspects of connectivity, accessibility and usability with respect to different cognitive entities present in the digital world, via a confluence of technologies including virtual reality, artificial intelligence and 2D digital environments, in a way that recognizes human factors and cognitive aspects as key issues. Devices, interfaces, and interacting entities can be enabled through IoD to share digital realities and to thereby build a new level of reality, using intelligent connections mostly based on immersive virtual scenarios and multi-modal interactions in both public and private networks. In this paper, we look into the infrastructural requirements of and challenges behind the Internet of Digital Reality, which must be solved in order to deliver a high-quality user experience while keeping the increasing complexity of these networks at bay.

Keywords: Digital Reality; Future Internet; Internet of Things; Internet of Everything; Internet of Digital Reality

1 Introduction

The term '*digital reality*' was discussed by the authors in Part I of this paper [1]. There, digital reality was defined as "*a high-level integration of virtual reality (including augmented reality, virtual and digital simulations and twins), artificial intelligence and 2D digital environments which creates a highly contextual reality for humans in which previously disparate realms of human experience are brought together*".

Internet of Digital Reality (IoD) is a set of technologies that enables digital realities to be managed, transmitted and harmonized in networked environments (both

public and private), focusing on a higher level of user accessibility, immersiveness and experience with the help of virtual reality and artificial intelligence. Connections among various cognitive entities also have to be handled not only at the end user level of virtual reality displays and software, but also at the levels of network protocols and network management, physical media (wired or wireless), hardware interfaces, and other equipment. AI is a key component of both digital reality and IoD, that enables a cohesion of context-driven content and intelligent network routing to emerge.

Internet of Things (IoT) introduced the world of networked "things" – e.g. sensors and actuators, wearables, digital twins – by integrating distributed computation with intelligent connections. Digital representations of physical entities in the real world can thus be connected, interacted with, managed, and they are able to communicate with each other even without constant human supervision. However, as artificial Intelligence, algorithms, and software robots are becoming sophisticated, reaching levels of partial or full autonomy, making decisions, and being able to evolve and mimic human actors in the virtual world, new possibilities are emerging, based on which the borders between users, operators and digital entities without physical counterparts are becoming blurred. These trends in intelligent data processing, curation and communication, together with the enhanced visual (and increasingly multi-sensory) experience provided by virtual reality technologies (including VR, AR and MR solutions, as detailed in Part I), IoT is gradually evolving into IoD [1]. This in turn raises aspects relevant to network infrastructure and capabilities, as well as various cognitive / human factors aspects, as well as legal and business issues, as described later in this paper.

To better understand the place in history and significance of IoD, it is important to consider how the means of interaction based on which humans can access information has evolved. In the earliest days of commercial IT, up until the late 1980s, the dominant means of interaction with digital systems happened through command-line interfaces (evolved from line terminals), like MS DOS. Then, in the 1990s, 2D graphical user interfaces became widespread (e.g., MS Windows) and the rapid adoption of 2D graphical web pages led to the dotcom boom. A natural next step of this evolution today seems to be to move forward and create 3D operating systems and the 3D Web – in fact, several recent papers clearly show that interactions, communication and analytics in 3D can be considerably more effective than in 2D. This transition, which we may refer to as the "*DOS – Windows – Spaces transition*" will require us to extend our view and understanding of the key terminologies that are in circulation today [1]. Adopting such a broader perspective is all the more important when we consider how artificial intelligence (AI) and the Internet-based network of AI systems are increasingly becoming a defining feature of our everyday digital environment. In order to increase the effectiveness of AI systems, it is important to enhance the level of communication between humans and AI – after all, data is

[1] It should be noted here that although Windows is the name of a proprietary operating system, here we use the word in its most general sense, to refer to the common experience of accessing applications through a 2D windowing system

often referred to as "the new oil" [2], without which even AI is powerless. Thus, it is suggested that today's Internet-based economy could benefit from merging with a new kind of 3D digital world enmeshed in big data, digital twins and AI.

In this paper, it is argued that besides changes in the *relationship* between natural cognitive systems (i.e. humans) and digital devices, a newly emerging, pervasive network of digital cognitive representations is also being formed, which is grounded on a combination of physical, biological and even virtual realities, but also supersedes them in important ways. This network is poised to become so deeply ingrained into daily life that it can be expected to radically alter the basic human experience, and can therefore be referred to as the **Internet of Digital Reality**. Further, in addition to this general notion of reality being altered, '*digital reality*' in this paper is also used in a particular sense of multi-modally accessible integration of VR, AI and 2D digital environments.

2 Evolution from IoT to IoE

Internet of Things (IoT) describes the network of physical objects – "things" – that are embedded with sensors, software, and other technologies for the purpose of connecting and exchanging data with other devices and systems over the Internet [3, 4, 5, 6].

Through time, the "things" underlying IoT have evolved due to the convergence of multiple technologies, capabilities for real-time analysis / machine learning, commodity sensors, and embedded systems. Traditional fields of embedded systems, wireless sensor networks, control systems, automation (including home and building automation), and others all contribute to enabling the Internet of Things. Today, smartphones and smart "things" each have a cloud representation. Not only for data but year by year more complex AI support. Therefore, whereas Internet of Things (IoT) was one of the first widespread terms used to focus on the connection between "non-human things" from simple sensors to complex highly integrated systems [7, 8, 9, 10, 11, 12], it is also a concept that is rapidly evolving and changing.

As a result, the concept of IoT has been and continues to be extended / qualified in many different ways. The **Internet of Nano Things (IoNT)** is a related concept in which the communication exists between nano-scale devices. The **Internet of Mission-Critical Things (IoMCT)** is used in critical missions such as rescue operations and on battlefields. The **Internet of Mobile Things (IoMT)** refers to communication between devices using mobile sensors [12].

The **Internet of Everything (IoE)** was defined by Cisco in 2013 as "*bringing together people, process, data, and things to make networked connections more relevant and valuable than ever before, turning information into actions that create new capabilities, richer experiences, and unprecedented economic opportunity for businesses, individuals, and countries*" [13, 14]. In this sense, IoE is the intelligent connection

of people, processes, data and things. It describes a world where billions of objects have sensors to detect measure and assess their status; all connected over public or private networks using standard and proprietary protocols. There is a fine line of difference between IoE and IoT and that is the intelligent connection. IoT is mostly about physical objects and concepts communicating with each other but IoE is what brings in network intelligence to bind all these concepts into a cohesive system. IoE is an extension of IoT which includes people, process, data and things in network connections.

Pillars of IoE are:

- People: Connecting people in more relevant, valuable ways.
- Data: Converting data into intelligence to make better decisions.
- Process: Delivering the right information to the right entity at the right time.
- Things: Physical devices and objects connected to the Internet and each other for intelligent decision making (IoT) [7]

However, IoE still does not deal with human factors, as the most important part, and other non-technological issues such as business, legal issues, and only partly with safety, security, ergonomics etc. Furthermore, it creates a hard boundary between "people" and "things".

The proliferation of fields called '*Internet-of-X*' (X being something different in each case) somewhat resembles the proliferation of more traditional fields focusing on different kinds of interactions – e.g. human-computer interactions, human-machine interactions, human-robot interactions etc. The emergence of such fields with similar concepts and methodologies (albeit applied to different contexts) was part of the impetus behind the definition of cognitive infocommunications (CogInfoCom) [15, 16, 17]. Similarly, we propose the term 'Internet of Digital Reality (IoD)' to partially integrate, partially complement and more importantly augment earlier notions of the form 'Internet-of-X'. After all, it can be argued that the real motivation behind all of these technological directions was always to merge, augment and share realities – an idea that is already present (excluding the network aspects) in Digital Reality. An overview of the relationship between IoT, IoE and IoD is shown in Figure 1.

3 Internet of Digital Reality – Technological Challenges

In one sense, IoD supersedes IoT and IoE where not only physical "things", but also complete digital reality are connected via a (public or private) network.

Today, cognitive entities and virtual / digital twins are strongly based on Internet connections [18]. Pillars of the Internet of Digital Reality include:

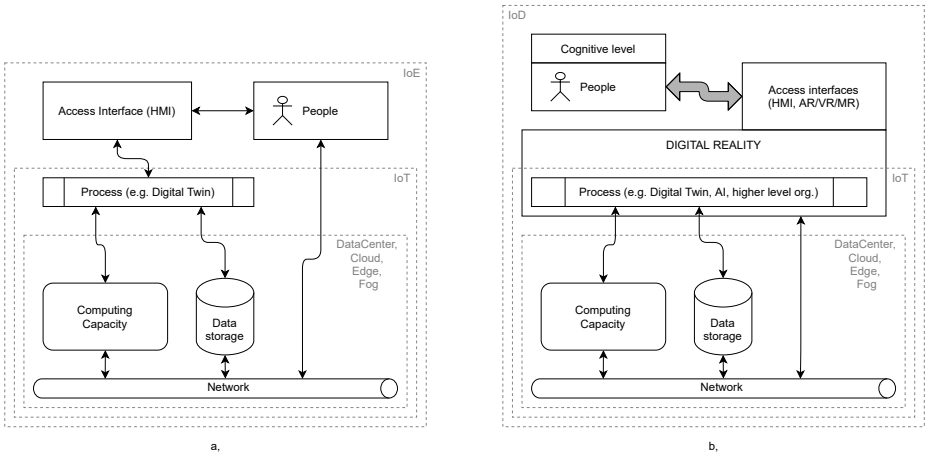

Figure 1
Overview of the different philosophies of IoT, IoE and IoD

- Cognitive entities (such as people, machines, "things", sensors, AI, digital twins, avatars, algorithms, bots, RPA, higher level organizations etc.) interacting in the digital realm.
- Information (data, web content, control).
- Communication networks (intelligent connection, wired and RF physical layers, public and private networks).
- Artificial intelligence, which gains new significance as a global network capable of distributed learning and continued evolution as digital realities become connected and shared across the globe
- Access devices and interfaces (headsets, tactile devices, AR/MR/VR spaces, 360-degree immersive scenarios, mobility and navigation)
- Cognitive infocommunications (sensation and perception, human factors and human-ICT co-evolution)
- Safety and security (data, information, or even the physical safety of the user etc.)
- Digital business and legal issues
- Digital Society (education, acceptance of technology, digital work, e-government, digital arts and gaming)

However, the most relevant aspect of IoD is that it connects digital realities, that is, combinations of technologies and data that create a higher-level functional integration. For example, IoD is the network through which combinations of 3D virtual

spaces and their real-world counterparts can be shared, together with all relevant data and interactive support for extended capabilities.

Since physical things may have digital twins, and in fact any single physical thing can have any number of digital twins, the connections between physical and digital can explode exponentially, causing “Big Data” and intelligent network management to play a crucial role in this equation. As a case in point, the volume and quality of internet traffic requires various improvements and new technological directions. For instance, today a remote cooperation on medical operations requires a very sophisticated and special internet solution in order to overcome latency and safety problems, however, when collaboration on 3D objects will grow increasingly common in VR environments, this technology will need to be generalised for popular cases, which also necessitates the integration of big data, AI and intelligent internet traffic management including the ability to address various security questions.

3.1 Cognitive Entities in the Digital World

Cognitive entities represented digitally are the basis of IoD. Cognitive entities can be conceived of as unique capabilities to effect change that arise via a merging and co-evolution of artificial and natural cognitive systems. This can include human beings, sensors, intelligent algorithms and more. The main characteristic of a cognitive entity is that its capabilities cannot be broken down along the borders between its constituents [16, 19, 20].

Cognitive entities can interact with each other, can be accessed (some only limited or by permission), and are able for transmit and/or receive information. Furthermore, they are present and "visible" in the virtual reality, thus, they offer access and communication interface of the highest level (e.g. during navigation and movement in the virtual space, via speech or any other interface suitable for communication in the virtual reality).

3.2 Communication networks

IoD can be implemented on a variety of communication networks, typically on multi-layered telecommunication networks, but high-speed wired or wireless connection will be a prerequisite. Currently available wired internet networks based on fibre optics, WLAN access points or the growing penetration of 5G (and beyond) mobile internet will serve as a network. Moving toward a future of being online and connected 24/7, RF networks providing access to the internet with mobile devices will stress the importance of 5G solutions for IoD [21, 22, 9].

It is important to emphasize, however, that not only does IoD depend on specific network technologies, it is also expected to shape them in novel ways, given the new requirements for e.g. QoS, logical network slicing and more, as detailed in Section 4.

3.3 Human Factors behind Accessing Devices and Interfaces

Cognitive infocommunications as a field integrates many aspects of human factors and users' perspective [23, 15, 24, 17]. Cognitive functions create boundaries and limitations around usability and accessibility and system designers have to deal with such issues by adopting a human centered approach.

Interfaces and devices that enable and establish the connections are also important from ergonomic and usability perspective. Especially in the case of headsets (audio and video playback) and VR gloves that give access to a fully tactile experience in IoD, issues of audio/video coding, spatial rendering, 3D vision, multichannel audio playback, sonification, speech production and recognition, spatial resolution of stimuli, latency, ergonomic design, sensation and perception of multimodal excitation signals are just some issues [25, 26, 27, 28].

Human factors, including how human users orientate, navigate, or get access to information influence the accessibility and usability of systems, especially if there are cognitive entities acting like other humans even when they have no human component.

IoD deals not only with the human perspective but also with all the other "needs" for cognitive entities to be operational. Even more importantly, IoD can be expected to shape what is meant by the concept of human factors in a way that is more integrated with the contextual details of daily life – e.g. where a user is situated, what devices a user has access to, what information the user is capable of providing as feedback.

3.4 Safety and security

Every communication system, including its components, raises safety issues, and therefore the need for security checks, authentication processes etc. [11]. In the case of IoD this is especially relevant, due to the personal or otherwise sensitive nature of the data involved, and the large variety of different cognitive entities interacting, often without knowing if they are human, artificial, a legal entity or some combination of these. A simple bank transfer that is currently effected on an internet-banking portal of a bank using credit card numbers can be later made in digital reality using gloves or speech communication with a virtual agent. Authentication, verification, transfer of sensitive data is therefore a point behind IoD applications. Furthermore, besides cybersecurity, people's physical safety during operation is a key part in immersive virtual environments (people can fall and get injured, or suffer from simulator sickness etc. [29, 30, 31]).

3.5 Digital Business and legal issues

From a non-technical point of view, a variety of business cases based on Digital Reality (trademarked by Deloitte) have emerged. According to Deloitte's definition, "*Digital Reality represents the next digital transformation. It changes how we engage with technology, through augmented-, virtual-, and mixed-reality, 360 video, and immersive experiences that are at once intuitive and data-rich, and which put the human user at the center of design.*" - with a strong focus on business cases using AR/VR [32, 33, 34, 35, 36, 37].

A recent analysis of cross-border e-commerce has revealed not only changes in costs related to trading goods but also changes in how people shop, consume, react to online ads and expect goods to be delivered [38]. As IoD is increasingly becoming a centerpiece of such services, new problems related to (and solutions to) various legal aspects are brought to light [39, 40, 41].

First of all, liability and responsibility in the digital world must be maintained, in order to increase trust in and acceptance of the technology [42, 43]. This aspect is clearly shown e.g. by the case of autonomous driving (i.e. who is to be held responsible when an accident occurs?).

The problem of intellectual property, copyright, original artwork vs. copies is even more significant in the digital and virtual world than before, given the ease with which artifacts can be copied. Virtual money (Bitcoin, Ether and others) and non-fungible tokens (NFT) – all of which are based on blockchain technology (see https://opensea.io/) – are expected to play a key role in this regard. An NFT is a unit of data that certifies a digital asset to be unique and therefore not interchangeable. NFTs can be used to represent the integrity and ownership of various types of digital files. While copies of these digital items are available for anyone to obtain, NFTs are tracked on blockchains to provide the owner with a proof of ownership that is separate from copyright and independent of how many copies of the digital item are made.

In immersive digital reality, where algorithms, deep learning solutions and more broadly speaking artificial intelligence have an active role to play, the question of who has the right to make certain decisions has far-reaching implications. If it is difficult to decide what kind of digital content and cognitive entities are present, and communicating with each other, there is an enormous risk for illegal activity from fraud to international terrorism and other activities.

3.6 Digital Society

Acceptance of new technology is a wide area to explore. Society includes not only technically educated individuals and experts, but also children, elderly users and people who are generally not familiar with and wary of new technologies. Increasing users' acceptance levels is a key point in all digital fields, not to mention in IoD

applications. Use cases in education, work, healthcare, e-government and administrative solutions etc. can help show the positive side of digital realities [44].

A Digital Society is a group of people who can use digital technologies to their benefit. The recent Coronavirus pandemic has shown how important it is for groups of people to be familiar with the same technological possibilities, whether they be related to education, shared working and / or home office environments, or whether they be simple tools of communication (as in the case of Zoom, Teams or Google Meet) [45, 46, 35]. Applications related to the fine arts and performing arts can also help familiarize soceity with the technological possibilities and far-reaching impacts of Digital Reality.

4 Connecting Digital Realities

Efficiency in communication is a key factor in any network. Efficiency can be increased if the network management is optimized for the requirements of common use cases and if the network can understand what entities are present and connected in the network. Network design and management optimization can be enhanced if the components of a digital reality can be grouped by some logic and functions in an actual task. Furthermore, they can be re-grouped or be a part of different set(s) of realities [47].

As an example, consider an 'integration' of a physical refrigerator, microwave oven, smart stove and deep fryer along with their corresponding digital twins, together with various further virtual objects in a shareable VR space, which also includes a 2D digital environment of collaborative cookbooks, cooking notes, cooking blogs, and video chats with a connection to the most renowned experts in the culinary arts – an example already detailed in Part I of this paper [1]. In such a scenario, the oven, stove and deep fryer, along with the various sensors, tablet displays etc. share the same physical network and instead of being independent or loosely connected, they may be logically grouped under the "cooking" label. At the same time, the smart fridge can be a member in the "what to buy at the grocery" group and the tablet can stream music as a member of the "infotainment" group. This might fit into the usual smart home and IoT concept, but IoD extends this in order for all of these components to be present in the same, integrated reality such that the user has access to all the relevant information and capabilities through AR/MR/VR glasses and/or haptic/tactile devices, voice commands and speech feedback and even AI-driven interfaces (e.g. chatbots) in a fully immersive way.

If the network is "smart" enough to be able to understand logically grouped components, it can be configured dynamically (and in an autonomous way), providing easy access for the user. The specific level of safety and security, communication and network management capabilities and key performance metrics (data rate, latency etc.) can be tailored to current requirements at any given time.

Increasing user experience relies also on reducing latency (increasing speed of control and feedback) in the system. By latency here we mean the time needed for handling an event initialized by inner status change of a component in Digital Reality, including the time for accessing, processing and transmitting of data over the network.The latency can be mission critical in some cases (real-time surgery, self-driving vehicle) in the order of milliseconds, but it can be also in the order of seconds, where time is not a limiting factor of the outcome.

Nowadays, different methods exist in computer networks for decreasing latency. In the case of IoD the following methods can be used or reconsidered, adapted to the needs of the network:

- QoS: different data types are sensitive to latency in different ways. The Quality of Service depends on the type of data (audio, video, etc.). In the scope of IoD QoS could be extended by differentiating network traffic not only by data-stream type, but by taking into account the logical grouping of entities.

- Logical Network Slicing: it would be beneficial, if logically grouped and geographically co-located digital entities shared the same physical network if possible allowing the shortest path for data transfer. Furthermore, fully digital entities such as algorithms, AIs not necessarily are near or of known origin. From the network side, a Software Defined Network can be helpful (that is a first class citizen in 5G), and from teh computing/resource side Cloud, Edge and Fog Computing.

- Multipath routing: in order to ensure low latency and add redundancy different network endpoints (e.g. WLAN, Mobile broadband and wired LAN) can be grouped and used together to transmit a single data stream [48].

- CDN: the idea behind a Content Delivery Network is that a logical digital entity (e.g. a movie file with audio and video) can be copied and multiplied. Copies then will be stored at different locations (servers), and users access the nearest provider for download or streaming. The question of copying is not only a technical problem (how do we make a replica of an AI?), but also a legal problem (property rights, copyright).

Conclusions

Part I of this paper introduced the concept of Digital Reality, which allows users to access, manipulate and interact with integrated sets of content – whether on display screens, immersive settings or overlaid on physical objects – that represent concepts and / or objects that can be both physical or digital, as well as both real or imagined. In Part II, an overview was given on Internet of Things and Internet of Everything, followed by a detailed discussion on the concept of Internet of Digital Reality. The discussion covered aspects relevant to technology, business use cases, legal issues and societal factors.

Acknowledgements This research was supported by the Digital Development Center in the national framework GINOP-3.1.1-VEKOP-15- 2016-00001 "Promotion and support of cooperations between educational institutions and ICT enterprises".

References

[1] P. Baranyi, Á. Csapó, T. Budai, and G. Wersényi, "Introducing the Concept of Internet of Digital Reality – Part I," *Acta Polytechnica Hungarica*, vol. 18, no. 7, pp. 225–240, 2021.

[2] C. Humby, "Data is the New Oil," *Proc. ANA Sr. Marketer's Summit. Evanston, IL, USA*, 2006.

[3] M. Rouse, "Internet of Things." `https://internetofthingsagenda.techtarget.com/definition/Internet-of-Things-IoT`, 2019.

[4] E. Brown, "21 Open Source Projects for IoT." `https://www.linux.com/news/21-open-source-projects-iot/`, 2016.

[5] ITU, "Internet of Things Global Standards Initiative," 2015.

[6] P. A. Laplante, M. Kassab, N. L. Laplante, and J. M. Voas, "Building caring healthcare systems in the Internet of Things," *IEEE Systems Journal*, vol. 12, no. 3, pp. 3030–3037, 2017.

[7] A. Banafa, "The Internet of Everything (IoE)," Aug 2018.

[8] S. Greengard, *The Internet of Things*. MIT press, 2015.

[9] S. Li, L. Da Xu, and S. Zhao, "5G Internet of Things: A survey," *Journal of Industrial Information Integration*, vol. 10, pp. 1–9, 2018.

[10] J. H. Nord, A. Koohang, and J. Paliszkiewicz, "The Internet of Things: Review and theoretical framework," *Expert Systems with Applications*, vol. 133, pp. 97–108, 2019.

[11] F. A. Alaba, M. Othman, I. A. T. Hashem, and F. Alotaibi, "Internet of Things security: A survey," *Journal of Network and Computer Applications*, vol. 88, pp. 10–28, 2017.

[12] C. Srinivasan, B. Rajesh, P. Saikalyan, K. Premsagar, and E. S. Yadav, "A Review on the Different Types of Internet of Things (IoT)," *Journal of Advanced Research in Dynamical and Control Systems*, vol. 11, no. 1, pp. 154–158, 2019.

[13] Cisco, "The Internet of Everything - Global Private Sector Economic Analysis." `https://www.cisco.com/c/dam/en_us/about/ac79/docs/innov/IoE_Economy_FAQ.pdf`, 2013.

[14] Cisco, "The Internet of Everything - Cisco IoE Value Index Study." `https://www.cisco.com/c/dam/en_us/about/business-insights/docs/ioe-value-index-faq.pdf`, 2013.

[15] P. Baranyi and Á. Csapó, "Definition and synergies of cognitive infocommunications," *Acta Polytechnica Hungarica*, vol. 9, no. 1, pp. 67–83, 2012.

[16] P. Baranyi, A. Csapo, and G. Sallai, *Cognitive Infocommunications (CogInfoCom)*. Springer, 2015.

[17] J. Katona, "A Review of Human–Computer Interaction and Virtual Reality Research Fields in Cognitive InfoCommunications," *Applied Sciences*, vol. 11, no. 6, p. 2646, 2021.

[18] D. Jones, C. Snider, A. Nassehi, J. Yon, and B. Hicks, "Characterising the Digital Twin: A systematic literature review," *CIRP Journal of Manufacturing Science and Technology*, vol. 29, pp. 36–52, 2020.

[19] P. Baranyi and A. B. Csapo, "Revisiting the concept of generation CE-Generation of Cognitive Entities," in *2015 6th IEEE International Conference on Cognitive Infocommunications (CogInfoCom)*, pp. 583–586, IEEE, 2015.

[20] L. I. Komlósi and P. Waldbuesser, "The cognitive entity generation: Emergent properties in social cognition," in *2015 6th IEEE International Conference on Cognitive Infocommunications (CogInfoCom)*, pp. 439–442, IEEE, 2015.

[21] E. Bastug, M. Bennis, M. Médard, and M. Debbah, "Toward interconnected virtual reality: Opportunities, challenges, and enablers," *IEEE Communications Magazine*, vol. 55, no. 6, pp. 110–117, 2017.

[22] A. A. Shchurov, "A multilayer model of computer networks," *arXiv preprint arXiv:1509.00721*, 2015.

[23] W. P. Neumann, S. Winkelhaus, E. H. Grosse, and C. H. Glock, "Industry 4.0 and the human factor–A systems framework and analysis methodology for successful development," *International Journal of Production Economics*, vol. 233, p. 107992, 2021.

[24] Á. Csapó and G. Wersényi, "Overview of auditory representations in human-machine interfaces," *ACM Computing Surveys (CSUR)*, vol. 46, no. 2, pp. 1–23, 2013.

[25] L. Xue, C. J. Parker, and H. McCormick, "A virtual reality and retailing literature review: Current focus, underlying themes and future directions," *Augmented Reality and Virtual Reality*, pp. 27–41, 2019.

[26] J. L. Rubio-Tamayo, M. Gertrudix Barrio, and F. García García, "Immersive environments and virtual reality: Systematic review and advances in communication, interaction and simulation," *Multimodal Technologies and Interaction*, vol. 1, no. 4, p. 21, 2017.

[27] Á. Csapó, G. Wersényi, H. Nagy, and T. Stockman, "A survey of assistive technologies and applications for blind users on mobile platforms: a review

and foundation for research," *Journal on Multimodal User Interfaces*, vol. 9, no. 4, pp. 275–286, 2015.

[28] S. Spagnol, G. Wersényi, M. Bujacz, O. Bălan, M. Herrera Martínez, A. Moldoveanu, and R. Unnthorsson, "Current use and future perspectives of spatial audio technologies in electronic travel aids," *Wireless Communications and Mobile Computing*, vol. 2018, 2018.

[29] E. Chang, H. T. Kim, and B. Yoo, "Virtual reality sickness: a review of causes and measurements," *International Journal of Human–Computer Interaction*, vol. 36, no. 17, pp. 1658–1682, 2020.

[30] K. Stanney, B. D. Lawson, B. Rokers, M. Dennison, C. Fidopiastis, T. Stoffregen, S. Weech, and J. M. Fulvio, "Identifying Causes of and Solutions for Cybersickness in Immersive Technology: Reformulation of a Research and Development Agenda," *International Journal of Human–Computer Interaction*, vol. 36, no. 19, pp. 1783–1803, 2020.

[31] S. Nichols and H. Patel, "Health and safety implications of virtual reality: a review of empirical evidence," *Applied ergonomics*, vol. 33, no. 3, pp. 251–271, 2002.

[32] Deloitte, "The Internet of Everything (IoE)." `https://www2.deloitte.com/us/en/pages/consulting/topics/digital-reality.html`, 2021.

[33] D. O. Baecker, "Digital Reality explained... in under 100 words." `https://www2.deloitte.com/ch/en/pages/innovation/articles/digital-reality-explained.html`, 2021.

[34] P. D. Ramani Moses, Nikita Garia, "Digital Reality – A technical primer." `https://www2.deloitte.com/insights/us/en/topics/emerging-technologies/digital-reality-technical-primer.html`, 2021.

[35] E. Mitrofanova, I. Bogatyreva, and V. Tarasenko, "Digital reality and perspective of the management of educational organizations," in *International Scientific Conference "Digital Transformation of the Economy: Challenges, Trends, New Opportunities"*, pp. 390–397, Springer, 2019.

[36] S. Sharma and C. Bach, "An exploratory research on virtual reality and how it affects future of shopping and immerging fields," *European Journal of Engineering and Technology Research*, vol. 1, no. 6, pp. 34–43, 2016.

[37] N. O. Stolyarov, E. S. Petrenko, O. A. Serova, and A. S. Umuralieva, "The digital reality of the modern economy: new actors and new decision-making logic," in *Institute of Scientific Communications Conference*, pp. 882–888, Springer, 2019.

[38] E. Gomez-Herrera, B. Martens, and G. Turlea, "The Drivers and Impediments for Cross-Border E-Commerce in the EU," *Information Economics and Policy*, vol. 28, pp. 83–96, 2014.

[39] M. R. Carrillo, "Artificial intelligence: From ethics to law," *Telecommunications Policy*, vol. 44, no. 6, p. 101937, 2020.

[40] J. S. Spiegel, "The ethics of virtual reality technology: social hazards and public policy recommendations," *Science and engineering ethics*, vol. 24, no. 5, pp. 1537–1550, 2018.

[41] W. K. Robinson and J. T. Smith, "Emerging Technologies Challenging Current Legal Paradigms," *Minn. JL Sci. & Tech.*, vol. 19, p. 355, 2018.

[42] K. Siau and W. Wang, "Building trust in artificial intelligence, machine learning, and robotics," *Cutter Business Technology Journal*, vol. 31, no. 2, pp. 47–53, 2018.

[43] M. Nogel, G. Kovács, and G. Wersényi, "Regulation of Digital Reality in Nutshell," in *12th IEEE International Conference on Cognitive Infocommunications (CogInfoCom)*, pp. 1–7, IEEE, 2021.

[44] H.-K. Wu, S. W.-Y. Lee, H.-Y. Chang, and J.-C. Liang, "Current status, opportunities and challenges of augmented reality in education," *Computers & education*, vol. 62, pp. 41–49, 2013.

[45] G. Makransky, S. Borre-Gude, and R. E. Mayer, "Motivational and cognitive benefits of training in immersive virtual reality based on multiple assessments," *Journal of Computer Assisted Learning*, vol. 35, no. 6, pp. 691–707, 2019.

[46] L. Freina and M. Ott, "A literature review on immersive virtual reality in education: state of the art and perspectives," *The international scientific conference elearning and software for education*, vol. 1, no. 133, pp. 10–1007, 2015.

[47] M. Handosa, H. Schulze, D. Gracanin, M. Tucker, and M. Manuel, "An Approach to Embodiment and Interactions with Digital Entities in Mixed-Reality Environments," in *2018 IEEE Conference on Virtual Reality and 3D User Interfaces (VR)*, pp. 569–570, IEEE, 2018.

[48] Á. Kovács, "Evaluation of the Aggregation Capability of the MPT Network Layer Multipath Communication Library and Multipath TCP," *Acta Polytechnica Hungarica*, vol. 16, no. 6, pp. 129–147, 2019.

Hungarian Food Consumers' Preferences, from the Aspect of Ethnocentrism

Mónika Garai-Fodor[1], Anett Popovics[2]

Keleti Károly Faculty of Business and Management, Óbuda University
[1]fodor.monika@kgk.uni-obuda.hu; ORCID: 1 0000-0001-7993-2780
[2]popovics.anett@kgk.uni-obuda.hu; ORCID: 20000-0003-3050-6953

Abstract: This paper highlights ethnocentric food consumption or the favoring of domestically produced food products. One of the theoretical pillars of the study is the trend toward ethnocentrism. Several studies proved that consumers are more positive about products from their own region. We would like to examine the Hungarians' opinion concerning their own products within the Hungarian food market. The other pillars of the theoretical background of the study are general food consumer behavior models and theories within the frame, of which, we analyzed the most important changes of the mindset of food consumers and the main structural diversion of food preferences. In the primary research, quantitative strategy, has been used, with the help of a pre-tested standardized questionnaire and snowball sample taking methods, 1447 questionnaires were evaluated. These research tools typically include closed-ended questions: selective, combinative semantic differential scales and ranking in the form of question types. The main aim of the research was to analyze the Hungarian consumers' preferences, for case of food consumption and characterize the most important target markets of the Hungarian food industry. We examined the attitude of the respondents toward Hungarian foods, from affective, cognitive and conative aspects. We also investigated the general food-consumer preferences of our respondents and the main elements of preference for Hungarian food consumption. As a result, we could characterize the most important features that Hungarian food-consumers associate with Hungarian food, we could also understand the advantages and disadvantages of various Hungarian foods. In addition, we could distinguish food consumer patterns, based on food consumption preferences. The results of this work can serve as an orientation for the players in the Hungarian food markets, to characterize their potential target markets and access the most important consumer groups, for the case of Hungarian food promotion.

Keywords: food consumption; preferences; ethnocentrism

1 Introduction

Food consumer behavior is a part of the human behavior spectrum. A variety of cultural, psychographic and personal factors affect the consumer's, final decision. As a result, in several cases, it is important to use a multidisciplinary approach when studying consumer behavior, so we can understand and explore the system of correlations that underlie consumer decision-making only by considering these variables together. Ethnocentricism, which serves as the study's theoretical foundation, is a term that can be explained in a variety of ways, including cultural, emotional and/or value system differences. We aim to briefly summarize these theories and present their connection points, supplementing it with generation specific consumer behavior characteristics.

1.1 Consumer Behavior of Hungarian Foods

Based on the literature, we can examine the consumer behavior of Hungarian foods on two levels. On the one hand, our image of the given product or brand is influenced by the country of origin, the "country-of-origin" image, a part of the image of a product, which is based on the origin of the product in a given country. On the other hand, research proves that the role of regional origin can be demonstrated on the levels of the purchasing decision process.

The factor related to the concept of country of origin image is the so-called consumer ethnocentrism, according to which ethnocentric consumers rely more on country-of-origin information, consider purchasing products from abroad incorrect because it endangers the domestic economy while non-ethnocentric consumers judge both domestic and foreign products on the basis of its quality. This effect is the strongest in the case of food purchases as consumers also develop a kind of nostalgia-based emotional attachment to Hungarian food brands (e.g. Túró Rudi) and, based on tradition, these products are also attributed to good quality [1].

According to the research of Verlegh and Steenkamp [2], if the consumer is confident enough that the origin of the product, the country of origin, guarantees good quality, then this factor demonstrably participates in the evaluation of the product. Otherwise, the consumer evaluates the product features one by one before making a purchase decision.

Although consumer ethnocentrism itself, belongs to the field of social psychology, its marketing-oriented consumer approach, has also provided the basis for a number of studies. Several consumer behavior surveys have shown that ethnocentrism influences purchasing decisions, affects both product evaluation and buying intentions [3, 4]. The consecutive ethnocentrism studies looked at buying intent and attitudes [5, 6].

It is essential to emphasize that both economic growth and consumer welfare have an effect on ethnocentrism [3, 7].

Consumers in economically developed countries have a higher level of confidence in goods made in their own country, so ethnocentrism is stronger while consumers in less developed countries have a much lower level of confidence in products made in their own country [8].

To understand consumers' motivations, they need to know their goals and knowledge of a particular product, as well as their attitudes, which together influence the decision-making process.

Some of the researches [9, 10] show that consumers have a more positive attitude towards products from their own region. The likelihood that a regional product will be included in the purchasing decision process depends to a large extent on how the consumer identifies it in the information gathering phase. Information about a regional product can be retrieved from memory when a purchasing problem occurs (internal information retrieval) or when the consumer encounters the product during the information retrieval phase (external information retrieval). Ittersum [9] found that consumers are interested in the region, information about the region, and therefore the increasing interest may enhance the likelihood of encountering the regional product. The perception of regional products is also related to culture: the more consumers are attracted to the culture of a given region, the more positive they are to regional products.

According to Chaney's [11] lifestyle model, food consumption is part of socio-cultural status, so food and drink are also indicators of taste, fashion, and demandingness among lifestyle traits. Regional foods also evoke nostalgia for the past when consumers were even younger or when they left, they spent his holiday in pleasant company. Especially people living in the city can evoke nostalgia for traditional flavors for rural holidays and rural pastimes. Local products re-evaluate the individual's cultural identity, these values and symbols contribute to the relocalization of culture [12].

The final conclusions of a series of Hungarian research were in line with the international findings. Hungarian products were normally devalued in Hungary at the time of the regime change, as opposed to those from Western countries [13, 14].

Berács and Malota [15] found that Hungarian respondents were generally positive about domestic products ten years later, but that the perception of products from developed countries was still more favorable.

Szakály et al. [10, 16] analyzed consumer habits and attitudes in the traditional Hungarian food market. Based on the results of the research, consumers understand the term traditional Hungarian food to be prepared only with Hungarian-flavored dishes prepared on the basis of an old recipe. 97% of the respondents consume some traditional Hungarian food, those who do not, they do

not buy the products due to the high price. The consumption of traditional foods is influenced by the taste and constant quality associated with the product, family preference and the quality guarantee brand. Further research has proved that the consumption of Hungarian food is part of everyday meal and cannot be linked to a specific festive or special occasion. People over the age of 40, one- and two-person households, and southern Hungarians are more likely to consume traditional foods.

In terms of food quality, it has also been shown that the quality of traditional foods is valued higher by consumers than by foreign products. More than 40% of the respondents think that the quality of Hungarian food is better than that of foreigners, and more than 80% of the respondents consider the average quality of traditional food to be good or excellent [17].

Median's [18] research has shown that Hungarian consumers make food choices based on the following order of importance: price, quality, health, Hungarian origin.

1.2 Generational Peculiarities in Consumer Behavior

The second literature pillar of our study is generation marketing.

As in our primary research we focused on the differences in food consumption due to age, we had to make a short overview of the most important features of Generation Z and Y, which were overrepresented, in our sample.

The values and ways of thinking of Generation Y and Z are characteristic only of them and different from the previous generations. Their consumer behavior and financial decisions can be influenced by the application of the appropriate communication strategy [19].

Törőcsik [20] examined the generational differences in food shopping in primary research, and found that young women shop with great enthusiasm and impulse, but store loyalty does not characterize them. Young men prefer to shop online rather than shopping in real life. Female members of the middle-aged generation either buy food with an action-sensitive, emotional charge, or in a functional, fast, goal-oriented way.

Examining the consumer habits of the Y generation, it can be said that compared to the previous generation, they have already grown up in the consumer society, all products have become available to them, they do not know the concept of a "shortage item". The motivations of their consumer habits move on several levels: on the one hand, they look for novelties, new experiences and are characterized by impulse buying. On the other hand, brand loyalty is not typical of them, they do not necessarily buy the most expensive, prestigious product. They prefer personalized options, comfort and flexibility in their decisions. Environmental awareness and social responsibility are also very important to them [21].

Based on the research of Varga [22] the offline purchasing decision of Generation Z is greatly influenced by the experience gained in the store. If they are attentive, they are kind in the store with them, if they feel they are an important customer, they value it more than gifts. The most popular and influential promotional tool is the discount but the need for entertainment, the shopping experience strongly influences the product choice of young people.

Generation Z has a strong purchasing power, but compared to members of Generation Y, the relationship with their parents is stronger, so their purchasing decisions are often made with them [23].

2 Method

In this study, in addition to the systematic processing of relevant domestic and international literature, we present the partial results of our primary research. We conducted quantitative research in the framework of primary data collection in the form of a pre-tested, standardized online questionnaire.

Subjects were recruited using a snowball sampling procedure, which resulted in 1447 questionnaires.

The research tool included only closed-ended questions, nominal measurement levels, single- and multiple-choice selective questions, Likert scale and a semantic differential scale to analyze consumer attitudes and values. Scale questions used a scale from 1 to 4. The reason for this is, on the one hand, the individual scale preference, which is typical of Hungarian respondents: due to the school classification system, our Hungarian respondents can interpret the scale up to five grades most stably against the 1-7, 1-9 or 1-10 scales.

We chose the even scale because in the case of the odd (1-5) scale, the mean value (3) is a kind of escape route, for the respondents. In the analysis of the attitude, in the case of those who choose the average value, the balance does not tilt in either direction, resulting in an excessive proportion of “indifferent” consumers, thus making it difficult to statistically and professionally evaluate segmentation [24]. Therefore, we opted for the even scale, which, by excluding the mean value, forces the respondent to take a more definitive position, thus better contributing to the successful segmentation. In addition, for the questions analyzed using the odd scale, it was not necessary for the mean, indifferent value to give either the “I don't know“ choice, because the cognitive level was filtered using separate questions.

The development of the topics of the research tool was realized as a result of the relevant secondary data analysis. Each response alternative was finalized – pre-tested of the research tool – in the light of qualitative results. As part of this

qualitative research phase, we conducted 10 mini-focus group interviews using a semi-structured interview outline. Qualitative sampling was also performed using the snowball method. The mini-focuses were group-directed conversations with a heterogeneous composition in terms of gender and age, with the participation of 3-4 people each. The main goal of the qualitative research was to establish the quantitative research, finalize the standardized questionnaire and outline the research hypotheses.

The topics of the quantitative research tool finalized as a result of the qualitative phase were the following: food buying habits, food consumption preferences, Hungarian food buying habits and domestic food consumption preference, assessment of Hungarian food (cognitive, affective and conative phase), socio-demographic data.

In the present study, we focus on the partial results of the quantitative phase of our research project. Within that, we also gave priority to food purchasing habits, possible segmentation opportunities based on preference, and the relationship of each food shopping segment to Hungarian food.

In the framework of quantitative research, we formulated one main and two sub-hypotheses. These are based on food consumer behavior theories [25, 26], that explain the buyer's decision, ethnocentric consumer behavior in the context of values [27, 28, 29]. What these concepts have in common is that an individual's consumer and consumer decision is interpreted as an external projection of their value system. [30, 31]. These hypotheses are:

(H1) There is a correlation between food customer preferences and attitudes towards Hungarian food.

(H1/a) Distinct consumer groups can be defined according to food consumer preferences

(H1/b) There is a statistically verifiable correlation between the segments formed according to the preferences of certain food buyers and the attitude towards Hungarian food.

In order to process the quantitative results and test the hypotheses, we used descriptive statistics, bivariate analyzes using SPSS 22.0 software. In case of the bivariate analyzes significance and F values were considered in the correlations examined by analysis of variance. In the case of Chi-square analyses, each relationship was subject to an internal correlation analysis based on the values of the corrected standardized residues (AdjR), which were interpreted as follows: Adj.R> = 2 indicates a positive deviation from the expected value with a 95% confidence level; Adj.R> = 3 indicates a positive deviation from the expected value with a 95% confidence level. In the case of a negative sign, the deviation from the expected value is negative at these value intervals [32].

3 Findings

3.1 Sociodemographic Characteristics of the Sample

60% of the respondents were women and 40% were men.

By age, 16-20 year olds had the highest proportion of respondents (31.1%), followed by young people aged 21-25 years. (24.5%). That is, more than half of the sample (55.5%) were respondents younger than 25 years, i.e., a member of Generation Z.

Unsurprisingly, in terms of age, 42% of respondents are single and 54% are married or in a cohabiting relationship. 42% of the respondents are residents of the capital, 38% live in cities and only 20% are residents of villages. In terms of educational attainment, those with secondary qualifications were absolutely over-represented (70%).

3.2 Food Shopping Habits

First, we examined the food buying habits of the respondents.

Sample members typically (32.8%) buy food themselves, and not surprisingly, the second most populous group (28.4%) who buy food with their parents in relation to the over-represented young target audience.

Table 1
Sample distribution by food purchasers

Those who buy food	Relative frequency % (several answers could be accepted)
Especially me	32.8
Typically my parents	28.4
Most of the time my spouse / partner	6.3
Typically me with my parents	12.2
Specialty shop	20.3
Especially me with my spouse / partner	32.8

Source: authors' own research, 2020 N= 1447

43.3% of respondents 27.3% buy food several times a week and 26.2% buy food twice a week.

The largest share (30.6%) was made up of those who spend between HUF 21,000 and HUF 30,000 on food on a monthly basis. The second most populous group of respondents (26.9%) spend between HUF 10,000 and HUF 20,000 for food.

The results show that respondents prefer discounts when buying food, and buy food at a specialty store the least.

Table 2

Food shopping locations in the sample

Type of market	Average (1= most often)	Standard deviation
Hypermarket	2.33	1.09
Supermarket	2.20	1.04
Discount	1.85	0.95
Convince store	2.68	1.09
Specialty shop	3.38	0.94
Traditional market	2.90	1.04

Source: authors' own research, 2020 N= 1447

The system of food preference was also examined separately. Based on the results, we observed the absolute dominance of comfort aspects, which, in our view is largely related to the fact that the majority of the sample members were young consumers under 25 years of age.

The durability, content value and easy accessibility of the food were the main aspects in the consumer preference system. The cheapness of food has also been relegated to the background in relation to these aspects. Given that discounts were preferred by subjects among the places where food is purchased, it can be assumed that the role of price already dominates in business choice and therefore additional considerations come to the forefront, in the case of product preference.

Table 3

Food purchase preference system in the sample

Aspects of food purchasing	**Average** (where 1 = not important at all, 4 = most important)	Standard deviation
Content values (taste, smell, calorie content)	**2.84**	1.02
Geographical origin (place of origin of the food)	2.26	0.98
Food must be cheap	**2.50**	0.92
Food must be on sale	2.34	0.93
Attractiveness of packaging	2.04	0.90
Food made exclusively from Hungarian ingredients	2.18	0.95
Brand	2.34	0.94
Practicality of packaging	2.22	0.90
Food durability, shelf life	**3.06**	0.96
Have a trademark on the packaging	2.25	1.00
Be easily accessible	**2.69**	1.00
Food advertising	1.75	0.86

Source: authors' own research, 2020 N= 1447

In terms of food shopping habits, overall, the majority of respondents buy food themselves, and prefer discounts. On a monthly basis, most respondents spend between HUF 21,000 and HUF 30,000 on food, the durability, content values and easy availability, are the main aspects in their selection, pushing the criterion of cheapness into the background.

3.3 Buying and Judging Hungarian Food

In the case of Hungarian foods, we also examined the criteria of food purchase separately, considering that our hypothesis H1 shows a difference compared to the normal food purchase preference. According to the results, the preference system for Hungarian foods has changed slightly: in the first place in this case, as well – although with a lower average value – the durability of the food came. In the case of Hungarian foods, the importance of the content values is more dominant compared to the general food purchase preference system, as well as the fact that it is made exclusively from Hungarian ingredients. Our respondents also pay more attention to the geographical origin when buying Hungarian food, but the cheapness of food is pushed into the background when buying Hungarian food compared to general food.

Table 4
Consumer preference for Hungarian foods

Aspects of purchasing	**Aspects of food purchasing**		**Aspects of Hungarian food purchasing**	
	Average (where 1 = not important at all, 4 = most important)	**Standard deviation**	**Average** (where 1 = not important at all, 4 = most important)	**Standard deviation**
Content values (taste, smell, calorie content,	**2.84**	1.02	**2.94**	1.09
Geographical origin (place of origin of the food	2.26	0.98	**2.51**	1.05
Food must be cheap	**2.50**	0.92	2.40	0.97
Food must be on sale	2.34	0.93	2.27	0.97
Attractiveness of packaging	2.04	0.90	2.01	0.89
Food made exclusively from Hungarian ingredients	2.18	0.95	**2.74**	1.05
Brand	2.34	0.94	2.35	0.96
Practicality of packaging	2.22	0.90	2.16	0.90

Food durability, shelf life	**3.06**	0.96	**3.00**	0.98
Have a trademark on the packaging	2.25	1.00	2.25	0.97
Be easily accessible	**2.69**	1.00	**2.64**	1.01
Food advertising	1.75	0.86	1.69	0.83

Source: authors' own research, 2020 N= 1447

In terms of the frequency of Hungarian food purchases, it surpasses normal food among the respondents: 47.5% of the respondents buy Hungarian food every day, 36% several times a week. According to the sample members, on average 30.33% of the food they buy is Hungarian food, which, in our opinion represents a rather large proportion.

We analyzed the opinions of the samples regarding Hungarian food, we were interested in how Hungarian food is perceived by consumers compared to normal food. According to the results, a significant part of the respondents (40.2%) do not perceive a difference in quality between Hungarian and normal food. However, there were a significant number (39.5%) who said that the quality of Hungarian food was better.

Table 5
Judging the quality of Hungarian food

The quality of Hungarian food compared to normal food	**Frequency (%)**
Right	**39.5**
Worse	5.7
Same	**40.2**
I do not know	14.7
TOTAL	**100.0**

Source: authors' own research, 2020 N= 1447

Regarding the reliability of Hungarian food, we obtained a similar value: the highest proportion was formed by the respondents who think that the reliability of normal and Hungarian food is the same. In this case, however, the range of those for whom Hungarian food is better was also significant in the case of reliability.

Table 6
Assessing the reliability of Hungarian food

Reliability of Hungarian food compared to normal food	**Frequency (%)**
Right	**37.5**
Worse	5.2
Same	**44.0**
I do not know	13.3
TOTAL	**100.0**

Source: authors' own research, 2020 N= 1447

Based on the affective component of the attitude towards Hungarian food, we could see that the vast majority of the sample is happy to buy Hungarian food because it supports domestic jobs.

Table 7
Judging Hungarian food

I like to buy Hungarian food because with this I support Hungarian jobs	**Frequency (%)**
Yes	**75.3**
No	27.7
The price of Hungarian food compared to normal food	Frequency (%)
Higher	44.3
Lower	13.4
Same	28.7
I do not know	13.5
Altogether	**100.0**
I only buy Hungarian food if it is cheaper than normal food	Frequency (%)
Yes	25.2
No	74.8
TOTAL	**100.0**

Source: authors' own research, 2020 N= 1447

The price of Hungarian food was considered high by a significant part of the sample.

In comparison, it is not even typical for the sample to buy Hungarian food at a special / cheaper price. Based on these answers, that is the reason, not the price or the price discount in the case of Hungarian food.

In the light of the results, it is also not typical for our respondents to buy Hungarian food out of fashion or to follow the behavior of their parents or friends.

Table 8
Motives of buying Hungarian food

Motives	**Frequency (%)**	
	Yes	No
I buy Hungarian food because it is fashionable and trendy	3.3	**96.7**
I buy Hungarian food because my parents buy it, too	**20.7**	79.3
I buy Hungarian food because my friends buy it ,too	**9.5**	90.5

Source: authors' own research, 2020 N= 1447

3.4 Purchase and Assessment of Hungarian Food as a Factor of Age

In order to test our hypothesis H2, we analyzed whether there is correlation between age and the extent of Hungarian food purchases. According to the results of the variance analysis (sig = 0.000) there is a statistically verifiable correlation between the two variables. Based on the values of the ANOVA table, it can be seen that the proportion of Hungarian foods purchased monthly increases with age.

Table 9
Proportion of Hungarian foods within the monthly level of food purchased (average)

Age groups	N (person)	Proportion of Hungarian foods within the monthly level of food purchased (average)
16-20 year	417	26.48
21-25 year	333	25.61
26-30 year	88	26.73
31-35 year	58	34.58
36-40 year	182	34.14
over 45 year	230	41.24

Source: authors' own research, 2020 N= 1447

In the course of the research, we also examined whether there is a correlation between the age of the respondents and the perception of Hungarian food. For this, we performed a Chi-square test, during which, the correlation could be detected based on Pearson's significance value (sig = 0.000). The corrected standardized residual (Adj.R) was used to analyze the internal correlations. In light of this, we could state that the proportion of respondents under the age of 25, i.e. Generation Z, was lower than expected or than those who rated the quality of Hungarian food as being better. However, among the respondents older than 36 years, i.e. belonging to Generation X, a larger proportion of respondents consider the quality of Hungarian food to be better than expected. Among those who considered the quality of Hungarian food to be the same, the proportion of young people was higher than the expected value and that of the older generation was lower. The same relationship is true for uncertain subjects ("don't know" answers).

According to the results of the research, we were able to establish a statistically verifiable correlation between age and the assessment of the reliability of Hungarian food (sig = 0.000). Based on the results, among the members of the older generation over the age of 45, those who considered Hungarian food to be more reliable were present in a higher percentage than expected, while in the case of young people (aged 16-20) they showed a smaller proportion than expected. In this case, too, the proportion of young people who considered the reliability of Hungarian food to be the same as normal food was higher than expected, and the proportion of young people over 45 was lower.

Table 10
Judging the quality of Hungarian food as a function of age

The quality of Hungarian food compared to normal food		Age groups						SUM (%)
		16-20 year	21-25 year	26-30 year	31-35 year	36-40 year	over 45 year	
Better	row %	21.8%	20.0%	7.6%	4.4%	17.2%	28.9%	100.0%
	column %	27.6%	32.3%	43.0%	41.0%	47.3%	60.4%	39.4%
	Adj.R	-6.1	-3.1	0.8	0.3	**2.5**	**7.8**	
Worse	row %	29.3%	34.1%	8.5%	3.7%	11.0%	13.4%	100.0%
	column %	5.4%	8.0%	7.0%	4.9%	4.4%	4.1%	5.7%
	Adj.R	-0.4	2.1	0.6	-0.3	-0.9	-1.3	
The same	row %	37.4%	26.8%	6.3%	4.9%	12.3%	12.3%	100.0%
	column %	48.3%	44.0%	36.0%	45.9%	34.6%	26.3%	40.2%
	Adj.R	**4.2**	1.7	-0.9	0.9	-1.8	**-5.2**	
I do not know	row %	39.5%	26.2%	6.7%	2.4%	13.3%	11.9%	100.0%
	column %	18.7%	15.7%	14.0%	8.2%	13.7%	9.3%	14.7%
	Adj.R	**2.9**	0.6	-0.2	-1.5	-0.4	**-2.8**	

Source: authors' own research, 2020 N= 1447

Table 11
Reliability of Hungarian food as a factor of age

Reliability of Hungarian food compared to normal food		Age groups						SUM (%)
		16-20 year	21-25 year	26-30 year	31-35 year	36-40 year	over 45 year	
Better	row %	23.9%	23.0%	6.9%	4.9%	14.4%	26.9%	100%
	column %	28.8%	35.1%	37.0%	42.6%	37.6%	53.3%	37.4%
	Adj.R	**-4.5**	-1.0	-0.1	0.9	0.1	**6.0**	
Worse	row %	37.3%	29.3%	6.7%	5.3%	12.0%	9.3%	100%
	column %	6.3%	6.3%	5.0%	6.6%	4.4%	2.6%	5.2%
	Adj.R	1.2	1.0	-0.1	0.5	-0.6	**-2.2**	
The same	row %	35.0%	26.0%	7.0%	4.3%	13.9%	13.9%	100%
	column %	49.4%	46.6%	44.0%	44.3%	42.4%	32.2%	43.9%
	Adj.R	**2.8**	1.2	0.0	0.1	-0.5	**-4.3**	
I do not know	row %	35.8%	21.8%	7.3%	2.1%	16.6%	16.6%	100%
	column %	15.5%	12.0%	14.0%	6.6%	15.6%	11.9%	13.5%
	Adj.R	1.5	-0.9	0.2	-1.6	1.0	-0.9	
SUM (N)		445	350	445	350	100	61	205

Source: authors' own research, 2020 N= 1447

Conclusions and Recommendations

As a conclusion of the research results, we could state that convenience factors increased, during food purchases and plays a more important role in the sample, than the price. The preference system of the Hungarian food purchase, shows a difference compared to the criteria of normal food purchases: The importance of the content values is more dominant as is the geographical origin and the fact that the food is made from Hungarian ingredients. However, the criterion of "cheapness" is pushed into the background when buying Hungarian food compared to general food (H1 has been confirmed).

We also examined how Hungarian respondents perceived Hungarian food compared to normal food. Based on the results, we found that a significant proportion of respondents (40.2%), do not perceive a difference in quality and most of them (44%), consider the two categories to be the same in terms of reliability.

Examining the motives for buying Hungarian food, we found that neither fashion nor following a pattern, within the family, characterizes the respondents.

Analyzing the correlation between the purchase of Hungarian food and age, in the light of the results, we were able to state that the proportion of Hungarian food in the consumer basket increases with the advancement of age (H2 / a). As we were able to prove statistically, that there is a correlation between age and the assessment of the reliability and quality of Hungarian food (H2 / b confirmed). Typically, the respondents belonging to Generation X, considered Hungarian food to be better and more reliable, the respondents of Generation Z (16-25 years old), rated Hungarian food as of the same quality and reliability, or they could not typically make a judgment.

According to the results, it can be said that the customers of Hungarian food, normally come from the members of Generation X, so according to age, they form the main target group. These consumers typically have a mature system of preferences and sufficient financial resources. In the case of the younger respondents (Generation Z), we could see many still insecure customers, the immaturity of their preference system, may be one of the main reasons why they do not statistically prefer Hungarian foods. Just as buying them is not considered a fashion pursuit, this trend would be worthwhile changing, knowing the values of a given generation. After all, trendy pattern-following, is dominant in their case, they are also looking for reference persons, samples, role models.

In our opinion, a communication campaign aimed at young people and involving them, could do a lot to promote Hungarian foods, among Generation Z. This can also be an important aspect, because the members of this generation, may soon represent a potential, solvent target group, with an independent income. In this form, they could play a significant role among Hungarian food consumers, in the future.

References

[1] Verlegh P.W.-Steenkamp J. (1999): *A Review and Meta-Analysis of Country of Origin Research*. Journal of Economy Psychology, Vol. 20. pp. 521-546

[2] Malota E. (2003): *Consumer ethnocentrism. The effect of stereotypes, ethnocentrism and image of national origin on the perception of domestic and foreign products*. Fogyasztói etnocentrizmus. A sztereotípiák, az etnocentrizmus és az országeredet-imázs hatása a hazai és a külföldi termékek megítélésére. PhD-értekezés, Budapesti Közgazdaságtudományi és Államigazgatási Egyetem

[3] Javalagi, G. R., Khare, P. V., Gross, C. A., & Scherer, F. R. (2005): *An application of consumer ethnocentrism model to French consumers*, International Business Review 14 (2005), pp. 325-344

[4] Khan, S. S., Yang, Y., Greaney, T., & Leung, P. (2020): *Who Leads the Price in Honolulu's Food Market? An Evaluation of the Competitiveness of Local Foods*, Journal of International Food & Agribusiness Marketing, 32 (5), pp. 464-481

[5] Sharma, S., Shimp, T. A., & Shin, J. (1995): *Consumer Ethnocentrism: A Test of Antecedents and Moderators*, Journal of the Academy of Marketing Science, 23 (1) pp. 26-37

[6] Klein, J. G., Ettenso, N. R., & Morris M. D. (1998) *The animosity model of foreign product purchase: An empirical test in the people's Republic of China*, Journal of Marketing, 62(1), pp. 89-101

[7] Shankarmahesh, M. N. (2006): *Consumer ethnocentrism: an integrative review of its antecedents and consequences*. International Marketing Review, Vol. 23, No. 2, pp. 146-172

[8] Wang, C., & Chen, Z. (2004): *Consumer ethnocentrism and willingness to buy domestic products in a developing country setting: Testing moderating effect*, Journal of Consumer Marketing, 21 (6), pp. 391-400

[9] Ittersum K. (2002): The role of region of origin in consumer decision-making and choice. PhD. dissertation, Mansholt Graduate School, Wageningen, Hollandia, 2002

[10] Szakály Z., Szigeti O., Szente V., Polereczki Zs. (2008): *Analysis of consumer habits and attitudes in the traditional Hungarian food market*. Fogyasztói szokások és attitűdök elemzése a hagyományos magyar élelmiszerek piacán. Kutatási tanulmány I-IV. Research Study I-IV. Budapest-Kaposvár

[11] Chaney D. (1996): Lifestylies, London: Routledge

[12] Ilbery B., Kneafsey M. (1999): *Niche markets and regional specialty food products in Europe*: towards a research agenda, environment and Planning. 31, pp. 2207-2222

[13] Csatáriné Dogi, I. (2015): Fogyasztói etnocentrizmust befolyásoló tényezők vizsgálata –szakirodalmi áttekintés *Analysis of affecting factors of consumer ethnocentrism a literature review* Journal of Central European Green Innovation 3 (3), pp. 37-44

[14] Németh, K., Birkner, Z., Katona, A., Göllény-Kovác, N., Bai, A., Balogh, P., Gabnai, Z., & Peter, E. (2018): *Can Energy be a "Local Product" Again? Hungarian Case Study*, Sustainability 2020, 12(3), 1118

[15] Berács, J., Malota, E. (2000): Fogyasztói etnocentrizmus, - az etnocentrizmus és az országeredet imázs kapcsolata a termékválasztásban. *Consumer ethnocentrism, - the relationship between ethnocentrism and country image in product choice*. Marketing & Menedzsment, 2000/2

[16] Szakály Z., Pallódé Kisérdi I., Nábrádi A. (szerk.) (2010): *Marketing in the traditional and regional food market.* Marketing a hagyományos és tájjellegű élelmiszerek piacán. Kaposvári Egyetem, Kaposvar University, 2010

[17] Popovics A. (2009): The possible role of geographical and traditional Hungarian products in food consumer behavior. A földrajzi helyhez kapcsolódó és a hagyományos magyar termékek lehetséges szerepe az élelmiszerfogyasztói magatartásban. PhD értekezés, PhD dissertation, Szent István Egyetem, Gödöllő

[18] Medián (2009): Should it be cheap or Hungarian? Olcsó legyen vagy magyar? - http://www.median.hu/printcikk.ivy?artid=7e7a6d29-ceb0-477d-b29a-3195f172ae15 (2019.09.01.)

[19] Garai-Fodor M., Csiszárik-Kocsir Á. (2018): *Validity of value-based consumer behavior models in the financial awareness of Generations Z and Y*. Értékrend alapú fogyasztói magatartásmodellek érvényessége a Z- és Y generáció pénzügyi tudatossága terén. Pénzügyi Szemle 2018/4, pp. 518-536

[20] Törőcsik M. (2017): *Consumer Behavior - Insight, Trends, Customers.* Fogyasztói magatartás – Insight, trendek, vásárlók. Akadémiai Kiadó, p. 225

[21] KPMG Tanácsadó Kft. (2018): *Consumer Drivers - What Drives a Versatile Consumer?* Fogyasztói mozgatóerők – Mi irányítja a sokoldalú fogyasztót? Kutatási tanulmány, https://home.kpmg/content/dam/kpmg/hu/pdf/KPMG_Fogyasztoi_mozgatoerok.pdf (2019.09.01.)

[22] Varga E. (2013): Living Generation Z and Promotion - Is Rewarding Expected? A Z generáció és a promóció megélése – elvárás a jutalmazás? OTDK dolgozat, 2013, pp. 29-53

[23] Pál E. (2013): *About the Z generation*. A Z-generációról. Pécsi Tudományegyetem, 2013, pp. 11-15

[24] Malhotra Naresh, K., Simon J. (2017): *Marketingresearch,* Marketingkutatás, Akadémiai Kiadó

[25] Horváth Á., Füredíné Kovács A., & Fodor M. (2005): *The effect of values on nutrition* Az értékrend hatása a táplálkozásra (In: Élelmiszer, táplálkozás, marketing, II. évf. (1-2)

[26] Horváth, A. (1996): A fogyasztói magatartás és az élelmiszerfogyasztás jellemzői. *Characteristics of consumer behavior and food consumption*. (PhD) Doktori értekezés, Doctoral Dissertation, GATE, Gödöllő

[27] Auruskeviciene, V., Vianelli, D., & Reardon, J. (2012): *Comparison of consumer ethnocentrism*. Transformations in Business & Economics, Vol. 11, No. 2, pp. 20-35

[28] Han, C. M. (1988): *The role of consumer patriotism in the choice of domestic versus foreign products*, Journal of Advertising Research, 1988, 3(1), pp. 25-32

[29] Liu, L., & Orth, U. (2021): *Cultural Differences in Design-Based Product Evaluation*: *The Role of Holistic and Analytic Thinking*, Sustainability, Vol. 13, 2775

[30] Gauthier, D. (1986): *Morals by Agreement Clarendon Press Oxford* In: S. Nagy, K. (szerk.) (2008): Értékek és Normák interdiszciplináris megközelítésben Values and Norms in an interdisciplinary approach Budapest: Gondolat Kiadó, 223 p.

[31] Hawkins, D.-Best R.-Coney K. (1992): *Consumer Behavior* 5th ed. Irwin, Boston M. A. In: Hofmeister-Tóth Á. (2003): Fogyasztói magatartás, Consumer behaviour Budapest: Aula Kiadó, 325 p.

[31] Sajtos L., & Mitev A. (2007): SPSS kutatási és adatelemzési kézikönyv, *SPSS Research and Data Analysis Manual* Budapest: Alinea Kiadó

Demand Forecasting in Python: Deep Learning Model Based on LSTM Architecture versus Statistical Models

Ing. Andrea Kolková, Ph.D., Ing. Miroslav Navrátil

VSB Technical University of Ostrava, Faculty of Economics, Department of Business Administration, Sokolská třída 33, Ostrava, Czech Republic
andrea.kolkova@vsb.cz, miroslav.navratil.st1@vsb.cz

Abstract: Demand forecasting for business practice is one of the biggest challenges of current business research. However, the discussion on the use of forecasting methods in business is still at the beginning. Forecasting methods are becoming more accurate. Accuracy is often the only criterion for forecasting. In the reality of business practice or management is also influenced by other factors such as runtime, computing demand, but also the knowledge of the manager. The goal of this article is to verify the possibilities demand forecasting using deep learning and statistical methods. Suitable methods are determined on based multi-criteria evaluation. Accuracy according to MSE and MAE, runtime and computing demand and knowledge requirements of the manager were chosen as the criteria. This study used univariate data from an e-commerce entity. It was realized 90-days and 365-days demand forecasting. Statistical methods Seasonal naïve, TBATS, Facebook Prophet and SARIMA was used. These models will be compared with a deep learning model based on recurrent neural network with Long short-term memory (LSTM) layer architecture. The Python code used in all experiments and data is available on GitHub (https://github.com/mrnavrc/demand_forecasting). The results show that all selected methods surpassed the benchmark in their accuracy. However, the differences in the other criteria were large. Models based on deep learning have proven to be the worst on runtime and computing demand. Therefore, they cannot be recommended for business practice. As a best practice model has proven Prophet model developed at Facebook.

Keywords: demand forecasting; deep learning model; TBATS; Prophet; SARIMA

1 Introduction and Literature Revue

At present, demand forecasting is gaining prominence in business economics research. Demand forecasting is now an integral part of corporate management, both operational and strategic management. Today, companies have to forecast a number of variables to be successful in the market, whether it is the number of

passengers for train seat planning [3], air traffic demand [28], electricity demand [10], demand forecasting in bike-sharing system [31], performing arts [25], forecasting call centre arrivals [23], LCD monitor market [17], or tourism [1]. The analysis of sales and demand is now insufficient and correct forecasting is a key source of information for companies.

This area of business management is also constantly expanding and increasing demands are being placed on the accuracy of forecasting. In this sense, researchers around the world have been developing new and expanding existing methods. Increasing studies are addressing the question whether methods based on machine learning can overcome the existing statistical models. An important contribution in this discussion is a study conducted by Makridakis [19], which has pointed out that machine learning methods cannot itself beat the statistical models in the accuracy of the forecasting. Another study [25], which focuses on the comparison of forecastign methods of COVID-19 active cases, also confirms the above-mentioned results. On the other hand, a study [7] conducted at the University of Porto concluded that the study presented by Makridakis is biased with low sample size. Each of the studies used different types of time series for its results.

Statistical methods are still used in business practice, namely, more complex or simple naïve methods or exponential smoothing. The ARIMA method is an often used example for forecasting in tourism in [1]. Already in the last century, statisticians have looked at whether simpler methods are better or worse than more complex ones [15], and at the beginning of this century, Zellner wrote about the need for simplicity of models in practice [32]. In 2018, Makridakis reopened this idea [19]. Time series forecasting is a topic that connects many disciplines [2], [26]. So far, no research has clearly identified the most appropriate method.

The goal of this article is to verify possibilities demand forecasting using deep-learnign and statistical methods. This methods will be used for of the company's 90-days and 365-days demand forecasting.

In this work, the naïve method will be used, it will also serve as a benchmark. Second method used is TBATS based on a study by DeLivera [8]. Another method used is Prophet, developed in practice by a team of experts from Facebook [29], and subsequently verified, for example [23]. Next method which will be used is SARIMAX, which is based on the Box-Jenkins model [6] and is used in pandemic predictions, for example H1N1 [16]. The last model, which will be used, is a deep learning model based on recurrent neural network with Long Short-Term Memory (hereafter only LSTM) layer architecture.

It is also important to mention that the resulting accuracy of the prediction is not necessarily a sign of the quality and usability of the model, but it is necessary to look at other factors, such as the computational demand of the prediction or the financial cost of maintaining such a model in real business operations. Gilliland [9], for example, states in his published discussion that even possibly increased accuracy of prediction, when using highly complex machine learning models, may

not have its justification in practical use, due to the above-mentioned factors. Among other things, this study aims to point out that future forecasting competitions should include more evaluation criteria and should focus more on real business usability.

2 Data Description and Methodology

The selected data set is divided into training data set and test data set, in the ratio 2/3: 1/3. As benchmark are used forecasting by the seasonal naïve forecast. This method are used to evaluate other advanced models.

All forecasts are modelled using Python. Python is being developed as an open source programming language with a number of other packages. It is an interpreted general-purpose project. It is often used for data analytics, but is also used for backend applications. For retrieve data is applied *Pandas* library, it is developed by Wes McKinney [20].

Pandas operate with the *Numpy* package, is is array-processing package and fundamental tool for Python scientific research. Used stucture is caled *data frame*, it can used a table or a two-dimensional array-like structure.

StatsModels and *PmdArima* (also called *PyramidArima*) libraries were also used in this study. Statsmodels was used for statistical tests and statistical data exploration.

2.1 Data Description

This study uses data from an e-commerce entity. E-shop is focused in the outdoor supplies for professional athletes. This company organizes outdoor training courses, seminars and competitions too. A lot of customers are in the B2B.

Individual daily demand form a data set. It is started at 1st September 2014 and ended 22th August 2020. Data set is geted using Google Analytics. Data set contains daily data of demand (number of conversions per day). Data is available at https://github.com/mrnavrc/demand_forecasting. All values was divided with the secret coefficient for trade secret, leading to a reduction in the size of demand in absolute terms. Does not change the trend, cycles and parameters necessary for forecasting. This was confirmed by the decomposition of the data. This decomposition confirmed the growing demand in the observed months in the summer months and in the period before Christmas. The cyclical development did not change throughout the observed period. Historical demand is graphically shown in Figure 1.

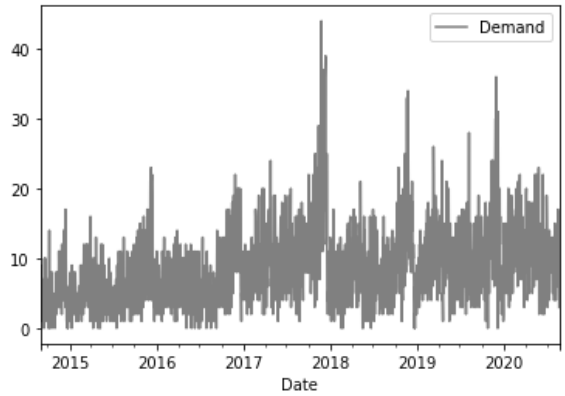

Figure 1
Demand of e-commerce entity from 1st September 2014 to 22th August 2020

Before forecasting, it is necessary to perform a statistical description and analysis of missing values and outliers. Missing values do not appear in the selected data file. There are some outliers. After analysis of the robustness of the selected models we decided let the outliers in the data set. In the histogram in Figure 2 we see the distribution of data around its mean value.

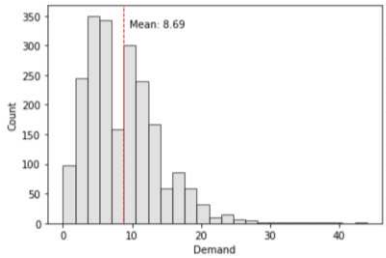

Mean:	8.69
Sum:	18966.00
Max demand:	44.00
Min demand:	0.00
Count:	2183.00
Median:	8.00
Std of demand:	5.44
Var of demand:	29.63

Figure 2
Histogram of demand of e-commerce entity

2.2 Applied Methods

The **seasonal naïve** forecast is based on the idea that the forecast will be equal to the previous period according to the selected time frame of the forecast. It is declarated [22]. This method is based on a simple formula (1).

$$\hat{y}_{T+h/T} = y_{T+h-m(k+1)} \text{ , where} \quad (1)$$

m is the seasonal period and *k* is the integer part of *(h−1)/m* (i.e. the number of complete years in the forecast period prior to time *T+h.)*

We make a demand forecast for the outdoor equipment, so can be expected a strong seasonal character. This could mean that this method will be too simple and less suitable for this data [12].

TBATS is acronym from the other models: **T**rigonometric seasonality, **B**ox-Cox transformation, **A**RMA errors, **T**rend and **S**easonal components [14]. This designation must be supplemented by appropriate arguments (ϖ, ϕ, p, q, m_1, $m_2 \ldots\ldots\ldots m_T$) to define Cox - Box parameters and damping parameters p and q to express the parameter of ARMA models and seasonal periodicity is expressed by arguments m_1, $m_2 \ldots\ldots\ldots m_T$. TBATS for modelling prediction automatically considers different models Box-Cox transformation. The best accuracy model will be chosen using Akaike information criterion [22]. The TBATS model is described by the relation (2).

$$\varphi \cdot p(L) \cdot \mu(L) \cdot y(\omega) \cdot t = \theta \cdot q(L) \cdot \delta(L) \cdot \varepsilon_t, \text{ where} \tag{2}$$

L is the lag operator, $\mu(L)$is $det(I-F \cdot L)$, $\delta(L) = w \cdot adj(I-F \cdot L)\ g \cdot L + det(I-208F \cdot L)$,

$\varphi \cdot p(L)$ and $\theta \cdot q(L)$ are polynomials of length p and q.

For this forecast we need around 298-461 seconds. TBATS is known for its high computational demand. The model applied grid research and no genetic evolution to set parameters faster.

Prophet is an open source library designed especially for business data forecasting. The prophet was developed by Facebook and has already been used in research [23]. Prophet uses the scikits-learn (*SKlearn*) library. It´s open-source library and contains functions for machine learning and statistical modelling. The model comes from a relationship (3).

$$y_t = g_t + s_t + h_t + \varepsilon_t, \text{ where} \tag{3}$$

g_t is the trend function, s_t is periodic changes, h_t is the effect of the holiday and ε_t is error.

It is possible to import public holidays and other events that affect demand into the Prophet model.

Based on the decomposition, it was found that this e-shop is significantly affected by Christmas, so it is included in the model. Other factors influencing the demand for sporting goods are sporting events such as the championship, Olympics, etc. The event can also be entered in prophet as an interval, many sporting events have an impact on demand many days before and after the event.

Model Prophet accuracy is based on a cross-validation function. In the model we can used accuracy by mean squared error (hereafter onlyMSE), root mean squared

erron (hereafter only RMSE), mean absolute error (hereafter only MAE), mean absolute percentage error (hereafter only MAPE) and coverage.

The *PmdArima* library contains the *auto_arima* function, which was used to calculate the **SARIMA** model. The model is based on arima models according to the relationship (4).

$$\widehat{y_t} = c + \emptyset_1 y_{t-1} + \emptyset_2 y_{t-2} + \cdots + \emptyset_p y_{t-p} + \varepsilon_t \tag{4}$$

Auto_arima work like grid-search. Defines a model in the form SARIMA (*p, q, d*). It means, that various sets of p and q (also P and Q for seasonal models) parameters are tested. The company sets whether it wants to select a model based on minimizes the Akaike information criterion (hereafter only AIC) or Bayesian information criterion (hereafter only BIC).

The parameters p and q are selected by the function itself using an automated iterative procedure. Parameter d must be set according to the stationarity tests, which are also part of the package. Prophet, for example, offers the augmented Dickey-Fuller test to test the stationarity and the Canova-Hansen test to test the seasonality.

This approach model parameters making is very time-consuming. It is better the stepwise function use. This stepwise function is definated by the strategy provided by Hyndman and Khandakar [13]. This model is currently considered to be the best model for step-in training process.

After determining the best model according to *auto_arima*, the *SARIMAX* function is used. This is part of the Statsmodels library. The result of *SARIMAX* is a diagnostic overview that can find a mistake or shortcoming in the semiautomatically approach [22]. After the diagnostic verified, a separate demand forecasting can be created.

The next model used is **Deep Learning**. For a deep learning model demand forecast it is used the *Keras* library. *Keras* library is high-level neural network application programming interface (hereafter only API). This library is created in Python. *Keras* supports convolutional networks, recurrent networks and their combinations too [22].

For demand forecasting by a deep learning using *Keras,* is difficult to adjust input data. Data set must be preprocessing and it must be converted to tensors. This is done by using the time series generator function. The deep learning model for demand forecasting can be demanding expertise and computing-time.

2.3 Multicriteria Approach to Method Evaluation

As mentioned, the prediction calculations will be performed for a period of 90 days and then for 365 days. The final evaluation is carried out on the basis of a multicriteria approach. The first evaluation criterion will be the degree of accuracy of the model.

Accuracy expresses the basic criterion for evaluating the quality of a model. In business practice, several indicators MAE, RMSE, MAPE and many others are used. The degree of accuracy decreases with the length of the forecast period. Forecasting can never be completely accurate, there is a certain amount of random component in each time series. MAE and MSE will be used in this study.

The mean absolute error (MAE), described relationship (5).

$$MAE = \frac{1}{M} \sum_{p=n+1}^{N} |y_p - \widehat{y_p}| \tag{5}$$

Some authors [18] point to the impossibility of comparing accuracy results between different time series. The MAE result is in units of original demand. In this paper, however, we have a time series of the same parameters, so the use of this criterion is possible.

The second accuracy used is MSE. This indicator is described by the relation (6).

$$MSE = \frac{1}{M} \sum_{p=n+1}^{N} \left(y_p - \widehat{y_p}\right)^2. \tag{6}$$

In the business situation, where the big error exponentially increases financial costs, is this parameter very important [4].

Another of the parameters of multicriteria comparison are runtime and computing demand. Not only the best accuracy is necessary to select the most suitable forecasting methods. Businesses usually do not have unlimited runtime or computing demand. Sometimes what can be calculated and predicted on campus, with the potential of using supercomputers and excellent computer equipment, is not realistic for business practice. These parameters are therefore crucial for evaluating the effectiveness of the methods used.

The last criterion is the complexity of the researcher's knowledge. Not all companies have top statistical experts and systems engineers. It is therefore necessary that financial and logistics managers be able to interpret or set methods in the company. Today, it is common for methods to be created by companies themselves (such as Google or Facebook), mainly due to the complexity of methods created in academic research.

3 Results

The results of the 90-days demand forecast according to the seasonal naïve method are shown in Figure 3 and Figure 4 for the 365-days demand forecast.

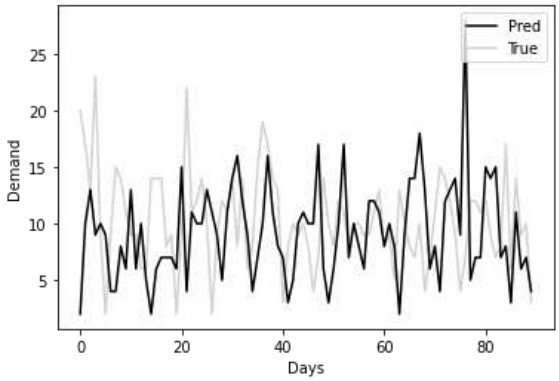

Figure 3
Results of 90-days demand forecasting using seasonal naïve method

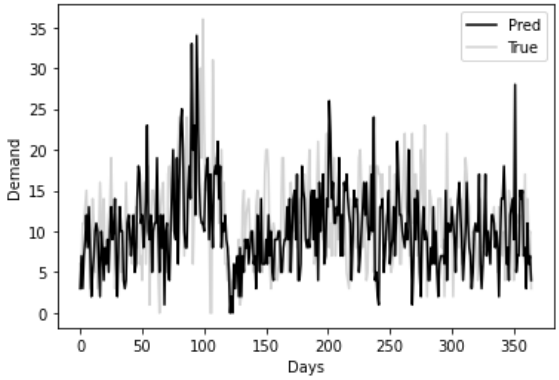

Figure 4
Results of 365-days demand forecasting using seasonal naïve method

Demand forecasting in Figure 4 shows, it will be very difficult to overcome the seasonal naïve forecast. Since the last period the demand changed only a little on data set and the seasonal patterns in demand stay constant. This is a problem with a change of weather in different seasons. This could mean a significant demand shift. Subsequently, there could be insufficient or, on the contrary, excessive supply and subsequent logistical problems.

When forecasting according to the TBATS method, an estimator including settings to handle multi-seasonality was selected based on the Akaike information

criterion, *estimator = 7,365*. Annual and weekly seasonality are including in estimator.

The results of this forecast are shown in Figures 5 and 6. Figure 5 expresses a 90-day demand forecast, Figure 6 for 365-days demand forecast.

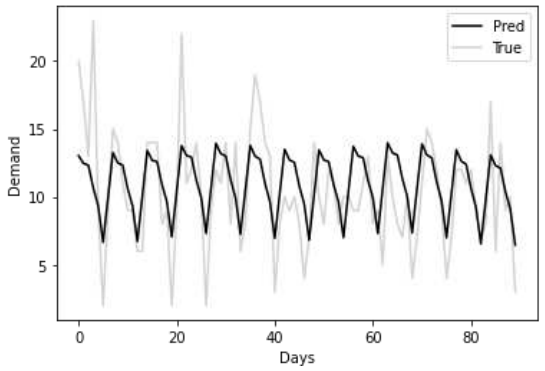

Figure 5
Results of 90-days demand forecasting using TBATS method

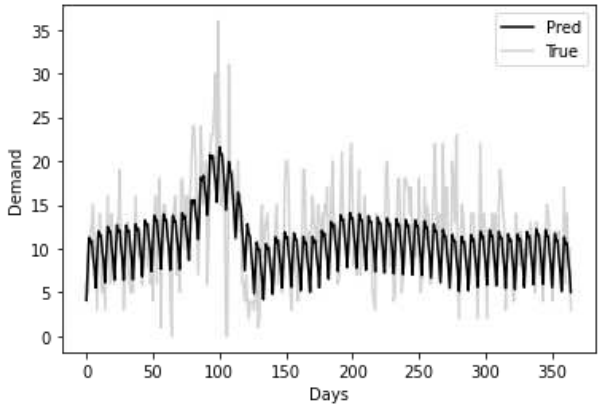

Figure 6
Results of 365-days demand forecasting using TBATS method

Based on the Prophet model, 90 and 365-days demand forecasts were again performed. The results are shown in Figures 7 and 8.

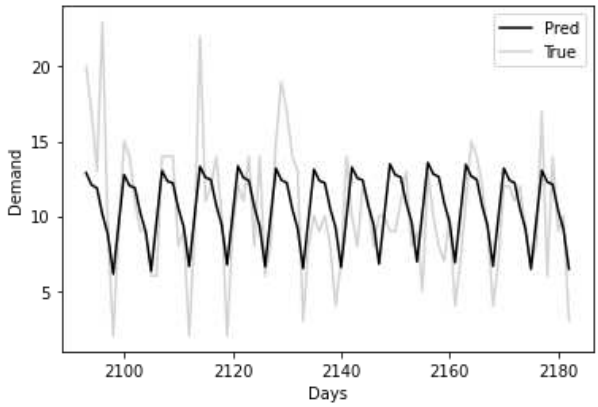

Figure 7
Results of 90-days demand forecasting using Prophet method

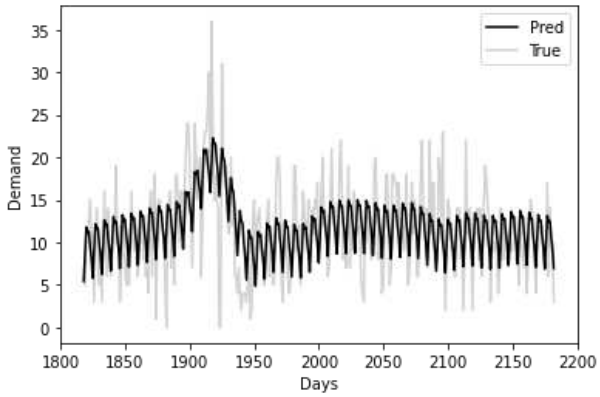

Figure 8
Results of 365-days demand forecasting using Prophet method

According to the methodology, the SARIMAX model was created. When evaluating the models, a model with parameters for 90 days,

SARIMAX (0, 1, 1) x (1, 1, 1, 7)

was selected by an automated process. For 365-days forecast,

SARIMAX (0, 0, 2) x (0, 1, 1, 7).

The resulting forecast is shown in Figures 9 and 10.

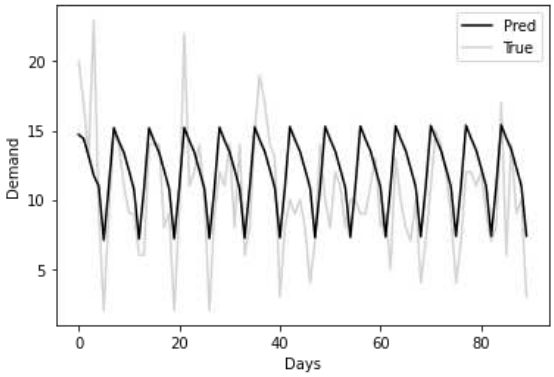

Figure 9
Results of 90-days demand forecasting using SARIMAX method

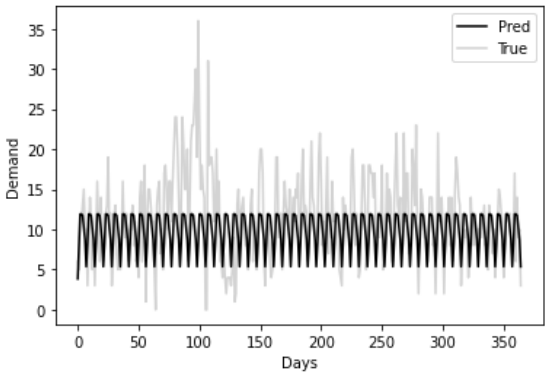

Figure 10
Results of 365-days demand forecasting using SARIMAX method

For Deep learning models, it is necessary to set more parameters. The calculation is therefore relatively demanding on the researcher's experience. Two models were chosen to solve the forecast using deep learning. The model A is based on shallow layers. Model B contains multiple hidden layer, so it is a deep neural network model to be able to compare both deep learning models. The only thing that will change will be the number of layers, and at the same time, both models must set around 360,000 parameters. This model should include more information, and be better to forecast demand curve [30]. This has not been confirmed. The model parameters are listed in Table 1.

Table 1
Parametrs Deep Learning models

Shallow Layers (model A)						**90-days demand forecasting parameters**
batch size	hidden layers	neurons	dropout	optimizer	epochs	
10	1	300	0.1	Adam	100	
Deep Layers (model B)						
batch size	hidden layers	neurons	dropout	optimizer	epochs	
10	3	405	0.1	Adam	100	
Shallow Layers (model A)						**365-days demand forecasting parameters**
batch size	hidden layers	neurons	dropout	optimizer	epochs	
10	1	30	0.1	Adam	100	
Deep Layers (model B)						
batch size	hidden layers	neurons	dropout	optimizer	epochs	
10	2	80	0.1	Adam	100	

The result of the deep learning MODEL A – shallow layer model for the 90-days forecast is shown in Figure 11 and of the deep learning MODEL B – deep layer in Figure 12.

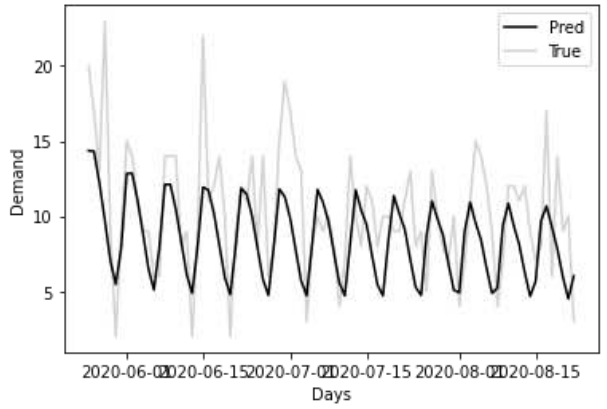

Figure 11
Results of 90-days demand forecasting using Deep learning MODEL A – shallow layer method

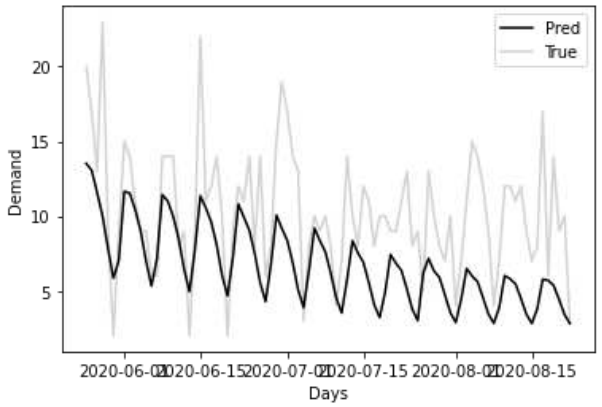

Figure 12
Results of 90-days demand forecast using deep learning MODEL B – deep layer method

The results of demand forecasting show that deep neural networks are not suitable for a simple univariete time series. Those models can be better for complex forecasting problems with mutlivariate data. The calculation of this model is even on an univariate date too time consuming, for this particular forecast the total computer time was 56 minutes. Therefore, it is not effective to continue optimizing for a possible improvement in accuracy.

For 365-days forecast and shallow layer, the results are shown in Figure 13 and deep layers in Figure 14.

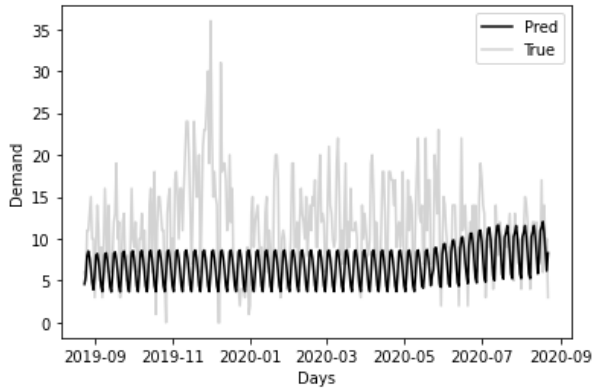

Figure 13
Results of Deep learning MODEL A – shallow layer method for 365-days demand forecast

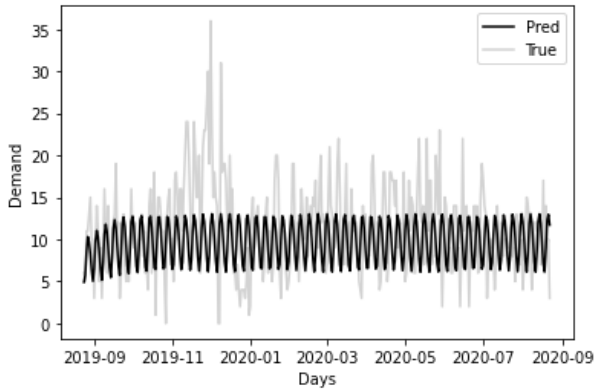

Figure 14

Results of Deep learning MODEL B – deep layer method for 365-days demand forecast

All models were evaluated on the basis of a multicriteria approach. Those criteria were the evaluation of MAE, MSE, runtime and computing demand and the knowledge and experience requirements of the researcher. All models based on the evaluation of accuracy (MAE, MSE) exceeded the benchmark of seasonal naive method. The individual criteria were evaluated in the order they received in the given criterion. Subsequently, the sum of the results of the individual orders was performed (lower is better).

As already mentioned, 5 criteria were evaluated, namely MAE, MSE, runtime, computing demand and researcher's expirence, namely on 90-days demand forecast and 365-days demand forecast.

In Table 2 are the results of multicriterial approach, which was applied in this study, based 90-days demand forecast. The Prophet model is under these criteria the best.

Table 2

Results of multicriteria evaluation models for 90-days demand forecast

90-days demand forecast										
Model		MAE	**Rank**	MSE	**Rank**	Runtime	**Rank**	**Computing demand - rank**	**Researcher's experience - rank**	Total Rank
Seasonal naive model		4.81	**5**	40.3	**6**	0.03s	**1**	**1**	**1**	14
TBATS		2.59	**2**	10.84	**2**	461.91s	**4**	**4**	**2**	14
Prophet		2.51	**1**	10.63	**1**	5.18s	**2**	**2**	**2**	8
SARIMA		2.94	**3**	12.98	**3**	17.94s	**3**	**3**	**2**	14
Deep Learning	**Shallow Layers**	2.94	**3**	14.6	**4**	2550.10s	**5**	**5**	**3**	20
	Deep Layers	3.94	**4**	24.09	**5**	3400.00s	**6**	**6**	**3**	24

Prophet also showed great results in the 365-days demand forecast, as shown in Table 3. In addition, the practical use of the Prophet model is supported by the conclusions of the already mentioned study, which suggested that information on promotions, holidays and events is very useful. This information can be very easily implemented into Prophet, so it further increases the possibility of use in practice. On the other hand, the exogenous time series that must be predicted (weather, macroeconomic data, etc.) did not bring any significant benefits [5]. And this is an area that needs more testing.

The worst results by this conditions achieved Deep learning model based on shallow layers and deep layers too. Especially for the 365-days demand forecast models using recurrent neural network showed the worst results, see Table 3. By 365-days demand forecasting is the best model Prophet, as well as by 90-days demand forecasting.

Table 3
Results of multicriteria evaluation models for 365-days demand forecast

365-days demand forecast										
Model		MAE	**Rank**	MSE	**Rank**	Runtime	**Rank**	**Computing demand - rank**	**Researcher's experience - rank**	Total Rank
Seasonal naive model		5.38	**6**	48.5	**6**	0.04s	**1**	**1**	**1**	15
TBATS		3.2	**2**	17.99	**2**	298.28s	**4**	**4**	**2**	14
Prophet		3.22	**1**	17.69	**1**	5.39s	**2**	**2**	**2**	8
SARIMA		3.64	**3**	24.84	**3**	88.62s	**3**	**3**	**2**	14
Deep Learning	**Shallow Layers**	5.27	**5**	46.33	**5**	1600.00s	**5**	**5**	**3**	23
	Deep Layers	4.85	**4**	37.5	**4**	3000.00s	**6**	**6**	**3**	23

Conclusions

The goal of this article was to verify the possibility demand forecasting using deep learning and statistical methods. Suitable methods are determined based on multicriteria evaluation. Accuracy according to MSE and MAE, runtime, computing demand and knowledge requirements of the manager were chosen as criteria. In this study was counted the forecast based on a deep learning method and based on statistical methods. Was realized by the e-commerce company 90-days and 365- days demand forecasting. Statistical methods Seasonal naïve, TBATS, Facebook Prophet and SARIMA were used. These models will be compared with a deep learning model based on recurrent neural network with Long short-term memory (LSTM) layer architecture.

The seasonal naïve model was chosen as a benchmark in this study. Visual presentation of the prediction indicated that it would be difficult to overcome this benchmark in univariate data. However, based on accuracy measures, the seasonal naïve model was eventually surpassed by all models.

The Propet model appears to be the most advantageous model for a company in the category of small and medium-sized enterprises. His demands for runtime, computing demand and researcher's experience were at a very good level. These parameters were surpassed only by the seasonal naive method, which had the worst accuracy. Prophet accuracy was the best for both the 90-days and 365-days demand forecast models. Therefore, the resulting multi-criteria comparison rated Prophet as the best.

The TBATS model according to the results can be called the second best. Its accuracy is comparable to the best model. However, TBATS is generally more computationally intensive and therefore its practical business use is likely to have its limitations.

Furthermore, this demand forecast indicate that SARIMA dont capture multi-seasonality and daily data. This is declareted other researches too [11]. SARIMA is also not suitable for practical use for demand forecasting due to its high degree of expertise of the processor and the manager working with the results of the model. Even though the resulting forecasting error is not so large, SARIMA cannot be recommended for wider business use.

The deep learning models exceeded the benchmark in the evaluation of accuracy measures and from this point of view they seemed applicable. However, their runtime and the need for high expertise put them in the last place. Small and medium-sized companies, such as the analysed one, usually do not have such computing capacity or relevant knowledge. The deep learning model can be improved. One option may be, setting better parameters as a study, which analysed Kaggles forecasting competitions, pointed out that a key to good performance of many machine learning models is the appropriate selection of hyperparameters and features [5]. However, this is not the subject of this study, because this study focuses only on comparing models in the basic setup without further optimization.

It may also indicated that machine learning models are not suitable for practical use in small and medium-sized companies due to high demands on finance and knowledge.

This is in in accordance with the results of the previous study by Makridakis [19]. His study declareted that on univariate time series classic statistical models is better to use than machine learning models.

Thus, this study supports the conclusion of a study that analysed Wikipedia web traffic and found that one of the weaknesses of recurrent neural networks is in modelling long-term dependencies such as yearly seasonality [5]. However, large multinational companies and companies engaged in professional forecasting invest a lot of money in the development of demand forecasting models. Therefore, neural networks may not be completely excluded now, their further development and possible further use for univariete data can be expected.

For smaller companies, however, this is not feasible. It is possible for them to use models only in the basic settings. Therefore deep learning models can be very helpful in predicting complex time series data with many exogenous inputs. Especially with the simultaneous use of statistical methods. After all, this was also confirmed by the M4 forecasting competition, where the best models include those based on a hybrid approach. In addition, another study suggests that the requirement for a successful use of machine learning models is cross-learning. That means using many time series to train a single model [27].

Acknowledgement

This work was supported by the Czech Science Foundation (GACR Project GA18-13951S).

References

[1] Andreeski, C. and Mechakaroska, D. Modelling, Forecasting and Testing Decisions for Seasonal Time Series in Tourism. Acta Polytechnica Hungarica, 2020, 17(10), pp. 149-171

[2] Farooq, U., Gu, J., Balas, V., Abbas, G., Asad, M. and Balas, M. A Hybrid Time Series Forecasting Model for Disturbance Storm Time Index using a Competitive Brain Emotional Neural Network and Neo-Fuzzy Neurons. Acta Polytechica Hungarica, 2019, 16(4), pp. 213-229

[3] Banerjee, N., Morton, A. and Akartunali, K. Passenger Demand Forecasting in Scheduled Transportation. European Journal of Operational Research, 2020, 286(3), pp. 797-810

[4] Barbieri, N. Approaches to Recommendations. 2014, California: Morgan and Claypool Publishers

[5] Bojer, C. and Meldgaard, J. Learnings from Kaggle's Forecasting Competitions. 2020, Work. Paper

[6] Box, G. E. P., Jenkins, G. M. and Reinsel, G. C. Time Series Analysis: Forecasting and Control. 1976, New York: John Wiley and Sons Inc.

[7] Cerqueira, V., Torgo, L. and Soares, C. Machine Learning vs. Statistical Methods for Time Series Forecasting: Size Matters. Machine Learning. ArXiv, 2019, abs/1909.13316

[8] DeLivera, A., Hyndman, R. J. and Snydera, R. D. Forecasting Time Series with Complex Seasonal Patterns Using Exponential Smoothing. Journal of the American Statistical Association, 2011, 106(496), pp. 1513-1527

[9] Gilliland, M. The Value Added by Machine Learning Approaches in Forecasting. International Journal of Forecasting, 2019, 36(1), pp. 161-166

[10] He, Y. X., Wang, M. Y., Guang, F. T. and Zhao, W. B. Research on the Method of Electricity Demand Analysis and Forecasting: The Case Of China. Electric Power Systems Research, 2020, 187

[11] Hyndman, R. Forecasting with Long Seasonal Periods. 2020, available at: https://robjhyndman.com/hyndsight/longseasonality/

[12] Hyndman, R. and Athanasopoulos, G. Forecasting, Principles and Practise. 2018, Middletown: Otext.

[13] Hyndman, R. and Khandakar, Y. Automatic Time Series Forecasting: The forecast Package for R. Journal of Statistical Software, 2008, 27(3)

[14] Hochreiter, S. and Schmidhuber, J. Long Short-term Memory. Neural computation, 1997, 9 (8), 1735-1780

[15] Chatfield, C. Simple is Best? International Journal of Forecasting, 1986, 2, pp. 401-402

[16] Choi S. B. and Ahn I. Forecasting Seasonal Influenza-Like Illness in South Korea after 2 And 30weeks Using Google Trends and Influenza Data From Argentina. PLoS ONE, 2020, 15(7)

[17] Lo, S. L, Wang, F. K. and Lin, J. T. Forecasting for the LCD Monitor Market. Journal of Forecasting, 2008, 27(4), pp. 341-356

[18] Macurová, P., Klabusayová, N. and Tvrdoň, L. Logistika, 2nd edition, 2018, Ostrava: VŠB-TU Ostrava

[19] Makridakis S, Spiliotis E. and Assimakopoulos V. Statistical and Machine Learning Forecasting Methods: Concerns and Ways Forward. PLOS ONE, 2018, 13(3)

[20] McKinney, W. Python for Data Analysis Book,: Data Wrangling with Pandas, NumPy, and IPython, 2nd edition, 2017, Sebastopol: O'Reilly Media, Inc.

[21] Millan-Ruiz, D. and Hidalgo, J. I. Forecasting Call Centre Arrivals. Journal of Forecasting, 2013, 32(7), pp. 628-638

[22] Navrátil, M. (2019) Comparison of Statistical Models with Deep Learning in Business Practice. Diploma thesis, VŠB –TU Ostrava, Department of Business Administration

[23] Navrátil, M. and Kolková, A. Decomposition and Forecasting Time Series in the Business Economy Using Prophet Forecasting Model. Central European Business Review, 2019, 8(4), pp. 26-39

[24] Ozhegov, E. M. and Ozhegova, A. Regression Tree Model for Prediction of Demand with Heterogeneity and Censorship. Journal of Forecasting, 2020, 39, pp. 489-500

[25] Papastefanopoulos, V., Linardatos, P. and Kotsiantis, S. COVID-19: A Comparison of Time Series Methods to Forecast Percentage of Active Cases per Population. Applied Sciences, 2020, 10(11)

[26] Parra, J., Fuentes, O., Anthony, E. and Kreinovich, V. Use of Machine Learning to Analyze and –Hopefully – Predict Volcano Activity. Acta Polytechnica Hungarica, 2020, 14(3), pp. 209-221

[27] Smyl, S. A Hybrid Method of Exponential Smoothing and Recurrent Neural Networks for Time Series Forecasting. International Journal of Forecasting, 2019, 36(1), pp. 75-85

[28] Solvoll, G., Mathisen, T. and Welde, M. Forecasting Air Traffic Demand for Major Infrastructure Changes. Research in Transportation Economics, 2020, 82

[29] Taylor, S. and Letham, B. Forecasting at Scale. The American Statistician, 2018, 72, pp. 37-45

[30] Wei, A. and Wei, J. Deep Learning Essentials: Your Hands-On Guide to the Fundamentals of Deep Learning and Neural Network Modelling. 2018, Birmingham: Pack Publishing

[31] Yang, Y. X., Heppenstall, A., Turner, A. and Comber, A. Using Graph Structural Information About Flows to Enhance Short-Term Demand Prediction in Bike-Sharing Systems. Computers Environment and Urban Systems, 2020, 83

[32] Zellner, A. Keep it sophisticatedly simple. Simplicity, Inference and Modelling: Keep it Sophisticatedly Simple, 2001, Cambridge: Cambridge University Press, pp. 242-262

Investigations of the Mechanical Properties of DLP 3D Printed Graphene/Resin Composites

Muammel M. Hanon[1,2*], Arsany Ghaly[3], László Zsidai[3], Zoltán Szakál[3], István Szabó[3], László Kátai[3]

[1] Mechanical Engineering Doctoral School, Szent István Campus, MATE University, Páter Károly u. 1, 2100 Gödöllő, Hungary; sharba.muammel.m.hanon@phd.uni-szie.hu

[2] Baquba Technical Institute, Middle Technical University (MTU), Muasker Al-Rashid Street, 10074 Baghdad, Iraq

[3] Institute of Technology, Szent István Campus, MATE University, Páter Károly u. 1, 2100 Gödöllő, Hungary; Ghaly.Arsany@stud.uni-mate.hu, zsidai.laszlo@uni-mate.hu, Szakal.Zoltan@uni-mate.hu, Szabo.Istvan@uni-mate.hu, katai.laszlo@uni-mate.hu

Abstract: Three-dimensional (3D) printing is an astonishing technology that has enabled the manufacturing of complex structures, with comparatively shorter times and the least material consumption. Currently, Graphene is gaining remarkable attention, as a filler material, used for the reinforcement of metal and polymer composites. In this paper, the 3D printing system, based on the digital light processing (DLP) method, is employed for the fabrication of bio-based resin specimens, to estimate their dynamic mechanical properties. For this purpose, two graphene concentrations (0.5 and 1 wt%) were mixed in resin (matrix) by a vortex mixer/shaker. The resultant mixture, in addition to the neat resin, was utilized for producing the test pieces, at three different layer thicknesses (35, 50, 100 μm). A comparison of the mechanical properties, between the DLP-printed neat resin and graphene/resin composite materials, was accomplished, to illustrate the impact of filler (graphene nanoplatelets) and the printing process settings (layer thickness). These determinants were assessed according to the microstructure and tensile characteristics of the examined materials. The results of scanning electron microscopy (SEM) showed a fairly even dispersion of graphene in the resin matrix. Moreover, it was found that smaller layer thicknesses provide a higher tensile strength. Further, a decrease in Young's modulus, tensile strength and elongation can be observed, with higher graphene concentrations.

Keywords: Photopolymerization; 3D Printing settings; Graphene platelets; Polymer composites; Tensile strength; Young's Modulus

1 Introduction

A universal method for enhancing the mechanical properties of machined items has not yet been suggested, despite the reports of numerous attempts. Thus, the investigation and development of new materials that demonstrate high potential outcomes are still being pursued. Graphene is one of the new materials exhibiting an extraordinary prospect for mechanical property enhancement. It has attracted considerable attention in the materials field over the last decade [1].

Due to the multi-functionality of this 2D-atomic crystal which combines unique properties, such as, high electron mobility (250,000 cm^2/Vs) at room temperature, elevated thermal conductivity (5000 W/mK), large surface area in the order of 2630 m^2/g, good electrical conductivity and a high modulus of elasticity, roughly 1 TPa, making it attractive for use in a broad range of applications [2]. The list of potential applications includes electromechanical systems, high-end composite materials, solar cells and supercapacitors [3].

Simultaneously additive manufacture (3D printing) is gaining more and more momentum owing to its versatility [4]. The ability of 3D Printing to create solid bodies layer by layer is magnificent [5] [6]. In mechanical engineering today's world, the applications of additive manufacture are very useful for the development and research of various components, covering from simple structures utilized in everyday life, up to complicated elements, in aerospace applications [7]. 3D printing supplies many advantages, such as, precision, simplicity, reliability, etc. [8].

One of the earliest additive manufacturing techniques was Stereolithography (SLA or SL) also known as optical fabrication, stereolithography apparatus, resin printing, or photo-solidification, which was invented by Chuck Hull in 1984 [9]. It harnesses the power of light, especially the ultraviolet light (UV), to cause chemical monomers and oligomers, to cross-link together, to create polymers, this process is called polymerization [10]. Digital light processing (DLP) is an additive manufacturing technology, also based on the photopolymerization principle, as SLA [11]. This method uses photocurable resins (polymer) to rapidly build an individual layer, of the desired 3D object, through spatially controlled solidification, using ultraviolet projected light [12]. It is characterized with less shrinkage, high resolution, produces smooth surface elements and fast performance [13] [14].

The study of graphene-based composites' mechanical properties is becoming increasingly common in academia and industry. Three techniques are being used to prepare graphene-composite or graphene oxide-composite:

In situ intercalative polymerization, where graphene or graphene oxide is first swollen (in the liquid monomer), then a suitable initiator is dispersed and polymerization reaction progresses by heat or radiation [15].

Melt intercalation, graphene or graphene oxide is mechanically mixed with polymer (thermoplastic) at raised temperatures [16]

Solution intercalation, which involves three steps: dispersion of graphene or graphene oxide in a suitable solvent, polymer addition, and removal of solvent [17].

The previous studies have reviewed the mechanical properties of graphene/polymer composites. The melt intercalation technique is usually used because controlling mixing and printing parameters are simple. The graphene has done a tremendous job in enhancing the mechanical properties of the polymers using the fused deposition modeling (FDM) technique [18-21]. Showing an increase in Young's modulus, stiffness, thermal and electrical conductivity. Some other researchers used powder bed fusion technology and added graphene to a metallic matrix [22].

Implementing graphene into photopolymerization technology (such as SLA/DLP) is very complex to control the homogeneity of the graphene within the polymer matrix (solution intercalation). This resulting in a nanocomposite material which is a perfect condition where layers of graphene are completely dispersed into the polymer matrix. The main challenge is how to diffuse graphene or graphene oxide equitably within the bulk. As a result, the number of published articles, is not sufficient to make a concrete conclusion concerning the effect of graphene on mechanical properties.

In all the previous work, especially using the photopolymerization method, the researchers were using sophisticated techniques to mix the graphene or the graphene oxide into the polymer matrix. The proportions that were used were under 1 wt%, in a controlled temperature. In this work, the effect of graphene on the mechanical (tensile) characteristics of graphene/resin composite 3D printed specimens, by the DLP technique, was studied. Meanwhile, robust industrial measures were carried out to mix the graphene within the resin using a relatively higher graphene percentage compared to the previous work. The composite mixture was with two graphene concentrations (0.5 and 1 wt%). The 3D printing was performed employing three printing layer thicknesses (35, 50, 100 μm). In addition, the microstructural features of graphene/resin composite were examined. Based on the obtained results, the influences of graphene existence and varying process parameters (layer height) on the mechanical properties of the composite were investigated.

2 Materials and Methods

2.1 Materials and Preparation of Composite

The Bio-based Photopolymer resin (eResin PLA) supplied by Shenzhen Esun Industrial Co., Ltd (China) was used as a matrix for the composite filler. This resin is a light-curable chemical liquid, with a white color. It could be cured at a wavelength range from 395 to 405 nm, to convert to a solid state. At 25 °C, it has a viscosity of 200-300 MPa.s, meanwhile, its density is 1.07-1.13 g/m^3. The chemical composition of the utilized photopolymer resin material as specified in the datasheet of the product is presented in Table 1 [23].

Table 1

Chemical ingredients of the employed photopolymer resin material [23]

Chemical name	**Percentage by weight (wt%)**
Polyurethane acrylate	30% min
Monomer	30% min
Photo initiators	5% max
Color pigment	5% max

Graphene nanoplatelets purchased from Nanografi Nano Technology Co. (Ankara, Turkey) [24] consisting of platelet-shaped graphene sheets (short stacks) in a planar form. This nanomaterial is colored black and with a purity of 99.90%. Its particles having a diameter of 1.5 μm and an average thickness of 3 nm besides a surface area of 800 m^2/g. Due to their pure graphitic composition, the graphene nanoplatelets are characterized by excellent thermal and electrical conductivity (1500-1980 s/m) [24].

The flowchart displayed in Figure 1 represents the sequence and steps of the experimental work that was accomplished in the present study. The experiments were conducted at Szent István Campus, MATE University, Gödöllő, Hungary, specifically in 3D printing and mechanical testing laboratories. Both 3D printing resin material (matrix) and graphene (filler) were used to prepare the composite and then fabricating the specimens. These materials concentration was weighed by means of a Sartorius brand laboratory scale (Sartorius AG Co., Gottingen, Germany) which has an accuracy of 0.001 g. Thereafter, the materials were put into a container to prepare the mixture. This container is a centrifuge tube (50 ml in volume) made of polypropylene plastic with a conical bottom shape. Further, aluminum foil was used to fully cover the tube and make it opaque to avoid any light transmission from the lab room into the resin which may cure it. A vortex mixer shaker (FOUR E's brand, FOUR E's Scientific Company, Guangzhou, China) device has been used to mix the components of the composite material (resin with graphene) put in the centrifuge tube at 3000 rpm shaking speed.

When the tube's conical bottom press onto the rubber piece of vortex mixer which is in contact with an electric motor, the rubber cap oscillates immediately in a circular motion owing to the motor running (See the **vortex mixer/shaker** in Figure 1). Thus, a vortex is created inside the tube as a consequence of the motion conveyed to the liquid. The mixture converts to fully black colored in a couple of seconds after starting the mixing process by the vortex mixer, despite the neat resin is white. This intimates the dispersion of graphene nanoplatelets throughout the resin. In order to increase the likelihood of a homogeneous mixture, the mixing process lasted for five minutes. Using this mixture (graphene/resin composite) as well as the neat resin (to determine the effect of graphene), the tensile testing specimens were fabricated with different parameters by 3D printing.

Moreover, post-processing was performed after the samples were printed to ensure that the resin was entirely cured. The post-printing process included heating the specimens for 30 minutes in the oven up to 60 °C. Then, these objects were exposed for 30 minutes to ultraviolet light (UV) at a wavelength of 405 nm as per recommended by Formlabs [25]. A schematic diagram of the UV light cure unit used is depicted in Figure 2a. This UV cure chamber was made from scratch where a nail salon UV lamp with 36 watts was modified to fit into a box for holding up the specimens. Aluminum (foil) mirror was employed for lining the box from inside to decrease the light losses by increasing the reflectivity. In addition, a transparent plastic sheet was added, as a shelf inside the box, to ensure UV light exposure, to all sides of specimens, at once.

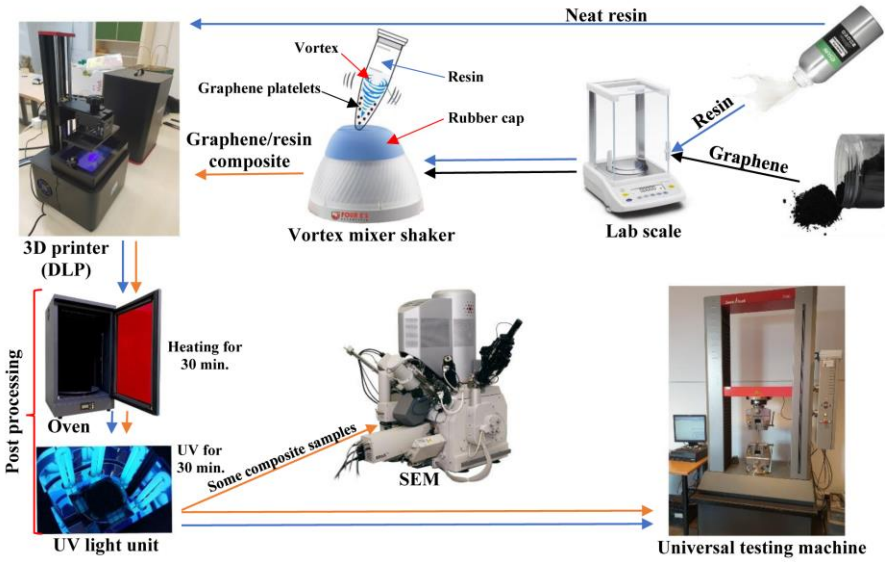

Figure 1
Flowchart for the experimental work sequence

Some graphene/resin composite samples were examined by scanning electron microscope (SEM) to inspect whether the graphene platelets were successfully incorporated. To this end, an EVO 40 SEM (Carl Zeiss AG Co., Oberkochen, Germany) was used to take many images for the surface morphology of the samples at various magnifications. Finally, the tensile tests were carried out for all manufactured specimens. More details about the 3D printing of specimens and tensile tests are described in the subsequent sections.

2.2 3D Printing of Test Specimens

Tensile test samples were produced with the WANHAO D7 V1.5 3D printer operating, according to a digital light processing (DLP) 3D printing method, that uses a photo-polymerization mechanism. AutoCAD program was utilized to design the specimens' 3D model. CreationWorkshop software which has as its file extension format, ".cws", was recommended by the manufacturer for the purpose of slicing the model. The course of action (procedure commands) of the sliced 3D model was uploaded into the 3D printer in accord with the parameters set during the slicing.

The tensile test pieces were the dog-bone shape modeled according to the standard ISO 527-2: 2012 type 1BA [26]. The specimens were built at an On-edge orientation (see Figure 2c) owing to the reliability of this build orientation as confirmed in literature [27-29]. These samples were fabricated at three layer heights (100, 50, and 35 μm) to investigate the influence of print layer thickness (see Figure 2d) on the mechanical properties. In terms of the printing materials, neat (pure) resin as well as graphene/resin composite with two different graphene concentrations (0.5 and 1 wt%) were used for the manufacture of specimens. This was done to assess the effect of graphene platelets' existence. At least, four identical specimens were printed for each print condition, i.e., for each individual manufacturing parameter, four similar pieces have been prepared. The actual physical appearance of the printed samples is pictured in Figure 2b.

Due to the diversity of parameters (different materials and print thicknesses), the specimens were highlighted with a description code for each one using various numbers and colors for easier traceability. The description included the layer height, graphene content, and the order of the sample within the same set. These identifying codes were manifested at the top face of the test pieces as displayed in Figure 2b. The tensile test specimens of graphene/resin composite material still fixed on the printing platform (after printing directly and before post-processing) are shown in Figure 2e.

2.3 Tensile Tests

As mentioned in section 2.2, the tensile test pieces were modeled following ISO 527-2, type 1BA, with an overall dimension of 75 mm × 10 mm × 2 mm (length × width × thickness, consecutively) for the measurement of tensile strength/modulus. Prior to measurement, the samples were conditioned for 24 hours in a room with a climatic of 23-25 °C and 45-50% as temperature (T) and relative humidity (RH), respectively. The tensile mechanical properties were examined for all printed specimens by a universal testing machine (Zwick / Roell Z100, Germany) with employing the standard for tensile testing of polymers ISO 527 [30]. During the test, both ends of the sample were attached to the grip, and testing was performed at a velocity of 5 mm/min until the test piece broke down. In order to yield confident data, four samples were tested for each condition and their average was calculated. The essential mechanical properties including Young's modulus (modulus of elasticity), ultimate tensile strength (UTS), elongation at break, and elongation at UTS were obtained from each specimen's stress-strain curve. The modulus of elasticity (E) was calculated using Hooke's law, in all stress-strain points:

$$E = \sigma/\varepsilon \tag{1}$$

where σ is the tensile stress (applied force/cross-sectional area) and ε is the tensile strain (change in length/initial length). For reliable results, the Young's modulus was determined by taking the gradient of the line on two points fitted at the 10% and 60% in the stress-strain plot. The stress-strain curves gained from specimens were compared to investigate the variance in specimens' mechanical properties fabricated in different conditions (layer height and graphene concentration). Table 2 provides a summary of the tensile specimen dimensions used and parameters performed throughout the tests.

Table 2
The specimen dimensions and the implemented parameters during the tensile tests

Parameter			**Value**
Specimen dimensions	Overall length		75 mm
	Gauge length		25 mm
	Gauge cross-section	Width	5 mm
		Thickness	2 mm
Testing standard			ISO 527-1:2012
Tensile velocity, v			5 mm/min
Relative humidity, RH			45-50 %
Ambient temperature, T			23-25 °C

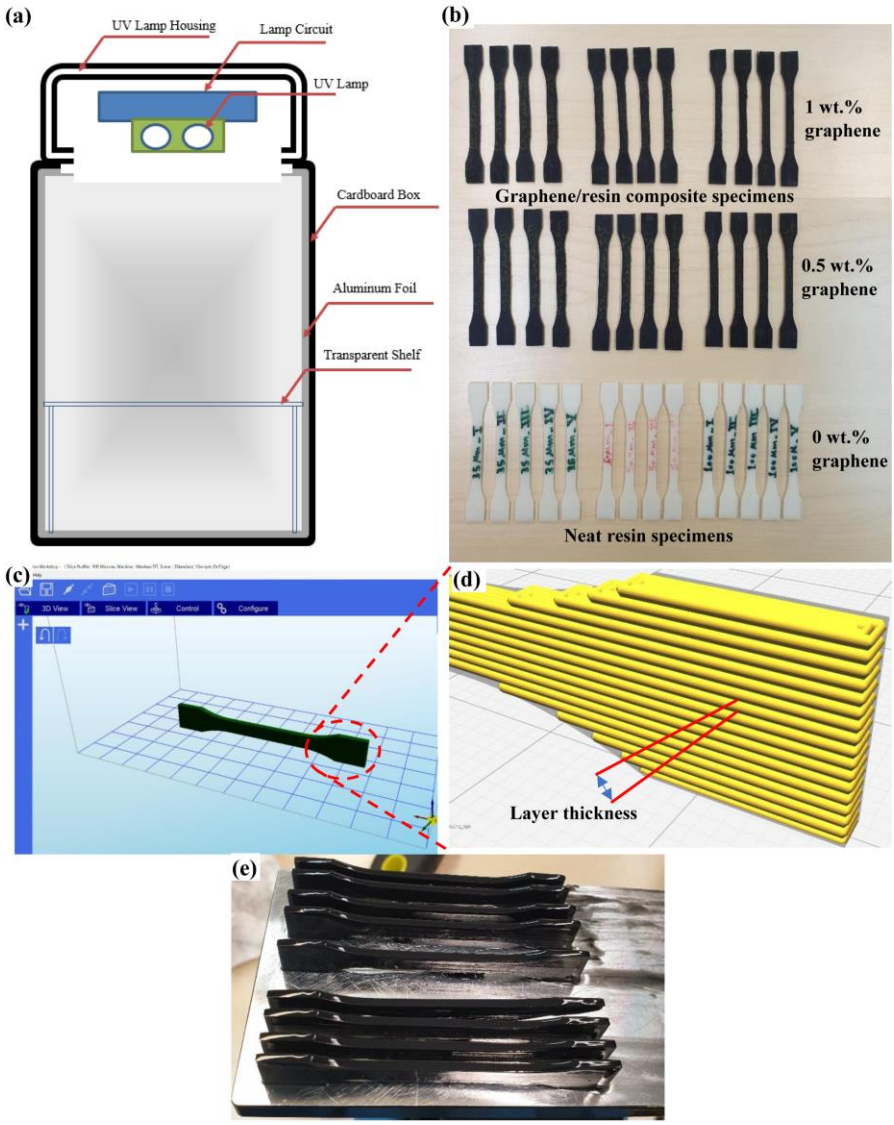

Figure 2

(a) Schematic of the used ultraviolet light unit. (b) The 3D printed tensile test specimens with different graphene content. (c) Screenshot from the slicing software for the tensile sample printed at On-edge build orientation. (d) Illustration for print layer height of test piece during the manufacture. (e) Specimens after printing instantly.

3 Results and Discussion

3.1 Microstructure Investigation

After mixing the graphene platelets with resin by the Vortex mixer/shaker, some pretest specimens were printed. The morphology and microstructure of these samples' surfaces were investigated by taking SEM images (Figure 3a-d). It was mentioned in Section 2.1 that the graphene platelets have a diameter of 1.5 μm and an average thickness of 3 nm, thus they are quite tiny. Figure 3a&b displays the surface morphology of the graphene/resin specimen where it can be seen that the graphene nanoparticles were successfully incorporated into the eventually printed structure. The graphene nanoplatelets seem to be spread throughout the matrix fairly. Some pits are also visible at the surface which indicates the existence of porosity that might be more prominent in the internal structure of printed pieces. The interior morphology of a fractured specimen is depicted in Figure 3c&d. The graphene nanoplatelets were also found and have appropriately integrated within the bulk.

In other respect, increasing the graphene addition to the polymer matrix made it somehow arduous to be printed especially beyond 2 wt%. This is due to the graphene nanoparticles give rise to scattering the UV light which causes difficulty to the resin for being fully cured. Numerous research in literature have reported that the photopolymerization 3D printing (light-based systems) of graphene/polymer composite could be only achieved with a low concentration of graphene, reached up to 0.1 wt% in these works [31] [32] and 0.5 wt% in others [16, 33]. However, for this study, the preparation method of the graphene/resin composite (by Vortex mixer/shaker) sounds excellent, as the composite material was efficiently printed with even a graphene concentration of 1 wt%.

3.2 Mechanical Behavior

The mechanical behavior of DLP 3D printed components is discussed in this chapter. To investigate the effect of strengthening the polymer composite, using graphene, on the mechanical properties, tensile test samples were 3D printed under different printing conditions. The variables of the experiment included the print layer thickness (height) and the graphene concentration to resin. Three print layer heights (35, 50, and 100 μm) were examined and two graphene ratios (0.5, and 1 wt%) were assessed. An average of four identical test pieces was taken for each inspected condition. The mechanical properties were reviewed through evaluating the stress-strain curves which implicitly assisted to obtain Young's modulus, ultimate tensile strength (UTS), elongation at break, and elongation at UTS for each specimen's data. The subsequent sections present the influence of layer thickness firstly, and then followed by the impact of graphene attendance.

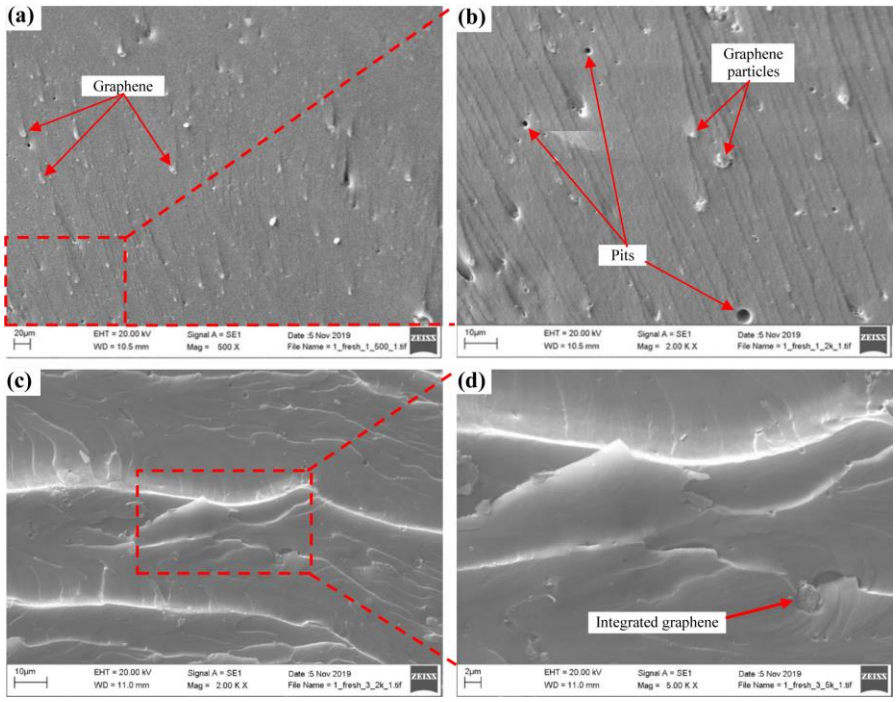

Figure 3
The morphology of graphene/resin specimen (a) & (b) at the surface; (c) & (d) in the interior structure after fracture

3.2.1 Impact of Layer Thickness

The stress versus strain curves under a load of tensile testing for different layer thickness (35, 50, and 100 µm) specimens are demonstrated in Figure 4. These curves for the test piece materials of 0 (neat resin), 0.5, and 1 wt% graphene concentration are displayed in Figure 4a, b, and c, respectively. In general, the highest tensile strength attitude was observed in the layer thickness of 35 µm (lowest height). This is because the strength of 3D printed objects enhances with the increase in the number of the layers [34], as the lower the layer height the more the number of layers. Therefore, the neat resin specimens reported a reduction of 11.62% and 22.1% in the average values of the tensile stress for 50 and 100 µm layer thickness, consecutively, as compared to the 35 µm. Further, a decrease of "7.25% and 25.78%" for the 50 µm layer height and "23.13% and 35.52%" for the 100 µm was noticed in the 0.5 wt% and 1 wt% graphene content samples, respectively, against the 35 µm specimens. This improvement in the 3D printed parts' tensile properties when the printing layer thickness reduces was also observed in other published research [35] [36]. They attributed the weaker

mechanical properties of the greater layer thickness to the bigger existed gaps. Which in turn prompts the porosity to develop in the element's cross-section and accelerates the failure.

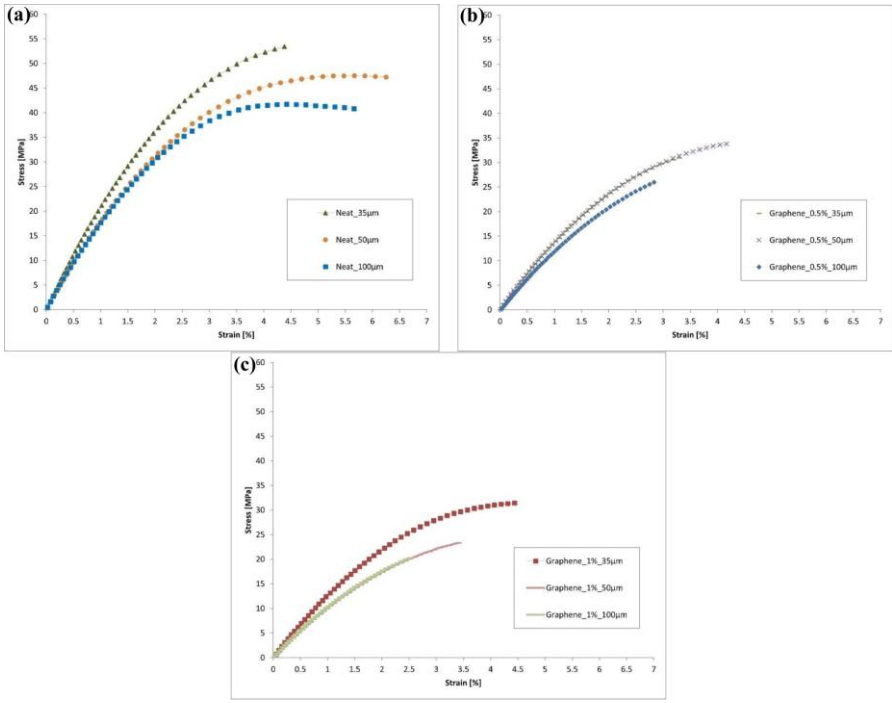

Figure 4

Tensile stress-strain curves of various layer thickness specimens at (a) Neat resin material; Composite with graphene concentration of (b) 0.5 wt% and (c) 1 wt%

3.2.2 Influence of Graphene Existence

Two different graphene concentrations of 0.5 and 1 wt% were tested. The charts in Figure 5 demonstrate how the addition of graphene, has affected the tensile stress and strain of DLP 3D printed resin, at various layer heights. The layer thickness specimen curves of 35, 50, and 100 µm are drawn in Figure 5 (a), (b) and (c), respectively. Moreover, Figure 5 (d) displays a comparison of stress-strain curves among all examined conditions. Based on these results, Young's modulus, UTS, elongation at UTS and elongation at break were calculated and represented in Figure 6 (a), (b), (c), and (d), consecutively. Furthermore, the values of all results with their standard deviation (SD), were summarized and tabulated in Table 3.

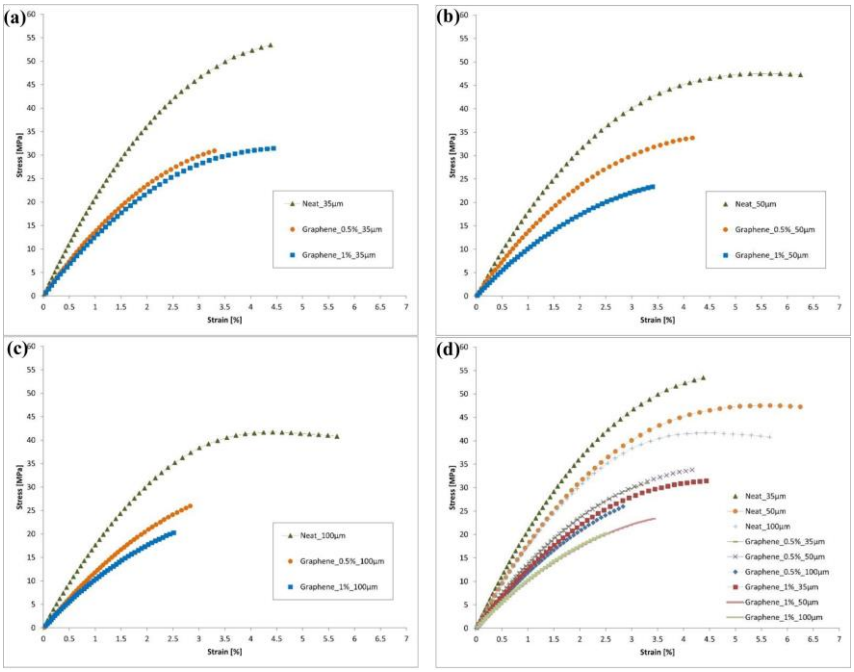

Figure 5

Tensile stress-strain curves of various graphene concentration (0, 0.5, 1 wt%) specimens at layer thickness of (a) 35, (b) 50, and (c) 100 µm; (d) comparison among all the used conditions

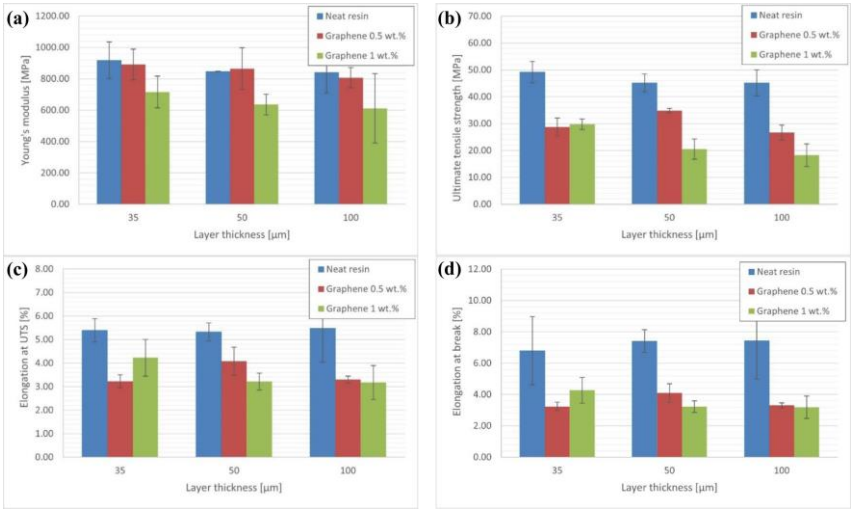

Figure 6

Comparison of mechanical behavior under different graphene concentrations and printing layer thickness in terms of (a) Young's modulus, (b) ultimate tensile strength (UTS), (c) elongation at UTS, and (d) elongation at break

Table 3
Average values aside with their standard deviation (SD) of Young's modulus, ultimate tensile strength (UTS), elongation at UTS, and elongation at break of samples manufactured in all tested conditions

Printing parameter			Young's modulus	SD	UTS	SD	Elong. at UTS	SD	Elong. at break	SD
Material	**Graphene content (wt%)**	**Layer height [µm]**	[MPa]	(±)	[MPa]	(±)	[%]	(±)	[%]	(±)
Neat resin	0	35	917.66	116.80	49.17	3.96	5.39	0.49	6.79	2.17
		50	847.46	1.81	45.17	3.31	5.33	0.38	7.40	0.73
		100	841.78	132.46	45.16	4.88	5.48	1.44	7.42	2.45
Graphene composite	0.5	35	890.87	98.25	28.74	3.30	3.23	0.27	3.24	0.28
		50	864.79	132.81	34.82	0.79	4.09	0.59	4.09	0.59
		100	807.09	63.90	26.66	2.80	3.30	0.15	3.31	0.16
	1	35	715.85	101.54	29.76	1.96	4.23	0.78	4.27	0.82
		50	635.78	65.69	20.53	3.82	3.22	0.36	3.22	0.37
		100	611.06	221.48	18.23	4.22	3.18	0.72	3.19	0.72

Despite the graphene is characterized with high mechanical qualities, however, it can be seen throughout the whole obtained results that the mechanical behavior was not improved when the graphene nanoplatelets were integrated. Also, it was noticed that with increasing the graphene concentration further, a much worse mechanical attitude was acquired. This might be attributed to the bubbles created within the matrix bulk during the DLP 3D printing due to the addition of graphene. Considering that the graphene contributes to scattering the UV light and decreases the curing which results in the presence of adjacent unpolymerized regions. In turn, played a role to boost the porosity existence, and subsequently, the effects of graphene platelets' stiffening and strengthening were critically hampered [31]. Markandan and Lai have observed large pores at higher graphene content (through microscopy images) of SLA-printed graphene/polymer composites. These pores caused an increase in the porosity in consistence with graphene concentration increment, where the overall porosity was generally around 8% [31].

On the contrary, the neat resin prototypes reported better mechanical properties (as compared to the graphene/resin composite) irrespective of the layer heights. The Young's modulus and UTS have revealed a difference of 33.41% and 62.92%, respectively, between the highest (in 35 µm neat resin) and lowest (in 100 µm graphene 1 wt%) given values (See Figure 6 (a) and (b)). Meanwhile, the distinction between the highest (in 100 µm, neat resin) and lowest (in 100 µm, graphene 1 wt%) values were approaching 41.97% and 57.01% for the elongation at UTS and elongation at break, sequentially (See Figure 6 (c) and (d)). The reduction values (variance) overall reviewed mechanical characteristics (Young's modulus, UTS, elongation at UTS, and elongation at break) in terms of the effect of layer thickness and the graphene incorporation are listed in Tables 4 and 5,

consecutively. The 35 µm layer thickness specimens (in Table 4) and neat resin specimens (in Table 5) of each used parameter were considered the reference for comparing.

Table 4

Variance in values regarding the layer thickness effect as compared to the reference specimen (35 µm layer thickness, highlighted with blue color) of each condition

Printing parameter		**Variance in values**			
Graphene concentration (wt%)	**Layer thickness [µm]**	**Young's modulus**	**UTS**	**Elongation at UTS**	**Elongation at break**
0	35	917.66 [MPa]	49.17 [MPa]	5.39 [%]	6.79 [%]
	50	-7.65 %	-8.14%	-1.11%	+8.98%
	100	-8.27%	-8.16%	+1.67%	+9.28%
0.5	35	890.87 [MPa]	28.74 [MPa]	3.23 [%]	3.24 [%]
	50	-2.92%	+21.15%	+26.63%	+26.23%
	100	-9.40%	-7.24%	+2.17%	+2.16%
1	35	715.85 [MPa]	29.76 [MPa]	4.23 [%]	4.27 [%]
	50	-11.18%	-31.01%	-23.88%	-24.59%
	100	-14.64%	-38.74%	-24.82%	-25.29%

Table 5

Variance in values concerning the graphene addition effect as compared to the reference specimen (neat resin material "0 graphene concentration", highlighted with blue color) of each condition

Printing parameter		**Variance in values**			
Layer thickness [µm]	**Graphene concentration (wt%)**	**Young's modulus**	**UTS**	**Elongation at UTS**	**Elongation at break**
35	0	917.66 [MPa]	49.17 [MPa]	5.39 [%]	6.79 [%]
	0.5	-2.92%	-41.55%	-40.07%	-52.28%
	1	-21.99%	-39.48%	-21.52%	-37.11%
50	0	847.46 [MPa]	45.17 [MPa]	5.33 [%]	7.40 [%]
	0.5	+2.04%	-22.91%	-23.26%	-44.73%
	1	-24.98%	-54.55%	-39.59%	-56.48%
100	0	841.78 [MPa]	45.16 [MPa]	5.48 [%]	7.42 [%]
	0.5	-4.12%	-40.97%	-39.78%	-55.39%
	1	-27.41%	-59.63%	-41.97%	-57.01%

A similar attitude was recognized by some researchers in recently published studies when mechanical properties of 3D printed graphene/polymer composites were investigated. A reduction in the tensile strength, the flexural strength, the tensile modulus of elasticity, and the flexural modulus of elasticity was detected with the increase in the graphene nanoplatelets (GnP) concentration [37] uploaded to ABS polymer. The mechanical response and tensile strength of a pure

thermoplastic PLA proved a better performance as compared to graphene/PLA composite [38]. The addition of 0.5% of graphene oxide (GO) to the matrix of DLP 3D printed resin caused a decrease of the mechanical features, as a higher amount of GO negatively influenced the curing process [33]. Several parameters can influence the mechanical characteristics of graphene-based composites including the preparation method, the structure of the filler, the dispersion of the graphene in the matrix, the orientation of the nanoplatelets (filler), and the filler matrix interactions [3]. In terms of the preparation methods effect, many studies have reviewed the mechanical properties of graphene-based polymer composites prepared with various procedures other than 3D printing. Vallés et al. have incorporated graphene oxide (GO) into an epoxy resin (matrix) at loadings from 0.5 to 5 wt% using sonication bath and then mechanical stirring. Tensile testing revealed moderate reinforcement of the polymer up to an optimal loading of 1 wt%. However, higher loadings beyond 1 wt% caused the mechanical features of the composites to deteriorate due to agglomeration of the GO flakes [39]. Another published research reported a comparable approach when polyurethane (PU) nanocomposites incorporated with graphene sheets (D-Graphene) by solution blending method. For this composite (D-Graphene/PU), the tensile strength enhanced up to a certain limit of graphene loading (0.24 vol%) but then reduced as loading increased [40]. This indicates that neither 3D printing nor other preparation methods can be considered free of disadvantages while graphene incorporated in a composite form. As 3D printing suffered from porosity existing whereas other methods showed filler flakes agglomeration which both contributed to weakening the mechanical features. Nevertheless, 3D printing has the advantage of manufacturing complex structures with a relatively shorter time and less material consumption.

Conclusions

In this work, the mechanical properties of 3D printed, neat resin and graphene/resin composite, using the DLP printing method were studied. Three printing layer thicknesses (35, 50, 100 μm) were used, during the fabrication of specimens and two different graphene concentrations (0.5 and 1 wt%) were tested. The effect of 3D printing layer thickness parameters and graphene nanoplatelets subsistence, were evaluated. Based on the experimental results, the following conclusions can be formed:

- The SEM images revealed that the graphene nanoplatelets were successfully incorporated into the printed structure. Furthermore, the graphene was properly dispersed throughout the specimen's bulk.

  The highest tensile strength attitude was observed in the lowest layer thickness (35 μm) specimens, due to the increase in the number of layers. The greatest decrease (35.52%) was noticed in the 100 μm layer thickness, against the 35 μm (at 1 wt% graphene content samples).

- The graphene contributed to scattering the UV light and decreased the curing, which resulted in the presence of adjacent unpolymerized regions. As a result it played a role in boosting the porosity of the material.

  The mechanical properties was not improved, when the graphene nanoplatelets were integrated throughout the obtained results. Also, a much worse mechanical attitude was gained when increasing the graphene concentration further, owing to the porosity increase.

The neat resin test pieces reported better mechanical properties (in terms of Young's modulus, UTS, elongation at UTS, and elongation at break) as compared to the graphene/resin composite, irrespective of the layer heights. The greatest difference of 33.41% and 62.92% concerning Young's modulus and UTS, respectively, between the highest (neat resin) and lowest (graphene 1 wt%) obtained values. Meanwhile, the variance was approaching 41.97% and 57.01% for the elongation at UTS and elongation at break, sequentially.

Obviously, with the addition of Graphene, as the rigid reinforcement to the polymer, caused a decrease in ductility. However, this can lead to the proposal, that the resultant graphene/polymer composite, may be a potential material, for sliding bearing applications, where the tribological properties, are much more important than the mechanical properties.

Acknowledgement

This work was supported by Szent István Campus, MATE University Research Fund (project number VEKOP-2.2.1-16-2017-00004), and the Stipendium Hungaricum Programme, Hungary.

References

[1] Kinloch I. A., Suhr J., Lou J., Young R. J., Ajayan P. M., "Composites with carbon nanotubes and graphene: An outlook", Science, Vol. 362, No. 6414, pp. 547-553, 2018

[2] Guo H., Lv R., Bai S., "Recent advances on 3D printing graphene-based composites", Nano Materials Science, Vol. 1, No. 2, pp. 101-115, 2019

[3] Papageorgiou D. G., Kinloch I. A., Young R. J., "Mechanical properties of graphene and graphene-based nanocomposites", Progress in Materials Science, Vol. 90, pp. 75-127, 2017

[4] Kátai L., Szabó I., Lágymányosi A., Lágymányosi P., Szakál Z., "Investigating the strength properties of a material used in additive manufacturing technology depending on the parameters of 3D printing", Gép, Vol. LXIX, No. 4, pp. 45-48, 2018

[5] Erdős F., Németh R., "AMT-based real-time, inter-cognitive communication model", Acta Polytechnica Hungarica, Vol. 16, No. 6, pp. 115-127, 2019

[6] Rafajłowicz E., "Data Structures for Pattern and Image Recognition and Application to Quality Control", Acta Polytechnica Hungarica, Vol. 15, No. 4, pp. 233-262, 2018

[7] Chaczko Z., Klempous R., Rozenblit J., Adegbija T., Chiu C., Kluwak K., Smutnick C., "Biomimetic Middleware Design Principles for IoT Infrastructures", Acta Polytechnica Hungarica, Vol. 17, No. 5, pp. 135-150, 2020

[8] Madhav C. V., Kesav R. S. N. H., Narayan Y. S., Importance and Utilization of 3D Printing in Various Applications (2016)

[9] Balletti C., Ballarin M., Guerra F., "3D printing: State of the art and future perspectives", Journal of Cultural Heritage, Vol. 26, pp. 172-182, 2017

[10] Bártolo P. J., Stereolithography: Materials, Processes and Applications, Springer US, Boston, MA, (2011)

[11] Mu Q., Wang L., Dunn C. K., Kuang X., Duan F., Zhang Z., Qi H. J., Wang T., "Digital light processing 3D printing of conductive complex structures", Additive Manufacturing, Vol. 18, pp. 74-83, 2017

[12] Hanon M. M., Zsidai L., "Sliding surface structure comparison of 3D printed polymers using FDM and DLP technologies", IOP Conference Series: Materials Science and Engineering, Vol. 749, pp. 012015, 2020

[13] Wu G.-H., Hsu S., "Review: Polymeric-Based 3D Printing for Tissue Engineering", Journal of Medical and Biological Engineering, Vol. 35, No. 3, pp. 285-292, 2015

[14] Hanon M. M., Zsidai L., "Tribological and mechanical properties investigation of 3D printed polymers using DLP technique", AIP Conference Proceedings, Vol. 2213, pp. 020205, 2020

[15] Xu Z., Gao C., "In situ Polymerization Approach to Graphene-Reinforced Nylon-6 Composites", Macromolecules, Vol. 43, No. 16, pp. 6716-6723, 2010

[16] Lin D., Jin S., Zhang F., Wang C., Wang Y., Zhou C., Cheng G. J., "3D stereolithography printing of graphene oxide reinforced complex architectures", Nanotechnology, Vol. 26, No. 43, pp. 434003, 2015

[17] Verdejo R., Bernal M. M., Romasanta L. J., Lopez-Manchado M. A., "Graphene filled polymer nanocomposites", J. Mater. Chem., Vol. 21, No. 10, pp. 3301-3310, 2011

[18] Mohan V. B., Bhattacharyya D., "Mechanical, electrical and thermal performance of hybrid polyethylene-graphene nanoplatelets-polypyrrole composites: a comparative analysis of 3D printed and compression molded samples", Polymer-Plastics Technology and Materials, Vol. 59, No. 7, pp. 780-796, 2020

[19] Prashantha K., Roger F., "Multifunctional properties of 3D printed poly(lactic acid)/graphene nanocomposites by fused deposition modeling", Journal of Macromolecular Science, Part A, Vol. 54, No. 1, pp. 24-29, 2017

[20] Mansour M., Tsongas K., Tzetzis D., "Measurement of the mechanical and dynamic properties of 3D printed polylactic acid reinforced with graphene", Polymer-Plastics Technology and Materials, Vol. 58, No. 11, pp. 1234-1244, 2019

[21] Del Gaudio C., "A feasibility study for a straightforward decoration of a 3D printing filament with graphene oxide", Fullerenes, Nanotubes and Carbon Nanostructures, Vol. 27, No. 8, pp. 607-612, 2019

[22] Tiwari J. K., Mandal A., Sathish N., Agrawal A. K., Srivastava A. K., "Investigation of porosity, microstructure and mechanical properties of additively manufactured graphene reinforced AlSi10Mg composite", Additive Manufacturing, Vol. 33, pp. 101095, 2020

[23] Esun Industrial Co. L., eResin-LC1001, Material Safety Data Sheet, Shenzhen, China (2019)

[24] Inc. N. N., Graphene Nanoplatelet-NG01GNP0109, Material Safety Data Sheet, Ankara, Turkey (2019)

[25] Formlabs, Form Cure Time and Temperature Settings (2018)

[26] International Organization for Standardization, ISO 527-2:2012: Plastics - Determination of tensile properties - Part 2: Test conditions for moulding and extrusion plastics (2012)

[27] Hanon M. M., Marczis R., Zsidai L., "Anisotropy Evaluation of Different Raster Directions, Spatial Orientations, and Fill Percentage of 3D Printed PETG Tensile Test Specimens", Key Engineering Materials, Vol. 821, pp. 167-173, 2019

[28] Hanon M. M., Alshammas Y., Zsidai L., "Effect of print orientation and bronze existence on tribological and mechanical properties of 3D-printed bronze/PLA composite", The International Journal of Advanced Manufacturing Technology, Vol. 108, No. 1-2, pp. 553-570, 2020

[29] Hanon M. M., Marczis R., Zsidai L., "Influence of the 3D Printing Process Settings on Tensile Strength of PLA and HT-PLA", Periodica Polytechnica Mechanical Engineering, Vol. 65, No. 1, pp. 38-46, 2020

[30] International Organization for Standardization, ISO 527-1:2012 - Plastics -- Determination of tensile properties -- Part 1: General principles (2012)

[31] Markandan K., Lai C. Q., "Enhanced mechanical properties of 3D printed graphene-polymer composite lattices at very low graphene concentrations", Composites Part A: Applied Science and Manufacturing, Vol. 129, pp. 105726, 2020

[32] Lai C. Q., Markandan K., Luo B., Lam Y. C., Chung W. C., Chidambaram A., "Viscoelastic and high strain rate response of anisotropic graphene-polymer nanocomposites fabricated with stereolithographic 3D printing", Additive Manufacturing, Vol. 37, pp. 101721, 2021

[33] Chiappone A., Roppolo I., Naretto E., Fantino E., Calignano F., Sangermano M., Pirri F., "Study of graphene oxide-based 3D printable composites: Effect of the in situ reduction", Composites Part B: Engineering, Vol. 124, pp. 9-15, 2017

[34] Sood A. K., Ohdar R. K., Mahapatra S. S., "Experimental investigation and empirical modelling of FDM process for compressive strength improvement", Journal of Advanced Research, Vol. 3, No. 1, pp. 81-90, 2012

[35] Ayrilmis N., Kariz M., Kwon J. H., Kitek Kuzman M., "Effect of printing layer thickness on water absorption and mechanical properties of 3D-printed wood/PLA composite materials", The International Journal of Advanced Manufacturing Technology, Vol. 102, No. 5-8, pp. 2195-2200, 2019

[36] Rankouhi B., Javadpour S., Delfanian F., Letcher T., "Failure Analysis and Mechanical Characterization of 3D Printed ABS With Respect to Layer Thickness and Orientation", Journal of Failure Analysis and Prevention, Vol. 16, No. 3, pp. 467-481, 2016

[37] Vidakis N., Maniadi A., Petousis M., Vamvakaki M., Kenanakis G., Koudoumas E., "Mechanical and Electrical Properties Investigation of 3D-Printed Acrylonitrile–Butadiene–Styrene Graphene and Carbon Nanocomposites", Journal of Materials Engineering and Performance, Vol. 29, No. 3, pp. 1909-1918, 2020

[38] Vidakis N., Petousis M., Savvakis K., Maniadi A., Koudoumas E., "A comprehensive investigation of the mechanical behavior and the dielectrics of pure polylactic acid (PLA) and PLA with graphene (GnP) in fused deposition modeling (FDM)", International Journal of Plastics Technology, Vol. 23, No. 2, pp. 195-206, 2019

[39] Vallés C., Beckert F., Burk L., Mülhaupt R., Young R. J., Kinloch I. A., "Effect of the C/O ratio in graphene oxide materials on the reinforcement of epoxy-based nanocomposites", Journal of Polymer Science Part B: Polymer Physics, Vol. 54, No. 2, pp. 281-291, 2016

[40] Yang L., Phua S. L., Toh C. L., Zhang L., Ling H., Chang M., Zhou D., Dong Y., Lu X., "Polydopamine-coated graphene as multifunctional nanofillers in polyurethane", RSC Advances, Vol. 3, No. 18, pp. 6377, 2013

Online Time Delay and Disturbance Compensation for Linear Non-Minimum Phase Systems

Özlem Demirtaş[1,2], Mehmet Önder Efe[3]

[1] Advanced Technologies & Systems Division, Roketsan Missiles Inc., Mamak 06852, Ankara, Turkey, ozlem.demirtas@roketsan.com.tr

[2] Hacettepe University, Graduate School of Science and Engineering, Beytepe, 06800, Ankara, Turkey, ozlem.demirtas@hacettepe.edu.tr

[3] Department of Computer Engineering, Hacettepe University, Beytepe Campus 06800, Ankara, Turkey, onderefe@hacettepe.edu.tr

Abstract: Herein, a disturbance observer is designed for linear non-minimum phase systems. A Smith Predictor is added to the system, using Recursive Least Squares (RLS), with a forgetting factor algorithm. The combination of both approaches, eliminates the restrictive feature of the classical disturbance observer, for non-minimum phase systems and removes the necessity for precise delay measurements, for the Smith Predictor structure. The results show that the proposed design procedure preserves system stability, in the presence of disturbances and time delays.

Keywords: Disturbance Observer; Recursive Least Squares; Smith Predictor

1 Introduction

Disturbances often occur in real systems and this has a negative effect on system stability and performance. In the past, a number of remedies have been proposed to enhance the stability and performance characteristics of feedback control systems [1].

The classical disturbance observer (DOB), estimates disturbances acting on the system, utilizing a proper inverse model and eliminates the disturbance from the control channel. However, the model inversion for non-minimum phase systems leads to unstable control loops, which require a special treatment for the right half plane (RHP) zeros [2]. This undesired situation narrows down both the simplicity and the capabilities of DOB.

Although researchers try to make the system robust by using more complex controllers due to restrictive effect of classical DOBs, the designed controllers often achieve one control target, making the system robust against disturbances, yet sacrificing other control objectives.

In addition to external disturbances, inherent time delays are also inevitable facts observed in dynamic systems, and similar to disturbances, they disrupt the system's stability and deteriorate its operation [3] [4] [5]. Smith Predictor (SP) [6] is often used to restore the stability of such systems. In this approach, negative feedback is made from the controller output to input by using time delay model and the delay becomes a multiplier of the delay free closed loop transfer function. However, in order to design the time delay model, the actual time delay must be measured precisely, which is usually not possible in practice [7].

In this study, the aim is to create a new control design, that removes the above-mentioned limitations of classical DOB and SP designs and can eliminate the negative effects of both disturbance and time delay concurrently. For this reason, both the DOB for non-minimum phase systems and the online SP design for systems with time delay are proposed to eliminate the negative effects of disturbances and time delays. As a non-minimum phase system, the altitude control of the Tower Trainer 60 unmanned aerial vehicle [8] is used and H_∞ based robust control design is preferred as the altitude controller.

In the first step, the design of a DOB for non-minimum phase systems is performed. The minimum phase approximation of the system is found by using a constrained optimization approach [9], and the inverse of the system is obtained by using this approximation. Then, input and output disturbances are fed to the system and the effect of the DOB on the system performance is observed.

In the second step, the online SP design using the Recursive Least Squares with Forgetting Factor (RLSWF) [10] method is proposed. In this phase, it is assumed that the nominal model of the system is known and the real system dynamics with delay are estimated using RLSWF. In this way the disruptive effect of delay on the system is eliminated in an online manner without the need for precise measurement of the time delay.

In the last phase, the studies done in the previous steps are combined to observe how the system stability is maintained for cases where the disturbance and delay are effective simultaneously. Then the closed loop system with uncertain elements is investigated with and without the presence of combination of proposed methods.

According to the results, it is seen that the controller alone is not capable of maintaining the stability under time delay and disturbances. On the other hand, for non-minimum phase and time delay systems, the response of the system is stable and it resembles the nominal system behavior with proposed time delay and disturbance estimation methods.

As a result, the following features in the presented study are superior to other studies in the literature:

1) A novel, simple and reliable DOB design has been created for non-minimum phase systems.
2) By making the SP design adaptive, time delay elimination is realized without the need for actual time delay measurement. Unlike the communication disturbance observer design [11], it can work for non-minimum phase systems without the need for extra design costs.
3) By combining the new SP and DOB designs, both delay and disturbance elimination is provided. 4) Both designs can be used both separately and in combination based on the system requirements.

This paper is organized as follows. Section 2 summarizes the previous work. Section 3 gives information about the DOB structure designed for linear non-minimum phase systems and shows the optimization results. Section 4 describes how the delay is compensated by combining SP and RLSWF when it occurs in the system. Section 5 shows how system works for the case where both methods are combined. Finally, Section 6 presents the conclusions.

2 Literature Background

In 2004, Chen, Zhai and Fukuda [12] used the least squares method to find the minimum phase estimation of the non-minimum phase system and incorporated it to the design of the classical DOB. However, this study focuses only on the inner loop of the system with DOB structure and the disturbance estimation. Therefore, in the presence of a controller, the performance of the closed loop system is not considered.

In 2010, Kim and Son [13] also designed a DOB for non-minimum phase systems and demonstrated that the designed observer executes robustly in the presence of time delay and time varying disturbance in the input signal. This study is important as it provides delay and disturbance compensation by combining non-minimum phase DOB and classical SP designs. However, the need for actual time delay measurement and the insufficiency for time varying delays of classical SP are the limitations of the study.

In 2010, Jo, Shim and Son [14] designed a parallel filter using the H_∞ synthesis technique for non-minimum phase system. Then, using this technique, they also incorporated a robust controller into the closed loop system and showed that without the proposed DOB, the corresponding controller can only achieve one design goal. Although this design provides the applicability of the classic DOB design for non-minimum phase systems, it has two drawbacks:

1) The input disturbance affecting the system is not injected the input of the parallel filter at runtime. For this reason, this situation leads to a small uncertainty in the design.
2) In order to calculate the parallel filter, a deep robust stability analysis is required.

In 2013, Sarıyıldız and Ohnishi [15] estimated the minimum phase equivalents by running an optimization method for the RHP zero(s) in the system and presented a study on which constraints should be considered when designing Q filter for such systems. In this method, the performance of the DOB is directly dependent on the performance of the optimization method used, and an approach with a high error rate affects the DOB performance and fidelity of the simulation negatively. Therefore, the cost function and optimization method should be selected in accordance with the non-minimum phase system to be used.

In 2014, Wang and Su [16] designed a DOB for non-minimum phase, delayed systems and they presented a Q filter optimization using H_∞ theory. In this study, disturbance rejection control using DOB for stable systems is investigated. However, although the study presents a design methodology considering both time delay and RHP zeros, the validity of the study only for stable systems and having a deep robust stability analysis are the limitations of the proposed method.

Observers are used quite often, not only for disturbance estimation, but also for estimating some system parameters. In 2014, Regaya et al. [17] estimated the speed in the induction machine using the sliding mode observer. Thus, they provided the control and determination of the unknown rotor speed without the need for the speed sensor. The simulation results support that the speed estimation was carried out successfully and the chattering in the controller was reduced.

The time delay problem is encountered in many different fields. In 2016, Muradore and Fiorini [18] examined the algorithms that will ensure the stability of communication between master and slave systems in dual teleoperation technologies and presented the advantages and disadvantages of these algorithms. These algorithms are based on passivity theory to guarantee the stability of teleoperation in the presence of time delay. Similarly, in 2017, Marton et al. [19] presented the modified bilateral control algorithm based on the time domain passivity concept, which guarantees system stability in the presence of time varying delays.

Although there exist DOB designs for non-minimum phase and delayed systems in the literature, an in depth stability analysis is required for designs using H_∞ theory [14] [16]. In other DOB designs for non-minimum phase systems, the delay is not included in the system [12] [15]. Even so, an accurate delay measurement is still required for SP design [13]. In this study, for non-minimum phase systems with time delays, delay compensation without precise delay information requirement is investigated and a practical optimization study for RHP zeros is conducted.

3 Disturbance Observer Design for Linear Non-Minimum Phase Systems

3.1 Classical Disturbance Observers

The structure of classical DOB is shown in Figure 1, where $P(s)$ is the real system, $P_n(s)$ is the nominal model of the system, $C(s)$ is the system controller and $Q(s)$ is a low pass filter.

As shown in Figure 1, the control signal exposed to the disturbance enters the plant via the control channel. The resulting –possibly- noisy output signal passes through the inverse of the nominal system dynamics and Q filter, respectively, and the estimated value of the disturbance is obtained.

The performance and stability of a closed loop system with a DOB depends tightly on the design of Q filter. In [20], a design procedure, which always guarantees the closed loop stability of the Q filter, is proposed. However, the use of inverse system dynamics in the design of DOB also requires some special considerations for non-minimum phase systems as the inverse of the nominal plant is unstable.

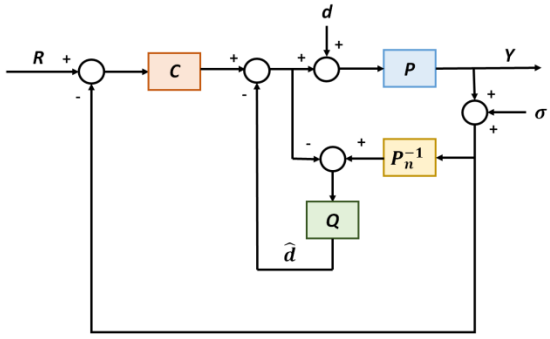

Figure 1
Classical DOB structure

3.2 Effect of Non-Minimum Phase Systems on Stability of Classical Disturbance Observer

If the stability condition is examined for the inner loop in which the classical DOB is located (See Figure 1), we have the following transfer functions from r to y in (1) and from d to y in (2). The measurement noise is denoted by σ and the transfer function from σ to y is given in (3):

$$P_{ry}(s) = \frac{P(s)P_n(s)}{P_n(s)+(P(s)- P_n(s))Q(s)} \tag{1}$$

$$P_{dy}(s) = \frac{P(s)P_n(s)(1-Q(s))}{P_n(s)+(P(s)-P_n(s))Q(s)} \tag{2}$$

$$P_{\sigma y}(s) = \frac{P(s)Q(s)}{P_n(s)+(P(s)-P_n(s))Q(s)} \tag{3}$$

If $P = P_n(1+\Delta)$, i.e. the uncertainty model is multiplicative, the characteristic equation of the closed loop system is as given in (4):

$$P_n(s)+\big(P(s)-P_n(s)\big)Q(s) = 0$$

$$P_n(s)\big(1+\Delta(s)Q(s)\big) = 0 \tag{4}$$

If (3) and (4) are combined, below transfer function is obtained:

$$P_{\sigma y}(s) = \frac{(P_n(s)+(1+\Delta(s)))Q(s)}{P_n(s)(1+\Delta(s)Q(s))} \tag{5}$$

In (5) P, Q and Δ are can be expressed as the ratio of polynomials such that $P_n = N_{P_n}/D_{P_n}$, $Q = N_Q/D_Q$ and $\Delta = N_\Delta/D_\Delta$. Rearranging (5) with these variables yields:

$$P_{\sigma y}(s) = \frac{N_Q(N_{P_n}D_\Delta + D_{P_n}D_\Delta + N_\Delta D_{P_n})}{N_{P_n}(D_\Delta D_Q + N_\Delta N_Q)} \tag{6}$$

In order to fulfill the internal loop stability condition, the denominator polynomial $N_{P_n}(D_\Delta D_Q + N_\Delta N_Q)$ specified in (6) must be Hurwitz. In this case, the nominal system must be minimum phase because N_{P_n} stands for the numerator of the nominal system.

3.3 Approximation of Non-Minimum Phase Systems

In order to invert the non-minimum phase system transfer function, minimum phase equivalents of the RHP zeros in the numerator of the nominal system that make the system non-minimum phase should be found for a certain frequency range. For this purpose, the approach specified in [15] is adopted with changes in the error function.

Suppose that the non-minimum phase causal system which we want to invert contains RHP zeros and N_P represents the polynomial consists of only RHP zeros. Also the non-causal, minimum phase transfer function that we calculated as the equivalent of N_P at the end of optimization is N_{approx}/D_{approx}. In this case, the error polynomial can be defined as in (7):

$$e := N_P - \frac{N_{approx}}{D_{approx}} \tag{7}$$

With this definition, the optimization problem can be cast as:

minimize

$$\mathrm{E} = x_{amp}(w)|e(jw)|^2 + x_{phase}(w)\big(arg\big(e(jw)\big)\big)^2$$

subject to:

E1: N_{approx} *and* D_{approx} *are Hurwitz polynomials.*

$$E2: 0 \leq w \leq min(Re(z_{RHP})) \tag{8}$$

$x_{amp}(w)$ and $x_{phase}(w)$ represent frequency dependent magnitude and phase weights. In the original solution, these coefficients are assumed to be constants. In the experiments, it is observed that taking these weights in the form of functions varying depending on the frequency yields more accurate results. In the minimization of the problem specified in (8), numerical solution is implemented by using the off-the-shelf interior point method and the solution is realized for frequency points up to the smallest of the RHP zeros.

3.4 Novel Disturbance Observer Design for Non-Minimum Phase Unmanned Aerial Vehicle

The Tower Trainer 60 autopilot design problem is used to test the new DOB method which is designed for non-minimum phase systems. The nominal transfer function of the system takes the elevator angle as input and provides altitude control. This transfer function's denominator degree is 5 and it has 3 zeros in total. One of these zeros is in the RHP and its value is approximately 12.449088. The transfer function coefficients are shown in (9):

$$P_n(s) = \frac{h(s)}{\delta_e(s)} = \frac{-34.16s^3-144.4s^2+7047s+557.2}{s^5+13.18s^4+95.93s^3+14.61s^2+31.94s} \tag{9}$$

In the first step, using (7), the following error polynomial is defined:

$$e(s) = (s - 12.449088) - \frac{N_{approx}}{D_{approx}} \tag{10}$$

Solving the optimization problem in (8) with the error polynomial specified in (10), the minimum phase approximation of the non-minimum phase part of the transfer function is estimated. $x_{amp}(w)$ and $x_{phase}(w)$ are chosen as $exp(-10 * w)$ and 10, respectively. The estimation is realized non-causal by selecting the numerator degree 2 and denominator degree 1 of the minimum phase transfer function. In order to obtain more accurate results, minimization can be carried out for different numerator and denominator degrees by providing the condition of being non-causal. Equation (11) shows the minimum phase and non-causal transfer function obtained as a result of minimization:

$$\frac{N_{approx}}{D_{approx}} = \frac{-0.183s^2-5.486s-72.63}{s+6.963} \tag{11}$$

In Figure 2, the RHP zero polynomial (s - 12.449088), minimum phase approximation and symmetric zero polynomial (-s - 12.449088) is compared in Bode diagrams. In this figure, Bode diagrams display acceptable similarity up to

the RHP zero frequency, which is used as the maximum frequency point in minimum phase approximation. This figure also shows us that the new DOB design has a bandwidth of 12 rad/sec and system responses are acceptable at frequencies below this value.

In the presence of new DOB, the robustness of the closed loop system for both input and output disturbances is studied after the minimum phase approximation of the non-minimum phase autopilot design. H_∞ synthesis method is used in the design of system controller. In this controller design type, a closed loop weighted transfer function is obtained by using the system's sensitivity and complementary sensitivity. Then, the optimal transfer function minimizing the norm of this weighted transfer function is used as system controller. Sensitivity and complementary sensitivity functions of the closed loop system are shaped using weights. For this purpose, the weighting method given in [14] is used in the control design. Values of weights are given as:

$$W_{Sensitivity}(s) = \frac{s^2+1.84s+0.846}{0.001s^3+1.002s^2+1.84s+1.84e\text{-}06}$$

and

$$W_{Cosensitivity}(s) = \frac{s}{5} \times \frac{s}{s - 0.001}$$

The gain and phase margins of the system are calculated as 38.5 dB and 76.1 degrees, respectively. The reference signal, input disturbances and output disturbances are defined as $r(t) = step(t)$, $d(t) = \sin(t)$ and $\sigma(t)$ is the output measurement noise, which has uniform distribution in between ±1e−3, respectively.

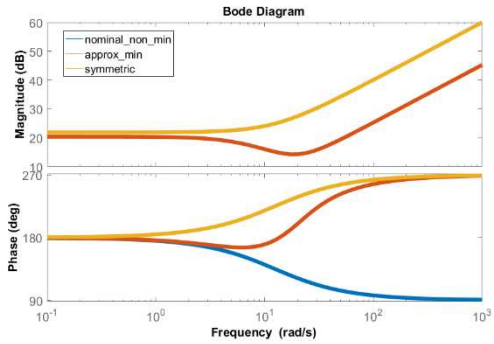

Figure 2

Bode diagrams of non-minimum phase, approximate minimum phase and symmetric polynomials. Blue, red and orange curves indicate non-minimum phase, approximate minimum phase and symmetric polynomials, respectively.

In Figure 3 the system response obtained in the absence of DOB when input and output disturbances affect the closed loop system is shown. As can be seen from the figure, when disturbances are active, the controller becomes incapable of alleviating it and this causes oscillations in the system response.

In Figure 4 the system response obtained in the presence of controller and DOB is compared with the system responses obtained only in the presence of a controller. As can be seen from the figure, the proposed DOB design used with the controller makes the system more robust against disturbances and provides a response close to the nominal system's response.

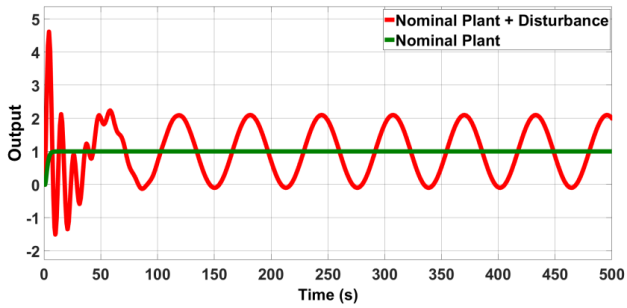

Figure 3

Closed loop responses of the system. Red and green curves show system responses in the presence and absence of both input and output disturbances, respectively.

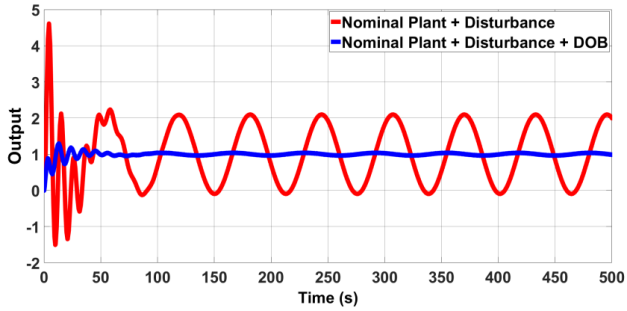

Figure 4

Closed loop responses of the system. Red and blue curves show system responses against input and output disturbances in the absence and presence of new non-minimum phase DOB, respectively.

4 Smith Predictor Design Using Recursive Least Squares

4.1 Classical Smith Predictor

SP is a simple yet effective design that ensures a stable response from a closed loop system when time delay is available in the loop. In this design, the accurately known delay term of the system is removed perfectly from the system's characteristic equation and the negative effect of the delay on the response is eliminated. Classical SP structure is illustrated in Figure 5. As shown in the figure, the delay that adversely affects the closed loop system is compensated using the predictor transfer function $P\,(1- e^{-\tau s})$.

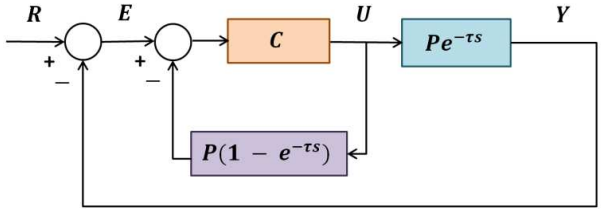

Figure 5
Classical SP structure

If the system structure is expressed using the following equations, then:

$$\frac{U}{E} = \frac{C}{1+PC(1-e^{-\tau s})} \tag{12}$$

$$\frac{Y}{R} = \frac{\frac{U}{E}\frac{Y}{U}}{1+\frac{U}{E}\frac{Y}{U}} = \frac{\frac{PCe^{-\tau s}}{1+PC(1-e^{-\tau s})}}{1+\frac{PCe^{-\tau s}}{1+PC(1-e^{-\tau s})}} = \frac{PCe^{-\tau s}}{1+PC} \tag{13}$$

are obtained. Equation (13) expresses the ideal design expected in the presence of controller and SP. However, in real systems, SP efficiency depends tightly on the exact measurement of delay and correct modeling of the real system. These are rather restrictive conditions for a successful application of SP.

In Figure 6, the delayed real system $P(s)\,e^{-\tau s}$ is modeled and $P_{ref}(s)\,e^{-\tau_{ref} s}$ is obtained. Then the SP design is studied on this new block structure. The transfer function of the new SP design is obtained as follows:

$$\frac{Y}{R} = \frac{\frac{PCe^{-\tau s}}{1+P_{ref}C(1-e^{-\tau_{ref} s})}}{1+\frac{PCe^{-\tau s}}{1+P_{ref}C(1-e^{-\tau_{ref} s})}} \tag{14}$$

$$\frac{Y}{R}=\frac{PCe^{-\tau s}}{1+P_{ref}C+C(Pe^{-\tau s}-P_{ref}e^{-\tau_{ref}s})} \tag{15}$$

As can be understood from (15), if the modeling error of the real system with delay is minimized and a sufficient level of fidelity is achieved, the ideal SP design expressed in (13) is obtained by assuming $\left(Pe^{-\tau s}-P_{ref}e^{-\tau_{ref}s}\right)\approx 0$.

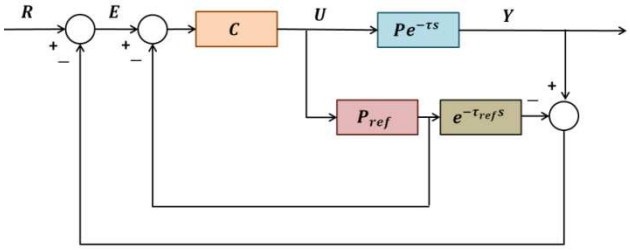

Figure 6
SP structure by modeling real system and delay

In modeling the real system with delay, classical mathematical modeling methods can be used as well as system identification techniques. In this context, RLSWF algorithm, which is a system identification method in time domain, is used in modeling the real delayed system.

4.2 Recursive Least Squares with Forgetting Factor

RLS algorithm is an iterative implementation of the Least Squares (LS) regression algorithm. The method allows the LS algorithm to be dynamically applied to time series obtained in real time. Algorithm is a member of Kalman filter family and exhibits an adaptive mechanism in terms of execution method. In addition, it is adjustable according to time varying input data and it has a fast convergence rate. In this respect, it clearly shows a better performance than the LS algorithm.

The basis of the LS algorithm is the identification of the linear model with unknown parameter values by minimizing the square of the difference between the real and estimated system outputs. This situation can be defined as optimizing the cost function specified in (16). In this equation, T is the sampling time, y is real system output, x is identification input and w is the vector of linear system parameters we want to obtain at the end of the identification.

$$\epsilon(w)=\frac{1}{2}\sum_{i=1}^{m}\left(x^T(iT)w-y(iT)\right)^2 \tag{16}$$

If closed form solution is developed, then:

$$\frac{d\epsilon}{dw}(w)=\sum_{i=1}^{m}x(iT)(x^T(iT)w-y(iT))\ =0 \tag{17}$$

$$\sum_{i=1}^{m}\left(x(iT)x^{T}(iT)w\text{-}x(iT)y(iT)\right)=0 \tag{18}$$

$$w\sum_{i=1}^{m}\left(x(iT)x^{T}(iT)\right)\text{-}\sum_{i=1}^{m}\left(x(iT)y(iT)\right)=0 \tag{19}$$

$$w=\sum_{i=1}^{m}\left(x(iT)x^{T}(iT)\right)^{-1}\sum_{i=1}^{m}\left(x(iT)y(iT)\right) \tag{20}$$

is obtained. In the RLS algorithm, it is aimed to recursively update the equation given in (20) as the real time data are obtained. If $A(mT)=\sum_{i=1}^{m}(x(iT)x^{T}(iT))$ and $B(mT)=\sum_{i=1}^{m}(x(iT)y(iT))$, then:

$$w(mT)=A^{-1}(mT)B(mT) \tag{21}$$

is obtained. The aim is to calculate the value of $w(mT)$ using the data we have obtained at time $(m\text{-}1)T$. In this case, the value of $w((m\text{-}1)T)$ is obtained as:

$$w((m\text{-}1)T)=A^{-1}((m\text{-}1)T)B((m\text{-}1)T) \tag{22}$$

If the values of $A(mT)$ and $B(mT)$ are also calculated using $A((m\text{-}1)T)$ and $B((m\text{-}1)T)$, then:

$$A(mT)=A((m\text{-}1)T)+x(mT)x^{T}(mT) \tag{23}$$

$$B(mT)=B((m\text{-}1)T)+x(mT)y(mT) \tag{24}$$

are obtained. However, as specified in (21), $A^{-1}(mT)$ is needed to obtain the $w(mT)$ value. From the matrix inversion formula:

$$A^{-1}(mT)=A^{-1}((m\text{-}1)T)\text{-}\frac{A^{-1}((m\text{-}1)T)x(mT)x^{T}(mT)A^{-1}((m\text{-}1)T)}{1+x^{T}(mT)A^{-1}((m\text{-}1)T)x(mT)} \tag{25}$$

is obtained. If the covariance matrix $P(mT)$ and Kalman gain $L(mT)$ are shown as $A^{-1}(mT)$ and $P((m\text{-}1)T)x(mT)\left(1+x^{T}(mT)P((m\text{-}1)T)x(mT)\right)^{-1}$ respectively, $P(mT)$ can also be expressed as:

$$P(mT)=(I\text{-}L(mT)x^{T}(mT))P((m\text{-}1)T) \tag{26}$$

In this case, to find the value of $w(mT)$ recursively, the following equations are used:

$$\begin{aligned}
&w(mT)=P(mT)B(mT)\\
&=P(mT)\left(A((m\text{-}1)T)w((m\text{-}1)T)+x(mT)y(mT)\right)\\
&=P(mT)\left(\left(A(mT)\text{-}x(mT)x^{T}(mT)\right)w((m\text{-}1)T)+x(mT)y(mT)\right)\\
&=w((m\text{-}1)T)\text{-}P(mT)x(mT)x^{T}(mT)w((m\text{-}1)T)+P(mT)x(mT)y(mT)\\
&=w((m\text{-}1)T)+L(mT)\left(y(mT)\text{-}x^{T}(mT)w((m\text{-}1)T)\right)
\end{aligned} \tag{27}$$

The algorithm structure used for RLS is similar to the one used in many recursive estimation algorithms. Differences between algorithms are mostly achieved by changing the Kalman gain. In cases where the linear system parameters are time varying, the RLS algorithm alone may not be sufficient. In this case, the forgetting factor, which is a more effective and heuristic approach, is used with RLS. This method allows more focus on recently observed data by reducing the weighting of old data points used during identification. In this case, the cost function used in the RLS algorithm, the covariance matrix P and the Kalman gain L are updated in the RLSWF algorithm respectively as follows:

$$\epsilon(w) = \frac{1}{2}\sum_{i=1}^{m} \lambda^{m-i}(x^T(iT)w\text{-}y(iT))^2 \tag{28}$$

$$P(mT) = (\frac{1}{\lambda})\left(I\text{-}L(mT)x^T(mT)\right)P(\left(m\text{-}1\right)T) \tag{29}$$

$$L(mT) = P(\left(m\text{-}1\right)T)x(m\mathrm{T})\left(\lambda + x^T(mT)P(\left(m\text{-}1\right)T)x(mT)\right)^{-1} \tag{30}$$

The forgetting factor (λ) value varies in between 0 and 1, and this value provides a compromise between the stability and tracking performances of the algorithm. As this value approaches 0, the tracking capability of the algorithm is improved, but negatively affects stability.

4.3 Combination of Smith Predictor Solution and Recursive Least Squares with Forgetting Factor

In the new SP design, the classical SP structure is combined with the RLSWF algorithm, aiming to eliminate the adverse effect of delay without entailing precise delay measurement. The structure used in the new SP design is shown in Figure 7. Unlike the system shown Figure 6, it is assumed that the nominal model of the system is known and only the delayed system is modeled using RLSWF. In addition, it is aimed to model only the delayed system by eliminating the necessity of modeling the delay separately.

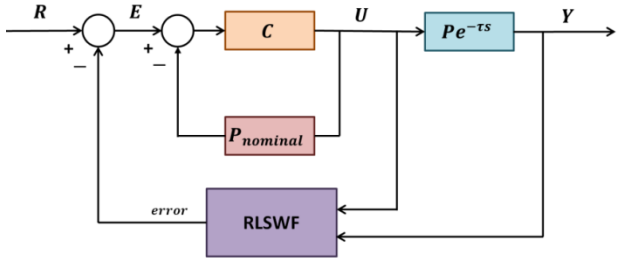

Figure 7
New SP design

In this structure, the RLSWF algorithm uses the inputs and outputs of the delayed system for identification and yields the error value between the real and the estimated system as output. This value is then subtracted from the reference signal. Similarly, the difference between the error signal and the nominal system output is given to the system controller as input. The execution performance of the new solution is directly dependent on the performance of the RLSWF algorithm. As specified in (15), if the modeling of the delayed system is done with a sufficient level of fidelity and $\left(Pe^{-\tau s} - P_{ref}e^{-\tau_{ref}s}\right) \approx 0$ is obtained, the ideal SP design is achieved. Therefore, if the RLSWF algorithm also performs high-fidelity identification and obtains the error value between the real and the identified delayed systems close to zero, more acceptable delay compensation is achieved by approaching the ideal SP design.

4.4 Novel Smith Predictor Design for Unmanned Aerial Vehicle with Delay

In order to compare the new SP design with the classical SP design, the autopilot of the Tower Trainer 60 unmanned aerial vehicle is used, in which the DOB design presented in the previous section, is also tested. In Figure 8 and Figure 9, it is observed how robust the system is against delays in the presence of a controller obtained using the H_∞ design method. Delay values are chosen as $\tau = 0.1$ s and 1 s, respectively. The reference input is a step signal. As can be seen from the results, the controller maintains a very precise tracking under the presence of process delay. In this case, there is no need for an external structure other than the controller to reduce the deteriorating effect of the delay in the presence of the specified delay values.

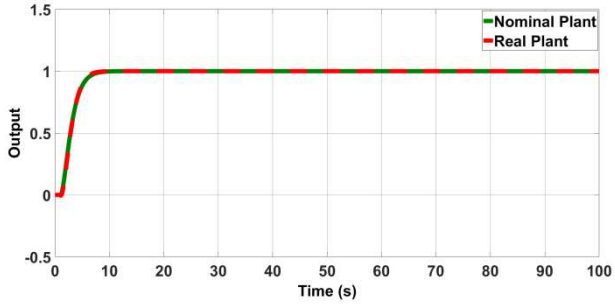

Figure 8

Closed loop responses of the system. Red and green curves show system responses in the presence and absence of $\tau = 0.1\ s$, respectively.

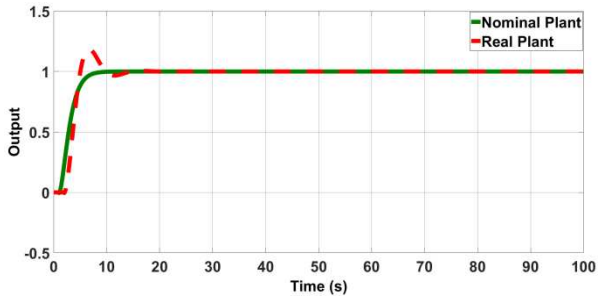

Figure 9

Closed loop responses of the system. Red and green curves show system responses in the presence and absence of $\tau = 1\ s$, respectively.

In Figure 10 the responses of nominal and delayed real systems are compared by choosing τ = 10 s. As can be seen from the figure, the system response loses its stability at high delay values and the controller cannot perform the satisfactory performance. For this reason, the novel SP design approach created using the RLSWF algorithm is added to the closed loop system and responses are examined.

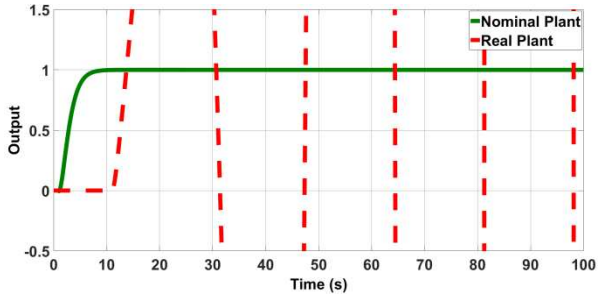

Figure 10

Closed loop responses of the system. Red and green curves show system responses in the presence and absence of $\tau = 10\ s$, respectively.

In Figure 11, the response of the closed loop system in which this design is used and the response of the system obtained in the presence of a controller only are compared. As can be seen from the figure, the new design ensures a stable response from the system by eliminating the deteriorating effect of the delay without the need for the actual delay information, even at high delay values. In this design, the performance of the RLSWF algorithm directly affects the performance of the SP design. Because as specified in Figure 7, RLSWF identifies the real system with delay and uses the identification error value in the closed loop system. Therefore, identification should be done at a high level of fidelity and this error rate should be kept low. Figure 12 shows both the response of linear system with τ = 10 s delay and the estimated system. As can be seen from the figure, the closed loop response of the linear system estimated by RLSWF is close to the real system response.

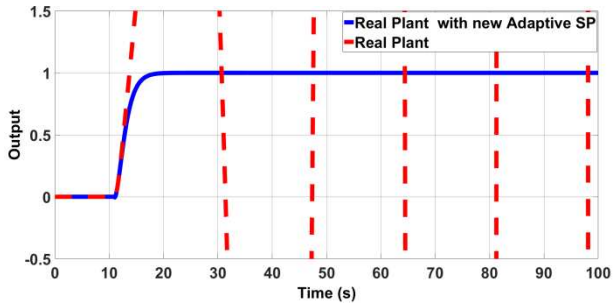

Figure 11

Closed loop responses of the system. Red and blue curves show system responses when $\tau = 10\ s$. The loop in the presence (blue) and absence (red) of new SP approach produces radically different responses.

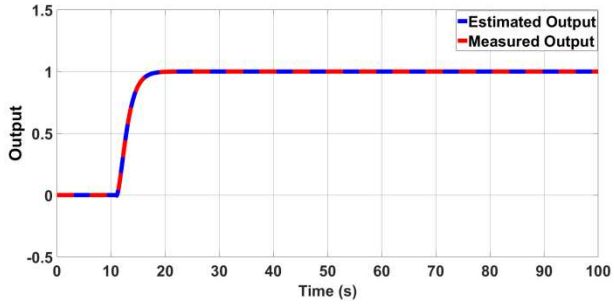

Figure 12

Identification results of the system. Blue and red curves show estimated and measured output of RLSWF, respectively.

Finally, in the Figure 13, the performances of the new SP design and classical SP design are compared in the presence of $\tau = 10\ s$ delay. As can be seen from the figure, while the new SP design performs better in terms of accuracy and speed, it does not require prior knowledge of precise measurement or delay.

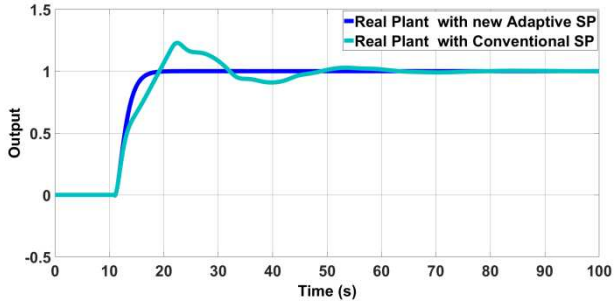

Figure 13

Responses of both classical SP and new SP design. Turquoise and blue curves indicate system responses with classical and new SP designs, respectively.

5 Online Disturbance and Delay Compensation Design

In this study, the novel DOB designed for non-minimum phase systems and the SP design which is implemented without relying on the actual delay measurement are combined to create a robust system against both time delays and disturbances. The system structure formed when two designs are combined can be seen in the Figure 14. Both designs can be developed and used independently, or they can be combined as shown in the figure. However, if the two designs are used together, the nominal delay value is required for the design of the non-minimum phase DOB. Because the process of inverting the delayed non-minimum phase system is performed once and before the system is started. For this reason, although an exact measurement of the actual delay value is not needed, only for the DOB design, the presumed nominal delay value is needed. In this way, for an actual non-minimum phase system where the delay occurs, the inverse operation can be performed accurately. During the DOB design, the delay model is approximated as $e^{-\tau s} \approx \frac{1}{\tau s+1}$. The unmanned aerial vehicle model, which is used for testing purposes in the proposed SP and DOB designs, is also used as a test system for the case, where the two designs are operating together.

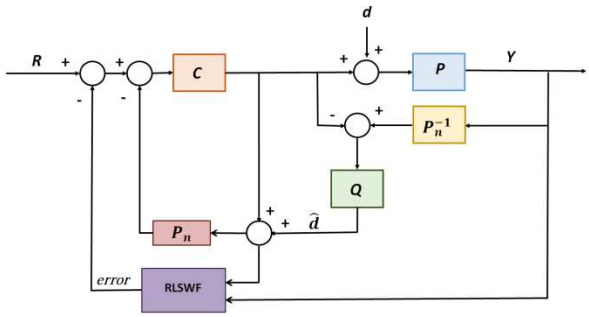

Figure 14
Online disturbance and delay compensation design

By applying the disturbances to the system with delay, system response in the presence of a controller and system responses when two designs are used together are compared. $R(t)=step\ (t)$ is given to the system as a reference input. Disturbance is chosen as $d=\sin(t)$. Figure 15 shows the case where the delay $\tau=5\ s$ and the input disturbance is given to the control signal of the system. Similarly, Figure 16 shows system response where the delay is $\tau=10\ s$ and with the same disturbance signal. As can be seen from the system responses, when both designs are used in combination, the system exhibits better tracking performance under the presence of delay and disturbances.

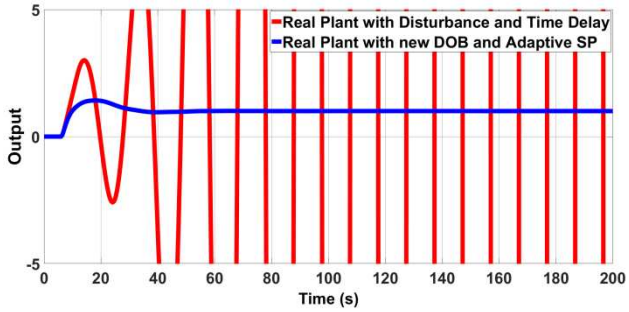

Figure 15

Closed loop responses of the system. Red and blue curves show system responses against delay $\tau = 5\ s$ and input disturbance in the absence and presence of new design, respectively.

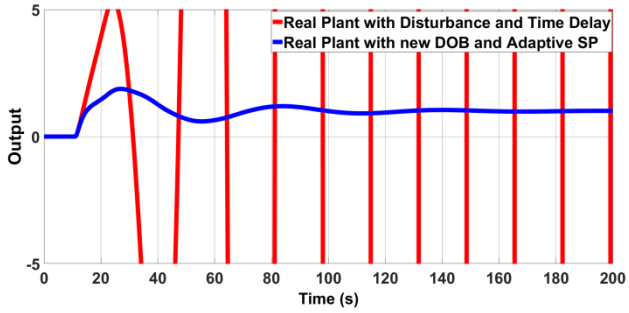

Figure 16

Closed loop responses of the system. Red and blue curves show system responses against delay $\tau = 10\ s$ and input disturbance in the absence and presence of new design, respectively.

Conclusions

This study combines SP and DOB approaches with an online identification mechanism. The following advantages of the proposed approach are as follows:

- The DOB design developed for non-minimum phase systems is used by updating the minimization problem specified in [15], and the requirement for the system to be the minimum phase is removed.
- In systems with delay, the classical SP design, which is proposed to be combined with the RLSWF algorithm, eliminates the need for precise measurement of the delay.
- Both designs can be used combined or separately. In this way, the system is made more robust when the controller alone is insufficient against delays and disturbances.

However, in cases where both designs are used together, the nominal value of the delay is needed, to correctly obtain the inverse of the non-minimum phase system.

In future work, we intend to use the RLSWF algorithm, also in a DOB design, in order to eliminate the abovementioned delay value dependency.

Acknowledgement

This study is a part of the M.S. Thesis of the first author.

References

[1] A. Turnip, & J. Panggabean: Hybrid controller design based magneto-rheological damper lookup table for quarter car suspension, Int. J. Artif. Intell, Vol. 18(1), 2020, pp. 193-206

[2] H. Shim, N. H. Jo: An almost necessary and sufficient condition for robust stability of closed loop systems with disturbance observer, Automatica, Vol. 45, 2009, pp. 296-299

[3] T. Haidegger, L. Kovács, R. E. Precup, S. Preitl, B. Benyó, Z. Benyó: Cascade control for telerobotic systems serving space medicine. IFAC Proceedings Volumes, Vol. 44(1), 2011, pp. 3759-3764

[4] T. Haidegger, L. Kovács, R. E. Precup, B. Benyó, Z. Benyó, S. Preitl: Simulation and control for telerobots in space medicine, Acta Astronautica, Vol. 81(1), 2012, pp. 390-402

[5] V. M. Aparanji, U. V. Wali, R. Aparna: Multi-Layer Auto Resonance Network for Robotic Motion Control, Int. J. Artif. Intell, Vol. 18(1), 2020, pp. 19-44

[6] Y. Sun, C. Xu, H. Yu: Research of adjusted Smith predictor based on immune feedback, IEEE International Conference on Measuring Technology and Mechatronics Automation, Vol. 2, 2010, pp. 1072-1075

[7] O. Camacho, F.D. la Cruz: Smith Predictor Based-Sliding Mode Controller for Integrating Processes with Elevated Deadtime, ISA Transactions, Vol. 43, 2004, pp. 257-270

[8] I. Barkana: Classical and simple adaptive control for non-minimum phase autopilot design, J. Guidance, Control, and Dynamics, Vol. 28, No. 4, 2005, pp. 631-638

[9] A. S. Nemirovski, M. J. Todd: Interior-point methods for optimization, Acta Numerica, Vol. 17, 2008, pp. 191-234

[10] A. Vahidi, A. Stefanopoulou, H. Peng: Recursive least squares with forgetting for online estimation of vehicle mass and road grade: theory and experiments, Vehicle System Dynamics, Vol. 43, No. 1, 2005, pp. 31-55

[11] A. Krejčí, T. Popule, and M. Goubej: Closing the motion control loops via industrial ethernet network, in Proceedings of the 2014 15th International Carpathian Control Conference, 2014, pp. 273-278

[12] X. Chen, G. Zhai, T. Fukuda: An approximate inverse system for non-minimum phase systems and its application to disturbance observer, Systems & Control Letters, Vol. 52, 2004, pp. 193-207

[13] I. H. Kim, Y. I. Son: Robust Control for Input Time Delay Systems: A Disturbance Observer Approach, SICE Annual Conference, 2010, pp. 179-183

[14] N. H. Jo, H. Shim, Y. I. Son: Disturbance Observer for Non-minimum Phase Linear Systems, International Journal of Control, Automation, and Systems, Vol. 8, 2010, pp. 994-1002

[15] E. Sarıyıldız, K. Ohnishi: A New Solution for the Robust Control Problem of Non-minimum Phase Systems using Disturbance Observer, IEEE International Conference on Mechatronics (ICM), 2013, pp. 46-51

[16] L. Wang, J. Su: Disturbance rejection control for non-minimum phase systems with optimal disturbance observer, ISA Transactions, Vol. 57, 2014, pp. 1-9

[17] C. B. Regaya, A. Zaafouri, A. Chaari: A new sliding mode speed observer of electric motor drive based on fuzzy-logic, Acta Polytechnica Hungarica, Vol. 11(3), 2014, pp. 219-232

[18] R. Muradore, P. Fiorini: A review of bilateral teleoperation algorithms, Acta Polytechnica Hungarica, Vol. 13(1), 2016, pp. 191-208

[19] L. Márton, Z. Szántó, T. Haidegger, P. Galambos, J. Kövecses: Internet-based bilateral teleoperation using a revised time-domain passivity controller, Acta Polytechnica Hungarica, Vol. 14(8), 2017, pp. 27-45

[20] H. Shim, Y. J. Joo: State space analysis of disturbance observer and a robust stability condition, IEEE Conf. on Dec. and Control, 2007, pp. 2193-2198

Torque Prediction of Ankle Joint from Surface Electromyographic Using Recurrent Cerebellar Model Neural Network

Hai-Yan Jiang[1,2], Shou-Yan Yu[1], Chih-Min Lin[3,*], Yan Chen[1,2], Shu-Ping Huang[1,2]

[1] College of Electrical Engineering and Automation, Fuzhou University, Fuzhou, 350108, Fujian, China, jianghaiyan@fzu.edu.cn, n170127071@fzu.edu.cn, n180127014@fzu.edu.cn, n190127024@fzu.edu.cn

[2] Fujian Key Lab of Medical Institute and Pharmaceutical Technology, Fuzhou University, Fuzhou, 350108, Fujian, China

[3]Department of Electrical Engineering, Yuan Ze University, Tao-Yuan 320, Taiwan, cml@saturn.yzu.edu.tw

*Corresponding author

Abstract: Joint torque prediction plays an important role in quantitative limb rehabilitation training and the exoskeleton robot. The Surface electromyography signal (sEMG) with the advantages of non-invasive and easy collection can be applied to the prediction of human muscle force. By utilizing the sEMG, the recurrent cerebellar model neural network (RCMNN), which has better generalization and computational power than the traditional neural network has been used to predict the joint torque. In this work, a smooth function with adaptive coefficient is employed to polish the results of RCMNN, the proposed method shows great performance on torque prediction with the correlation coefficient between the torque and the estimation result up to 98.43%, such advanced model paves the way to the application on the quantitative rehabilitation training.

Keywords: Torque prediction; ankle joint; sEMG; RCMNN

1 Introduction

Joint torque prediction plays an important role in quantitative limb rehabilitation training and exoskeleton robots [1]. A number of kinematics and non-invasive methods have been proposed to estimate the joint torque, but most of these require special measuring apparatus, such as isokinetic dynamometers, which made these methods unsuitable for application in patients' daily lives and operations outside the lab. The Surface electromyographic (sEMG) signals are a kind of biological

electrical signals recorded on the skin surface, containing movement intentions of the human body [2]. Generally, compared with electromyographic (EMG) signals collected by needle electrodes, sEMG signals are widely used in rehabilitation medicine and sports medicine [3-6] because of their advantages in terms of simple operation, non-invasive and multi-point measurement. Moreover, due to the transmission time, sEMG signal is generated 30-150 ms earlier than human muscle movements, which makes it a valuable signal source for man-machine interaction technology [7]. Therefore, it is of significance to use the sEMG signals in the joint torque prediction.

Several nonlinear models have been proposed for estimation of ankle joints torque from the sEMG signals, such as artificial neuron network (ANN) and fuzzy model (FCM) [8-13], which actually obtained good results in various nonlinear modeling. Kim et al. [14] using deep neural network to estimate the torque by the sEMG signal. Lu et al. [15] developed an sEMG-based torque estimation control strategy for a soft elbow exoskeleton. Xu et al. [16] proposed an sEMG-based joint torque estimation strategy combining with hill-type muscle model by using radical basis function neural network to make the results of muscular movement digitized. Currently, artificial neuron network (ANN) as a nonlinear model is still the most popular model used in torque prediction [17-19]. However, the learning of the neural network is slow since all the weights are updated during each learning cycle. The cerebellar model neural network (CMNN) has been widely used in high-precision control fields due to its simple structure, good generalization, rapid learning speed and good convergence [20-26]. A recurrent unit, which considers the effect of the previous moment on the current moment, is added to the CMNN to make it a recurrent CMNN (RCMNN). Since the prediction problem is relative to time sequence, the prediction performance of RCMNN is better than CMNN. Therefore, utilizing the sEMG and RCMNN to predict joint torque is an essential project in a wide range of real-time applications.

In this paper, an sEMG-driven RCMNN is introduced to predict the torque of the ankle joint. A group of processed signals consisting of the joint angular velocity, accelerometer signals, and sEMG signal related to the joint torque are sent to the predictor and then the prediction output result is obtained. At last, a smoothing function with the adaptive coefficient is used to process the output result of the RCMNN to obtain the final torque prediction result.

2 Data Acquisition

To estimate the ankle joint torque, Delsys Trigno Wireless System was used for collecting sEMG signals, and BIODEX System 4 Pro Strength Testing System was applied for collecting angular velocity, accelerometer, and torque signals

(Fig. 1(a)). Five Trigno sEMG sensors were placed on the subject muscles, including gastrocnemius, tibialis anterior, peroneus Longus, extensor halluces longus, and extensor digitorum longus, for detecting the sEMG signals on the disinfected skin surface. Then the subjects were fixed on BIODEX System 4 Pro Strength Testing System to swing ankle joint eversion and inversion as described in Fig. 1 (b). The raw data from the sEMG and position sensors are sampled at rates of 2000 Hz and 418 Hz using a 16-bit A/D converter, respectively. Note that all the subjects, ranging in age from 17-42 years participated in this study, are in ankle health, and none of them has a history of injuries.

(a) (b)

Figure 1
The system setup for the experiment

After data acquisition, a serial of raw sEMG data were collected and shown in Fig. 2.

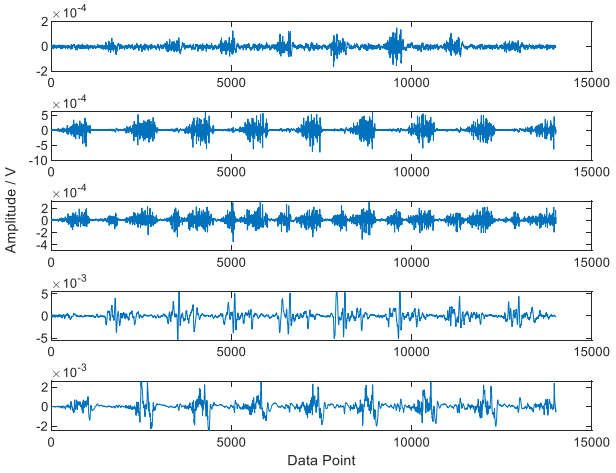

Figure 2
The raw sEMG signals

In Fig. 2, from top to bottom are the amplitudes of gastrocnemius, tibialis anterior, longus tibialis, extensor pollicis, extensor digitalis longus.

3 Data Processing

3.1 Outlier Processing and De-noising

Due to the undesirable noise and disturbances, the raw sEMG signals are hardly estimated the ankle joint torque. As known, the surface muscle telecommunications energy is mainly concentrated between the frequency bands of 20 Hz and 500 Hz. For this reason, the raw signal can be filtered by removing the uncorrelated frequency band and the 50 Hz power frequency. In this study, the signal is processed by Fourier transform using a filter with the amplitude of the incoherent frequency at zero. Then, the inverse transform is performed to obtain the processed data of tibialis anterior shown in Fig. 3.

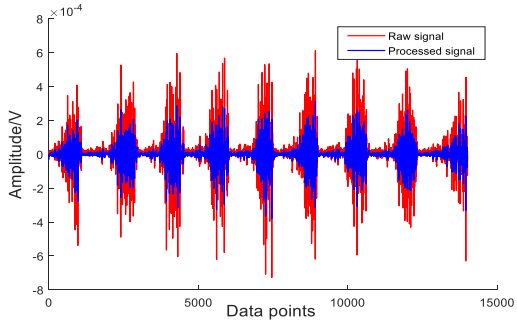

Figure 3
Contrast between raw signal and denoised signal

It can be seen that the processed signal effectively restrains the noise and preserves the peaks and the abrupt part so that it can retain the characteristics of the raw signal.

3.2 De-redundancy

However, redundancy may exist between the sEMG signals of five muscles [27], which will limit the prediction accuracy of the neural network and increase the calculation amount and the prediction time of the model.

In this section, a correlation coefficient is employed to determine the degree of coupling among different sEMG signals of muscles. The formula is described as follows

$$\sigma_i = \sqrt{\frac{1}{N}\sum_{n=1}^{N}(f_i(n)-\bar{f}_i)}\,,\ n=1,2...N \tag{1}$$

$$C_{ij} = \frac{1}{N}\sum_{n=1}^{N}(f_i(n) - \bar{f}_i)(f_j(n) - \bar{f}_j), n = 1,2...N \tag{2}$$

$$\rho_{ij} = \frac{C_{ij}}{\sigma_i \cdot \sigma_j} \tag{3}$$

where σ_i is the standard deviation of the sEMG signal on the *i*-th muscle surface, and C_{ij} and ρ_{ij} are the covariance and correlation coefficients of the sEMG signals on the *i*-th and *j*-th muscle surfaces.

Finally, the correlation coefficient of the five muscles is shown in the following table.

Table 1
Correlation coefficient between muscles

Muscle 1 / Muscle 2	Gas	T-A	L-T	E-P	E-D-L
Gas	1	0.0277	-0.0868	0.2175	0.0589
T-A	0.0277	1	-0.4539	-0.0684	0.1451
L-T	-0.0868	-0.4539	1	0.0140	-0.1261
E-P	0.2175	-0.0684	0.0140	1	-0.0898
E-D-L	0.0589	0.1451	-0.1261	-0.0898	1

P.S. Gas, T-A, L-T, E-P, and E-D-L represent gastrocnemius, tibialis anterior, Longus tibialis, extensor pollicis, extensor digitalis longus respectively.

Furthermore, to determine whether there is redundancy between the data, a method shown as Fig. 4 is used.

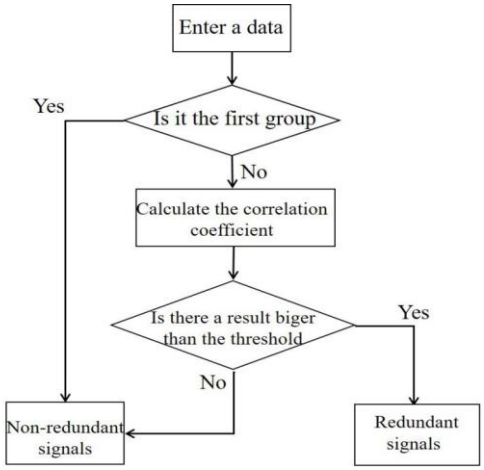

Figure 4
Redundancy decision flowchart

In this flowchart, all the data is divided into redundant signals and non-redundant signals. The first group of data, the gastrocnemius signal, is put into non-redundant information and a threshold (absolute value is 0.4) is set. Then, the second group data is input, and calculate the correlation coefficient between group 2 and non-redundant information. The correlation coefficient of the data is compared with the threshold value. When the correlation coefficients are bigger than the threshold value, the data is considered as redundant data, otherwise for the non-redundant data. Repeat the second step until all the data is judged.

According to Table 1 and Fig. 4, the signals of the tibialis anterior and longus tibialis are redundant.

3.3 Resampling

Because the sampling frequency of sEMG (2,000 Hz) is higher than that of joint angle and joint force. In order to match the length of the sEMG signal the in time-domain, the joint torque data are also re-sampled and are then smoothed. To test the effect of redundancy, in this paper, the data set is divided into a redundant group and a non-redundant group. The redundant data set includes processed 5 channels of sEMG, joint angular velocity and accelerometer signals, and the non-redundant data group includes 4 channels of sEMG except gastrocnemius, as well as joint angular velocity and accelerometer signals. The redundant group and non-redundant group data after resampling are 7-dimensional and 6-dimensional feature vectors respectively, and they will be inputted into the RCMNN.

4 Review of RCMNN

4.1 Structure of RCMNN

The schematics of the RCMNN are shown in Fig. 5 with the input space, the association memory space, the receptive-field space, the weight memory space, and the output space [28].

Input Space For a given input data I_i, i=1,2,…,m, each input variable I_i is quantized into n discrete regions (called “elements” or “neurons”) according to given control space. The value of neurons n is called resolution. Based on this n element, n layers are defined in total.

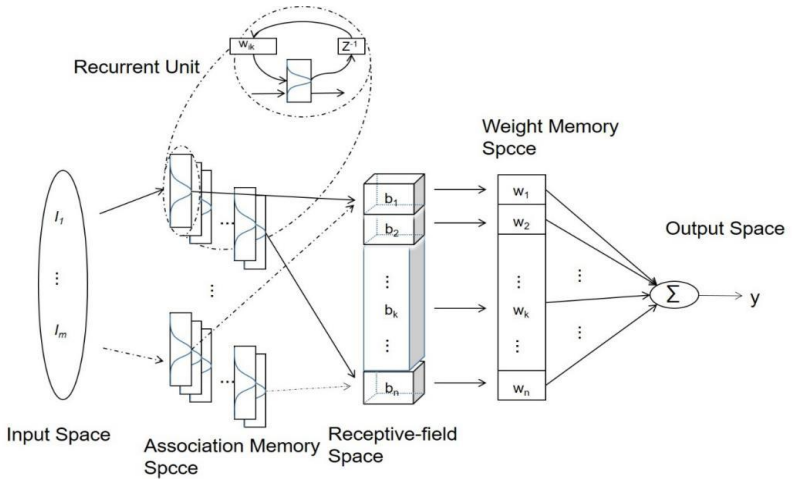

Figure 5
Architecture of a RCMNN [28]

Association Memory Space In the space, the Guass function is used as the receptive-field basis function, which can be expressed as

$$r_{ik} = \exp[-\frac{(I_{ik} - m_{ik})^2}{\sigma_{ik}^2}], i = 1,2,...,m, k = 1,2,...,n \tag{6}$$

where r_{ik} represents the output of the *k*-th receptive-field basis function for the *i*-th input, and the mean m_{ik} and variance σ_{ik} represent the center point and width of the Gaussian function. In addition, I_{ik} is the result of the recurrent unit and can be represented by

$$I_{ik}(\mathrm{t}) = I_i(t) + w_{ik} r_{ik}(t-1) \tag{7}$$

where t denotes the time step, and $r_{ik}(t-1)$ is the value of r_{ik} through a time delay; w_{ik} is the recurrent gain, and the size of the value represents impact of the information of one previous point to the current moment.

To further understand w_{ik} here, a linear function instead of the Gaussian function is chosen as basis function and is defined as

$$r_{ik}(t) = I_{ik}(t) \tag{8}$$

Then, (7) can be expressed as

$$r_{ik}(\mathrm{t}) = I_i(t) + w_{ik} r_{ik}(t-1) \tag{9}$$

Since

$$r_{ik}(\text{t-1}) = I_i(t-1) + w_{ik} r_{ik}(t-2) \tag{10}$$

Equation(9) becomes

$$\begin{aligned} r_{ik}(\text{t}) &= I_i(t) + w_{ik} r_{ik}(\text{t-1}) \\ &= I_i(t) + w_{ik} I_i(t-1) + w_{ik}{}^2 r_{ik}(\text{t-2}) \\ &= I_i(t) + w_{ik} I_i(t-1) + \ldots + w_{ik}{}^{n-1} I_i(t-n+1) + w_{ik}{}^n r_{ik}(t-n). \end{aligned} \tag{11}$$

Obviously, the output of RCMNN in the associative memory space contains the information of all previous parameters.

Receptive-Field Space The *k*-th multidimensional receptive-field function is defined as

$$\text{b}_k = \prod_{i=1}^{m} r_{ik}, \; k = 1,2,\ldots,n, \; i = 1,2,\ldots,m \tag{12}$$

The output of the space indicates the excitation intensity for the last space.

Weight Memory Space The weight of the receptive-field space with the output space is stored in the space and denoted in a vector as

$$w = [w_1,\ldots,w_k,\ldots,w_n]^T \tag{13}$$

Output Space The output of RCMNN is the algebraic sum of the Receptive-Field Space in the weight memory space and is shown as

$$y = \sum_{k=1}^{n} (w_k \cdot b_k) \tag{14}$$

4.2 Learning Algorithm of RCMNN

In this section, backpropagation (BP) is applied to update the parameters m_{ik}, σ_{ik}, w_{ik} and w of RCMNN. While BP is the iterative gradient decent algorithm designed to minimize the mean square error of an objective function defined as

$$E = \frac{1}{2}(y_0 - y)^2 = \frac{1}{2}e^2 \tag{15}$$

where $e = y_0 - y$, y_0 is the previous known value for the testing data and the expected output of neural network.

The parameter updating rule based on the gradient descent algorithm is derived according to

$$P(N+1) = P(N) + \Delta P = P(N) + \eta_P \frac{-\partial E(N)}{\partial P} \tag{16}$$

where η_p is a learning rate, and if P is replaced by m_{ik}, σ_{ik}, w_{ik} and w then it denotes the updating rule for mean, variance, recurrent gain, and output weight, respectively.

The changed values of the above parameters are calculated by the chain rule represented as

$$\begin{aligned} \Delta w_k &= -\eta_{\mathrm{w}} \frac{\partial E}{\partial w_k} = \frac{\partial E}{\partial y}\frac{\partial y}{\partial w_k} \\ &= \eta_{\mathrm{w}} (y_0 - y) \cdot b_k \end{aligned} \tag{17}$$

$$\begin{aligned} \Delta m_{ik} &= -\eta_m \frac{\partial E}{\partial m_{ik}} = \frac{\partial E}{\partial y}\frac{\partial y}{\partial b_k}\frac{\partial b_k}{\partial r_{ik}}\frac{\partial r_{ik}}{\partial m_{ik}} \\ &= \eta_m (y_0 - y) \cdot w_k \cdot b_k \cdot \frac{2(I_{ik} - m_{ik})}{\sigma_{ik}^2} \end{aligned} \tag{18}$$

$$\begin{aligned} \Delta \sigma_{ik} &= -\eta_\sigma \frac{\partial E}{\partial \sigma_{ik}} = \frac{\partial E}{\partial y}\frac{\partial y}{\partial b_k}\frac{\partial b_k}{\partial r_{ik}}\frac{\partial r_{ik}}{\partial \sigma_{ik}} \\ &= \eta_\sigma (y_0 - y) \cdot w_k \cdot b_k \cdot \frac{2(I_{ik} - m_{ik})^2}{\sigma_{ik}^3} \end{aligned} \tag{19}$$

$$\begin{aligned} \Delta w_{ik} &= -\eta_{\mathrm{wik}} \frac{\partial E}{\partial w_{ik}} = \frac{\partial E}{\partial y}\frac{\partial y}{\partial b_k}\frac{\partial b_k}{\partial r_{ik}}\frac{\partial r_{ik}}{\partial I_{ik}}\frac{\partial I_{ik}}{\partial w_{ik}} \\ &= \eta_{\mathrm{wik}} (y_0 - y) \cdot w_k \cdot b_k \cdot \frac{2(m_{ik} - I_{ik})}{\sigma_{ik}^2} \cdot r_{ik}(t-1) \end{aligned} \tag{20}$$

4.3 Convergence Analyses [29]

Theorem 1 Let η_p be the learning-rates for the P in (16). Then, the convergence of tracking error is guaranteed if η_p is chosen as

$$0 < \eta_P < \frac{2}{Y^2} \tag{21}$$

where $Y = \dfrac{\partial y(N)}{\partial P}$.

Proof Define a Lyapunov functions as

$$V(N) = \frac{1}{2} e(N)^2 \tag{22}$$

Then, the change of the Lyapunov function is obtained as

$$\begin{aligned}\Delta V\ (N) &= V(N+1)-V(N)\\ &= \frac{1}{2}(e(N+1)^2-e(N)^2)\\ &= \frac{1}{2}(e(N+1)+e(N))\cdot\Delta e(N)\end{aligned} \tag{23}$$

According to the Taylor formula and the chain rule, the error function variation can be expressed as

$$\Delta e\ (N) \cong \frac{\partial e(N)}{\partial P}\cdot\Delta P \tag{24}$$

Among these,

$$\frac{\partial e(N)}{\partial P} = \frac{\partial e(N)}{\partial y(N)}\cdot\frac{\partial y(N)}{\partial P} = -1\cdot\frac{\partial y(N)}{\partial P} \tag{25}$$

and

$$\Delta P = -\eta\frac{\partial E(N)}{\partial P} = -\eta\cdot(-e(N)\cdot\frac{\partial y(N)}{\partial P} = \eta\cdot e(N)\cdot\frac{\partial y(N)}{\partial P}. \tag{26}$$

Using (25) and (26), (24) becomes

$$\begin{aligned}\Delta e\ (N) &\cong \frac{\partial e(N)}{\partial P}\cdot\Delta P\\ &= (-1\cdot\frac{\partial y(N)}{\partial P})\cdot(\eta\cdot e(N)\cdot\frac{\partial y(N)}{\partial P})\\ &= -\eta\cdot e(N)\cdot(\frac{\partial y(N)}{\partial P})^2 \equiv -\eta\cdot e(N)Y^2.\end{aligned} \tag{27}$$

From (27), $\Delta V(N)$ can be represented as

$$\begin{aligned}\Delta V\ (N) &= \frac{1}{2}(2e(N)+\Delta e(N))\cdot\Delta e(N)\\ &= \frac{1}{2}\eta e(N)^2Y^2(\eta Y^2-2)\end{aligned} \tag{28}$$

If η_P is chosen as $0<\eta_P<\frac{2}{Y^2}$, $\Delta V(N)<0$ is guaranteed obviously. And easily, for any $0\le y_0(N)\le 1$, $0\le y(N)\le 1$, there is $V(N)\ge 0$. Therefore, the Lyapunov stability of $V(N)\ge 0$ and $\Delta V(N)<0$ is guaranteed, which can explain the convergence of tracking error. The derivation results prove that the convergence of RCMNN model is guaranteed.

5 Simulation Result

In this experiment, the goal of the model training is to find the values of the parameters m_{ik} , σ_{ik} , w_{ik} and w that minimizes the overall error. We take the 7-dimensional redundant data set and 6-dimensional non-redundant data set as the input data of the RCMNN (Fig. 5) respectively, and the joint signals as output data. We randomly selected 80% data for training and verification, 20% data for testing. To compare the RCMNN with other methods, we use CMNN, and the most popular artificial neural network BP. The performance of trained models was subsequently tested by comparing predicted torque values from the model and the measured torque values. RMSE (Root Mean Square Error), NMAE (Normalized Mean Absolute Error), NRMSE (Normalized Root Mean Square Error), and CC (Correlation Coefficient) between the predicted joint torque and the measure joint torque data are used to evaluate network performance.

5.1 The Updated RCMNN

In the training of RCMNN, in order to make the RCMNN converge faster, the learning-rate η_p is set as

$$\eta_p = \frac{c}{t} \tag{29}$$

In which c is a constant, and t is the training times. Obviously, the equation is in line with the law of error convergence. Because as the number of training increases, the error will continue to decrease, and when the error is small enough, an excessive learning rate will cause the error to oscillate. Thereby a decreasing learning rate accelerates the rate of convergence during model training, making the model meet the standard faster.

After 50 times training, the results are drawn in Fig. 6 (a). Note that the output of RCMNN is generally close to the true value with a slight vibration, which is obvious at the bottom of the waveform. To smooth the waveform, the smooth function is applied in RCMNN, which is represented as follows

$$f(t) = c_1 f(t) + c_2 f(t-1) + c_3 f(t-2) \tag{30}$$

where $f(t)$ is the data point at time t, and c_1 ,c_2 ,c_3 are set as 0.5, 0.3, 0.2, respectively.

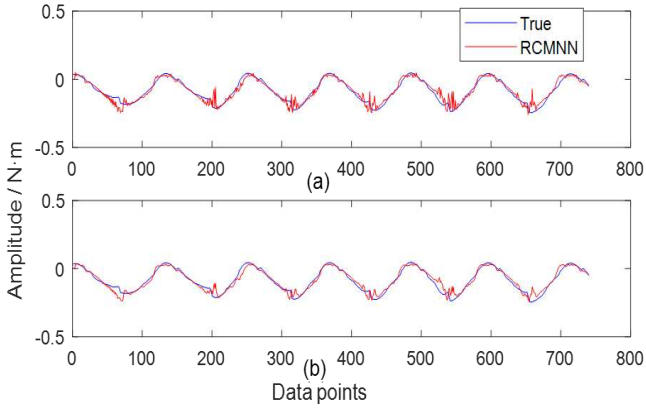

Figure 6
Result of training data

Table 2
Comparison of the three cases

Results	RMSE	NMAE	NRMSE	CC
(a)	0.0273	0.1937	0.2299	0.9454
(b)	0.0239	0.1828	0.2009	0.9582

P.S. RMSE (Root Mean Square Error) = $\sqrt{\frac{1}{n}\sum_1^n (y_0 - y)^2}$

NMAE (Normalized Mean Absolute Error) = $\sum_1^n |y_0 - y| / \sum_1^n |y_0|$

NRMSE (Normalized Root Mean Square Error) = $\sqrt{\sum_1^n (y_0 - y)^2 / \sum_1^n (y_0)^2}$

CC (Correlation Coefficient) shown on formula (2)

As shown in Fig. 6 (b) and Table 2, the frequency and amplitude of oscillation have a great reduction compared to the original output (Fig. 6 (a)).

In the testing of RCMNN, the input data is sent to the predictor, and the prediction results and smoothed results are shown in Fig. 7 and the specific parameters are shown in Table 3.

Table 3
Comparison of the two cases

Results	RMSE	NMAE	NRMSE	CC
a	0.0281	0.2333	0.2483	0.9555
b	0.0254	0.2188	0.2248	0.9640

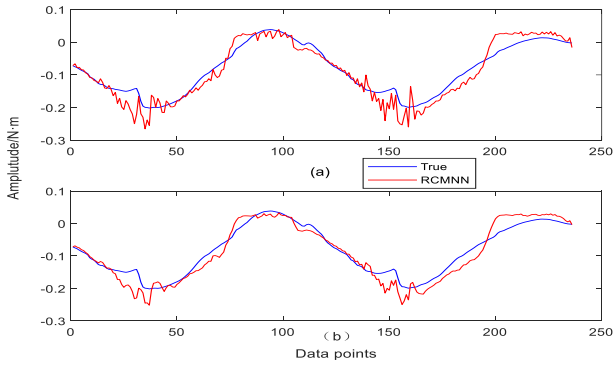

Figure 7
Result of testing data

Results show the peaks and troughs of the output of the model appear significantly earlier than the sample output, while the smoothed RCMNN greatly improves the situation of oscillation, proving the validity of RCMNN.

5.2 Results

The results obtained by the RCMNN, CMNN, and BP network of the redundant group and the non-redundant group are shown in Table 4 and Table 5 respectively. Table 4 and Table 5 show that the performance of the RCMNN is better than that of BP and CMNN, due to its recurrent unit. In addition, according to Table 4 and Table 5, although the redundant group has one more dimensionality information related to the torque of ankle than the non-redundant group, the latter generally has better performance, like RMSE, NMAE, NRMSE, and CC. Hence, our subsequent experiments use the non-redundant data group.

Table 4
Results of the redundant group

	RCMNN	CMNN	BP
RMSE	0.0254	0.0358	0.0254
NMAE	0.2188	0.3267	0.2157
NRMSE	0.2248	0.3168	0.2252
CC	0.9640	0.8826	0.9495

Table 5
Results of the non-redundant group

	RCMNN	CMNN	BP
RMSE	0.0213	0.0335	0.0233
NMAE	0.1810	0.2878	0.2056
NRMSE	0.1881	0.2957	0.2068
CC	0.9639	0.9035	0.9488

In the previous section, equation (30) is employed to smooth the output of RCMNN, and make an excellent result with a not suitable enough coefficient. In this part, an algorithm is summarized in Algorithm 1 to get a more appropriate coefficient.

Algorithm 1 adaptive coefficient algorithm

1 : Set: X(t)=[y(t-2),y(t-1),y(t)]; Y(t)=y_0(t); a weight vector with same number to the number of formula (30) coefficient and a threshold *m*.

2 : Train: Divide X(t) and Y(t) into training data and testing data; train the network until the correlation coefficient between the output of BP and is bigger than *m*.

3 : Finish: Assign the weight to the coefficient of formula (30), and use testing data to verify whether the coefficient is suitable.

With the coefficient gotten by Algorithm 1, the non-redundant group shows its experimental results as Table 6.

Table 6
The results with the coefficient gotten by algorithm 1

Subjects	RMSE	NMAE	NRMSE	CC
1	0.0023	0.0266	0.0291	0.9864
2	0.0026	0.0194	0.0235	0.9866
3	0.0025	0.0364	0.0427	0.9843
4	0.0028	0.0216	0.0226	0.9867

In Table 6, after the weights obtained after training by the BP neural network are used as the coefficients of Formula (30), the experimental results obtained by the predictor are greatly improved. The correlation coefficient between the experimental output results and the torque data has been increased by more than two percentage points, and the improved performance of other parameters are also obvious. One of the curves on training data and testing data is drawn as follows.

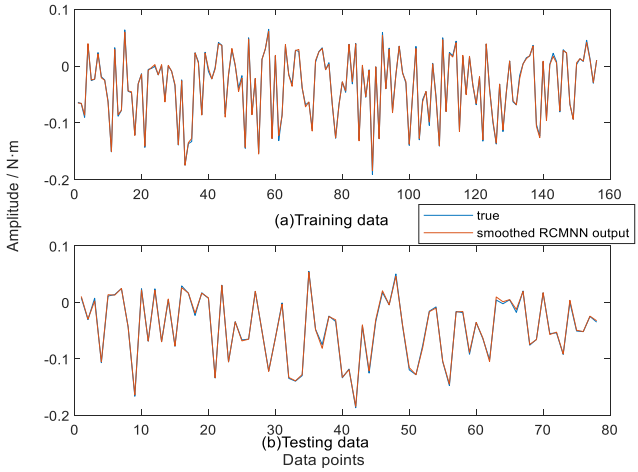

Figure 8
Performance of RCMNN after smoothing

Conclusions

In this study, a RCMNN is employed as a predictor to estimate torque of ankle joint from velocity, position and sEMG signals. RCMNN shows excellent fitting ability in torque prediction, that is the correlation coefficient between torque and estimation result reaches 98.43%, and other performance parameters like RMSE, NMAE, and NRMSE are also satisfactory. Moreover, RCMNN accelerates the torque prediction, making the predictor a control source of the bionic prosthesis and rehabilitation robot. Hence, the outstandingly fitting ability of RCMNN has great application prospects on torque prediction.

References

[1] T. Kikuchi, C. Sato, K. Yamabe, et al. "Upper limb training/assessment program using passive force controllable rehabilitation system," IEEE International Conference on Rehabilitation Robotics, pp. 505-510, 2017

[2] Q. B. Lin, S. C. Chen and C. M. Lin, "Parametric fault diagnosis based on fuzzy cerebellar model neural networks," IEEE Transactions on Industrial Electronics, Vol. 66, No. 10, pp. 8104-8115, 2019

[3] R. Merletti and P. Parker, "Electromyography: physiology, engineering, and noninvasive applications." New York, USA: IEEE Press, pp. 381-425, 2004

[4] M. Atzori, A. Gijsberts, C. Castellini, et al. "Clinical parameter effect on the capability to control myoelectric robotic prosthetic hands," Journal of Rehabilitation Research & Development, Vol. 53, No. 3, pp. 345-58, 2016

[5] C. S. Li , Y. Q. Zhou and Y. Li, "The signal processing and identification of upper limb motion based on sEMG," Wireless Personal Communications, Vol. 103, No. 1, pp. 887-896, 2018

[6] B. P. Xiong, N. Y. Zeng, H. Li, et al. "Intelligent prediction of human lower extremity joint moment: an artificial neural network approach". IEEE Access, Vol. 7, pp. 29973-29980, 2019

[7] J. Chu, I. Moon, Y. Lee, S. Kim and M. Mun, "A supervised feature-projection-based real-time EMG pattern recognition for multifunction myoelectric hand control," IEEE/ASME Transactions on Mechatronics, Vol. 12, No. 3, pp. 282-290, 2007

[8] W. Y. Cheng, C. F. Juang. "A fuzzy model with online incremental SVM and margin-selective gradient descent learning for classification problems," IEEE Transactions on Fuzzy Systems, Vol. 22, No. 2, pp. 324-337, 2014

[9] R. E. Precup, T. A. Teban, A. Albu, et al. "Evolving fuzzy models for prosthetic hand myoelectric-based control," IEEE Transactions on Instrumentation and Measurement, Vol. 69, No. 7, pp. 4625-4636, 2020

[10] C. F. Juang, Y. Y. Lin, R. B. Huang, "Dynamic system modeling using a recurrent interval-valued fuzzy neural network and its hardware implementation," Fuzzy Sets & Systems, Vol. 179, No. 1, pp. 83-99, 2011

[11] R. Zall and M. R. Kangavari, "On the construction of multi-relational classifier based on canonical correlation analysis," International Journal of Artificial Intelligence, Vol. 17, No. 2, pp. 23-43, 2019

[12] E. Hedrea, R. Precup, R. Roman, et al. "Tensor product- based model transformation approach to tower crane systems modelling," Asian Journal of Control, DOI: 10.1002/asjc.2494, 2021

[13] C. Pozna, R. E. Precup, "Applications of signatures to expert systems modelling," Acta Polytechnica Hungarica, Vol. 11, No. 2, pp. 21-39, 2014

[14] H. Kim, H. Park, S. Lee, et al. "Joint torque estimation using sEMG and deep neural network," J. Electr. Eng. Technol. Vol. 15, pp. 2287-2298, 2020

[15] L. Lu, Q. Wu, X. Chen et al. "Development of a sEMG-based torque estimation control strategy for a soft elbow exoskeleton," Robotics and Autonomous Systems, Vol. 111, pp. 88-98, 2019

[16] D. Xu, Q. Wu, and Y. Zhu, "Development of a sEMG-based joint torque estimation strategy using hill-type muscle model and neural network," Journal of Medical and Biological Engineering, pp. 1-11, 2020

[17] M. H. Jali, T. A. Izzuddin, Z. H. Bohari, et al. "Predicting EMG based elbow joint torque model using multiple input ANN neurons for arm rehabilitation," 2014 UKSim-AMSS 16th International Conference on Computer Modelling and Simulation, pp. 188-193, 2014

[18] Y. Liu, S. M. Shih, S. L. Tian, et al. "Lower extremity joint torque predicted by using artificial neural network during vertical jump". Journal of Biomechanics, Vol. 42, No. 7, pp. 906-911, 2009

[19] J. Han, Q. Ding, A. Xiong and X. Zhao, "A state-space EMG model for the estimation of continuous joint movements," IEEE Transactions on Industrial Electronics, Vol. 62, No. 7, pp. 4267-4275, 2015

[20] J. S. Albus, "A new approach to manipulator control: the cerebellar model articulation control," Journal of Dynamic System, Measurement and Control, Vol. 97, No. 3, pp. 220-227, 1975

[21] J. S. Albus, "Data storage in the cerebellar model articulation controller (CMAC)," Journal of Dynamic Systems, Measurement and Control, Vol. 97, No. 3, pp. 228-233, 1975

[22] J. S. Guan, C. M. Lin, G. L. Ji, L. W. Qian and Y. M. Zheng, "Robust adaptive tracking control for manipulators based on a TSK fuzzy cerebellar model articulation controller," IEEE Access, Vol. 6, pp. 1670-1679, 2018

[23] T. L. Le, T. T. Huynh, and C. M. Lin, "Self-evolving interval type-2 wavelet cerebellar model articulation control design for uncertain nonlinear systems using PSO" International Journal of Fuzzy Systems, Vol. 21, No. 8, pp. 2524-2541, 2019

[24] J. Zhao, Z. Zhong, C. M. Lin and H. K. Lam, "H ∞ tracking control for nonlinear multivariable systems using wavelet-type TSK fuzzy brain emotional learning with particle swarm optimization" Journal of the Franklin, Vol. 358, No. 1, pp. 650-673, 2021

[25] C. M. Lin, V. H. La and T. L. Le, "DC - DC converters design using a type-2 wavelet fuzzy cerebellar model articulation controller", Neural Computing and Applications, Vol. 32, No. 7, pp. 2217-2229, 2020

[26] T. T. Huynh, C. M. Lin, T. L. Le, H. Y. Cho, T. T. T. Pham, N. Q. K. Le and F. Chao, "A new self-organizing fuzzy cerebellar model articulation controller for uncertain nonlinear systems using overlapped Gaussian membership Functions," IEEE Transactions on Industrial Electronics, Vol. 67, No. 11, pp. 9671-9682, 2020

[27] M. Sartori, M. Reggiani, D. Farina and D. G. Lloyd, "EMG-driven forward-dynamic estimation of muscle force and joint moment about multiple degrees of freedom in the human lower extremity," PLoS ONE, Vol. 7, No. 12, pp. e52618, 2012

[28] C. M. Lin, L. Chen and D. S. Yeung, "Adaptive filter design using recurrent cerebellar model articulation controller," IEEE Transactions on Neural Networks, Vol. 21, No. 7, pp. 1149-1157, 2010

[29] T. L. Le, T. T. Huynh and C. M. Lin, "A K-means interval type-2 fuzzy neural network for medical diagnosis", *International Journal of Fuzzy Systems*, Vol. 21, No. 7, pp. 2258-2269, 2019

Efficient Prediction of the First Just Noticeable Difference Point for JPEG Compressed Images

Boban Bondžulić[1], Nenad Stojanović[1], Vladimir Petrović[2], Boban Pavlović[1], Zoran Miličević[1]

[1] Military Academy, University of Defence in Belgrade
Veljka Lukića Kurjaka 33, 11000 Belgrade, Serbia

[2] Faculty of Technical Sciences, University of Novi Sad
Trg Dositeja Obradovića 6, 21000 Novi Sad, Serbia

e-mails: boban.bondzulic@va.mod.gov.rs, nenad.m.stojanovic@vs.rs, vladimir.petrovic@uns.ac.rs, boban.pavlovic@va.mod.gov.rs, zoran.milicevic@vs.rs

Abstract: In this paper, we show that a high-level of correlation exists between a simple image feature – mean gradient magnitude and the peak signal-to-noise ratio (PSNR) of the first just noticeable difference point for JPEG image compression. On the basis of this observation, we proposed a method to estimate the JPEG quality factor which represents the effective limit between perceptually lossy and lossless coding as the PSNR of the first just noticeable difference point. The goal is optimal image/video coding, at the lowest compression bit-rate that ensures perceptually lossless output image quality. We also show that this feature can be used to predict higher PSNR just noticeable difference points.

Keywords: JPEG; just noticeable difference points; peak signal-to-noise ratio; perceptually lossless

1 Introduction

In recent years there has been a rapid development of systems for digital processing, transmission, and display of image/video content [1, 2]. This development has led to great interest in efficient image compression techniques, which are capable of improving the compression ratio and image quality [3, 4].

Various compression standards have been developed for image archiving and transmission, such as JPEG and JPEG 2000, and intraframe profiles of H.264, H.265, and VVC video coding techniques have been used [5]. Among these techniques, JPEG compression is the most common due to its low complexity [6].

Image compression techniques eliminate coding and spatial redundancy, taking into account some of the features of the human visual system (HVS) – visual redundancy. Thanks to these features, various perceptual quantization schemes, and perceptual models have been developed and built into coding systems. Thus, by applying just noticeable difference (JND) models, compression efficiency can be improved. JND models estimate the maximum degradation of the visual signal that the HVS will not notice [7]. Therefore, JND can be viewed as a perceptual threshold in image/video processing applications and can be used for perceptual image compression. In addition to compression, JND is successfully used in the objective assessment of image quality, in all three assessment techniques (no-reference [8], reduced-reference [9], and full-reference [10]), leading to performance improvements.

Existing research on JND can be divided into three main areas: 1) subjective research with the aim of collecting JND annotations, 2) mathematical modeling of the distribution of JND points and 3) prediction of the distribution of JND points for a given image or video [5]. The research in this paper can be classified in the third area, with the aim of efficiently predicting the first JND point of images with JPEG compression.

2 Related Works

Traditional JND models can be divided into pixel-wise models, in which the JND threshold is determined for each pixel individually, and sub-band models in which JND thresholds are determined for each sub-band coefficient after switching to one of the transform domains. In most pixel-wise models, the effects of luminance adaptation and contrast masking are used, while in the sub-band model, the contrast sensitivity function plays a dominant role in determining the visibility threshold [11]. As in these models, the JND threshold is determined for each pixel or sub-band separately, and which does not properly reflect the total effect of image masking, in recent years picture-wise JND has been investigated, which measures the maximum image difference that HVS will not notice [12].

Recent research shows that observers differentiate between a finite number of image quality levels, as well as, that the relationship between perceptual distortions and bit-rate/distortion level is not a smooth but rather a step-wise function [13-15]. The steps of this function represent the JND points. The first and most significant JND point refers to the transition between a pristine and an image with visible distortions, or rather the transition from perceptually lossless to perceptually lossy encoding [16]. The second JND point was obtained by detecting noticeable differences from the first JND point (anchor). Lower JND points are used as anchors to determine higher JND points.

JND points can be used to determine the satisfied-user-ratio (SUR) curves, taking into account that the user is satisfied with the visual test signal in relation to the reference visual signal, i.e. the difference in the quality of these two signals is below the JND threshold. SUR modeling that reflects user satisfaction is more suitable for streaming and coding applications than mean opinion scores which generally use a five-level scale (from the worst to excellent) [17].

JND-based subjective quality analysis has been conducted on JPEG [13, 18, 19], JPEG 2000 [19, 20], H.265 [20] and VVC compressed images [21, 22], and on H.264 [14, 15] and H.265 compressed videos [23], with results in publicly available JND-based image/video datasets.

Several JND prediction methods were proposed based on these data. JND prediction described in [24] uses local quality and masking models to form a feature vector used in a support vector regressor (SVR) with the aim of predicting the SUR curve from which the first JND can be derived. This method was extended to predict the second and third JND points in [25]. In [23] a feature set derived from the non-compressed source is input into a SVR to predict the first JND. A deep learning approach in [26] defines the quality factor of the first JND based on learning the SUR curve of the JPEG compressed image. In further research, the authors from [26] optimized the proposed architecture and applied a feature learning instead of a fine-tuning approach, which led to a significant reduction in computational cost and performance improvement [27]. A sliding-window-based search strategy to predict JND based on a deep learning perceptually lossy/lossless predictor was proposed in [28]. These prediction methods can be used in perceptual quality assessment and adaptive perceptual image/video coding [29].

Research in this paper is focused on the most widespread type of image distortion, JPEG compression. Therefore, the JND analysis was performed on MCL-JCI image dataset [13], which contains information on the JND points of JPEG compressed images. This database was used to predict JND points in [26-28]. The mean absolute error (MAE) of the PSNR between the predicted and ground truth JND distributions was used as a prediction accuracy measure. In [26] a convolutional neural network using a 12,288-dimensional vector trained on 45 and tested on the remaining 5 sources over 10 iterations yielded a MAE for the first JND point of 0.69 dB. The deep learning approach from [27] uses a 30,144-dimensional vector, and it achieved an even better result in estimating the first JND point with an MAE of 0.58 dB. Through five-fold cross-validation, the deep learning approach from [28] reached an MAE of 0.79 dB.

In this paper, we show that a much simpler approach using the mean gradient magnitude (MGM) of the source non-compressed image can be used to reliably predict the first JND point of JPEG compression. The method does not require complex vision or masking models and determines the optimal JPEG quality factor (QF) through a simple rate-distortion function using the computationally efficient PSNR metric for objective quality assessment. Reaching the desired

PSNR value of JPEG lossy compressed images has been the subject of various studies [30-34], and the results can be used here to accelerate the proposed approach.

3 Dataset Description

Prediction of the first JND (JND #1) was performed on the MCL-JCI dataset, which consists of 5,000 JPEG compressed high-resolution images (1080x1920) [13], obtained by varying the JPEG quality factor from 1 (worst) to 100 (best quality) to generate 100 compressed images for each of the 50 different source images. A total of 150 observers evaluated the images using the bisection method with at least 30 scores gathered for each image. In this method, observers compare compressed images obtained with different quality factors and determine the visual threshold when there are no differences between them. Bisection search was adopted to speed up the procedure, i.e. to reduce the number of comparisons through an iterative procedure with division into half-quality intervals. The distribution of multiple JND points was modeled by a Gaussian mixture model [13].

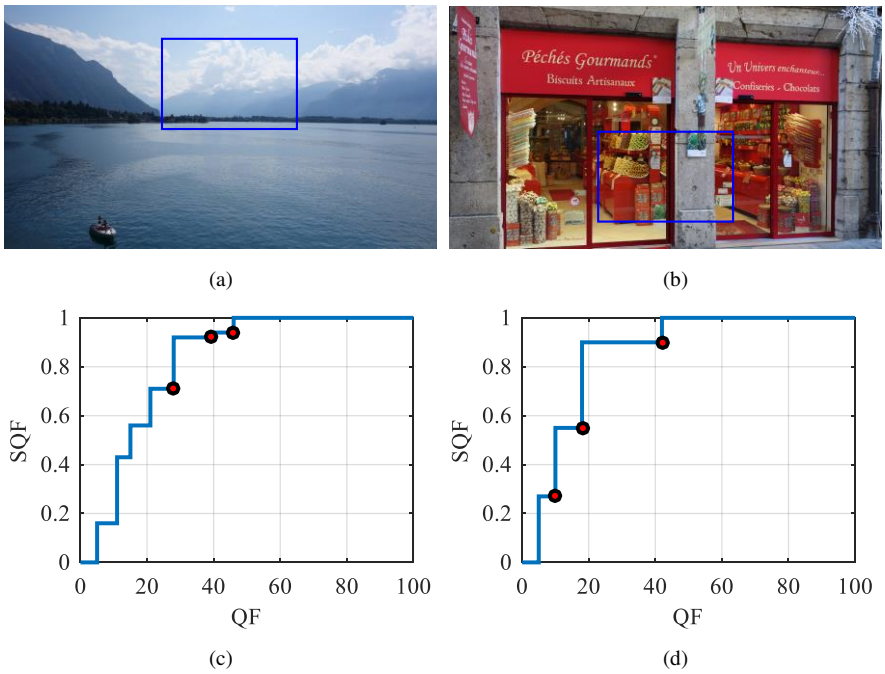

Figure 1
(a) original image with some large homogeneous areas, (b) original image rich with details, (c) and (d) are SQF functions of corresponding images above

(a) original

(b) original

(c) JND #1 (QF=46, SQF=0.94)

(d) JND #1 (QF=42, SQF=0.90)

(e) JND #2 (QF=39, SQF=0.92)

(f) JND #2 (QF=18, SQF=0.55)

(g) JND #3 (QF=28, SQF=0.71)

(h) JND #3 (QF=10, SQF=0.27)

Figure 2
Regions from the original and JPEG coded images (denoted by the red dots in Fig. 1)

The subjective trial results are presented through stair quality functions (SQF) obtained through analysis and post-processing of raw JND data. They show that human observers differentiate between 4 and 8 quality levels. Also, the results are mapped into 243 SQF points (linking all quality factors which do not produce a noticeable difference), with each original image having at least 3 JND points mainly depending on the complexity of the depicted scene.

For images that are rich in detail, due to the masking effect, the number of JND levels (points) will be lower than for images that have large homogeneous regions. Examples for two images are given in Fig. 1, one with large homogeneous regions (Fig. 1a) and the other rich in detail (Fig. 1b). Along with original images, SQF functions (higher is better) are provided – Figs. 1c and 1d. Zoomed versions (blue rectangles in Figs. 1a and 1b) of original and JPEG coded images at three lowest successive SQF levels (red dots in Figs. 1c and 1d) are shown in Fig. 2.

From Fig. 2 it can be seen that the images corresponding to JND #1 are of high quality and that there is no noticeable difference from the original. On the other hand, block effects can be seen in images corresponding to higher JNDs, and the difference from the original is noticeable.

4 Results and Analysis

As the images from MCL-JCI dataset are in RGB color format, their conversion to grayscale (luminance) images was first performed, using the weighted sum of the R (red), G (green) and B (blue) components:

$$f(n,m) = 0.299R(n,m) + 0.587G(n,m) + 0.114B(n,m). \tag{1}$$

We analysed a set of simple features derived from the grayscale images in the MCL-JCI dataset – signal standard deviation, entropy, and MGM, and determined that MGM has the best agreement with PSNR of the first JND point. Specifically, MGM was determined on an *N*x*M* grayscale image from the responses to 2D Sobel filters applied to it (g_x and g_y):

$$\begin{aligned} g_x(n,m) = {} & f(n+1,m-1) + 2f(n+1,m) + f(n+1,m+1) \\ & -[f(n-1,m-1) + 2f(n-1,m) + f(n-1,m+1)] \end{aligned}, \tag{2}$$

and

$$\begin{aligned} g_y(n,m) = {} & f(n-1,m+1) + 2f(n,m+1) + f(n+1,m+1) \\ & -[f(n-1,m-1) + 2f(n,m-1) + f(n+1,m-1)] \end{aligned}. \tag{3}$$

From the resulting g_x and g_y oriented gradient components, MGM information is easily obtained according to:

$$MGM = \frac{1}{NM}\sum\nolimits_{\forall n,m}\frac{1}{g_{\max}}\sqrt{g_x^2(n,m)+g_y^2(n,m)}\,, \tag{4}$$

where $g_{\max}$ is the maximum magnitude value, taken as $g_{\max}$=4.472 for grayscale images with a dynamic range 0 to 1 [35] (image **f** which is an 8-bit unsigned integer array with a range of 0 to 255 is linearly scaled to a dynamic range of 0 to 1 with double-precision 64-bit format).

Mean gradient magnitude can be viewed as a descriptor of image contrast and texture, which are relevant for visibility masking estimation because in regions that contain more non-uniform contents more distortion can be tolerated than in regions with homogeneous content. This is confirmed in the Fig. 3, which shows the original uncompressed images from the MCL-JCI dataset with the smallest and largest MGM values. For these two images, the first JND points correspond to JPEG compression quality factors of QF=63 and QF=32 [13], respectively. Fig. 3 also shows JPEG compressed versions of the original images with QF=32, which corresponds to the first JND point of the image with the maximum MGM value. For this image, no compression degradations are observed, while for an image with a minimum MGM value, the image degradations are noticeable in uniform regions.

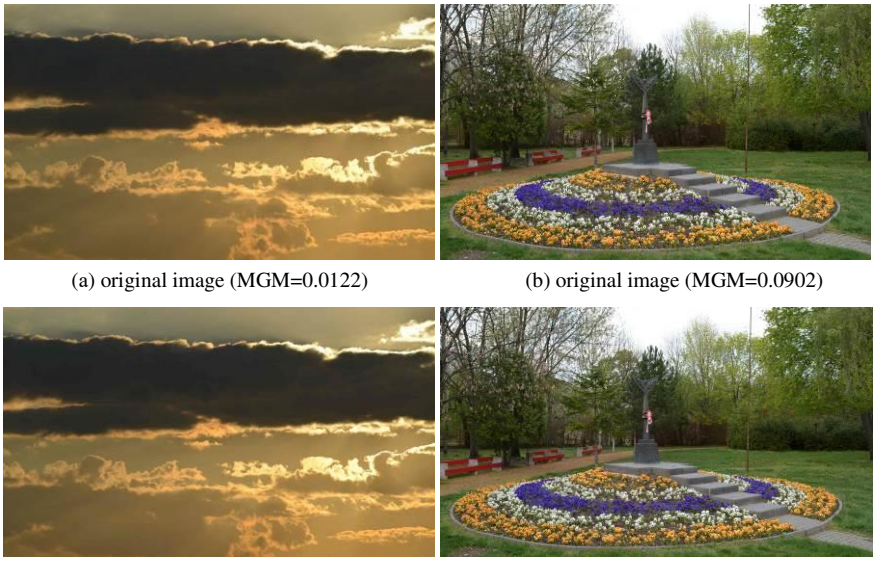

(a) original image (MGM=0.0122) (b) original image (MGM=0.0902)

(c) JPEG compressed image (QF=32) (d) JPEG compressed image (QF=32)

Figure 3

Original images from the MCL-JCI dataset with: (a) the smallest and (b) the largest MGM values and (c) and (d) their JPEG compressed versions with QF=32

PSNR is the most widely used full-reference metric and is defined via the mean squared error (MSE), computed by averaging the squared intensity differences of distorted (**d**) and reference (**f**) images, [36]:

$$MSE(\mathbf{d},\mathbf{f}) = \frac{1}{NM}\sum_{n=1}^{N}\sum_{m=1}^{M}\left(d(n,m)-f(n,m)\right)^2 \tag{5}$$

$$PSNR(\mathbf{d},\mathbf{f}) = 10\cdot\log_{10}\left(L^2 / MSE(\mathbf{d},\mathbf{f})\right) \tag{6}$$

where N and M are the image dimensions and L is the dynamic range of the image.

Fig. 4 shows the correlation which we obtained between MGM and PSNR of JND #1 modelled through a second-order mapping function. Based on this observation, we divided the MCL-JCI data into a training set of 25 randomly selected source images which we used to train a mapping function between MGM and corresponding PSNR of JND #1 points on the condition that it is a falling function, which effectively stays constant after reaching its minimum:

$$PSNR(MGM) = \begin{cases} p_1 MGM^2 + p_2 MGM + p_3, MGM \le MGM_c \\ PSNR_{\min}, MGM > MGM_c \end{cases}, \tag{7}$$

where MGM_c is the mean gradient magnitude for which the mapping function reaches its minimum value ($PSNR_{\min}$).

Obtained least-squares fit parameters, p_1, p_2, and p_3 were then used to predict the PSNR of the JND #1 of the remaining 25 source images (test set). Such randomised dataset division, training, and evaluation was repeated 200 times.

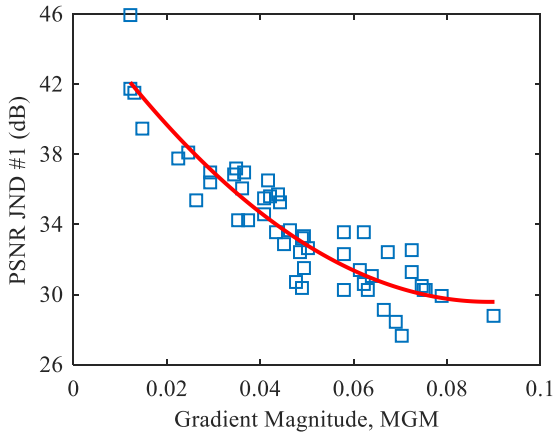

Figure 4

Mean gradient magnitude and PSNR of the first JND of the MCL-JCI source images (second order mapping function, solid line)

Prediction function obtained using mean parameter values over the 200 training runs, $[p_1, p_2, p_3] = [2115.5, -377, 46.4]$, is shown on Fig. 5, and is given by:

$$PSNR(MGM) = \begin{cases} 2115.5MGM^2 - 377MGM + 46.4, MGM \le 0.0896 \\ 29.58, MGM > 0.0896 \end{cases}, \quad (8)$$

where for MGM=0.0896 the mapping function reaches its minimum value ($PSNR_{min}$=29.58 dB).

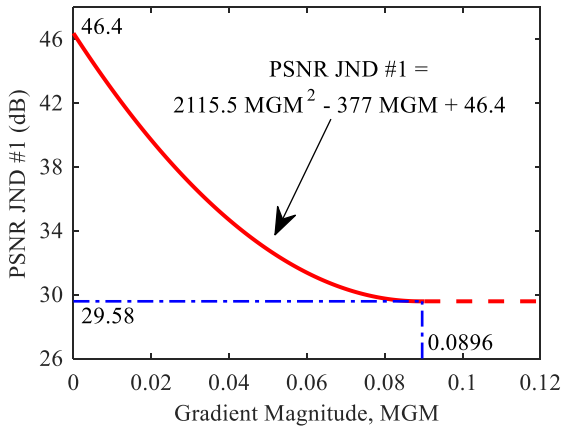

Figure 5
PSNR prediction of the first JND point based on MGM

Agreement between predicted and actual PSNR values of JND #1 over 200 runs measured through linear correlation (LCC), Spearman and Kendall rank-order correlations (SROCC, KROCC), and MAE is provided in Table 1 (mean agreement). The metrics show a high level of agreement between the predicted and ground truth PSNR of JND #1 (determined from subjective experiments).

Table 1
Mean agreement between the predicted and ground truth PSNR of JND #1

LCC (%)	SROCC (%)	KROCC (%)	MAE (dB)
91.54	90.44	75.05	1.21

This can be compared to five- and ten-fold cross-validation deep learning approaches [26-28] which yielded a MAE of 0.69 dB, 0.58 dB, and 0.79 dB, respectively. We show that an MAE of just 0.6 dB more can be obtained with a significantly simpler and faster approach on a far less favourable 50/50% dataset split.

Fig. 6 shows predicted PSNR values of JND #1, PSNR(MGM), obtained using the proposed approach and their relationship to the ground truth of the first three JND points, obtained through subjective trials and sorted in ascending JND #1 order.

Prediction function used mean parameter values obtained over the 200 training runs, Eq. 8.

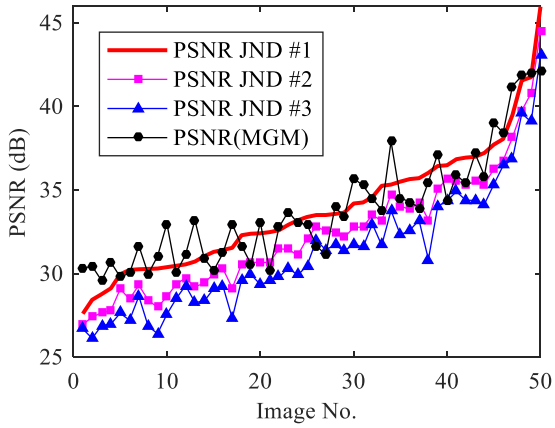

Figure 6
Predicted PSNR of JND #1 and PSNR values of the first three JND points obtained from subjective trials

From Fig. 6 it can be seen that the predicted JND #1 PSNR is greater than PSNR of JND #2 in 43 out of 50 sources and greater than PSNR of JND #3 in 46 out of 50, which suggests that a small bias in the predicted PSNR, of ~1.2 dB (MAE in Table 1), would eliminate practically all prediction errors and ensure that we always obtain an image with no visible compression artifacts. Another way to achieve this would be to use a minimum regional MGM instead of a globally determined value, which could focus on the most sensitive region but would also reduce the achievable compression ratios and thus our method's efficiency.

The proposed prediction method trained and validated on the MCL-JCI data was tested using independent high resolution (1600x1280) source images from a different dataset – JPEG XR [37]. Fig. 7 shows the relationship between PSNR and quality factor QF for JPEG XR images *woman* and *p30* with marked target JND #1 PSNR and corresponding QF, 38 and 28 respectively. QF is shown in its full range, 1 to 100, while in real applications PSNR of JND #1 could be sought in iterative procedures over a significantly narrower practical range.

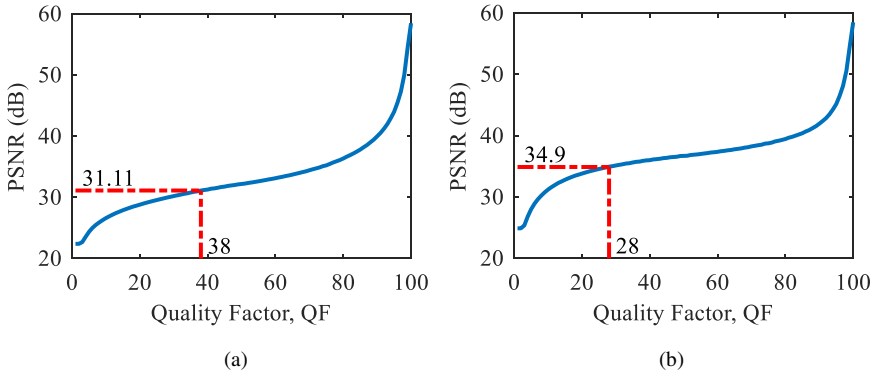

Figure 7
Relationship between PSNR and compression level (quality factor) of test images from the JPEG XR dataset: (a) test image *woman* and (b) test image *p30*

Fig. 8 shows JPEG XR test images *woman* and *p30* optimally compressed using QF to match the PSNR of JND #1 predicted through Eq. 8 using parameters defined above, where no distortions are apparent on normal viewing, as well as zoomed 160x160 pixel sections (1.25% of image size) showing that images were indeed compressed with blocky artifacts visible only after enlargement – Fig. 8c and Fig. 8d. Using perceptually lossless compression preserves the quality of source signals while significantly reducing the bit length required to encode them from 2 MB to 182 and 102 kB, with compression ratios of 11 and 20 respectively. For reference, lossless JPEG encoding on these images achieves image sizes of 1.36 MB and 1.17 MB respectively. Also, according to some research, websites such as Google and YouTube use JPEG compression with a QF of about 75 [5]. By applying the proposed method, significant bit-saving performance in signal archiving can be achieved, without perceptual loss of information (for the two selected images the optimal QF values are 38 and 28).

The results shown here were obtained for grayscale images, but analogous results can be achieved when the proposed method is applied to color images in the MCL-JCI dataset. In that case, even greater compression ratios can be achieved for pristine images.

Furthermore, we also found that a good correlation exists between MGM and PSNR of the higher JND points – Fig. 9, and we can use this to allow even greater latitude in practical systems setting quality/compression compromise automatically. Fig. 9d shows second-order PSNR prediction functions for the first four JND points, exhibiting a similar trend, with relative differences of approximately 1.4 dB (#1 vs. #2), 1.07 dB (#2 vs. #3) and 0.93 dB (#3 vs. #4). Linear correlation between the proposed second-order gradient-based prediction and ground truth PSNR of JND points #2, #3, and #4 is above 91%.

(a) (b)

(c) (d)

Figure 8

Test images compressed using the quality factor determined by the proposed method: (a) *woman* image compressed using JPEG QF=38, (b) *p30* image compressed using JPEG QF=28, (c) top left 160x160 pixels of image on Fig. 8a and (d) central 160x160 pixels of image on Fig. 8b

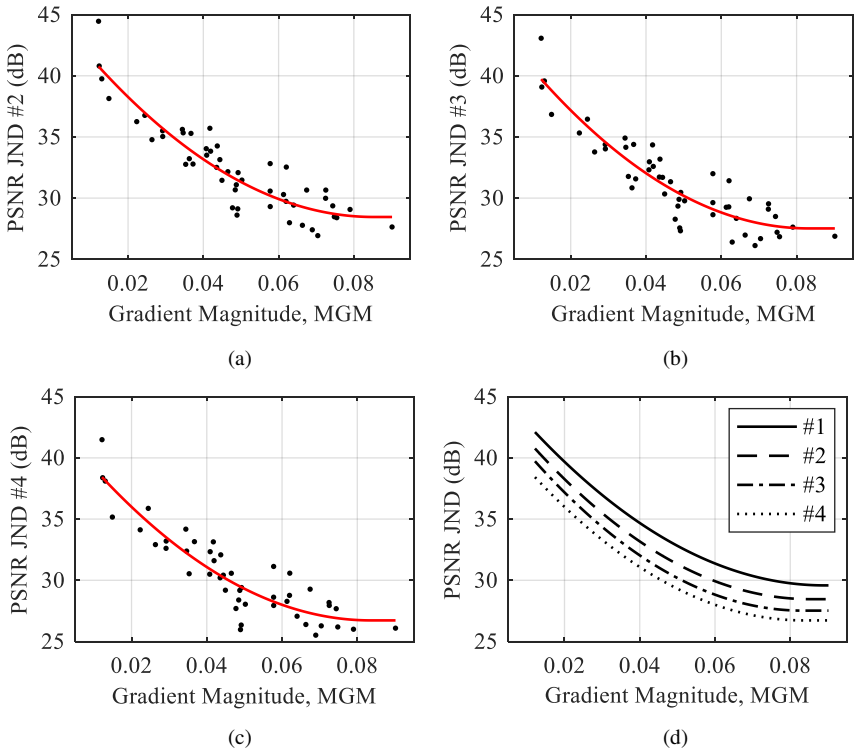

Figure 9
Predicted PSNR of JND: (a) #2 (LCC=91.87%), (b) #3 (LCC=91.41%), (c) #4 (LCC=93.2%) and (d) second order mapping functions for the first four JND points

One way to reach the desired PSNR value is by applying an iterative procedure with multiple compression and decompression, quality assessment, and changing the QF value [30]. However, thanks to the orthogonality of DCT, it is possible to estimate the PSNR of the spatial domain based on the MSE calculated in the DCT domain [31, 32]. This avoids multiple compression/decompression.

Suppose that for an p-th block (p=1,…,P, where P is the total number of non-overlapping blocks) reference image has a set of DCT coefficients $F(p,k,l)$ and the distorted image has a set of DCT coefficients $D(p,k,l)$, where k=0,…,7 and l=0,…,7. $F(p,0,0)$ and $D(p,0,0)$ are the direct current (DC) coefficients that relate to the means in the p-th blocks. The differences between coefficients in the block are:

$$\Delta D(p,k,l) = D(p,k,l) - F(p,k,l), \tag{9}$$

and based on them the MSE in the p-th block can be determined:

$$MSE_p = \frac{1}{64}\sum_{k=0}^{7}\sum_{l=0}^{7}\left(\Delta D(p,k,l)\right)^2. \tag{10}$$

Finally, the estimates of MSE and PSNR in the DCT domain for the entire image are:

$$MSE_{DCT} = \frac{1}{P}\sum_{p=1}^{P} MSE_p = \frac{1}{64P}\sum_{p=1}^{P}\sum_{k=0}^{7}\sum_{l=0}^{7}\left(\Delta D(p,k,l)\right)^2, \tag{11}$$

$$PSNR_{DCT} = 10\cdot\log_{10}\left(L^2 / MSE_{DCT}\right). \tag{12}$$

Fig. 10 shows a scatter plot between the PSNR values calculated in spatial (Eq. 6) and in DCT domains (Eq. 12) for 243 JPEG images from MCL-JCI dataset (all JND points). It is easy to see that the PSNR values calculated in the spatial domain are practically equal to the PSNR values calculated in the DCT domain.

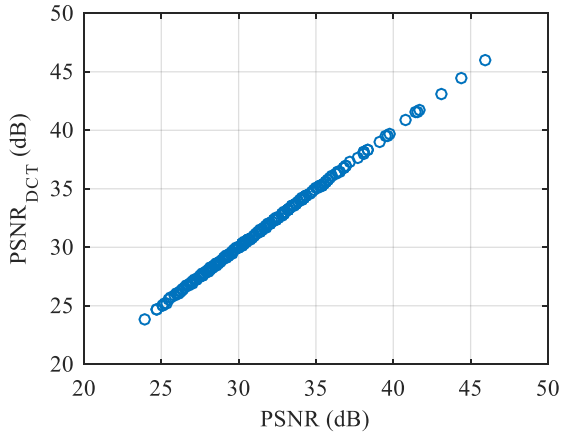

Figure 10
Scatter plot of PSNR vs. PSNR$_{DCT}$ for JPEG MCL-JCI images

The relationship between the PSNR values calculated in the spatial and DCT domains is further illustrated in Fig. 11, using a different degree of compression of the same image (test image *p30* from the JPEG XR dataset). In the DCT domain, compression was introduced using quality factors, on the basis of which quantization matrices are determined [4]. In this case, too, it is noticed that the PSNR values calculated in the spatial domain are practically the same as the PSNR values calculated in the DCT domain. In this way, by determining the array of DCT coefficients of all image blocks, it is possible to make a prediction of MSE and PSNR. Additionally, by changing the quality factor QF, it is possible to adjust the QF to reach the desired MSE or PSNR value without iterative compression/decompression. Although in this way an accelerated process of reaching the desired value of PSNR has been achieved, in our future research we will analyze the achievement of the desired value of PSNR JND #1 without iterations [33], through two steps [34] and through the use of a limited number of blocks [30].

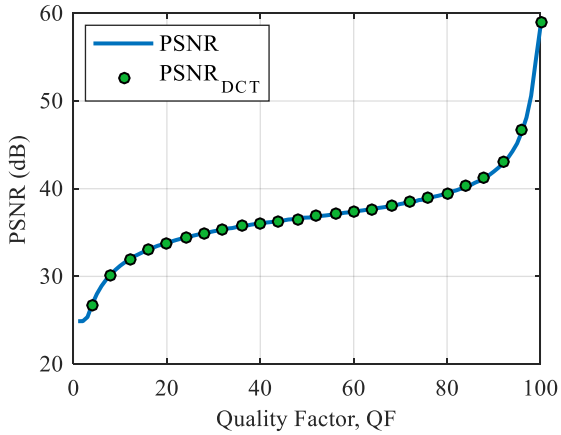

Figure 11
Relationship between PSNR and $PSNR_{DCT}$ of test image *p30* from the JPEG XR dataset for different compression levels (quality factors)

Prediction of the first JND point for MCL-JCI JPEG compressed images can be achieved in the PSNR, QF, and bits per pixel (bpp) domains [28]. Therefore, the correlation between ground truth values (determined from subjective experiments) and their predictions in these three domains were analyzed (Eq. 8 is used for prediction with optimal set parameters [p_1, p_2, p_3] defined above). The scatter plots between predicted and ground truth measures values of JND #1 are shown in Fig. 12, and quantitative indicators of the degree of their agreement (correlations) are given in Table 2.

Fig. 12 and Table 2 show the lowest degree of agreement between QF ground truth and predicted values (LCC=40.58%). In the vicinity of the QF ground-truth value of JND #1 there is a very wide region of QF values for which the difference between compressed images is very difficult to observe by observers (see Fig. 1). The width of this region depends on the content of the image. The wider this region, the higher the probability that the predicted values will deviate from the ground truth values, so there is a small degree of their mutual correlation. The degree of agreement between PSNR ground truth and predicted values are significantly higher (LCC=92.02%), so it can be concluded that it is necessary to use the PSNR domain to predict the first JND point.

Table 2
Agreement between the predicted and ground truth PSNR, bpp and QF of JND #1

	LCC (%)	SROCC (%)	KROCC (%)
PSNR	92.02	91.38	75.18
bpp	78.71	80.04	61.96
QF	40.58	48.37	35.37

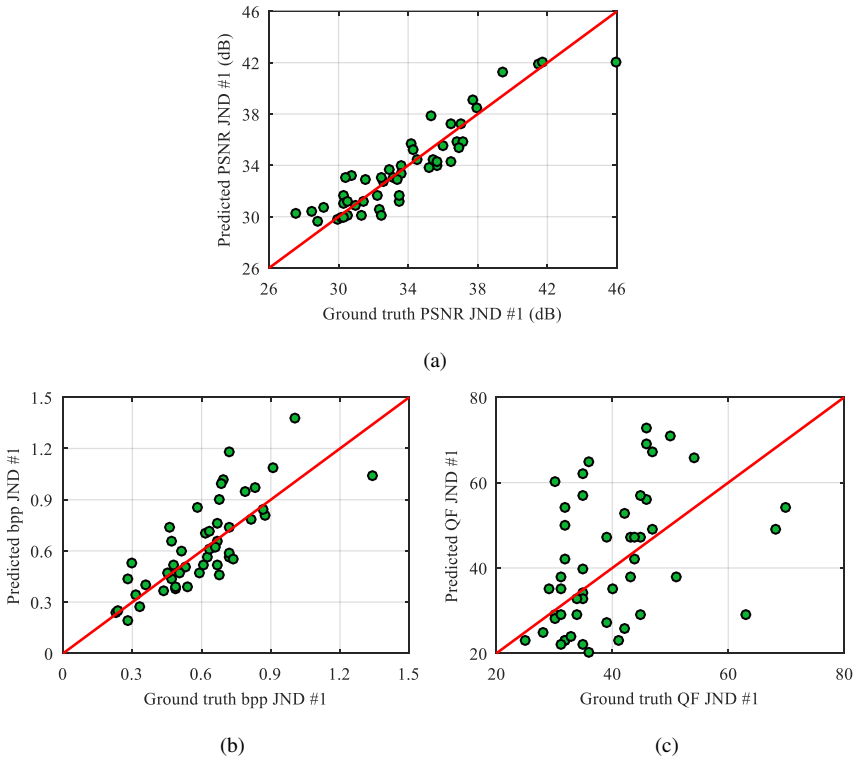

Figure 12

Predicted vs. ground truth metrics of JND #1: (a) PSNR, (b) bpp and (c) QF

Conclusions

This paper demonstrated that simple to compute mean gradient magnitude can be used to reliably predict the PSNR of the first just noticeable difference point as the limit between perceptually lossless and lossy JPEG image coding. This allows adaptive setting and optimisation of compression ratios meaning the proposed method can efficiently reach optimally high compression ratios without visible distortions or information loss. Furthermore, it can be used to set optimal compression ratios over a wider range of increasingly perceptually visible differences points. Additionally, this approach can be used to guide watermark or hidden message embedding, allowing the embedded information to remain undetected by observers. The agreement (linear correlation) between the proposed second-order gradient-based prediction and ground truth PSNR for the first four JND points is above 91%. Furthermore, the mean absolute error between predicted and ground-truth PSNR values of the first and the most important just noticeable difference points is 1.21 dB, which is only 0.6 dB worse than the best result achieved by applying a significantly more complex deep learning approach on the same image dataset. Also, the paper shows that reaching the desired value of

PSNR can be accelerated by its determination in the DCT domain. The proposed picture-wise approach can be used in the efficient compression of grayscale and color images.

As different parts of the image (or blocks) may have non-uniform and homogeneous content, different just noticeable difference values correspond to them. Therefore, one of the directions of further research will be a block-based prediction of perceptual visual redundancy. Also, in further work, the possibility of applying the gradient magnitude as a feature in the video compression just noticeable difference points will be analyzed.

Acknowledgment

This research has been a part of the project No. VA-TT/3/20-22 supported by the Ministry of Defence, Republic of Serbia.

References

[1] Bovik, A. C.: Automatic prediction of perceptual image and video quality, Proceedings of the IEEE, 2013, Vol. 101, No. 9, pp. 2008-2024

[2] Ilic, S., Petrovic, M., Jaksic, B., Spalevic, P., Lazic, Lj., Milosevic, M.: Experimental analysis of picture quality after compression by different methods, Przeglad Elektrotechniczny, 2013, Vol. 89, No. 11, pp. 190-194

[3] Ernawan, F., Kabir, N., Zamli, K. Z.: An efficient image compression technique using Tchebichef bit allocation, Optik – International Journal for Light and Electron Optics, 2017, Vol. 148, pp. 106-119

[4] Poth, M., Trpovski, Z., Loncar-Turukalo, T.: Analysis and improvement of JPEG compression performance using custom quantization and block boundary classifications, Acta Polytechnica Hungarica, 2020, Vol. 17, No. 6, pp. 171-191

[5] Tian, T., Wang, H., Zuo, L., Kuo, C.-C. J., Kwong, S.: Just noticeable difference level prediction for perceptual image compression, IEEE Transactions on Broadcasting, 2020, Vol. 66, No. 3, pp. 690-700

[6] Wang, Z., Tran, T.-H., Muthappa, P. K., Simon, S.: A JND-based pixel-domain algorithm and hardware architecture for perceptual image coding, Journal of Imaging, 2019, Vol. 5: 50, pp. 1-29

[7] Wu, J., Shi, G., Lin, W.: Survey of visual just noticeable difference estimation, Frontiers of Computer Science, 2019, Vol. 13, pp. 4-15

[8] Kim, M., Song, K.-S., Kang, M.-G.: No-reference image contrast assessment based on just-noticeable-difference, in Proc. IS&T International Symposium on Electronic Imaging – Image Quality and System Performance XIV, Burlingame, CA, USA, 2017, pp. 26-29

[9] Miao, X., Lee, D.-J.: Just-noticeable difference binary pattern for reduced reference image quality assessment, Optical Engineering, 2019, Vol. 58, No. 9, Article no. 093105

[10] Seo, S., Ki, S., Kim, M.: A novel just-noticeable-difference-based saliency-channnel attention residual network for full-reference image quality predictions, IEEE Transactions on Circuits and Systems for Video Technology, 2021, Vol. 31, No. 7, pp. 2602-2616

[11] Wang, H., Yu, L., Liang, J., Yin, H., Li, T., Wang, S.: Hierarchical predictive coding-based JND estimation for image compression, IEEE Transactions on Image Processing, 2021, Vol. 30, pp. 487-500

[12] Li, H., Jenadeleh, M., Chen, G., Reips, U.-D., Hamzaoui, R., Saupe, D.: Subjective assessment of global picture-wise just noticeable difference, in Proc. IEEE International Conference on Multimedia & Expo Workshops, London, UK, 2020, pp. 1-6

[13] Jin, L., Lin, J. Y., Hu, S., Wang, H., Wang, P., Katsavounidis, I., Aaron, A., Kuo, C.-C. J.: Statistical study on perceived JPEG image quality via MCL-JCI dataset construction and analysis, in Proc. IS&T International Symposium on Electronic Imaging – Image Quality and System Performance XIII, San Francisco, CA, USA, 2016, Article no. IQSP-222

[14] Wang, H., Gan, W., Hu, S., Lin, J. Y., Jin, L., Song, L., Wang, P., Katsavounidis, I., Aaron, A., Kuo, C.-C. J.: MCL-JCV: a JND-based H.264/AVC video quality assessment dataset, in Proc. IEEE International Conference on Image Processing, Phoenix, AZ, USA, 2016, pp. 1509-1513

[15] Wang, H., Katsavounidis, I., Zhou, J., Park, J., Lei, S., Zhou, X., Pun, M.-O., Jin, X., Wang, R., Wang, X., Zhang, Y., Huang, J., Kwong, S., Kuo, C.-C. J.: VideoSet: a large-scale compressed video quality dataset based on JND measurement, Journal of Visual Communication and Image Representation, 2017, Vol. 46, pp. 292-302

[16] Huang, J., Feng, H., Xu, Z., Li, Q., Chen, Y.: A robust deblurring algorithm for noisy images with just noticeable blur, Optik – International Journal for Light and Electron Optics, 2018, Vol. 168, pp. 577-589

[17] Zhang, X., Yang, C., Wang, H., Xu, W., Kuo, C.-C. J.: Satisfied-user-ratio modeling for compressed video, IEEE Transactions on Image Processing, 2020, Vol. 29, pp. 3777-3789

[18] Liu, X., Chen, Z., Wang, X., Jiang, J., Kwong, S.: JND-Pano: database for just noticeable difference of JPEG compressed panoramic images, Lecture Notes in Computer Science, 2018, Vol. 11164, pp. 458-468

[19] Ahar, A., Mahmaoudpour, S., Van Wallendael, G., Paridaens, T., Lambert, P., Schelkens, P.: A just noticeable difference subjective test for high dynamic range images, in Proc. 10th International Conference on Quality of Multimedia Experience, Cagliari, Italy, 2018, pp. 1-6

[20] Fan, C., Zhang, Y., Hamzaoui, R., Jiang, Q.: Interactive subjective study on picture-level just noticeable difference of compressed stereoscopic images, in Proc. IEEE International Conference on Acoustics, Speech and Signal Processing, Brighton, UK, 2019, pp. 8548-8552

[21] Shen, X., Ni, Z., Yang, W., Zhang, X., Wang, S., Kwong, S.: A JND dataset based on VVC compressed images, in Proc. IEEE International Conference on Multimedia & Expo Workshop, London, United Kingdom, 2020, pp. 1-6

[22] Shen, X., Ni, Z., Yang, W., Zhang, X., Wang, S., Kwong, S.: Just noticeable distortion profile inference: a patch-level structural visibility learning approach, IEEE Transactions on Image Processing, 2021, Vol. 30, pp. 26-38

[23] Huang, Q., Wang, H., Lim, S. C., Kim, H. Y., Jeong, S. Y., Kuo, C.-C. J.: Measure and prediction of HEVC perceptually lossy/lossless boundary QP values, in Proc. Data Compression Conference, Snowbird, UT, USA, 2017, pp. 42-51

[24] Wang, H., Katsavounidis, I., Huang, Q., Zhou, X., Kuo, C.-C. J.: Prediction of satisfied user ratio for compressed video, in Proc. IEEE International Conference on Acoustics, Speech and Signal Processing, Calgary, Canada, 2018, pp. 6747-6751

[25] Wang, H., Zhang, X., Yang, C., Kuo, C.-C. J.: Analysis and prediction of JND-based video quality model, in Proc. Picture Coding Symposium, San Francisco, CA, USA, 2018, pp. 278-282

[26] Fan, C., Lin, H., Hosu, V., Zhang, Y., Jiang, Q., Hamzaoui, R., Saupe, D.: SUR-Net: predicting the satisfied user ratio curve for image compression with deep learning, in Proc. 11th International Conference on Quality of Multimedia Experience, Berlin, Germany, 2019, pp. 1-6

[27] Lin, H., Hosu, V., Fan, C., Zhang, Y., Mu, Y., Hamzaoui, R., Saupe, D.: SUR-FeatNet: Predicting the satisfied user ratio curve for image compression with deep feature learning, Quality and User Experience, 2020, Vol. 5, No. 5, pp. 1-23

[28] Liu, H., Zhang, Y., Zhang, H., Fan, C., Kwong, S., Kuo C.-C. J., Fan, X.: Deep learning based picture-wise just noticeable prediction model for image compression, IEEE Transactions on Image Processing, 2020, Vol. 29, pp. 641-656

[29] Yuan, D., Zhao, T., Xu, Y., Xue, H., Lin, L.: Visual JND: a perceptual measurement in video coding, IEEE Access, 2019, Vol. 7, pp. 29014-29022

[30] Kozhemiakin, R., Lukin, V., Vozel, B.: Image quality prediction for DCT-based compression, in Proc. 14th International Conference The Experience of Designing and Application of CAD Systems in Microelectronics, Lviv, Ukraine, 2017, pp. 225-228

[31] Kozhemiakin, R. A., Abramov, S. K., Lukin, V. V., Vozel, B., Chehdi, K.: Output MSE and PSNR prediction in DCT-based lossy compression of remote sensing images, in Proc. Image and Signal Processing XXIII, Warsaw, Poland, 2017, Article no. 1042721

[32] Lu, K.-S., Ortega, A., Mukherjee, D., Chen, Y.: Perceptually inspired weighted MSE optimization using irregularity-aware graph Fourier transform, in Proc. IEEE International Conference on Image Processing, Abu Dhabi, United Arab Emirates, 2020, pp. 3384-3388

[33] Minguillon, J., Pujol, J.: JPEG standard uniform quantization error modeling with applications to sequential and progressive operation modes, Journal of Electronic Imaging, 2001, Vol. 10, No. 2, pp. 475-485

[34] Krivenko, S., Demchenko, D., Dyogtev, I., Lukin, V.: A two-step approach to providing a desired quality of lossy compressed images, in Proc. Nechyporuk, M., Pavlikov, V., Kritskiy D. (eds): Integrated Computer Technologies in Mechanical Engineering, Advances in Intelligent Systems and Computing, 2020, Vol. 1113, pp. 482-491

[35] Bondzulic, B., Petrovic, V., Andric, M., Pavlovic, B.: Gradient-based image quality assessment, Acta Polytechnica Hungarica, 2018, Vol. 15, No. 4, pp. 83-99

[36] Bondzulic, B. P., Pavlovic, B. Z., Petrovic, V. S., Andric, M. S.: Performance of peak signal-to-noise ratio quality assessment in video streaming with packet losses, Electronics Letters, 2016, Vol. 52, pp. 454-456

[37] De Simone, F., Goldmann, L., Baroncini, V., Ebrahimi, T.: Subjective evaluation of JPEG XR image compression, in Proc. SPIE 7443, San Diego, CA, USA, 2009, Article no. 74430L

The Effect of Ultrasound on Strain-hardened Metals

Endre Ruszinkó, Ali H. Alhilfi

Óbuda University, Népszínház u. 8, H-1081 Budapest, Hungary
ruszinko.endre@uni-obuda.hu; alihameed@stud.uni-obuda.hu

Abstract: This paper addresses the case when acoustic energy is applied to plastically deformed metals when the "Ultrasonic recovery phenomenon" is observed, which manifests itself in a decrease of dislocation density, hardness and yield strength. Based on the analysis of the processes occurring in the sonicated material's microstructure, a model has been developed within the terms of the synthetic theory of irrecoverable deformation. We introduce into the equation governing recovery processes a term for expressing the oscillating stress amplitude. The model results show good agreement with the experimental data.

Keywords: ultrasound; plastic deformation; recovery

1 Introduction

Ultrasound energy is an effective tool in metallurgy, metal forming, and many other industry branches and technological processes. With the effects of ultrasound upon metals' deformational properties, the following phenomena can be listed:

(i) *Ultrasonic hardening*. Acoustic energy propagating through an annealed specimen increases the number of crystalline grid defects – mainly dislocations and vacancies. As a result, the material's yield strength grows as a function of the sonication duration (Fig. 1a). One can see that the *yield strength ~ sonication time* dependency first increases and then reaches a plateau. The yield strength increment saturation is explained by the gradual restrain of Frank-Read sources caused by dislocations nucleated in preceding cycles. The annihilation of oppositely oriented dislocations emitted by sources on parallel atomic planes also contributes to the gradual decay in the yield strength's increase. Numerous experiments show that the ultrasonic hardening effect is a function of the ultrasonic field's intensity [1]-[4].

(ii) *Effect of acoustic energy upon the creep characteristics.* Creep experiments for materials subjected to the preliminary sonication treatment – sonication + annealing – show that the ultrasonic treatment exerts a positive impact upon the steady-state creep rate. Fig. 1b schematically demonstrates the decrease in the creep rate for copper (one minimum) and aluminum (two minimums) caused by the dislocation substructure formed during the preliminary ultrasonic treatment. As one can see, there are optimal ranges of the sonication duration when the creep rate shows low values, which is due to the thermal stability of the ultrasonic defect structure. Beyond the optimal ranges, the dislocation substructure loses its capacity to impede the creep deformation, and the creep rate tends to its initial value. The number of minimums in Fig. 1b depends on the recovery mechanisms governing the creep – polygonization for materials with high stacking fault energy (SFE) such as aluminum and recrystallization for low SFE (copper) [4]-[7].

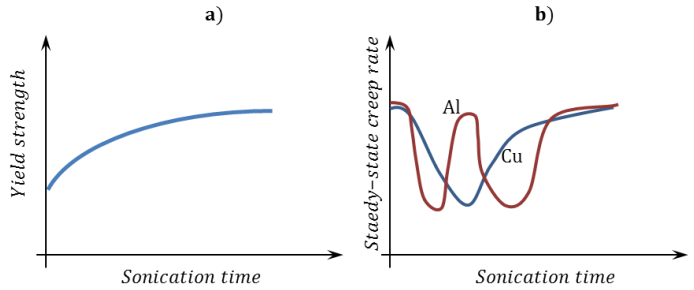

Figure 1

Schematic plots for the ultrasonic effects upon metals' properties– **a)** ultrasonic hardening, **b)** dependences of the creep rate upon the duration of preliminary sonication

(iii) *Ultrasonic temporary softening* manifests itself when a unidirectional loading is coupled with an oscillating one. Fig. 2 schematically demonstrates the effect of acoustic energy upon the development of plastic deformation in uniaxial tension. When the ultrasound is applied, the value of tensile stress decreases in a step-wise manner, and the further development of plastic deformation takes place at lesser value of the unidirectional stress. The stress-drop amount is measured to be proportional to the energy of acoustic energy or oscillating stress amplitude. Although the mechanism of the ultrasonic temporary softening is far from clear, researchers use the following suggestions or their combination:

a) A stress superimposition mechanism implies that ultrasonic waves activate anchored dislocations, hardened under ordinary deformation, and decrease stresses for further inelastic deformation,

b) An analogy between the effects of hot deformation and ultrasound action – numerous researches suggest that ultrasonic vibration induces sufficient heat input to the sample to produce some softening of microstructure. [8]-[15].

(iv) *Ultrasonic residual softening or hardening* (Fig. 2) are observed after the ultrasound is Off, and the material deforms under the action of the static load alone. The appearance of one of the phenomenon depends on the changes in the material structure during acoustoplasticity. Thus, if acoustic energy induces dynamic recrystallization or other softening processes, the residual softening will be observed (Fig. 2a). In the case when, e.g., polygonized structure forms during the ultrasound-assisted deforming, more significant stress is needed for the further development of plastic deformation as ultrasound is Off (residual hardening, Fig. 2b) [16]-[18].

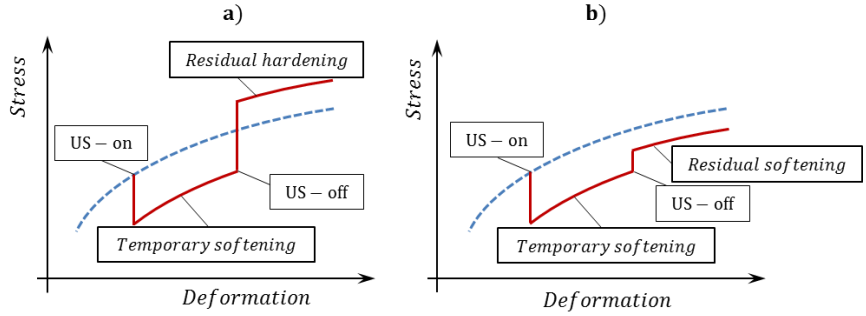

Figure 2
Schematic plots for the ultrasonic effects upon the plastic deformation: **a)** residual hardening, **b)** residual softening

While the modeling of the phenomena above can be found in Rusinko's early works [1] [5] [19], the phenomenon discussed below so far was out of the authors' sight.

(v) *Ultrasonic recovery effect*. Acoustic energy has a recovery effect upon strain hardened materials.

Kulemin [4] conducted X-ray investigations to study the interference patterns evolution during the sonication of plastically deformed aluminum specimens ($\varepsilon = 5\ \%$) at 20°C (Fig. 3). Due to the plastic deformation, clear interference spots of 0.3-1.0 mm radius of the annealed specimen blur out to 8 mm and 2-3 mm in the azimuthal and radial direction. After the ultrasonic action, the interference spot blurring decreases in both radial and polar directions, which testify to the relaxation of stresses of the second kind arisen due to the elastic distortions of crystalline grids in plastic deforming. Fig. 4 shows the decrease in the dislocation density, caused by the sonication at 20°C of the plastically hardened aluminum. As one can see, the dislocation density for the deformed material monotonically decreases to its initial value (annealed state) as a function of the sonication duration.

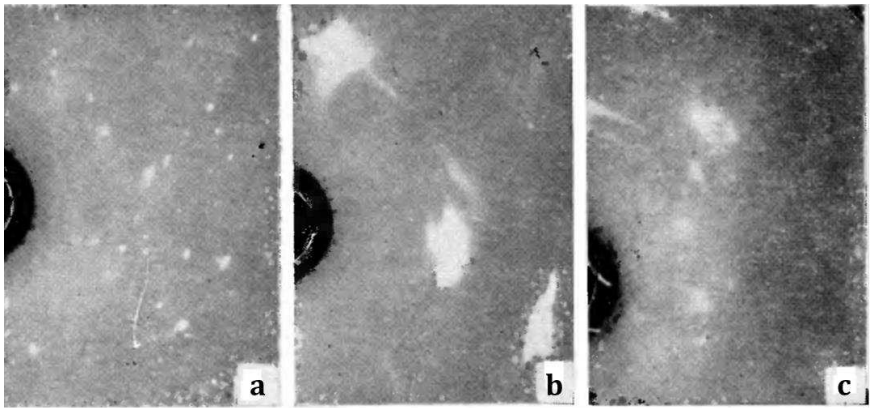

Figure 3

X-ray micrograph of aluminum specimen – **a)** annealed state, **b)** plastic deformation of 5%, **c)** sonication of the deformed specimen; oscillating stress amplitude 16 MPa, duration 100 min [4]

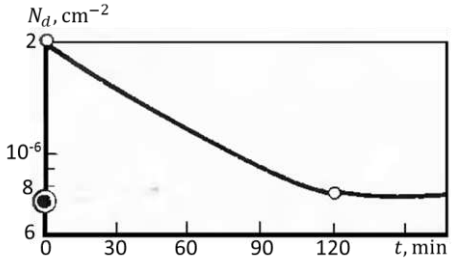

Figure 4

Dislocation density vs. sonication time at stress amplitude of 16 MPa [4]

The ultrasonic recovery is suggested to proceed through polygonization when dislocations are built into low-angle boundaries. As a result, the initially distorted lattice is rearranging into stress-free blocks separated by the boundaries consisting of one sign's dislocations. The formation of the polygonized substructure requires the dislocations to leave their slip planes and climb parallel ones. As it is well known, the dislocation climb needs vacancies inflow which can be thermally activated as it is typical, for example, in elevated-temperature creep or during annealing. But since the results from Figs. 3 and 4 are obtained at room temperatures, the energy needed for the nucleation and migration of vacancies is provided by ultrasound. This result is harmonized with the established fact, that one of the features of sonication is an abundant number of point defects (vacancies). Fig. 5 confirms the above-considered thoughts about the dislocation-climb-nature of the ultrasonic recovering. Indeed, the straight slip lines from the plastic deformation (Fig. 5a) split into numerous intersected curved lines (Fig. 5b).

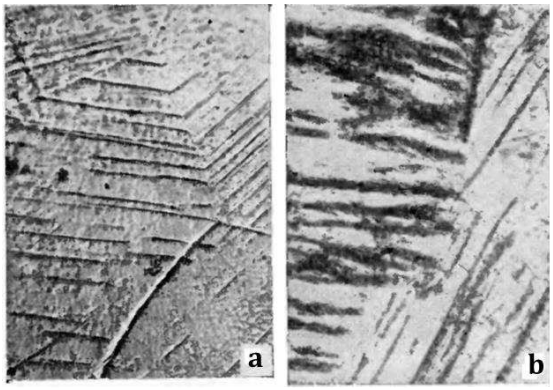

Figure 5
Slip lines on the surface of aluminum specimen – **a)** after plastic deformation, **b)** after the sonication of the plastically deformed specimen, t = 20°C. × 400 [4]

Similar results were obtained at the sonication of cold-rolled steel strips [20], which indicate the yield strength decrease in the acoustic field.

With the intensity of the ultrasonic recovery, the following can be summarizing [4] [19]:

(i) There is a lower limit for the oscillating stress (σ_m) beneath which the recovery effect is not observed (for example, while $\sigma_m = 4.3$ MPa and $\sigma_m = 5.6$ MPa gives no changes in the hardening-decrease, $\sigma_m = 8.4$ MPa already yields the recovery effect [4])

(ii) The increase in σ_m leads to a much steeper decrease of hardness/yield strength of the strain hardened material

(iii) At a given value σ_m, the acoustic energy causes more intensive recovery for more significant plastic deformations – the ultrasound-assisted recovery mechanisms are accelerating at the greater deformation energy cumulated in the material

(iv) with the sonications time, at significant values of σ_m, the ultrasonic recovery can be succeeded by some hardening (in a wave manner), but the overall trend remains unchangeable, decreasing hardness/yield strength. Such cases are not considered here.

Our paper is aimed to model the ultrasonic recovery effect in terms of the synthetic theory of irrecoverable deformation, which has already shown satisfactory results in the analytical description of ultrasonic softening and hardening [1] [5] [19] [21].

2 The Synthetic Theory and Its Extensions for the Case of the Ultrasonic Recovery

2.1 Basic Equations

In terms of this theory [20], plastic deformation at a point of the body – plastic strain deviator vector ($\vec{\mathbf{e}}$) – is determined via deformations at the micro-level of material, i.e., as a sum of plastic shifts in active slips systems where the Schmidt law conditions are met – the resolved shear stress exceeds the material yield strength:

$$\vec{\mathbf{e}} = \iiint_V \varphi_N \vec{\mathbf{N}} dV \tag{1}$$

φ_N – plastic strain intensity – is an average measure of plastic deformation within one slip system.

The synthetic theory formulates a yield criterion and strain hardening rule in terms of three-dimensional stress deviator space S^3. It does not deal with a yield surface itself, but with its tangent planes, i.e., the yield surface is considered an inner envelope of the tangent planes. The location of planes is defined by their distances (H_N) and unit normal vectors $\left(\vec{\mathbf{N}}\right)$. For a virgin state, the synthetic theory works with the Von-Mises yield criterion, which results in the set of equidistant planes in all directions (Fig. 6a).

A stress vector ($\vec{\mathbf{S}}$) represents loading, whose coordinates are composed of the stress deviator tensor components. During the loading, the stress vector shifts at its endpoint a set of planes from their initial positions (Fig. 6b). The planes' movements at the endpoint of the stress vector are translational, i.e., the plane orientations keep changeless. Planes, which are not located at the endpoint of the vector $\vec{\mathbf{S}}$, remain stationary. The plane's displacement at the stress vector's endpoint represents a plastic flow within the corresponding slip system.

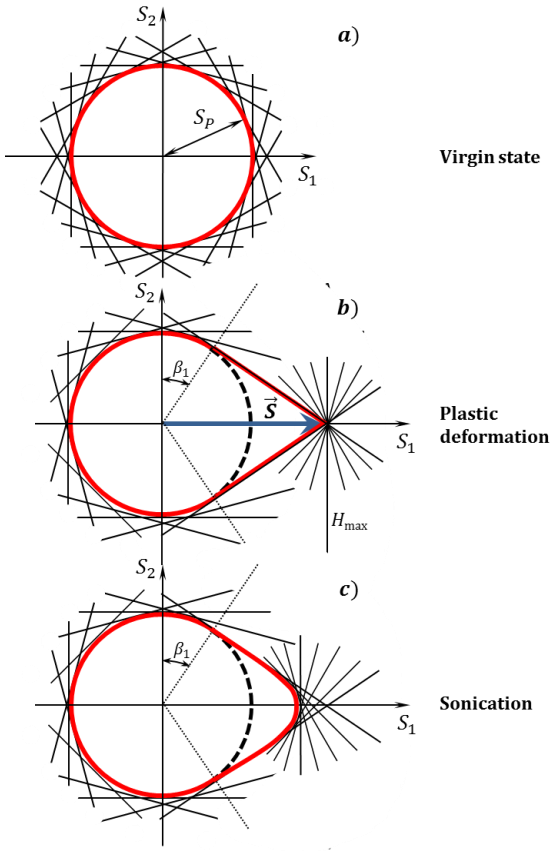

Figure 6

Yield and loading surface in terms of the synthetic theory in S_1-S_2 coordinate plane for uniaxial tension ($\lambda = 0$)

We define the plastic strain intensity – the plastic flow rule on the micro-level of material – through the carriers of irrecoverable deformation, defect-intensity (ψ_N):

$$d\psi_N = rd\varphi_N - K\psi_N dt \tag{2}$$

where r is the model constant determining the slope of the stress-strain diagram in its plastic portion, and K is a function of temperature and acting stress, which governs the steady-state creep rate [20]:

$$K = K_1(T)K_2(\tau_0), \tag{3}$$

$$K_1(T) = \exp\left(-\frac{Q}{RT}\right), \tag{4}$$

$$K_1(\tau_0) = \frac{9\sqrt{3}cr}{2\sqrt{2}\pi}\tau_0^{k-2}. \tag{5}$$

In the formulae above Q is the thermal activation energy, T is the temperature, τ_0 is the Von-Mises stress, c and k are the model constants.

The hardening rule of a material is defined through the distances to the tangent planes

$$\psi_N = H_N^2 - S_S^2 = \begin{cases} (\vec{\mathbf{S}}\cdot\vec{\mathbf{N}})^2 - S_S^2 & \text{for planes reached by } \vec{\mathbf{S}}\text{: } H_N = \vec{\mathbf{S}}\cdot\vec{\mathbf{N}} \\ 0 & \text{for planes not reached by } \vec{\mathbf{S}}\text{: } H_N > \vec{\mathbf{S}}\cdot\vec{\mathbf{N}} \end{cases} \tag{6}$$

S_S is a radius of the Von-Mises sphere; $S_S = \sqrt{2/3}\sigma_S$, where σ_S is the yield strength of a material in uniaxial tension. It is clear from (6) that the greater plane distance is, the more significant stresses are needed to continue plastic deforming.

In uniaxial tension, the stress vector $\vec{\mathbf{S}}(\sqrt{2/3}\sigma, 0, 0)$ extends along the S_1 axis, and the plane distances are

$$H_N = S_1 N_1 = \sqrt{2/3}\sigma \sin\beta\cos\lambda \tag{7}$$

For plastic deformation, when the time-dependent term in (2) can be neglected, we get from (2) and (6) the following expression

$$r\varphi_N = \psi_N = (2/3)[(\sigma sin\beta\ cos\lambda)^2 - \sigma_S^2] \tag{8}$$

The loading surface consists of two parts: a) sphere as the envelope of stationary planes and b) cone whose generator is constituted by the boundary planes (angle β_1 in Fig. 6b) shifted by $\vec{\mathbf{S}}$.

Now, the integration in (1) gives the component of plastic strain vector component as

$$e = \frac{4\pi}{3r}\int_{\beta_1}^{\pi/2}\int_0^{\lambda_1}[(\sigma sin\beta cos\lambda)^2 - \sigma_S^2]sin\beta cos\lambda cos\beta d\lambda d\beta = a_0\Phi(b) \tag{9}$$

where

$$a_0 = \frac{\pi\sigma_S^2}{9r}, \tag{10}$$

$$\Phi(b) = \frac{1}{b^2}[2\sqrt{1-b^2} - 5b^2\sqrt{1-b^2} + 3b^4 \ln \frac{1+\sqrt{1-b^2}}{b}], \tag{11}$$

$$b \equiv \sin\beta_1 = \frac{\sigma_S}{\sigma}. \tag{12}$$

2.2 Post-deformed State, Ultrasonic Recovery

After the plastic strain is over ($d\varphi_N = 0$), Eq. (2) takes the following form

$$d\psi_N = -K\psi_N dt. \tag{13}$$

The solution of the differential equation above gives

$$\psi_N = \psi_{N0} \exp(-Kt), \tag{14}$$

where ψ_{N0} reflects the number of defects cumulated in the material during plastic deforming, Eq. (8).

Formula (14), together with (6), means that the tangent planes start moving towards the origin of coordinates (Fig. 6c):

$$H_N = \sqrt{\sigma_S^2 + \frac{3}{2}\psi_{N0} \exp(-Kt)}. \tag{15}$$

As it follows from (6) and (15), only the planes translated by the stress-vector during plastic deforming take part in the movement.

To adopt Eq. (14) for modeling the phenomenon that the acoustic energy leads to the recovery of work-hardened materials' mechanical properties, we propose the following.

Since the ultrasonic recovery experiments were held at the stress-free state, the function K defined via formulae (3)-(5) is inapplicable because $K = 0$ at $\tau_0 = 0$ and we obtain no change in H_N. Further, since the thermally activated processes at room temperature exert a feeble effect, we need to insert into the function K a term that expresses the recovery processes induced by ultrasound.

We replace the function K from (15) by

$$K_U = K + A_1 \left(\sigma_m H_{\max}\right)^{A_2}, \tag{16}$$

where σ_m is the oscillating stress amplitude, $H_{\max}$ is the maximum plane distance for the whole loading history, A_1 and A_2 are the model constant to be chosen for the best fit between the analytic and experimental results.

Therefore, now the degree of hardening – the plane distances in terms of the synthetic theory – obeys the following relationships:

$$H_{NU} = \sqrt{\sigma_S^2 + \frac{3}{2}\psi_{N0}\exp(-A_1\left(\sigma_m H_{\max}\right)^{A_2} t)}. \tag{17}$$

Let us analyze the modification proposed in Eqs. (16) and (17). The appearance of a term depending on the intensity of sonication (σ_m) in the function that governs the decrease of the plane distances reflects the experimental fact that the acoustic energy can induce alone the recovery processes in plastically deformed materials. It is clear that $K_U = K$ in the absence of ultrasonic energy ($\sigma_m = 0$), i.e., we return to the case as with formula (3). Further, we defined K_U via the product $\sigma_m H_{\max}$ to reflect another experimental fact that the greater values of strain hardening (plastic deformation) lead to more intensive recovery during the sonication at a given intensity of ultrasound and its duration. $H_{\max}$ is defined via formula (7) at $\beta = 0$ and $\lambda = 0$:

$$H_{\max} = S_1 N_1 = \sqrt{2/3}\sigma \tag{18}$$

So $H_{\max}$, via σ, bears in itself the information on the degree of plastic deformation.

2.3 Results and Discussion

To inspect the modifications we proposed above, let us compare model results with experimental data [4] on the temporary decrease of Vickers hardness number (*HV*) of aluminum specimen plastically deformed in uniaxial tension on two values: $\varepsilon_1 = 3.6\ \%$ and $\varepsilon_2 = 6.8\ \%$ (Fig. 7). The sonication of the strain hardened specimen is conducted by the longitudinal oscillation of amplitude $\sigma_m = 10$ MPa . Both the plastic deforming and the sonication take place at room temperature. To relate the value of *HV* to the yield strength in uniaxial tension σ_S , we address the results on the correlation between Vickers hardness number and yield strength for aluminum, which states that $HV = 17.4$ corresponds to $\sigma_S = 23.4$ MPa [22]. We preserve the relation $R \equiv HV / \sigma_S = 0.744$ not only for the start of plastic deforming but for formula (17) as well:

$$HV = R \cdot \sqrt{\sigma_S^2 + \frac{3}{2}\psi_{N0}\exp(-A_1\left(\sigma_m H_{\max}\right)^{A_2} t)}. \tag{19}$$

To apply the formula above, first, we need to choose the constant r to make sure that it gives correct HV for the plastically deformed specimens. For this purpose,

(i) We utilize formulae (9)-(12), which give $\varepsilon \sim \sigma$ relation

(ii) From the $\varepsilon \sim \sigma$ relationships, we take those values of the stresses ($\sigma_1 = 31.0\text{MPa}$ and $\sigma_2 = 33.6$ MPa) that correspond to $\varepsilon_1 = 3.6$ % and $\varepsilon_2 = 6.8$ %

(iii) On the base of (8), we calculate ψ_{N0} for σ_1 and σ_2

(iv) Formula (19) at $t = 0$ gives the values of HV for the plastic deformation caused by σ_1 and σ_2

As a result, we obtain two points on the $HV \sim t$ diagram at $t = 0$

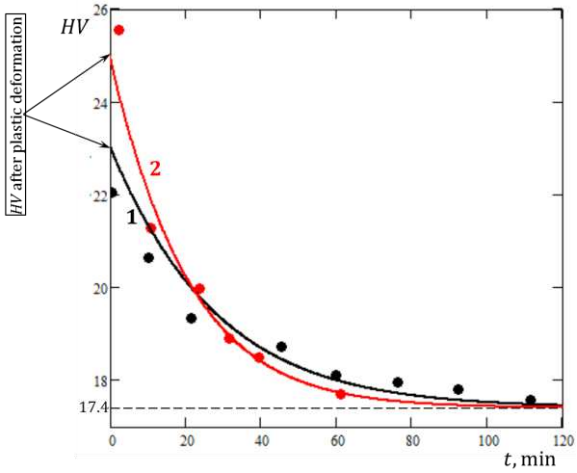

Figure 7
HV vs. *sonication time* plots for the plastically deformed aluminum specimen: $\varepsilon_1 = 3.6$ % and $\varepsilon_2 = 6.8$ % . • - experiment [4], lines - model

The next step is to model the decrease in HV as a function of sonication time by formula (19). Fig. 7 demonstrates the model $HV \sim t$ curves constructed at the following constants' values: $A_1 = 7.136 \times 10^{14} \left(\text{MPa}^{2A_2} \cdot \text{s}\right)^{-1}$, $A_2 = 4.0$. As in the experiment, the model curve at $\varepsilon_2 = 6.8$ % shows a quicker decrease in HV than that at $\varepsilon_1 = 3.6$ %. It is in full accordance with the experimental fact that the initial strain hardening increase boosts the acoustic field's recovery processes.

Conclusions

In this work we developed a model that analytically describes the phenomenon of ultrasonic recovery. For the mathematical apparatus, we utilized the synthetic theory of irrecoverable deformation, which has shown itself to be an effective tool for modelling the various problems that are related to ultrasound-assisted processes. We extend the synthetic theory, via the introduction of a new term

accounting, for the presence of oscillating stress. As a result, we obtained a plot for the micro-hardness of plastically deformed aluminum specimens, that are subjected to sonication. The results show a good agreement with the experimental data.

Acknowledgment

This work was supported by Doctoral School on Materials Science and Technologies, ID 215, Óbuda University.

References

[1] Rusinko, A.: Analytical description of ultrasonic hardening and softening. *Ultrasonics*, **51**, 709-714, 2011

[2] Peslo, A.: Ultrasonic hardening of aluminium alloys. *Ultrasonics,* **22**, 37-41, 1984

[3] A. Kozlov, N. Mordyuk: The influence of preliminary ultrasound treatment on the strength of metals, *Ultrasonic vibrations and their impact upon the mechanical characteristics of metals, Kiev,* 1986, pp. 31-34

[4] Kulemin, A.: *Ultrasound and Diffusion in Metals.* Moscow, Metallurgia, 1978

[5] Rusinko, A.: Influence of preliminary ultrasonic treatment upon the steady-state creep of metals of different stacking fault energies. *Ultrasonics*, **54**, 90-98, 2014

[6] Bazeljuk, G. et al.: Influence of preliminary ultrasonic irradiation and mechanics-thermal treatment upon the high-temperature creep and microhardness of copper, *Fizika metallov i metallovedenije*, **29**: 508-511, 1970

[7] Bazeljuk, G. et al.: Influence of preliminary ultrasonic irradiation and mechanics-thermal treatment upon the creep-resistance of aluminum, *Fizika metallov i metallovedenije*, **32**: 145-151, 1971

[8] Bagherzadeh, S. & Abrinia, K.: Effect of ultrasonic vibration on compression behavior and microstructural characteristics of commercially pure aluminum. *Journal of Materials Engineering and Performance*, **24**, 4364-4376, 2015

[9] Blagoveshchenskii, V., Panin, I.: An increase in the rate of plastic deformation under the effect of ultrasound. *The Physics of Metals and Metallography*, **103**, 424-426, 2007

[10] Daud, Y., Lucas, M. & Huang, Z.: Modelling the effects of superimposed ultrasonic vibrations on tension and compression tests of aluminium. *J. Mater. Process. Technol,* **186**, 179-190, 2007

[11] Deshpande, A., Tofangchi, A., & Hsu, K.: Microstructure evolution of Al6061 and copper during ultrasonic energy-assisted compression. *Materials Characterization,* **153**, 240-250, 2019

[12] Geibler, U., Schneider-Ramelow, M., & Reichl, H.: Hardening and softening in AlSi1 bond contacts during ultrasonic wire bonding. *IEEE Transactions on Components and Packaging Technologies,* **32**, 794-798, 2009

[13] Graff, K.: Ultrasonic metal forming: processing. *Power Ultrasonics, Edited by Juan A. Gallego and Karl F. Graff, Woodhead Publishing*, pp. 377-438, 2015

[14] Huang, H., Pequegnat, A., Chang, B., Mayer, M., Du, D. & Zhou, Y.: Influence of superimposed ultrasound on deformability of Cu. *Journal of Applied Physics,* **106**, 113514, 2009

[15] Malygin, G. A.: Acoustoplastic effect and the stress superimposition mechanism. *Physics of the Solid State,* **42**, 72-78, 2000

[16] Yao, Z., Kim, G. Y., Wang, Z., Faidley, L., Zou, Q., Mei, D., & Chen, Z.: Acoustic softening and residual hardening in aluminum: modeling and experiments. *International Journal of Plasticity*, **38**, 75-87, 2012

[17] Zhou, H., Cui, H., and Qin, Q.: Influence of ultrasonic vibration on the plasticity of metals during compression process. *J. Mater. Process. Technol.*, **251**, 146-159, 2018

[18] Lum, I., Huang, H., Chang, B., Mayer, M., Du, D., and Zhou, Y.: Effects of superimposed ultrasound on deformation of gold. *Journal of Applied Physics,* **105**, 024902, 2009

[19] A. Rusinko, Ali H. Alhilfi: Evolution of loading surface in the ultrasonic field, *Proceedings of the Engineering Symposium at Bánki*, Budapest 2020, pp. 35-40

[20] Susan, M. M., Dumitras, P. G. and Iliescu, V. G:. Experimental research of the ultrasonic softening in cold-rolled steel strips. *Электронная обработка материалов* №1, 2007

[21] Rusinko, A. & Rusinko, K.: *Plasticity and Creep of Metals.* Berlin, Springer, 2011

[22] Arbtin Jr., E., Murphym G.: Correlation of Vickers hardness number, modulus of elasticity, and the yield strength for ductile metals. *Ames Laboratory ISC Technical Reports*, 1953

Proactive Maintenance as a Tool of Optimization for Vehicle Fleets, in Terms of Economic and Technical Benefits

Ľubomír Ambriško[1] and Katarína Teplická[2]

Institutes of [1]Logistics and Transport and [2]Earth Resources
Technical University of Košice, Faculty of Mining, Ecology, Process Control and Geotechnologies, Letná 1/9, 042 00 Košice, Slovakia
lubomir.ambrisko@tuke.sk, katarina.teplicka@tuke.sk

Abstract: Maintenance is one of the more important processes that affect productivity and creates added value, for the main process within every company. The aim of this paper is to highlight the process of vehicle fleet maintenance and the evaluate the economic and technical benefits, in terms of optimizing the maintenance process. We used economic, comparative analysis to evaluate the maintenance process. Pareto analysis on the principle (80/20%) presents critical service activities for each type of bus. Critical services of the maintenance process are shock absorbers, cooler, planning service, brake lines. Important features of the maintenance process are cost optimization, capacity planning, workload utilization, optimal material delivery and monitoring the fulfillment of the plan for every company, in various areas of industry. The solution to the problems of fleet maintenance is the introduction of a proactive maintenance approach, aimed at improving the individual activities and capabilities of the vehicles used in the process.

Keywords: maintenance; efficiency; plan; life cycle; vehicle fleet

1 Introduction

Since early 2000, proactive maintenance in Europe, and prognostic and health management in the US have been developed to go beyond classical maintenance strategies. Both use the monitoring parameters, which allow the failure prevision of machines [1]. Preventive maintenance is planned and is performed before the machines fail [2] e. g. it prevents the machines from closing due to the degrading [3] (deterioration, such as wear, fatigue, and corrosion are common [4]). The aim of proactive maintenance is using historical data, empirical tests and statistical calculations to avoid machine breakdowns [5]. Urban buses require different levels of preventive maintenance. The higher level of the preventive maintenance, the more maintenance cost will arise [6].

Buses, in bus transportation companies, are maintained regularly in a fixed time or mileage intervals in maintenance depots [7]. The important component in the bus transit operations planning process is the scheduling of maintenance activities [8]. In work [9] was compared the operational efficiency of the urban buses in various stages of their operational life. Work [10] deals with the implementation of the prescribed maintenance of buses and the maintenance costs were analyzed by Pareto. Maintenance has changed from corrective to preventive to predictive and proactive [11].

Proactive maintenance is a key instrument for the vehicle fleet of bus transport. Her significance is in economic, technical, social, environmental benefits. Industry 4.0 concept or in integrating the smart system in transport is also an important step around the sustainability of bus transport in every state. High costs and high energy consumption are factors for changes in the vehicle fleet of bus transport areas. Rajput et.al said Industry 4.0 is progressing exponentially and offers a productive output in terms of circular economy and cleaner production to attain ethical business by achieving accuracy, precision, and efficiency also in the vehicle fleet [12]. Preventive maintenance in bus transport is an instrument for improvement. Proactive maintenance is a strategy to prevent malfunctions. Proactive maintenance has tasks that we divide into three categories: planned renewal, planned decommissioning, determining the conditions for monitoring the condition [13]. This strategy includes both preventive and predictive maintenance (Figure 1). Maintenance is one of the important processes of vehicle fleets. All processes affect the efficiency and functionality of the fleet vehicles, for bus transport purposes.

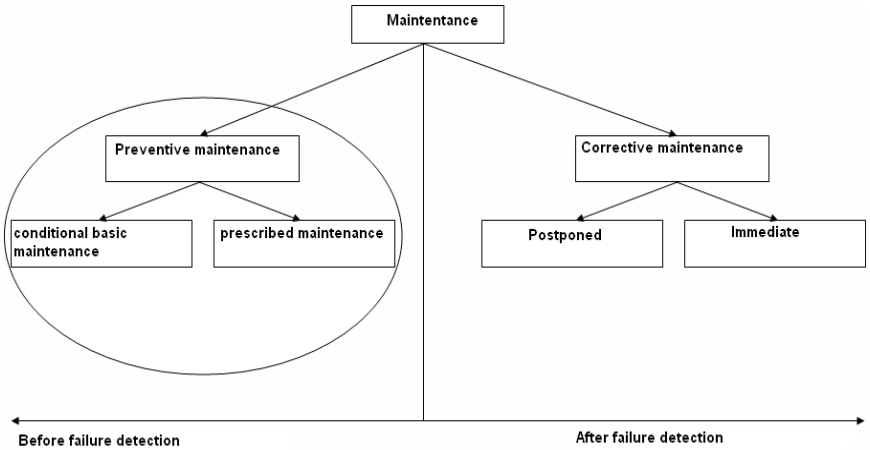

Figure 1
Maintenance according STN EN 13 306

The method of maintenance management is an important element of effective management of the entire organization. Maintenance is the process of managing technical and administrative activities throughout the life cycle of an object (*Figure 2*).

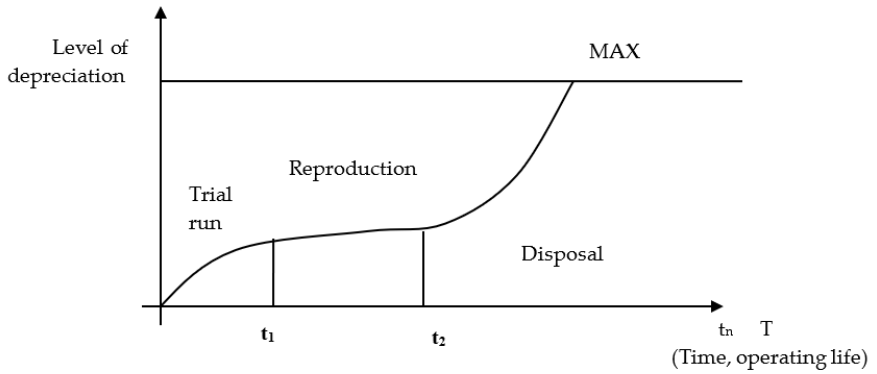

Figure 2
Economic life cycle of vehicle [13]

The aim of proactive maintenance is to maintain or restore its condition in which it can vehicle perform the required function, considering optimal costs and quality, safety, and environmental requirements. Maintenance is a set of activities that ensure the technical competence, readiness, and economic operation of the basic vehicle. It is a set of measures for securing and assessing the actual condition of machinery and equipment, as well as for maintaining and restoring their desired condition. The scope of maintenance activities is not specifically specified, this includes treatment (maintenance by cleaning and lubrication), inspection, repairs in case of equipment failures. Bashar et. al. commented that total productive maintenance (TPM), people management (HRM), and organizational performance are connected and influence the business profit of organizations [14]. The next possibility of bus transport is a hybrid system. Wang et al. [15] presented a hybrid system for sustainable cities that contains a combination of a bus system with a bike system. It means a low-carbon transport system because the bus system creates high CO_2 emissions. The hybrid system reaches the most environmentally friendly state for big cities. The change of fuel to biodiesel can significantly reduce CO_2 emission and energy consumption of the current bus system. The next problem in the bus transport area is periodic maintenance and long-term plan for daily parking, the assignment of bus blocks in the frame of compatibility. David et al. [16] have solved the problem with public transit, which aims to assign vehicle blocks of a planning period to buses in the fleet of a transportation company. They suggest a state-expanded multi-commodity flow network. This model takes bus parking constraints into account and assigns preventive maintenance. An important part of bus transport is bus stop and information at the bus stop for customers. Intelligent systems create opportunities for improvement in bus

transport. These include smart meters, smart street lightings, smart gas stations, smart parking lots, and smart bus stops. Kamal et al. [17] said that the advent of smart sensors, single system-on-chip computing devices, the Internet of Things (IoT), and cloud computing is facilitating the design and development of smart devices and services in bus transport. They present major enhancements to the bus stops by installing air-conditioning units, but without any remote monitoring and control features. They present a smart IoT-based environmentally friendly enhanced design for existing bus stop services. Lauth et al. [18] present a methodology that addresses the challenges of designing a depot for electric vehicle fleets - bus. The wide variety of possible solutions are structured using a morphological matrix. A modular simulation and planning tool are introduced which takes technical and operational aspects into account. All these changes create an innovative approach in bus transport and services like maintenance, parking. In cities, public transportation service plays a vital role in the mobility of people. Introduction of a new route or increase in the frequency of buses, the nonrevenue kilometers covered by the buses increases as a depot and route starting/ending points are at different places. This problem is the next opportunity for improvement. Mahadikar et al. [19] said, that the reduction of dead kilometers is necessary for the economic growth of the public transportation system. They obtained information that minimizing dead kilometers depend on optimizing the allocation of buses to depots depending upon the shortest distance between the depot and route starting/ending points. On the base, this information began to solve the reduction of dead kilometers. Regular maintenance, which is performed according to a predetermined schedule, represents preventive maintenance. A special case of a preventive strategy is predictive maintenance and is focused on detecting warning signs of damage that has already begun [20]. Periodic resp. on-line condition monitoring and maintenance will be performed if the deterioration of the condition to a certain specified extent is detected [21]. In this case, however, maintenance will only work on parts whose condition has been recorded as deteriorated. This prevents the fault, but usually does not eliminate the primary cause of the deterioration.

2 Material and Methods

As part of the research, we proceeded based on the algorithm of steps (Figure 3), which was the basic tool for managing the implemented project. Various methods were used in solving the project, such as analytical, simulation, experimental, graphical. We deal with the economic life cycle of vehicles in the phase of reproduction and the phase of disposal. The economic life-cycle of vehicles in the phase of reproduction means the modernization of vehicles, repair of vehicles, or buying new vehicles with the same characteristics.

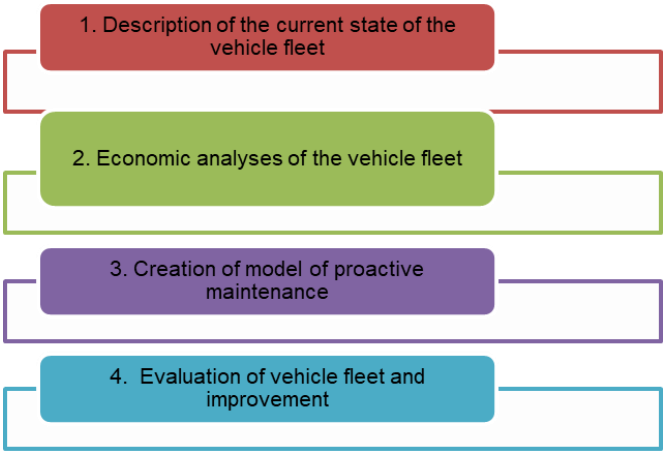

Figure 3
Algorithm of research

In the area of economic analysis, we used Pareto analysis. In the field of quality management, it is one of the most effective, commonly available and easy-to-apply tools. It states that 20% of the causes, are causally related, to 80% outcomes of poor quality. It makes it possible to separate the essential factors of a certain problem from the less significant ones and to show which direction to focus on efforts to eliminate shortcomings in the quality assurance process. We rank the causes from the largest to the smallest value. Let us create a bar graph.

We determine the percentage of causes based on the formula Structure (S):

$$S\,(\%)\frac{Xi}{SUM\ Xi} * 100(\%) \tag{1}$$

Then we determine the Lorenz curve using cumulative percentages and plot a line graph. According to the Lorenz curve, we determine the maintenance services that are critical and that need to be addressed in the transport company, because they represent high costs for buses maintenance.

2.1 Description of the Current State of the Vehicle Fleet

To carry out the research of the vehicle fleet, it was necessary to prepare a description of the current state of the vehicle fleet-buses. The research was focused on the fleet of buses operated by the transport company. The aim of the research was to determine the condition of the vehicle fleet and the efficiency of the bus maintenance process, due to the technical and economic problems of the transport company. The first prototype of the SOR NB 12 (*Figure 4*) bus was

manufactured in 2006 by the Czech manufacturer SOR Libchava. It was put into operation in 2012.

Figure 4
Vehicles SOR NB 12

Iveco Crossway LE 12M (*Figure 5*) was manufactured in 2008. The buses were manufactured at the Irisbus Iveco plant in Vysoké Mýto in Czech Republic.

Figure 5
Vehicle Iveco Crossway LE 12M

Iveco First FCLLI buses (*Figure 6*) were manufactured in Slovakia in the company Rošero - P in the year 2008. The reason for purchasing this bus was the need to provide transport, more economically, on connections that are unprofitable for classic buses. They started in operation in 2009.

Figure 6
Vehicle Iveco First FCLLI

3 Results

In the research analytical portion, we focused on the economic analysis of the maintenance process in the bus fleet. In the first step, we monitored the activities in the maintenance process according to category M1 for selected buses. As part of the fleet research, we performed an analysis of service activities (*Table 1*) in the category: Service standard. The basic criteria for the service standard category are the distance traveled 40,000 km, complete bus service once a year, or the number of bus hours 800 hours. Some service activities are not necessary for the specified category M1.

Table 1
Analysis of service activities

Type of service activities M1	**SOR NB12**	**IVECO CROSSWAY LE12M**	**IVECO FIRST FCLLI**
Engine oil change	•	•	•
Engine oil filter replacement	•	•	•
Fuel pre-filter cartridge replacement			•
Engine blow by filter replacement	•	•	
Replacement of the antifouling filter	•	•	
Checking the fluid level in the hydraulic system	•	•	•
Total chassis lubrication	•	•	
Checking the condition of various belts	•	•	•
External radiator wash	•	•	
Checking the effectiveness of the axle vent			•

Type of service activities M1	**SOR NB12**	**IVECO CROSSWAY LE12M**	**IVECO FIRST FCLLI**
Inspection of tie rods, joints, and steering shaft			•
Check the tightness of the hydraulic brake lines and the cooling system	•	•	•
Check the wear rate of the brake discs and brake pads	•	•	•
Check the engine EDC system with E.A.SY			•
Ad blue device test using E.A.SY function	•	•	
Check on the road	•	•	•

Based on detailed economic analyzes for the service activities of the bus fleet, we found the activities that are financially the most expensive for the transport company (*Table 2*). These activities include in particular: Planning service, Belts, Replacement engine oil, Testing of failure, Oil filter, Radiator wash, Brake lines, Cooler, Shock absorbers. In addition to these critical activities and spare parts, other important activities are performed in the bus maintenance system, and various spare parts are needed. However, they are not that expensive and do not pose a significant problem within the fleet maintenance system. Given that the bus fleet maintenance system presents both economic and technical problems, it is necessary to analyze critical service activities.

Table 2

Type of critical service activities

Type of service activities, replacement parts (€)	**SOR NB12**	**IVECO CROSSWAY LE12M**	**IVECO FIRST FCLLI**
Planning service	1800	850	180
Belts	1400	560	60
Replacement engine oil	1200	1100	80
Testing of failure	800	300	95
Oil filter	750	600	35
Radiator wash	500	200	25
Brake lines	350	750	110
Cooler	2100	4500	350
Shock absorbers	2860	3000	460

3.1 Economic Analyses of the Vehicle Fleet

Based on the performed Pareto analysis according to formula (1), we found critical service services that are very costly for individual types of buses.

The type of bus SOR NB12 (*Figure 7*), based on Pareto analysis, presents critical service activities as an 20/80% split, the critical services are shock absorbers, cooler, planning service, belts and the replacement of engine oil. The critical activity limit is determined based on a point on the Lorenz curve of 80% and are perpendicular to the x-axis. The economic aspect is the movement of costs at the level from 1200 € to 2860 €. Those activities or spare parts are the critical category 20% of maintenance activities and 80% costs of maintenance.

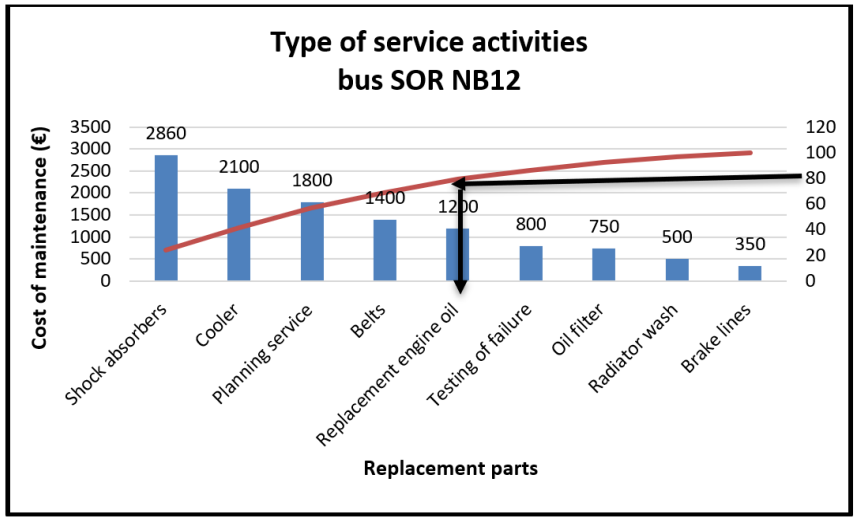

Figure 7
Pareto analysis SOR NB12

The type of bus IVECO CROSSWAY LE12M (*Figure 8*) based on Pareto analysis presents critical service activities on the principle (20/80%). They are cooler, shock absorbers, replacement engine oil, planning service. The critical activity limit is determined based on a point on the Lorenz curve of 80% and a perpendicular to the x-axis. The economic aspect is the movement of costs at the level from 850 € to 4500 €. Those activities or spare parts are the critical category 20% of maintenance activities and 80% costs of maintenance.

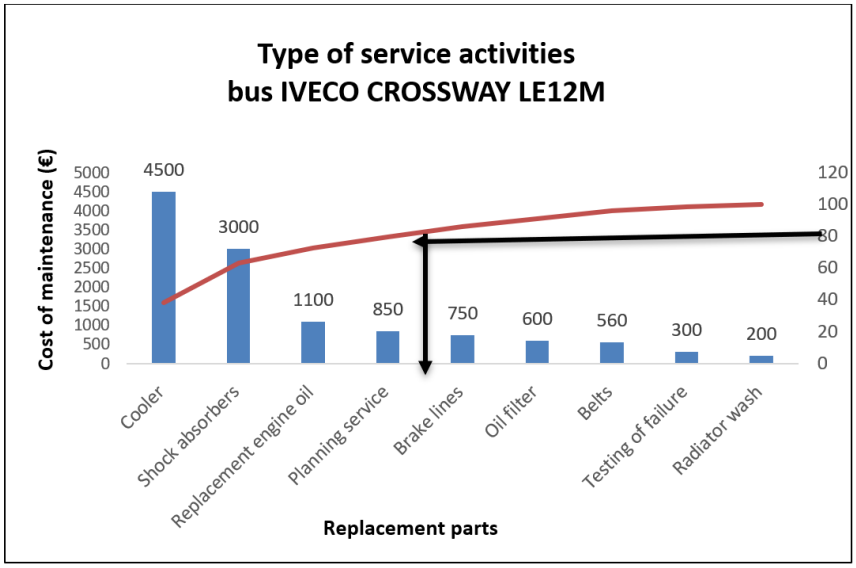

Figure 8
Pareto analysis IVECO CROSSWAY LE12M

The type of bus IVECO FIRST FCLLI (*Figure 9*) based on Pareto analysis presents critical service activities on the principle (20/80%). They are shock absorbers, cooler, planning service, brake lines. The critical activity limit is determined based on a point on the Lorenz curve of 80% and a perpendicular to the x-axis.

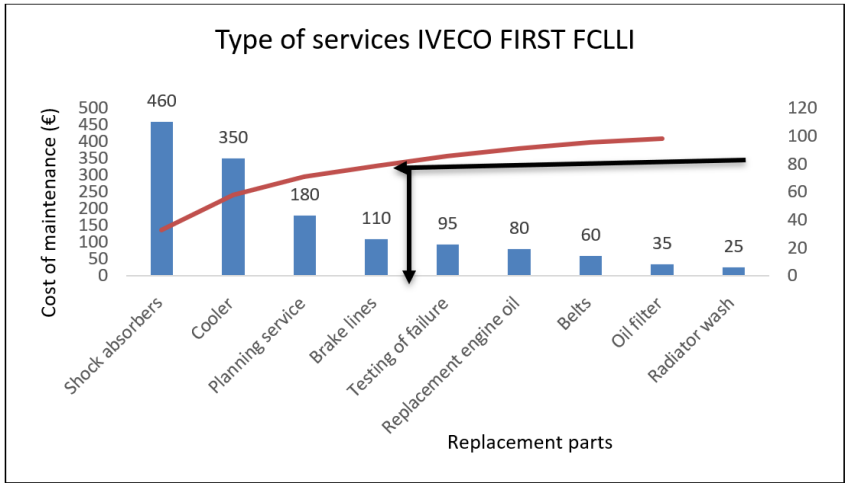

Figure 9
Pareto analysis IVECO FIRST FCLLI

The economic aspect is the movement of costs at the level from 110 € to 460 €. Those activities or spare parts are the critical category 20% of maintenance activities and 80% costs of maintenance. 20% of maintenance activities account for 80% of maintenance costs and therefore it is necessary to pay attention to these activities in the maintenance process.

3.2 Creation of Model of Proactive Maintenance

Critical maintenance activities as cooler, shock absorbers, replacement engine oil, planning service, brake lines, belts need to be planned as part of preventive maintenance. It is important to plan for these critical activities in the maintenance process for the bus fleet as part of proactive maintenance (*Figure 10)* to minimize the cost of spare parts and critical activities in the maintenance process.

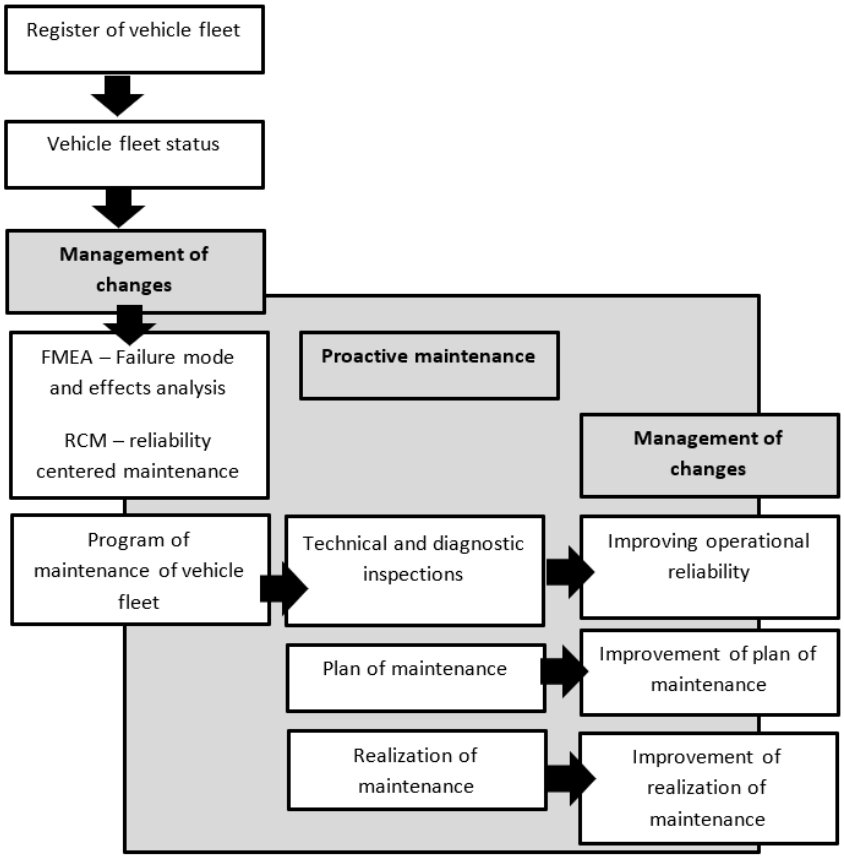

Figure 10
Proactive model of maintenance management

Proactive maintenance requires the planning of activities that prevent bus breakdowns. In this way, they minimize activities related to repairing faults, replacing spare parts, and performing regular preventive service activities. The proactive maintenance model is based on the use of change management approaches in terms of technical and diagnostic control of vehicles - buses, maintenance planning focused on preventive maintenance, implementation of maintenance activities with a focus on cost minimization.

3.3 Evaluation of Vehicle Fleet and Improvement

Based on the above approach, it is possible to achieve changes in the maintenance process and create an effective maintenance system in the transport company's bus fleet. High bus maintenance costs, lack of spare parts, lack of functional buses are problems for the vehicle fleet. Focusing on the new three approaches according to the proactive maintenance model will bring the transport company improved maintenance planning, improvements in the implementation of maintenance activities, improved operational reliability of vehicles-buses, which ultimately means satisfying customer requirements.

4 Discussion

Proactive maintenance is orientated on new innovative approaches in maintenance (TPM, RCM). According to the level of generations of maintenance, all the firms can decide, what form of maintenance use from the view of care for vehicles (*Figure 11)*. The tendency of maintenance depends on the character of the firm. The third generation of maintenance level is orientated on reliability, security, quality, costs, environment, and durability of the vehicle. This approach is preferred around maintenance management circles today.

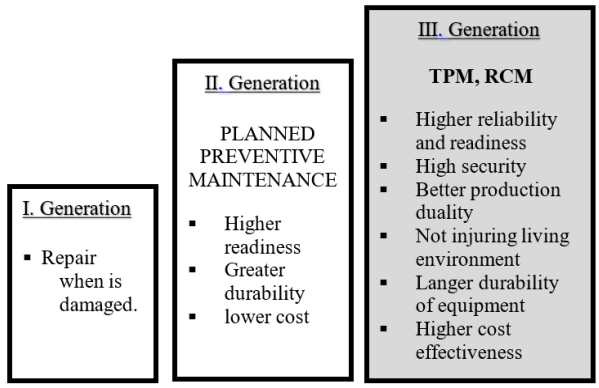

Figure 11
Generation of maintenance management

Rajput et. al [12] said Industry 4.0 offers a productive output in terms of circular economy and efficiency. This approach is used in transport companies so, that bring implementation proactive maintenance in vehicle fleet for buses. This proactive maintenance brings economic benefit in reduction of costs and technical benefit for the realization of maintenance activities and buying new spare parts for vehicle fleet buses. Bashar et al. [14] commented that total productive maintenance (TPM), people management (HRM), and organizational performance are connected and influence the business profit of organizations. This connection brought for the vehicle fleet important significance because the transport company implemented proactive maintenance, the employees of maintenance absolved training, the performance of the transport company was improved, and maintenance reduced all cost for three buses of the vehicle fleet. Wang et al. [15] presented a hybrid system for sustainable cities that contains a combination of a bus system with a bike system. This transport company offer service for cities in bus system only. Transport company does not competencies for implementation hybrid system, because it is opportunities for the public sector. It is possible to create a hybrid system with a bus system, bike system, train transport.

Conclusion

Maintenance is one of the most important processes that affect productivity and creates added value, for the main process, within every company. Proactive maintenance is a key instrument for the operation of vehicle fleets of bus transport and its significance is in terms of economic, technical, social and environmental benefits. High costs and high energy consumption are factors for changes in the vehicle fleet of bus transport areas. The aim of this work was to describe the process of vehicle fleet maintenance and provide an evaluation of economic and technical benefits, in terms of the optimization of the entire maintenance process. We used economic, comparative analysis to evaluate the maintenance process and the Pareto analysis, based on the 80/20% principle. The results provide critical service activities for each type of bus. Critical services of the maintenance process are shock absorbers, cooler, planning service, brake lines. Paramount, in the maintenance process, is cost optimization, capacity planning, workload utilization, optimal material delivery and monitoring the fulfillment of the plan in each company and in various areas of industry. The Industry 4.0 concept, or in integrating the smart system in transport, is also, an important step in the sustainability of bus transport.

Acknowledgement

The article was prepared with the support from the project VEGA 1/0429/18 and VEGA 1/0317/19.

References

[1] Laloix, T., Voisin, A., Deeb, S., Romagn, E., Iung, B., Lorange, F.: Industrial system functioning/dysfunctioning-based approach for indicator

identification to support proactive maintenance, IFAC PapersOnLine 50-1, 2017, pp. 13704-13709

[2] Exner, K., Schnürmacher, C., Adolphy, S., Stark, R.: Proactive maintenance as success factor for use-oriented Product-Service Systems, Procedia CIRP 64, The 9th CIRP IPSS Conference: Circular Perspectives on Product/Service-Systems, 2017, pp. 330-335

[3] Zhou, B., Qi, Y., Liu, Y.: Proactive preventive maintenance policy for buffered serial production systems based on energy saving opportunistic windows, Journal of Cleaner Production, 253, 2020, pp. 1-14

[4] Yang, L., Zhao, Y., Peng, R., Ma, X.: Hybrid preventive maintenance of competing failures under random environment, Reliability Engineering & System Safety, 174, 2018, pp. 130-140

[5] Škerlič, S., Sokolovskij, E., Erčulj, V.: Maintenance of heavy trucks: an international study on truck drivers, Eksploatacja i Niezawodnosc – Maintenance and Reliability, 22 (3), 2020, pp. 493-500

[6] Zhou, Y., Kou, G., Xiao, H., Peng, Y., Alsaadi, F. E.: Sequential imperfect preventive maintenance model with failure intensity reduction with an application to urban buses, Reliability Engineering and System Safety, 198, 2020, pp. 1-11

[7] Zhou, R., Fox, B., Lee, H. P., Nee, A. Y. C.: Bus maintenance scheduling using multi-agent systems, Engineering Applications of Artificial Intelligence, 17, 2004, pp. 623-630

[8] Haghani, A., Shafahi, Y.: Bus maintenance systems and maintenance scheduling: model formulations and solutions, Transportation Research Part A, 36, 2002, pp. 453-482

[9] Niewczas, A., Rymarz, J., Debicka, E.: Stages of operating vehicles with respect to operational efficiency using city buses as an example, Eksploatacja i Niezawodnosc – Maintenance and Reliability, 21 (1), 2019, pp. 21-27

[10] Ambriško, Ľ.: Analysis of public transport vehicles maintenance costs, CLC 2018 Carpathian Logistics Congress, Ostrava, 2019, pp. 368-373

[11] Horváth, C., Gaál, Z.: Operating maintenance model for modern printing machines, Acta Polytechnica Hungarica, 5 (3), 2008, pp. 39-47

[12] Rajput, S., Singh, S. P.: Indurstry 4.0 model for circular economy and cleaner production, Journal of Cleaner Production, 277, 2020, 123853

[13] Teplická, K., Straka, M.: Sustainability of extraction of raw material by a combination of mobile and stationary mining machines and optimization of machine life cycle, Sustainability, 12 (24), 2020, pp. 1-13

[14] Bashar, A., Hasin, A. A., Jahangir, N.: Linkage between TPM, people management and organizational performance, Journal of Quality in Maintenance Engineering, 2020, 10.1108/JQME-11-2019-0105

[15] Wang, S. S., Wand, H., Xie, P. Y., Chen, X. D.: Life-cycle assessment of carbon footprint of bike-share and bus systems in capus transit, Sustainability, 13 (1), 2021, 1-14

[16] David, B., Kresz, M.: Multi-depot bus schedule assignement with parking and maitenance constraints for intercity transportation over a planning period, Transportation Letters – the International Journal of Transportation Research, 12 (1), 2020, pp. 66-75

[17] Kamal, M., Atif, M., Jujahid, H., Shanableh, T., Al-Ali, A. R., Al Nabulsi, A.: IoT based smart city bus stops, Future Internet, 11 (11), 2019, 1-11

[18] Lauth, E., Mundt, P., Gohlich, D.: Simulation based planning of depots for electric bus fleets considering operations and charging management, The 4th International Conference on Intelligent Transportation Engineering, 2019, pp. 327-333

[19] Mahadikar, J., Mulangj, R. H., Sitharam, T. G.: Optimization of bus allocation to depots by minimizing dead kilometers, Journal of Advanced Transportation, 49 (8), 2015, pp. 901-912

[20] Ambriško, Ľ., Marasová, D., Cehlár, M.: Investigating the tension load of rubber composites by impact dynamic testing, Bulletin of Materials Science, 40 (2), 2017, pp. 281-287

[21] Ambriško, Ľ. Et al.: Mechanical properties and chemical composition of rubber gaskets, Przemysł Chemiczny – Chemical Industry, 99 (4), 2020, pp. 598-601